1-1-2006

The chemical and mechanical effects of binding chitosan to implant quality titanium

Holly Joy Martin

THE CHEMICAL AND MECHANICAL EFFECTS OF BINDING CHITOSAN TO IMPLANT QUALITY TITANIUM

By

Holly Joy Martin

A Dissertation
Submitted to the Faculty of
Mississippi State University
in Partial Fulfillment of the Requirements
for the Degree of Doctor of Philosophy
in Chemical Engineering
in the Dave C. Swalm School of Chemical Engineering

Mississippi State, Mississippi

December 2006

THE CHEMICAL AND MECHANICAL EFFECTS OF BINDING CHITOSAN TO IMPLANT QUALITY TITANIUM

By

Holly Joy Martin

Approved:

Kirk H. Schulz Professor of Chemical Engineering Dean of the James Worth Bagley College of Engineering (Director of Dissertation)	Joel D. Bumgardner Associate Professor of Biomedical Engineering University of Memphis (Committee Member)
Jerome A. Gilbert Professor of Biological Engineering Associate Provost for Academic Affairs (Committee Member)	Adrienne R. Minerick Assistant Professor of Chemical Engineering (Committee Member)
Judith A. Schneider Associate Professor of Mechanical Engineering (Committee Member)	Keisha B. Walters Assistant Professor of Chemical Engineering (Committee Member)
Rudy E. Rogers Professor of Chemical Engineering Director of Graduate Studies in the Dave C. Swalm School of Chemical Engineering	Roger L. King Professor of Electrical Engineering Associate Dean of the James Worth Bagley College of Engineering

Name: Holly Joy Martin

Date of Degree: December 8, 2006

Institution: Mississippi State University

Major Field: Chemical Engineering

Major Professor: Dr. Kirk H. Schulz

Title of Study: THE CHEMICAL AND MECHANICAL EFFECTS OF BINDING CHITOSAN TO IMPLANT QUALITY TITANIUM

Pages in Study: 486

Candidate for Degree of Doctor of Philosophy

Biomedical implants are commonly made from commercially pure titanium and other metal alloys, which are chosen for their strength and density. To improve the stability and promote bone cell growth into the implant, efforts to bond coatings to metal have been extensively studied. Many coatings used are considered bioactive, which promote the adhesion and growth of the bone cells surrounding the implant [A.1]. Of these, the most commonly investigated coating is a ceramic called hydroxyapatite, which is brittle, leading to flaking and inadequate bone cell growth [A.2]. Alternate bioactive coatings are being examined, including chitosan, the deacetylated form of chitin. Chitin is the second most abundant polymer in nature [A.3] and is found in the exoskeletons of insects and shellfish [A.4]. Chitosan has been proven to have excellent biocompatibility [A.5], be non-toxic [A.3], and promote the adhesion and growth of bone cells [A.6 – A.7].

In this research, four treatment combinations were developed and tested in an attempt to improve film bonding. These treatment combinations were created using one of two silane molecules, aminopropyltriethoxysilane and triethoxsilylbutyraldehyde, and one of two metal treatments, passivation and piranha treatment. XPS was used to characterize the reaction steps for each of the treatment combinations. A significant decrease in TiO, along with significant increases in SiO_x groups, C – N – H, and C = O, indicated that the reactions were proceeding as expected. XPS also indicated that, chemically, the chitosan films were not significantly different and were unchanged by the treatment combinations.

Following chemical analysis, mechanical testing was performed on the four treatment combinations. No changes to the bulk properties were seen as demonstrated by nano-indentation, further indicating that the four treatment combinations did not change the chemical properties of chitosan. The bulk adhesion of the films was greatly improved for all four treatment combinations, as demonstrated by tensile testing. The highest value from this research, 19.50 ± 1.63 MPa, was significantly higher than the previously published results of 1.6 – 1.8 MPa [A.10].

Overall, the treatments developed in this study significantly improved the adhesion of the chitosan film on the titanium substrate, without modifying the chemical or structural properties of chitosan.

DEDICATION

I would like to dedicate this dissertation to my mother, Emily C. Prine, and my husband, Eric J. Martin. Without their encouragement and support, this doctorate degree would not have been possible.

ACKNOWLEDGEMENTS

I would like to convey my heartfelt appreciation to several people without whom this research would not have occurred. I would first like to thank Dr. Kirk H. Schulz, my advisor, for his time and effort to assist me throughout my doctoral program, research questions, and dissertation writing process. Second, I would like to thank Dr. Keisha B. Walters for her guidance and suggestions for choosing the silane molecules, the metal treatment, and the solvent to improve the bonding of the chitosan film to the titanium substrates. I would also like to thank Dr. Joel D. Bumgardner for providing the chitosan used in the creation of the films and his assistance in performing bulk adhesion tests and contact angle measurements. I would next like to thank Dr. Judy A. Schneider for her guidance in choosing mechanical tests and for accessing the SHaRE program at Oak Ridge National Laboratory. Finally, I would like to thank Dr. Jerome A. Gilbert and Dr. Adrienne R. Minerick for serving on my committee. In addition to my committee, I would like to thank Dr. Sang Hoon Shim for his guidance and direction while performing the mechanical tests at Oak Ridge National Laboratory.

TABLE OF CONTENTS

CHAPTER Page

CHAPTER Page

LIST OF TABLES

TABLE Page

TABLE Page

TABLE Page

TABLE Page

TABLE Page

TABLE Page

TABLE Page

LIST OF FIGURES

FIGURE Page

FIGURE Page

FIGURE Page

FIGURE Page

FIGURE Page

CHAPTER I

LITERATURE REVIEW

1.1 Introduction

Metal has been used as implants in the human body for at least two thousand years, when ancient civilizations used gold for dental purposes [1.1]. Since first being developed to treat diseased teeth in the ancient world, the purpose and size of implants has dramatically changed [1.1]. As our knowledge of the human body, the immune system, and toxicology has increased, so has the realization that the metal implants used in the human body are not as un-reactive as once believed. Implants that were once considered inert and passive are degraded by the human body, through the leaching of metal ions and the destruction of surrounding bone cells [1.14 – 1.16], along with particulate formation caused by fretting [1.18].

This realization, and the human body's mechanisms to remove foreign bodies, has increased the efforts to improve the implant – tissue interface, to minimize the immune reaction to the implant, to promote the growth of bone cells into and surrounding the implant, and to stabilize the implant. Improvements have been made in creating coatings that are bioactive, or promote an interface between tissue and coating [1.2]. These improvements focus mainly on the interaction between the coating and the tissue, with very little attention being paid to the implant surface – coating interface. As a result, reaction mechanisms and bonding strengths of the various methods to produce coatings

are not well understood. In order to improve the tissue – coating interface, information must be obtained on ways to strengthen the coating – implant interface. The increase in interface strength is needed in order to reduce or prevent the fracture of the coating from the implant surface during implantation and to extend the life of the implant.

1.2 Implant Criteria

The first implants were originally used more than fifty years ago and were made of common, commercially available polymers and metals [1.2]. However, these materials were tested for their wear-patterns in the "outside" world, not in the fluids of the human body. As physicians implanted these materials, some patients began developing hypersensitivity reactions to these implants over time, leading physicians and material – implant specialists to realize that a material chosen must meet several criteria. Any implant used in the human body must meet all of the following characteristics [1.1]:

- Low toxicity
- Biocompatibility
- Proper anatomical fit
- Performance requirements

The implant should not be toxic to the surrounding tissues, nor should the byproducts of the degradation of that implant be toxic [1.1]. A material or chemical is considered toxic if it kills cells [1.3]. An exposure dose of that chemical is examined to determine the effect on the cells. The exposure dose is measured with respect to the entire animal. For example, the toxicity of pharmaceuticals are commonly characterized by an LD50, which is the toxic dose of a drug that kills 50% of the population of rats [1.4]. With implants, the toxicity effect of a chemical is examined using target cells, which are those cells that are the most susceptible to that chemical. Usually, the target

cells are cells normally surrounding the implant *in vivo* [1.3]. The target cell test is a much more sensitive toxicity determination method than the whole animal toxicity test, which accounts for the large differences in toxicity numbers between whole organism and target cell test methods.

The implant should be biocompatible to the surrounding tissues, with the definition of biocompatibility being determined based on the purpose of the implant [1.1]. The most basic definition of biocompatibility is given as "the ability of a material to perform with an appropriate host response in a specific situation" [1.5], where a host reaction is defined as "the reaction of a living system to the presence of a material" [1.5]. There are two major types of implants – those designed to remain for a patient's lifetime and those designed to be degraded by the body. The implants designed to remain permanently in the patient, such as joint replacements, should not adversely affect the host tissue nor should the tissue detrimentally change the implant [1.6]. The implants that are designed to be degraded by the body, such as drug delivery systems, may release toxic products, such as cancer drugs [1.1]. Therefore, unlike permanent implants, the implants that are designed to be degraded may adversely affect the host tissue; also, the surrounding tissue should detrimentally change the implant as the implant is degraded and removed [1.6].

An implant must be designed for the location and must fit that location properly [1.1]. Certain factors, such as movement, the fluid surrounding the material, and use will determine the shape and features of the implant. For example, a joint implant must be able to support movement, as the natural joint would do [1.1]. However, an implant that

is designed to be placed in a vein or artery does not need to allow movement, but must allow the blood to pass through it [1.1].

Finally, performance requirements are the last criterion needed for implant success. These requirements are based on the location of the implant and the purpose of the implant and must account for three different categories: mechanical performance, mechanical durability, and physical properties [1.1]. An implant should be designed to perform properly for its location within the human body, last more than ten years, and utilize the bulk material properties, such as density or ductility. For example, a hip implant should be strong and rigid to support the weight of the human body, it should last for at least 10 years, and it should be constructed of metals that are considered strong, but possess a low density, to reduce the weight of the implant while maintaining the strength of the metal [1.1].

With these criteria in mind, physicians and material scientists began working together more closely during the last thirty years to produce quality implants that would better serve the patients who needed them.

1.3 Metal Implants

Different types of metal have been used in the human body for centuries. More than 2000 years ago, gold was used in dentistry by the Romans, Chinese, and Aztec [1.1]. Since that time, advances have been made in both the understanding of toxicology and the understanding of the human body and its immune system's interaction with foreign bodies.

The metals originally chosen for implantation were commercially available metals [1.2]. These metals were not treated in any specific manner nor were they chosen for their chemical composition, but instead for their strength, durability, and availability. Eventually, though, material scientists began to realize that the manufacturing and composition of the metal implant had a major impact on the ability of the body to react with the implant, whether that was through degradation of the implant or the appearance of sensitivity reactions [1.2]. Today, the metals used are all chosen based upon their interaction, or lack thereof, with the host tissue. All three of the major implant metals can easily be treated to form a passive oxide layer, which does not allow interaction between the bone tissue and the metal implant. The metals are also chosen based on their density, elastic modulus, yield strength, and tensile strength; the yield strength and tensile strength can easily be changed by different methods of machining.

The manufacturing process of a standard metal implant begins with an ore, which contains the desired metal as well as other elements and contaminants [1.2]. The metal is removed from the ore through a standard treatment process designed for that specific raw metal [1.2]. The raw metal is then converted into an alloy by the addition of specific amounts of other chemicals, such as chromium or carbon in the creation of stainless steel, or the removal of other chemicals, such as oxygen in the creation of titanium metals [1.2]. Once the raw metal has been made into the proper composition, the metal is processed into stock shapes, which are sold to implant manufacturers. The manufacturers then fabricate the implant into its final form [1.2]. Once the implant is completely formed, the surface is cleaned and a passive oxide layer is created on the surface, following ASTM standards [1.2].

The composition of the different implant metals is very important to the mechanical properties, specifically tensile strength and yield strength. However, just as the composition is important, so is the method in which the implant is fabricated. Annealing a material refers to the method of exposing a metal to an elevated temperature for an extended time period and then slowly cooling that metal [1.7]. Annealing is done in order to relieve stress, increase ductility, and/or produce a specific microstructure [1.7]. Cold-working refers to the process of plastically deforming a metal, causing that metal to become harder and stronger [1.8]. It is used to increase the yield strength and tensile strength. However cold-working does result in a decrease in both ductility and percent elongation. Cold-forging, which is different from cold-working, refers to the method of mechanically working a metal; forging a metal results in the formation of tightly packed, well-defined grain structures and the best combination of physical properties [1.9]. Some metals are difficult to melt and machine. These metals, when cast by creating a molten material, result in casting defects and undesirable grain formations [1.2]. Powder metallurgy is used on those difficult metals to reduce the defects and prevent the undesirable grain formation [1.2]. In powder metallurgy, a fine powder of the metal is compacted and then sintered together using the appropriate pressure and temperature [1.2].

Currently, there are three types of metals used in the majority of implants, with several different compositions available for each metal. Table 1.1 lists the most common metals and the compositions of these metals that are used in implants.

Table 1.1. Commonly used biomedical implant metals and their compositions [1.2].

Implant Metal	Composition (in wt %)	
Stainless Steel, Grade 2, 316L	60.0 – 65.0	Iron
	17.0 – 19.0	Chromium
	12.0 – 14.0	Nickel
	2.0 – 3.0	Molybdenum
	< 2.0	Manganese
	< 0.5	Copper
	< 0.03	Carbon
	< 0.1	Nitrogen
	< 0.025	Phosphorus
	< 0.075	Silicon
	< 0.01	Sulfur
Cobalt-Chrome, F75	58.0 – 69.5	Cobalt
	27.0 – 30.0	Chromium
	5.0 – 7.0	Molybdenum
	< 1.0	Manganese
	< 1.0	Silicon
	< 1.5	Nickel
	< 0.75	Iron
	< 0.35	Carbon
Cobalt-Chrome, F90	45.5 – 56.2	Cobalt
	19.0 – 21.0	Chromium
	14.0 – 16.0	Tungsten
	9.0 – 11.0	Nickel
	< 3.0	Iron
	1.0 – 2.0	Manganese
	0.05 – 0.15	Carbon
	< 0.04	Phosphorus
	< 0.40	Silicon
	< 0.03	Sulfur
Commercially Pure Titanium, Grade 4	> 98.9	Titanium
	< 0.10	Carbon
	< 0.5	Iron
	< 0.0125 – 0.015	Hydrogen
	< 0.05	Nitrogen
	< 0.40	Oxygen
	< 0.18	Oxygen (Grade 1)
Ti – 6Al – 4 V	88.3 – 90.8	Titanium
	5.5 – 6.5	Aluminum
	3.5 – 4.5	Vanadium
	< 0.08	Carbon
	0.0125	Hydrogen
	< 0.25	Iron
	< 0.05	Nitrogen
	< 0.13	Oxygen

As Table 1.1 shows, stainless steel is mostly iron alloyed with chromium, nickel, and molybdenum. Chromium was added to create corrosion – resistant steel. This corrosion resistance is due to the formation of a strongly bonded, passive oxide film [1.2]. However, chromium tends to migrate to the ferritic phase, as well as molybdenum and silicon; the ferritic phase is the weaker of the two major phases in stainless steel [1.2]. In order to stabilize the stronger austenitic phase, nickel is added [1.2]. Stainless steel comes in many different alloys, with one major difference being the amount of carbon present [1.2]. Even 316 stainless steel is different from 316L stainless steel [1.2]. The "L" in 316L stands for low, indicating that the carbon percentage is extremely small [1.2]. The smaller amount of carbon present, the lower the rate at which the metal corrodes [1.2]. This occurs since the carbon bonds to the chromium, which reduces the ability of the chromium to form the passive oxide layer [1.2]. Adding the different chemicals to stainless steel and adjusting the method in which the stainless steel is processed changes the yield strength and tensile strength, as shown in Table 1.2.

Table 1.2. Properties of commonly used implant metals: their density, elastic modulus, and tensile strength.

Implant Metal	ASTM	Density (g/cm^3)*	Elastic Modulus (GPa)*	Yield Strength (MPa)**	Tensile Strength (MPa)**
Stainless Steel, Grade 2	F138, F139				
Annealed		8.00	193	331	586
30% Cold-Worked		8.00	193	792	930
Cold Forged		8.00	193	1213	1351
Cobalt-Chrome	F75				
Annealed		8.29***	210**	448-517	655-889
Powder Metallurgy		8.29***	253**	841	1277
Cobalt-Chrome	F90				
Annealed		9.13	236	448-648	951-1220
40% Cold-Worked		9.13	236	1606	1896
Commercially Pure Titanium	F67				
Grade 1, 30% Cold-Worked		4.51	103	170	760
Grade 4, 30% Cold-Worked		4.51	103	485	760
Ti – 6Al – 4 V	F136				
Forged Annealed		4.43	114	896	965
Forged Heat-Treated		4.43	114	1034	1103

* From reference [1.10] ** From reference [1.2] ***From reference [1.87]

As expected, cobalt-chrome is created mostly from cobalt and chromium, along with quantities of molybdenum or tungsten, as shown in Table 1.1 [1.2]. Cobalt-chrome was originally created to make use of the strength that the two elements create when combined together [1.2]. In the process of developing cobalt-chrome, it was determined that the grain structure of cobalt-chrome is very difficult to control using casting with subsequent annealing methods [1.2]. Cobalt rich grains are formed, with grain-boundary carbides consisting of carbon combined with only one of the following: molybdenum, chromium, or cobalt [1.2]. This combination of cobalt-rich grains and carbide-rich grains causes the formation of an electrochemical gradient, with the cobalt-rich grains being anodic and the carbide-rich grains being cathodic [1.2]. In addition to cobalt-chrome being difficult to anneal in a desired manner, cobalt-chrome is also very difficult to machine. The addition of two elements, tungsten and nickel, improved the machining and fabrication ability of the metal [1.2]. Table 1.2 shows the significant increase in yield strength and tensile strength when the original cobalt-chrome alloy (ASTM F75), which cannot be cold-worked, is compared with the cobalt-chrome alloy with added nickel and tungsten (ASTM F90) that can be cold-worked.

Titanium has increasingly been considered for use in implant materials due to the density of the material, which is about half of stainless steel and cobalt-chrome. The lower density results in a lighter material, a desirable attribute in a metal that is placed in bone and carried daily by the implant patients. The two major types of titanium are commercially pure titanium and titanium with 6% aluminum and 4% vanadium added (Ti-6Al-4V) [1.2]. As shown in Table 1.2, with commercially pure titanium, an increased presence in oxygen content from grade 1 to grade 4 increases the yield strength as it

increases the strength of the interstitial areas, or those areas between the "host atoms" [1.11]. The increased presence of oxygen also helps form a surface layer of TiO_2, helping resist corrosion of the metal [1.2]. The addition of aluminum and vanadium, to form Ti – 6Al – 4V, increases the yield and tensile strengths of the metal as aluminum helps stabilize the alpha phase while vanadium helps stabilize the beta phase [1.2].

No metal implant is without problems, as major technical drawbacks exist. To begin with, metal implants are usually smooth, with an un-reactive surface. The smooth surface is not osteoconductive, so it does not promote the growth of bone cells into the implant [1.12]. Without the growth of bone cells into the implant, the implant cannot be stabilized; eventually, the instability of the implant will lead to slipping of the implant within the bone surface [1.18]. A type of mechanical corrosion called fretting can then occur, eventually leading to biological corrosion and the necrosis of surrounding bone. As a result of biological corrosion, by-products are produced which are transported throughout the body; these by-products can then cause severe systemic reactions. Corrosion of the implant, both mechanically and biologically, along with the local and systemic problems created by the corrosion by-products, are the major issues surrounding metal implants.

Corrosion of biomedical implants has multiple different causes. A mechanical type of corrosion, called fretting, occurs when materials under a load experience either vibration or begin to slip [1.13]. A biological type of corrosion, called biocorrosion, or corrosion caused by a biological attack, begins with a uniform attack through the leaching of metal ions [1.14 – 1.16] and continues with pitting [1.14], or corrosion that occurs in

an extremely localized area resulting in holes in the metal [1.17]. Each type of corrosion can cause long-term negative effects to the patient.

The stress load of the impact caused by walking can lead to implant slippage and fretting corrosion. While one might not think that slipping occurs in the area surrounding the implant, very little slippage is required; as little as 10^{-8} cm is all that is necessary to produce damage due to fretting [1.13]. The surface of the metal begins to wear off in the form of oxide debris and fractures due to fatigue and pitting can then result [1.13]. Also, since the oxide debris formed is located between the bone and the implant, the oxide debris can rub against the bone cell membranes, causing the rupture and death of the cells. The death of the surrounding bone cells causes the loosening of the implant, which can create a need for the replacement of the implant [1.18]. Fretting also can destroy the passive oxide film, leading to another types of corrosion [1.18].

Fretting, or mechanical corrosion, can lead to biological corrosion and the formation of pits. However, biocorrosion does not need the assistance of fretting to begin. In the human body, when a foreign body is detected, macrophage cells are sent to the site of the foreign object [1.19]. These cells are designed to destroy the foreign body by releasing chemicals and then engulfing of the object, such as viruses or bacteria [1.19]. While all of the metals used in the most common implants exhibit passivity, or the loss of chemical reactivity [1.17], the macrophage cells begin releasing chemicals that attack the passive surface [1.19]. Eventually, the chemical attack can lead to the leaching of metal ions, as seen in stainless steel 316L [1.14]. It was demonstrated that certain chemicals, such as nickel, were removed from the surface of the metal, while other chemicals, such as chromium, were bonded to compounds which were not originally

present in large quantities, such as sulfur [1.14]. The implants also showed pitting [1.14], which is often difficult to detect, as the pits are small and usually covered by the corrosion by-products [1.17]. The failure that occurs is often very sudden and unexpected and can occur even though only a very small amount of implant weight has been lost [1.17]. Biocorrosion does not only affect stainless steel 316L, however. Cobalt-Chrome, or ASTM F75, has also been shown to corrode using a human cell culture model [1.15]. Even though pitting was not demonstrated over a nine day period, the osteoblasts that surrounded the implant metal did leach out varying amounts of both cobalt and chromium [1.15]. A similar *in vivo* study on Cobalt – Chrome showed that nickel and molybdenum were also leached [1.16].

The bone tissue that surrounds the implants is responsible for the leaching of chemicals from the surface of the implant. Some of these leached chemicals may be taken up by the surrounding bone cells for use in cellular processes [1.15]. Within the human body, there are several biological processes that need metals to perform their activities, such as hemoglobin utilizing iron to fix oxygen within the red blood cells [1.20]. Cobalt and chromium are considered essential metals, or those metals that are needed to perform physiological activities [1.21]. Following the leaching of the metal ions, the chemicals from the implant are then transported extracellularly throughout the body. However, an extended period of time is needed to accumulate the chemicals to values higher than background amounts. This accumulation, due to the leaching and transportation of implant chemicals, can be an indication that the implant is loosening, since the levels of metal within the body are typically higher for patients with loose implants [1.16]. A contributing factor to this loosening, however, is the necrosis, or

death, of the surrounding tissue. This is caused by the inability of the osteoblasts to proliferate [1.15]. With weight loss experienced by the implant due to the leaching of metal ions and the bone cells surrounding the implant dying, eventually too much space between the bone and the implant will exist. At this point, the implant has been loosened and will need to be surgically removed and replaced.

Loosening of the implant, through the leaching of chemicals and the necrosis of the surrounding bone cells, is not the only problem with corrosion, however. The chemicals are not just leached for use in physiological activities, though, but instead leached indiscriminately. All of the leached chemicals can be found throughout the human body, absorbed and stored by cells in different tissues, and/or eliminated as waste in the urine [1.16, 1.21]. For example, chromium is found in the blood stream in high amounts, but is rarely found in the urine, indicating that the red blood cells bind and store the chromium [1.16, 1.21]. The leaching of chemicals, however, is considered to be chronic, or persistent, and ongoing throughout the life of the implant [1.21]. The amount of metals leached yearly is considered very low, but these chemicals will accumulate in certain areas of the body, such as the lungs, liver, kidneys, and spleen [1.16, 1.21]. The long-term effects of the accumulation of these chemicals are just now being studied. Several of the elements used in the creation of the metal implants, including nickel, cobalt, and chromium, have previously been shown to be carcinogenic [1.21]. Ultimately, though, the chemical state of the element determines if the element is carcinogenic or not. Chromium, for example, is a necessary metal when it is in the Cr^{3+} state; however, when chromium is in the Cr^{6+} state, it is a known carcinogen [1.21]. With the transportation of the chemicals throughout the body, an implant patient may or may

not develop cancer that is related to the implant [1.14]. The transportation of chemicals throughout the body is not just an issue with cancer. Transportation of the chemicals throughout the body can lead to long-term sensitivity reactions, including, but not limited to, asthma and urticaria [1.21]. Corrosion by-products, while not causing an immune reaction on their own, often react with native proteins causing the formation of a foreign body and the activation of an immune response [1.22]. If this immune response occurs in the lungs, asthma can result. Urticaria, the formation of sensitive, itchy red round welts on the skin, can be a major consequence if the immune response occurs in near the skin [1.22, 1.23]. Short-term sensitivity reactions to metal can also arise [1.22, 1.23]. Hypersensitivity reactions can occur with any metal present in the body; however, the most common reactions occur with nickel, cobalt, and chromium, respectively [1.22]. While it usually takes several hours to several days for the hypersensitivity immune response, the resulting cascade of events will eventually cause severe tissue damage surrounding the implant [1.22]. These hypersensitivity reactions eventually lead to the removal and replacement of the implant [1.22]. In general, implants created from stainless steel or cobalt-chrome alloys have resulted in more hypersensitivity reactions, as compared with titanium and titanium alloys [1.22]. However, titanium and titanium alloys are not exempt from hypersensitivity reactions. All metals that are used in implants can result in hypersensitivity reactions and may be one reason that a metal implant fails [1.22]. When an implant was functioning poorly, 60% of the patient population studied had hypersensitivity reactions to the metal in their implant [1.22]. When an implant was functioning properly, only 25% of the patient population studied had hypersensitivity reactions to the metal in their implant [1.22]. While hypersensitivity

reactions may not be the only cause in failure of the implant, it is believed that metal sensitivity is a contributing factor to implant failure [1.22].

Even though the corrosion of several different types of implants has been investigated, titanium is not likely to corrode [1.1]. The major problem with titanium is the lack of osseointegration, or the incorporation of the implant into the surrounding bone [1.12]. Osseointegration is important, as this helps stabilize the implant [1.12]. Methods are currently being investigated to reduce or prevent the degradation of the implant and improve the growth of bone cells into the implant. One method to prevent corrosion, both biological and mechanical, and to improve osseointegration is to create a coating, which prevents the macrophage cells from reaching the implant surface while giving the bone cells a surface onto which they can attach and grow.

1.4 Implant Coatings

While the strength and durability of an implant are determined by the bulk properties of the material, the reaction of the host tissue is determined by the surface chemistry of the implant [1.2].

No matter which method is used to improve the tissue – implant interface, the created layer must be resistant to delamination, which is the separation of the film from the metal surface [1.2]. Many different methods to coat metals exist and include:

- Plasma-spraying
- Immersion coating
- Dip coating and sintering
- Hot isostatic pressing
- Sputtering
- Chemical reactions

Plasma-spraying occurs by injecting powder into a very high temperature plasma flame where it is heated to a molten material and then accelerated to a very high velocity [1.24]. The molten material hits the substrate and rapidly cools, bonding to the substrate and forming a coating [1.24]. Plasma-spraying is very costly and complex. Due to the high temperature, only compounds that can be melted without losing their bulk properties can be used, which virtually eliminates all polymers [1.24]. However plasma-spraying is used commonly with certain materials, such as ceramics, that can withstand the molten phase [1.25 – 1.28].

Immersion coating occurs when a sample is placed into a solution containing the desired coating material. In the literature, this usually means that the desired coating material has been melted [1.29]. Dip coating occurs when a sample is placed, or dipped, into a solution containing the desired coating material, removed, and allowed to dry [1.29]. The dipping process may be repeated multiple times [1.29]. Sintering occurs when a sample with the desired powder coating is heated to a high temperature. The coating will bond to itself and to the substrate without becoming a liquid [1.29 – 1.30]. The porosity of the powder is reduced as the atomic spacing decreases [1.30]. In hot isostatic pressing, heat and pressure are both applied while the powder is being sintered [1.29]. This produces a solid material with a much lower porosity than normal sintering produces [1.29 – 1.30].

Sputtering occurs when a beam is directed at a target containing the desired material [1.31]. Atoms are released as a result of the bombardment of the target by energetic ions [1.31]. Different methods for sputtering exist, with some using an ion beam [1.29] and others using radio-frequency [1.32]. Sputtering is commonly used on targets made of metals, oxides, fluorides, and other chemical compounds [1.88]. The targets are created by melting the materials or hot-pressing powders [1.32]. Both of the methods to create the sputtering targets could not be used for polymers, as the heat would destroy the polymer chains [1.88].

Finally, chemical reactions occur when the surface of the implant metal is treated with a chemical that will bind to the metal surface [1.33 – 1.35]. Silanes can be used to covalently bond with a metal surface and produce a desirable reactive surface group, such as an amine (NH_3) or an aldehyde (HC=O) [1.1, 1.33 – 1.35].

All of the various surface treatments described above have a single goal – to improve the bonding of a coating to metal. The most desirable coatings for biomedical implants are those which are considered bioactive. These bioactive materials develop "an adherent interface with tissues that resist substantial mechanical forces" [1.2]. The adhesion between tissue and implant coating is highly desirable, since it can stabilize the implant. Without adhesion between tissue and coating, a fibrous tissue of variable thickness forms; this fibrous tissue cannot stabilize or support the implant [1.2].

Compounds and chemicals that are considered bioactive are present in nature, both inside and outside of the human body. Examples that have been examined in the literature include physiological fluids, such as synovial fluid surrounding human joints, hydroxyapatite, ($Ca_{10}(PO_4)_6(OH)_2$) which is usually bioactive and resorbable [1.1, 1.25 –

1.27, 1.29], calcium phosphate, (CaP) [1.32, 1.36], bioactive glass [1.28], and biologically functional materials, such as enzymes and proteins [1.33 – 1.35].

Several problems exist with the current coatings that are based on the properties from the bulk material. Every material, from ceramics to metals to polymers, can be compared based on the moduli of elasticity, tensile strength, and yield strength. The modulus of elasticity relates to the stiffness of the material [1.37]. Ceramics typically have a modulus of elasticity higher than that of metals, while the modulus of elasticity of polymers are usually much lower than that of metals [1.10, 1.37]. However, to think of the modulus of elasticity as proving how elastic a material is would be deceiving. The modulus of elasticity measures a material's resistance to elastic deformation: the higher the modulus of elasticity, the stiffer the material [1.37]. Modulus of elasticity is not the only measure to determine a material's resistance to change and should not be the only value examined when determining which material to use. The elongation of a material is a sign of the ductility of the material, or its ability to deform plastically before fracture [1.37]. While metals and ceramics exhibit much higher moduli of elasticity, an indication of stiffness, polymers exhibit much higher percentages of elongation, an indication of ductility [1.10, 1.37]. Metals can typically elongate no more than between 15% and 60%, depending upon the metal being examined [1.10], while ceramics possess ductilities of less 5%, which is defined as possessing no elongation ability. Polymers, on the other hand, typically can elongate from between 400% and 1200% [1.10], indicating an ability to give to stresses from scratching, a type of plastic deformation.

The largest problem with coatings is based on the type of material used. Hydroxyapatite and calcium phosphate are both ceramics, while bioactive glass is

classified as a glass – ceramic [1.2]. These three materials possess typical ceramic and glass bulk properties; they are extremely hard, but very brittle with fracturing occurring before any type of plastic deformation can occur [1.38]. This brittle behavior can lead to flaking, cracking, and scratching of the coating during implantation [1.26, 1.39]. The destruction of the coating can lead to pitting and crevice corrosion since the macrophage cells can get to the implant surface, defeating the purpose of the coating [1.26]. One method of improving hydroxyapatite is to incorporate it into a polymer, such as polylactic acid [1.40 – 1.41], collagen [1.42], chitosan [1.39, 1.43], or polyethylene [1.44 – 1.45]. The addition of hydroxyapatite to the polymers showed an increase in the modulus of elasticity of the polymer; however, a point was reached when so much hydroxyapatite was present that a brittle fracture occurred [1.41, 1.44]. Even with the addition of a polymer to hydroxyapatite, the ability of the coating to survive a scratch should always be questioned.

Another method of increasing the bioactivity of the coating is to include compounds within the coating materials that will encourage and support the growth of the bone tissue. Examples of these materials include enzymes and proteins that the host tissue will recognize and to which they will favorably respond. Model enzymes and proteins have also been studied to ensure that bonding via silanation will not cause inactivation of the enzyme [1.34 – 1.35]. The use of silanes or plasma deposition has not reduced the enzymatic activity of alkaline phosphatase [1.33], trypsin [1.34 – 1.35], or lysosyme [1.46]. Some proteins previously bound to the surface of metal implants include a model protein, albumen [1.33], and a protein that can encourage bone cell differentiation and growth called bone morphogenetic protein [1.46]. These proteins

were also not affected by silanation [1.33] or using plasma deposition and a linker molecule to bind the protein [1.46].

Enzymes and proteins are not the only biologically produced materials. Polymers can also be biologically produced. As previously stated, with a low modulus of elasticity and high percents of elongation, polymers should be able to withstand the stresses of implantation without flaking or cracking. There are several different types of polymers, with different functions, that are produced biologically [1.2]. Collagen and glycosaminoglycans are two types of polymers that are produced by the human body, reside in the connective tissues, and are used for mechanical support and movement [1.2]. Other biologically produced polymers include silk, chitin, deoxyribonucleic acid (DNA), and ribonucleic acid (RNA) [1.2]. Each of the polymers have specialized functions, such as protection, shape, and protein synthesis [1.2]. The biologically produced polymer, chitin, is considered bioactive [1.47] and is of special interest in this research.

1.5 Chitosan - Properties and Uses

Chitin is the second most abundant form of polymerized carbon in the world, only behind cellulose [1.48]. It is present in the exoskeletons of most crustaceans, such as shrimp, crabs, and lobster [1.47], along with insects, some fungi, and micro-organisms [1.47 – 1.48]. Chitin is a straight polymer composed of N-acetyl glucosamine [1.48]. Treatment of chitin with concentrated bases, such as sodium hydroxide, results in the deacetylation of the polymer and the creation of chitosan [1.47 – 1.48]. Chitosan is a co-polymer composed of glucosamine and N-acetyl glucosamine [1.48]. The polymer is called chitin when the degree of deacetylation (DDA) is below 50% and chitosan when

the degree of deacetylation is 50% or above [1.49]. Of the two polymers, chitosan is more often investigated for use both inside and outside of the body [1.49]. Chitosan is used because it is soluble in dilute organic acids, allowing the hydroxyl and amine groups to be utilized in chemical reactions [1.48 – 1.49]. Upon dissolution, the amine group in chitosan becomes protonated, resulting in a positively charged polysaccharide that can attract and promote cell adhesion [1.50]. Figure 1.1 shows the chemical structure of chitin as compared to chitosan. Chitosan contains a decreased concentration of acetamide groups, but an increased concentration of amine groups. These amine groups will allow bonding to the terminal groups of the silane molecules selected in this research.

Besides the positively charged amine group, chitosan exhibits many properties, both physiochemical and biological, which are useful for a wide range of applications. Chitosan was originally examined for use in water treatment [1.47, 1.51]. The use of this polymer for water treatment emerged due to its physiochemical property of chelating metal ions [1.47] or coagulating proteins, dyes, and amino acids [1.47]. Chitosan is also used in agriculture, as a fertilizer [1.47], seed coating [1.47, 1.52 – 1.53], or leaf coating [1.47]; it is employed because of biodegradability and fungistatic activity [1.47, 1.52 – 1.53]. The biomedical community, however, has done the most research with respect to chitosan. The investigation into chitosan exists because it possesses many desirable biological properties.

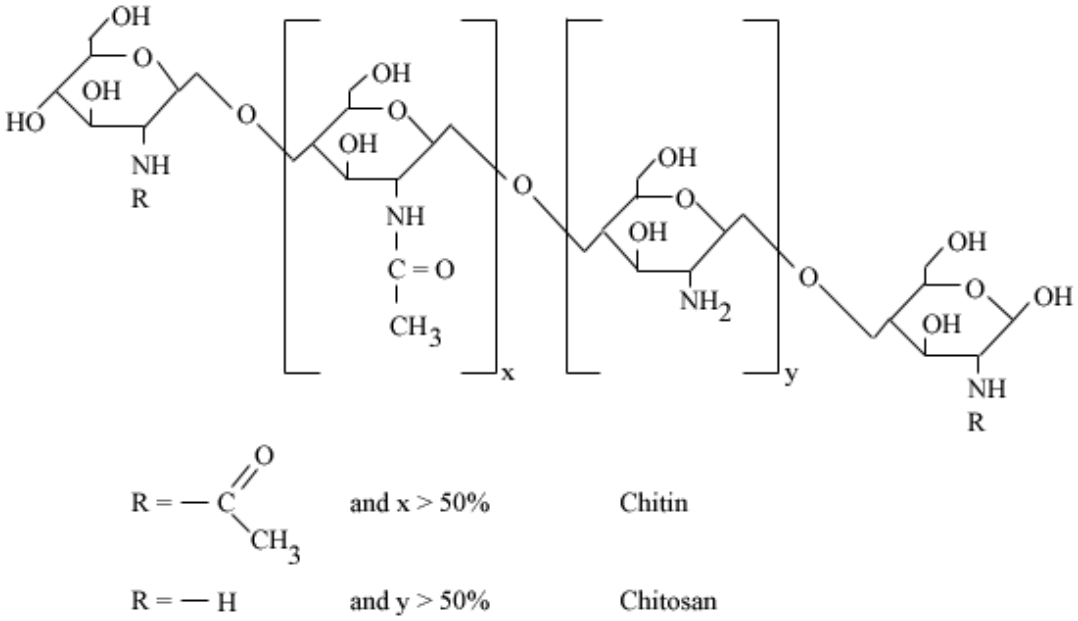

Figure 1.1. Schematic representation of chitin and chitosan [1.49].

To begin with, chitosan is non-toxic, with an LD50 of greater than 16 g/kg [1.48]. In addition to being a fungistatic polymer, chitosan is also bacteriostatic [1.53 – 1.54]. Chitosan, in amounts as low as 0.1%, stopped the growth and reproduction of *Staphylococcus epidermis*. In amounts as low as 1%, the polymer was able to stop the growth of *Staphylococcus aureus* and *Pseudomonas aeruginosa* [1.47]. These three bacteria are commonly found on the human skin and create problems for healing if the bacteria get into a wound [1.47]. Chitosan is not just bacteriostatic, but is also bactericidal against a large range of bacteria [1.54]. It is particularly useful against the yeast family *Candida* and gram-positive bacteria [1.54], while *S. aureus* and *S. epidermis* were completely killed by 8 mg of chitosan per mL of water. *P. aeruginosa*, while inhibited in the presence of chitosan, was never completed killed nor completely inhibited by the polymer [1.54].

Chitosan is considered a biocompatible polymer [1.50, 1.55 – 1.57], but also demonstrates bioactive behavior [1.50, 1.55 – 1.62]. The polymer is considered biocompatible since only a mild tissue reaction occurs after the material is placed into the host tissue [1.55 – 1.56]. The polymer is considered bioactive because it promotes the adhesion of cells [1.1, 1.47]. The cationic nature of chitosan promotes cell adhesion, differentiation, and growth of bone cells [1.57, 1.59 – 1.61]. Chitosan provides the cells a location to attach to the polymer, through the positively charged amine group [1.60]. When chitosan is present, the osteoprogenitor cells, those that produce bone cells, are almost doubled in number compared to locations without chitosan [1.59 – 1.60]. With the presence of the osteoprogenitor cells, chitosan then stimulates their differentiation, into the formation of bone cells [1.59]. Although the quantity of bone that was produced

by the osteoblasts was doubled [1.60], the most important effect was the organization of the bone tissue. The controls consistently had fibroblast type cells, while the chitosan was fibroblast free [1.60]. As compared to the controls, which were "spindle-shaped" or the shape of a fibroblast, the bone cells that were present on the chitosan surfaces maintained the "plump, spherical to polygonal form" [1.61]. This retention in shape is very important, as cell morphology changes, the cell functions also change [1.61]. The cells present on the chitosan surfaces continued to maintain their shape and cell-specific functions [1.61]. The lack of fibroblasts is very important, since this promotes proper healing, and the formation of bone tissue [1.60]. The ability of chitosan to prevent the attachment of fibroblast cells helped prevent the formation of fibroplasias and promoted the formation of organized tissue [1.60]. The prevention of scar tissue can also be attributed to chitosan, which helps enhance the production of hyaluronic acid, a material present in the extracellular matrix of connective tissue [1.59]. However, hyaluronic acid is not the only material present in the extracellular matrix surrounding connective tissues. Chitosan, as a foreign body, helps activate macrophages, which produce different types of growth factors [1.19]; these growth factors then promote and regulate the production of the extracellular matrix [1.62]. The production of the growth factors then promotes the growth of cells surrounding the macrophages, which helps promote the differentiation and growth of bone cells [1.19].

Chitosan is also considered biodegradable; the byproducts produced by the degradation of chitosan are part of normal metabolism, which include CO_2, glucosamines, and saccarides [1.50, 1.57]. While chitosan can be degraded, specifically by lysozyme [1.63 – 1.65], this polymer is usually only lightly degraded [1.50]. In fact,

as the degree of deacetylation increases the amount of degradation of chitosan decreases [1.50, 1.56 – 1.57]. With an increasing degree of deacetylation, the amount of cellular attachment increases [1.56 – 1.57]. This is mainly caused by the increased presence of the positively charged amine group attracting the negatively charged cells [1.56 – 1.57]. The decreased degradation is explained by the close packing of chitosan molecules [1.50]; without the presence of the acetamide group, the biopolymer chain can align more closely with other chains [1.50] and crystallinity can increase [1.50, 1.66]. The increase in crystallinity and the decrease in distance between the chains prevent enzymes, such as lysozyme, from degrading the chitosan [1.50].

Due to chitosan's biocompatibility, bioactivity, and biodegradability, other properties have also been investigated. Chitosan is also is haemostatic [1.48, 1.67], it possesses the ability to stop bleeding, which is particularly useful when applying wound dressings or artificial skin [1.47]. With the presence of the hydroxyl and amine groups, chitosan is also easy to modify chemically [1.48], allowing the researcher the ability to sulfate the chitosan, thereby producing chitosan that possesses an ability to prevent coagulation [1.47]. The ability to produce an anti-coagulating material is necessary when one is designing artificial blood vessels or dialysis machines [1.47].

While chitosan has many wonderful properties, both physiochemical and biological, there is one major disadvantage associated with chitosan. Any item used in medicine must be sterilized and chitosan has demonstrated a change in several properties following sterilization [1.50, 1.68, 1.72]. The most commonly used methods of sterilization include autoclaving, gamma irradiation, and ethylene oxide treatment

[1.68, 1.72]. Following sterilization, the film thickness, tensile strength, contact angle, and hemolysis, or the ability to rupture red blood cells, were measured and compared to pre – sterilization values. Autoclaving caused an increase in the thickness of the film, which was attributed to an increase in moisture deposited by the sterilization method [1.68, 1.72]. Gamma irradiation and ethylene oxide did not affect the thickness [1.68, 1.72]. The tensile strength of the film was markedly decreased, with the largest decrease created by the ethylene oxide and the smallest decrease caused by autoclaving [1.68, 1.72]. The films sterilized in the autoclave retained 96 – 97% of the tensile strength, while those sterilized in ethylene oxide retained only 80% of the tensile strength [1.68]. The decrease in tensile strength was caused by chain scissons, crosslinking, and hydrolysis of the chain by water molecules [1.68 – 1.70]. Using contact angle measurements, all of the films showed an increase in hydrophobicity following every method of sterilization [1.68]; however, the films did show a significant decrease when measuring hemolysis [1.68]. Autoclaving does appear to be the optimum method of sterilization, since no effects on biological performances *in vivo* were seen [1.71].

Chitosan is currently being examined for several uses within the biomedical community. Originally, chitosan was used for wound dressing [1.49] and bone filler, such as in the holes produced by wisdom teeth extraction [1.59, 1.77 – 1.79]. Very little testing has been done on the ability to bind chitosan to a substrate. In fact, most of the tests performed on chitosan have been on films formed in plastic or glass dishes, without consideration of surface bonding [1.72 – 1.74]. Tests have also been performed on chitosan containing other components, such as hydroxyapatite [1.39, 1.43], carbon nanotubes [1.75], clay nanocomposites [1.76], and bone morphogenetic protein [1.80].

Of those research efforts that involved coating a substrate with chitosan, several different techniques have been used. The simplest method involves evaporation, which does not use a chemical reaction to form the chitosan film, but instead allows the film to form as the water evaporates, creating interlinked chains [1.80]. Another method that does not use a chemical reaction is electrochemical deposition, which combines chitosan and hydroxyapatite to form a composite material [1.81 – 1.82]. In electrochemical deposition, a current is run through a cathode, the metal substrate, which attracts positive charges present in other molecules, such as the amine group in chitosan [1.17]. Chemical reactions have also been utilized and documented in the literature. One technique utilizes a self-assembly method by reacting polycations and polyanions [1.83 – 1.84]. In this technique, the substrate is dipped into polyethyleneimine followed by sodium hyaluronate and chitosan, respectively [1.83], or the substrate is dipped into polyethyleneimine followed by dipping into gelatin and chitosan, respectively [1.84]. This procedure was repeated until the desired thickness was obtained [1.83 – 1.84]. A more complex chemical reaction was also investigated. Hydroxyapatite or bioactive glass was placed onto Ti – 6Al – 4V through plasma deposition [1.85]. The chitosan was then reacted with the plasma deposited material and allowed to dry [1.85]. While plasma deposition is useful, it is very costly and complex [1.24]. Another chemical method was investigated which does not require the specialized equipment or personnel of plasma deposition. Silanation, which does not use any heat or specialized equipment, is a chemical reaction in which a silane is used to bond to hydroxyl groups present on the substrate [1.50, 1.86]. Based on the terminal group present, a linker molecule may be needed [1.50, 1.86]. Following the silanation and linker molecule reactions, chitosan is

reacted with the surface and allowed to evaporate to produce a film [1.50, 1.86]. While the literature reveals multiple different methods to bond chitosan to metal substrates, only one article discusses the adhesion of these techniques. Using a silanation reaction of isocyanatopropyltriethoxysilane in an ethanol/water mixture, an increase in the adhesion of the chitosan film using the evaporation method was seen, from 0.5 MPa to 1.6 MPa [1.50].

This research is focused on improving the attachment quality of films on commercially pure titanium grade 4. Commercially pure titanium grade 4 was chosen for two reasons. First, titanium is a very commonly used metal for implants due to its density and strength. Secondly, as shown in Table 1, there are very few elements present in this material besides titanium and oxygen. The reactions that occur on the surface of the metal will be with the titanium and not with other elements, which allows the researcher to fully determine the model reaction. The film being investigated in this research is chitosan, again chosen for two different reasons. The first reason is that chitosan, as previously detailed, demonstrates many desirable properties, including non-toxicity, biocompatibility, and biodegradability. The second reason for the use of chitosan is the ready availability of the material; it is a by-product of the seafood industry, which makes up a large portion of the state of Mississippi's economy. Finally, chemical reactions using silanes will be used to bond chitosan to the titanium metal coupons. Silane reactions were chosen for this research because of the ease of use; since no specialized equipment is needed, the cost is reduced as compared to many of the other deposition methods previously outlined.

1.6 Research Objectives

Currently, advancements are being made to improve the implant – tissue interface in order to minimize tissue necrosis, implant corrosion, and sensitivity reactions. These efforts are aimed primarily at preventing the tissue from contacting the implant surface through the creation of attached films. The films being examined usually incorporate bioactive materials, including ceramics, polymers, and biofunctional molecules. The osteoconduction properties of these materials have been well studied and manipulated. However, while research has been done to improve the film – tissue interface, there has been very little attention given to improve the film – substrate interface, or to understand the effects that different treatments have upon this interface. Presently, the reactions that occur at the surface to bind bioactive materials and the effects of these reactions on bond strength and film quality are not well understood.

The primary objective of this research is to improve the adhesion of chitosan films to commercially pure titanium grade 4. This objective will be accomplished by:

1. The chemical analysis of a published silane reaction.
2. The chemical analysis of four treatment combinations utilizing two metal treatments and two silane reactions.
3. The mechanical analysis of the films produced from the four treatment combinations.

The completion of these sub-objectives will develop insight into the chemical and mechanical bonding mechanisms of silane treated titanium which will aid in improving the strength of the film – substrate interface, thereby facilitating the development of high quality implant coatings able to withstand the stresses associated with implantation.

CHAPTER II

MATERIALS AND METHODS

2.1 Introduction

This research, broadly defined as the development of biologically compatible coatings on implant quality titanium, was performed using two different metal treatments, three different reaction series, and multiple experimental characterization methods. The metal treatments consist of a standard, commonly used method and a highly reactive method, with both treatments designed to form different types of oxide layers on the surface. The three different reaction series use different starting compounds and may or may not have a linker molecule. The only common material used for the two different metal treatments and the three different reaction series is the ending film created from chitosan. The results of these metal treatments and reaction series were examined using numerous experimental methods to determine the film quality, roughness, hardness, and elastic modulus, along with the polymer's reaction to stress. The experimental methods used were X-Ray Photoelectron Spectroscopy (XPS) for chemical analysis, Scanning Electron Microscopy (SEM) and Atomic Force Microscopy (AFM) for surface features and roughness determination, nano-indentation, scratch testing, and bulk adhesion for mechanical properties, and contact angle measurements for wettability properties.

2.2 Materials

Table 2.1 lists all of the chemicals used in this research, along with the manufacturer and location. The deionized water was obtained from a NANOpure diamond deionized water maker (Barnstead, Boston, MA) and utilized a D3750 hollow fiber filter with a maximum operating pressure of 50 psi and a 0.2 μm pore size rating.

Table 2.1. Chemicals and materials used in the creation of chitosan films.

Chemical	**Purity**	**Manufacturer**	**Location**
Glacial Acetic Acid	99.7+%, ACS	Alfa Aesar	Ward Hill, MA
Acetone	≥99.5%, ACS Reagent	Sigma Aldrich	St. Louis, MO
Instant Gel Adhesive	Prism 454, LT 45404	Loctite	Rocky Hill, CT
Aluminum Oxide Sandpaper	Grits of 600, 800, 1200	Norton	Worcester, MA
3-Aminopropyltriethoxysilane	98%	Alfa Aesar	Ward Hill, MA
Chitosan	87.4% DDA	Dr. Bumgardner	Memphis, TN
Commercially Pure Titanium, Grade 4	---	Titanium Industries, Inc.	Jacksonville, FL
Deionized Water	---	---	---
Ethanol, 200 proof	≥99.5%, ACS Reagent	Sigma Aldrich	St. Louis, MO
Gluteraldehyde	25% Aqueous Solution	Alfa Aesar	Ward Hill, MA
Hydrogen Peroxide	35% Aqueous Solution	Alfa Aesar	Ward Hill, MA
3-Isocyanatopropyltriethoxysilane	95%	Alfa Aesar	Ward Hill, MA
Isopropyl Alcohol	ACS Reagent	Acros Chemical	Morris Plains, NJ
Nitric Acid	ACS Reagent	Acros Chemical	Morris Plains, NJ
Sodium Hydroxide	1.0N in Water	Sigma Aldrich	St. Louis, MO
Sulfuric Acid	95-98%, ACS Reagent	Alfa Aesar	Ward Hill, MA
Toluene	99% min, Semiconductor Grade	Alfa Aesar	Ward Hill, MA
Triethoxsilylbutyraldehyde	90%	Gelest	Morrisville, PA
Ultra Pure Water	HPLC Grade	Alfa Aesar	Ward Hill, MA

2.3 Reaction Methods

The metal coupons used in this research were first cut from a bar and polished. A metal treatment was then applied to the polished coupons before being used in one of three silane reaction series. The metal treatments and chemical reactions are given in detail below.

2.3.1 Metal Preparation

The commercially pure titanium grade 4 was originally purchased as a 3 inch x 5 inch x ¼ inch bar. The bar was cut into approximately 1 inch x 1 inch x ¼ inch pieces using a Makita Cut-Off Saw (Makita, La Mirada, CA) with a carbide blade and without a water bath by BK Edwards Fabrication. These coupons were then sanded to a 1200 grit finish in a series of steps. An electric belt sander (BR300, Type 1, Black and Decker, Towson, MD), with a belt grit of 120, a belt width of 3" x 18", and a speed of 656 feet per minute, was used to smooth out the roughest areas of the metal pieces. A 320 grit sandpaper was then placed on a compressed air, dual action sander (Nikota, Whittier, CA) to remove the scratches made from the previous grit and to continue the smoothing process. Following the 320 grit sandpaper, the samples were sanded by hand for the remainder of the polishing. The first step to sanding by hand involved 600 grit, which was used to remove the scratches left from the 320 grit and to continue smoothing the metal surface. The metal was sanded in one direction and then rotated 90^{o} and sanded in one direction again. The coupons were continually sanded and rotated until the scratches left from the previous grit were removed as determined by visual inspection. The coupon was then sanded using 800 grit in the same method- one direction, then rotation of 90^{o}-

until all of the scratches from the 600 grit were removed as determined by visual inspection. Sandpaper of 1200 grit then followed the 800 grit in the same method- one direction, then rotation of 90°- until all of the scratches from the 800 grit were removed as determined by visual inspection.

2.3.2 Chemical Cleaning

One of the following two methods of chemical cleaning was performed on the polished metal coupons. The metal coupons were either treated using the passivation method or the piranha method, but never both on the same sample before a reaction series.

2.3.2.1 Passivation

Passivation was performed following ASTM F86, as shown in Figure 2.1. The coupons were sonicated for ten minutes in each of the following chemicals: acetone, 70% ethanol, and deionized water, respectively. The sonication is designed to remove particulates from the surface of the metal. Following sonication in deionized water, the coupons were placed in 30 vol. % nitric acid – 70 vol. % deionized water for 30 minutes at room temperature. The nitric acid is used to form a passive oxide layer on the surface of the titanium. Following the nitric acid treatment, the samples were rinsed with deionized water and placed in an ultra pure water bath with a lid for 24 hours. Figure 2.1a shows the steps involved in passivation of the metal coupons.

2.3.2.2 Piranha Treatment

The second metal treatment, or piranha treatment, can be extremely dangerous. **Care must be taken, as this reaction is highly exothermic and reacts strongly with carboneous materials. It can burn the skin from both the heat produced and the reaction of the chemicals with the skin.** The coupons are first sonicated for 30 minutes in 70 vol. % isopropyl alcohol and 30 vol. % deionized water, which is designed to remove particulates from the surface. Following sonication, sulfuric acid is poured into a beaker, with hydrogen peroxide slowly poured into the sulfuric acid at a ratio of 70 vol. % sulfuric acid to 30 vol. % hydrogen peroxide. The resulting mixture is then swirled gently to ensure mixing before being poured over the metal coupons. The coupons are left for ten minutes before being removed and placed in a second piranha mixture for five minutes. Care should be taken that only a few samples at a time are placed in the piranha solution, as a runaway reaction will occur with several samples. Also, care should be taken to remove the samples after ten minutes and after five minutes. Piranha does react with the exposed titanium and will etch the surface, if the samples are left too long in the solution [2.1]. After the second piranha treatment, the metal coupons were rinsed twice in ultra pure water before being placed in an ultra pure water bath for 24 hours. The ultra pure water bath is designed to allow the formation of Ti – OH groups. To prevent contamination, a container with a lid should be used to hold the ultra pure water and the titanium samples. Figure 2.1b shows the steps involved in the piranha treatment of the metal coupons.

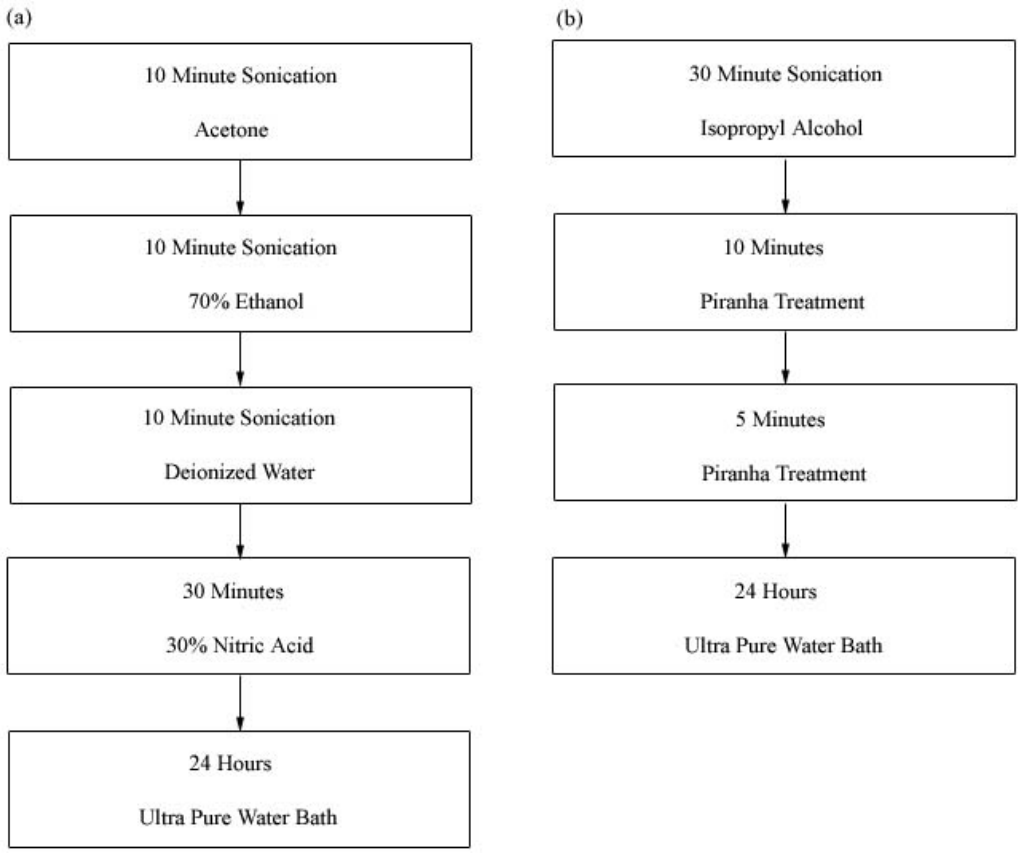

Figure 2.1. The necessary steps for metal treatments.

(a) Passivation and (b) Piranha treatment of the metal coupons.

2.3.3 Silane Reactions

For each sample, one of three different silane compounds was used. Following one of the metal treatments, the coupons were placed in one of the three following silane solutions. These silane reactions were designed to create a reactive terminal group to which a different compound could bind.

2.3.3.1 Isocyanatopropyltriethoxysilane Reaction Series

This reaction involves placing the passivated coupons into a solution containing 3-isocyanatopropyltriethoxysilane. This method has been described elsewhere [2.2], but is also given below. Three different reaction steps are used for this series.

The first reaction step involves the silane reaction. A mixture of 95 vol. % ethanol and 5 vol. % deionized water is created, to which 2 vol. % of 3-isocyanatopropyltriethoxysilane is added. The resulting solution is then stirred before the addition of the metal coupons. The metal coupons are then added to the stirring solution and left for ten minutes after which the coupons are removed and rinsed with ethanol followed by deionized water.

The second step in the reaction series involves the linker molecule, gluteraldehyde. A mixture of 98% deionized water and 2% by volume gluteraldehyde is stirred before the addition of the metal coupons. The metal coupons are then added to the stirred solution and left for 24 hours, during which time the solution is continually stirred. The pH is maintained at 4.5 using either 1N sodium hydroxide or 10M acetic acid to adjust the pH. Following the 24 hour time period, the metal coupons are removed and rinsed with deionized water.

The third step of the reaction involves the creation of the chitosan film. A solution of 2% by weight chitosan is combined with 2% by weight acetic acid and 96% by weight deionized water. The solution is stirred until the chitosan is fully dissolved and is then filtered through several layers of cheesecloth to remove any undissolved particulates. The metal coupons are then placed in a petri dish and the chitosan solution is poured over the coupons. The chitosan solution is then allowed to evaporate for 7-10 days; after which time, a yellowish film can be seen on the surface of the metal coupons. Figure 2.2 shows the anticipated reaction steps, with the reaction that should occur between the metal and 3-isocyanatopropyltriethoxysilane labeled as reaction step 1, the reaction between the terminal group of the silane and the gluteraldehyde molecule labeled as reaction step 2, and the reaction between the silane-gluteraldehyde complex and chitosan labeled as reaction step 3.

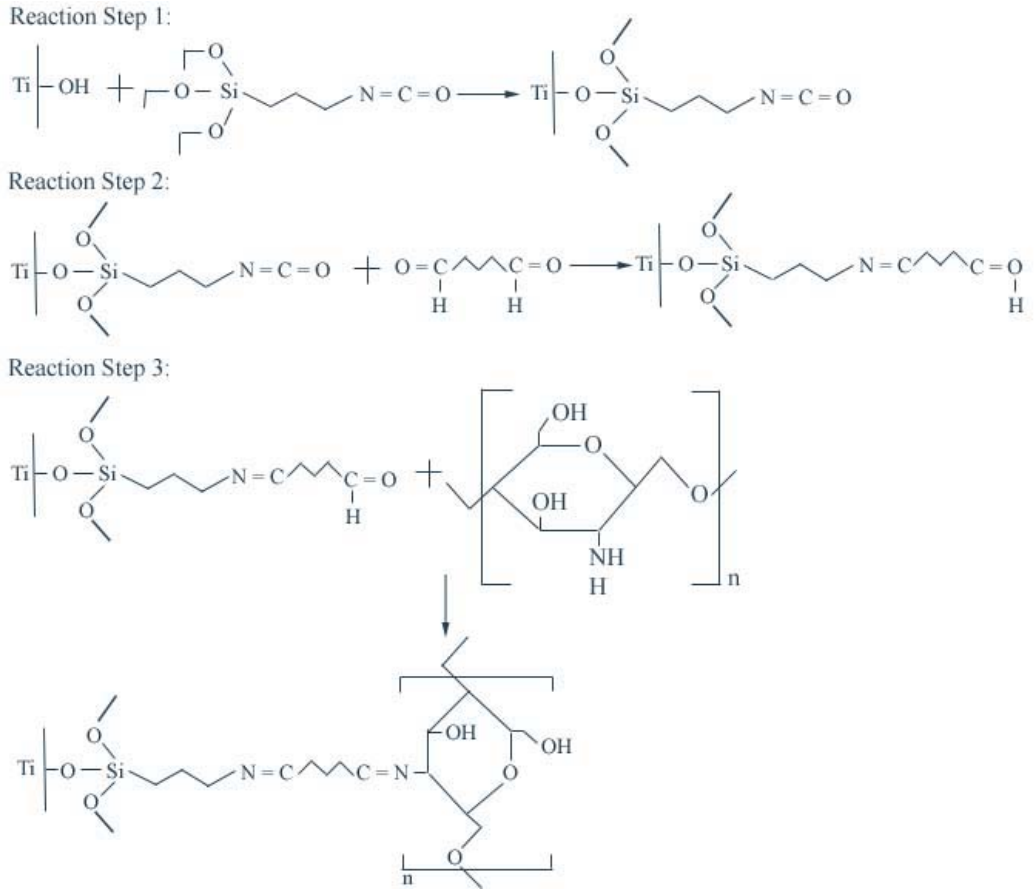

Figure 2.2. Isocyanatopropyltriethoxysilane anticipated reaction series.

Reaction step 1 shows isocyanatopropyltriethoxysilane bonding to the passivated metal surface. Reaction step 2 shows gluteraldehyde bonding to the isocyanatopropyltriethoxysilane-titanium complex. Reaction step 3 shows chitosan bonding to the gluteraldehyde-isocyanatopropyltriethoxysilane-titanium complex.

2.3.3.2 Aminopropyltriethoxysilane Reaction Series

The aminopropyltriethoxysilane reaction series involved placing either the passivated coupons or the piranha treated coupons into a solution containing 3-aminopropyltriethoxysilane. Three different reaction steps are used for this series.

The first reaction step involves the silane reaction. A mixture of 98% by volume toluene and 2% by volume aminopropyltriethoxysilane is created. The solution is stirred for 1 hour, with care given to ensure that a vortex did not form. The metal coupons were dried and placed in individual containers; the toluene – silane solution was poured over the samples, using 25 mL per container to ensure full coverage of the metal coupon. The containers were then sealed, covered with parafilm, and left for 24 hours. Following the 24 hours, the metal coupons were placed in pure toluene and sonicated for 30 minutes. The procedure of using fresh toluene and 30 minute sonications was repeated twice more, for a total sonication time of 90 minutes. The metal coupons were then rinsed with ethanol followed by deionized water before being dried to remove any toluene residue. Following the rinsing and drying process, the coupons were placed in individual containers.

The second step in the reaction series involves the linker molecule, gluteraldehyde. A mixture of 98% deionized water and 2% by volume gluteraldehyde is created and stirred for 1 hour, with care given to ensure a vortex did not form. The water – gluteraldehyde solution was poured over the samples, using 25 mL per container to ensure full coverage of the metal coupon. The containers were then sealed and left for 24 hours. Following the 24 hours, the samples were rinsed with deionized water and placed in a petri dish.

The third step in the reaction series involves the creation of the chitosan film. A solution of 1% by weight chitosan was combined with 2% by weight acetic acid and 97% by weight deionized water. The solution was stirred for 1 hour to ensure that the chitosan had dissolved and was then filtered through several layers of cheesecloth to remove any undissolved particulate. The chitosan solution was poured over the metal coupons placed in the petri dish. The solution was then allowed to evaporate for 7-10 days; after which time, a clear film can be seen on the surface of the metal coupons, as the reflection of light is different than on an untreated metal coupon. Figure 2.3 shows the anticipated reaction steps, with the reaction between the metal and the 3-aminopropyltriethoxysilane labeled as reaction step 1a, the reaction between the terminal group of the silane and the gluteraldehyde molecule labeled as reaction step 2a, and the reaction between the silane – gluteraldehyde complex and chitosan labeled as reaction step 3a.

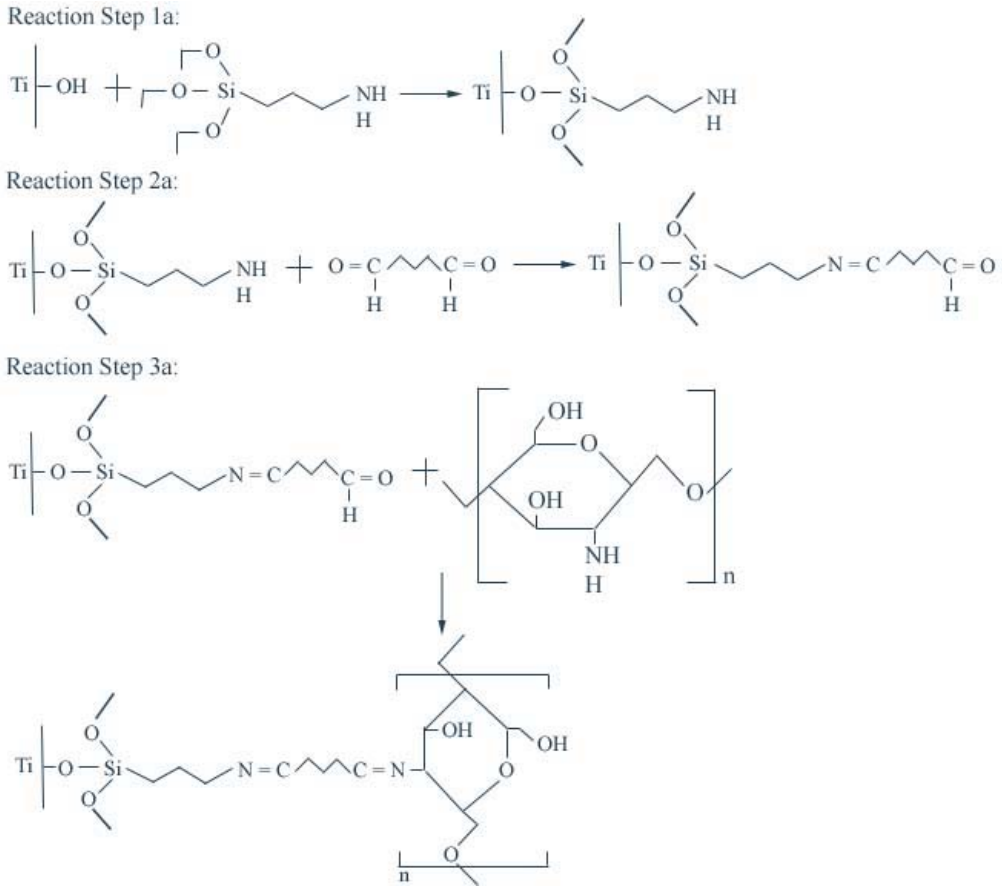

Figure 2.3. Aminopropyltriethoxysilane anticipated reaction series.

Reaction step 1a shows aminopropyltriethoxysilane bonding to the metal surface. Reaction step 2a shows gluteraldehyde bonding to the aminopropyltriethoxysilane-titanium complex. Reaction step 3a shows chitosan bonding to the gluteraldehyde-aminopropyltriethoxysilane-titanium complex.

2.3.3.3 Triethoxsilylbutyraldehyde Reaction Series

The triethoxsilylbutyraldehyde reaction series involved placing either the passivated coupons or the piranha treated coupons into a solution containing triethoxsilylbutyraldehyde. Two reaction steps are used for this series, as the triethoxsilylbutyraldehyde does not require a linker molecule.

The first reaction step involves the silane reaction. A mixture of 98% by volume toluene and 2% by volume triethoxsilylbutyraldehyde is created. The solution is stirred for 1 hour, with care given to ensure that a vortex did not form. The metal coupons were dried and placed in individual containers. The toluene – silane solution was then poured over the samples, using 25 mL per container to ensure full coverage of the metal coupon. The containers were sealed, covered with parafilm, and left for 24 hours. Following the 24 hours, the metal coupons were placed in pure toluene and sonicated for 30 minutes. The procedure of using fresh toluene and 30 minute sonications was repeated twice more, for a total sonication time of 90 minutes. The metal coupons were then rinsed with ethanol followed by deionized water before being dried to remove any toluene residue. Following the rinsing and drying process, the coupons were placed in a petri dish.

The second step in the reaction series involves the creation of the chitosan film. A solution of 1% by weight chitosan was combined with 2% by weight acetic acid and 97% by weight deionized water. The solution was stirred for 1 hour to ensure that the chitosan had dissolved and was then filtered through several layers of cheesecloth to remove any undissolved particulate. The chitosan solution was poured over the metal coupons located in the petri dish. The solution was then allowed to evaporate for 7-10 days; after which time, a clear film can be seen on the surface of the metal coupons, as

the reflection of light is different than on an untreated metal coupon. Figure 2.4 shows the anticipated reaction steps, with the reaction between the metal and the triethoxsilylbutyraldehyde labeled as reaction step 1b and the reaction between the terminal group and chitosan labeled as reaction step 2b.

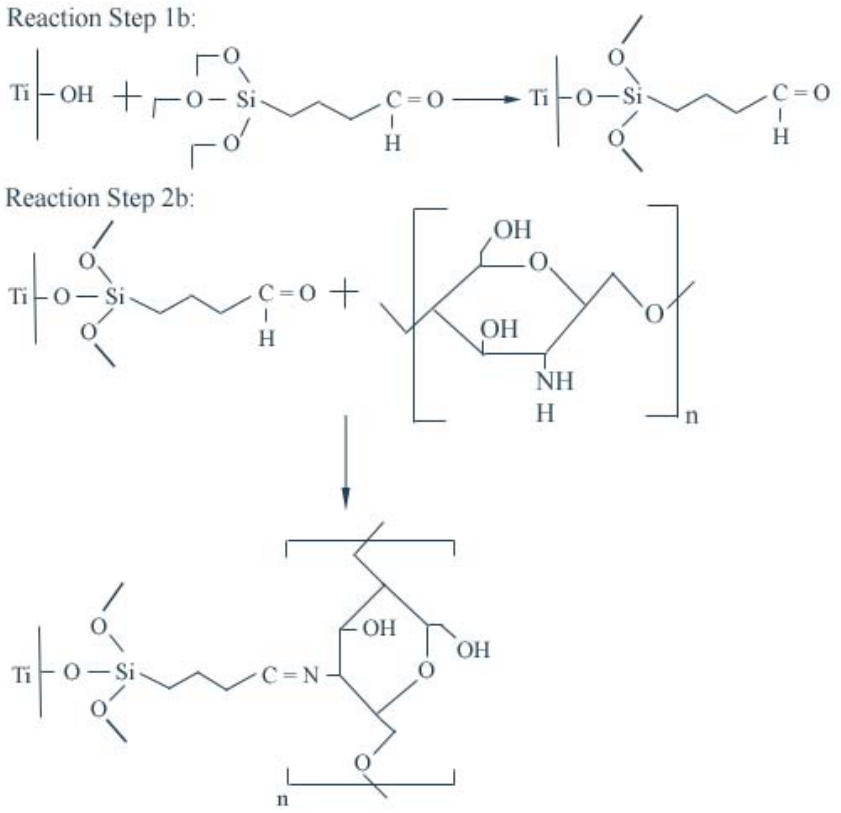

Figure 2.4. Triethoxsilylbutyraldehyde anticipated reaction series.

Reaction step 1b shows triethoxsilylbutyraldehyde bonding to the metal surface. Reaction step 2b shows chitosan bonding to the triethoxsilylbutyraldehyde-titanium complex.

2.4 Experimental Methods

The experimental methods used in this research were all chosen based on the data desired. Since this research revolves around growing high quality chitosan films on implant quality metal, both the reactions performed and the film produced must be examined. X-Ray Photoelectron Spectroscopy (XPS) was used to examine the individual reaction steps to determine the differences between the elements present based on the various silane and metal treatments. Scanning Electron Microscopy (SEM) was used to examine the films produced for differences in film features. Nano-indentation was used to examine the hardness and elastic modulus of the films and scratch testing was used to examine the adhesion of the films. SEM was also used to examine the nano-indentation marks and scratches produced. Atomic Force Microscopy (AFM) was used to examine the roughness of the films and the nano-indentation marks to determine how the film reacted to stresses. Bulk adhesion measurements were used to determine if the bond strength between the film and the titanium substrate was greater or less than the bond strength of the glue. Contact angle measurements were used to determine if changes to the film's interaction with water occurred due to the different metal treatments and silanes.

2.4.1 X-Ray Photoelectron Spectroscopy

XPS is a useful surface analysis technique that allows the user to determine the elements present and the chemical composition of those elements. When using XPS, a filament of either magnesium or aluminum is energized to produce soft x-rays of 1253.6 eV or 1486.6 eV, respectively [2.3]. The photons released then hit the surface of the

material, reaching a depth of no greater than 100 angstroms [2.3]. The photon then energizes an electron, which is released as a photoelectron. The ejected photoelectrons are collected by an energy analyzer, which counts the number of photoelectrons to determine the intensity of the element present [2.3]. An electron in the outer shell then drops into the "hole" produced by the ejection of the photoelectron. In the process of relaxation, that electron also releases energy causing the ejection of an Auger electron [2.3]. Figure 2.5a demonstrates the excitation and ejection of a photoelectron, while Figure 2.5b demonstrates the relaxation, excitation, and ejection of an Auger electron.

XPS is useful because each element has at least one characteristic binding energy that corresponds to the shell present. Elements that have more than one shell will have more than one characteristic binding energy [2.4]. The number of electrons surrounding the nucleus of the atom determines the number of shells present [2.4]. After a shell is filled with electrons, another shell is formed; when several electrons are present in a shell, the shell may split, based on the spin of the electrons within that shell, as seen in calcium and titanium [2.3]. Table 2.2 shows the number of electrons that fit into each of the shells in the anticipated elements, and Table 2.3 shows the characteristic binding energies for the elements commonly seen in the metal surface, reaction steps, and films.

As previously stated, XPS is a surface technique that reaches a depth of no more than 100 angstroms. Because of this, XPS is an appropriate technique to examine the surface chemistry and to monitor the reaction steps. As the anticipated reaction steps proceed, a thin film is produced that will reduce, and ultimately cover, the titanium elemental peak. XPS can also be used to determine the chemical compounds present [2.3]. This occurs within each elemental peak [2.3]. As an element is bound in the form

of different compounds and molecules, chemical shifts occur. For example, elemental carbon has a binding energy of 284.5 eV and hydrocarbons have a binding energy of 285.3 eV. Every addition of an oxygen shifts the elemental carbon signal over 1.5 eV, to 286.0 eV for C – OH, 287.5 eV for C = O, and 289.0 eV for COOH [2.5]. These chemical shifts allow the researcher to determine the compounds present on the surface of the samples [2.3].

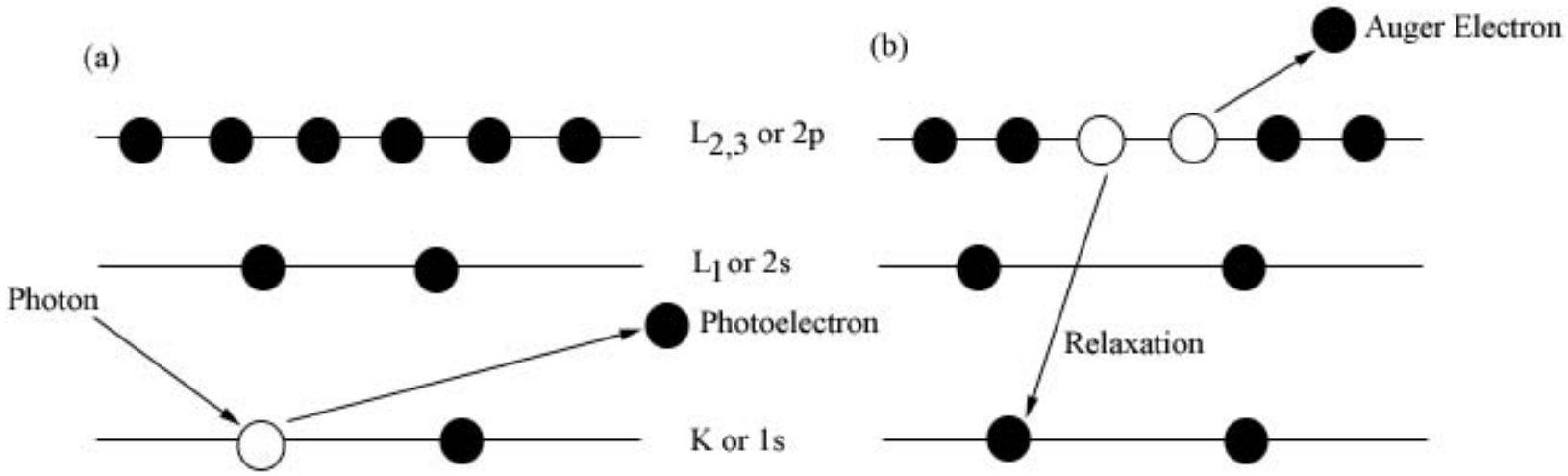

Figure 2.5. Excitation of electrons.

(a) Excitation and release of a photoelectron. (b) Relaxation, excitation, and release of an Auger electron. Adapted from [2.3].

Table 2.2. Electrons present in the shells of the anticipated elements [2.4].

Shell	**Electrons**
1s	2
2s	2
2p	6
3s	2
3p	6

Table 2.3. Anticipated elements based on the reaction steps.

The star indicates the major peak fitted for chemical composition [2.3].

Element	Atomic Number	Energized Shell	Binding Energy (eV)
Carbon	6	1s*	285
Nitrogen	7	1s*	398
Oxygen	8	1s*	531
		2s	23
Silicon	14	2s	151
		2p*	99
Calcium	20	2s	440
		2p1/2	351
		2p3/2*	347
		3s	45
		3p	26
Titanium	22	2s	561
		2p1/2	460
		2p3/2*	454
		3s	59
		3p	33

2.4.2 Scanning Electron Microscopy

SEM is an imaging tool that allows the user to examine the surface features of materials. In our research, SEM was used to examine the features of the chitosan films produced through the different silane reactions and metal treatments. When using SEM, a filament of either tungsten or LaB_6 is heated and the electrons are released due to the heat of the filament [2.6]. Since the filament and resulting electrons are negatively charged and the anode is positively charged, an electrical potential is formed [2.6]. These electrons are accelerated towards the anode, with the resulting voltage difference being referred to as the accelerating voltage [2.6]. Figure 2.6 demonstrates the charging of the filament and the voltage through the anode.

Following the passage of the electrons through the anode, the beam is focused through a series of electromagnetic lenses [2.6]. Figure 2.7 shows the multitude of lenses through which the electron beam passes [2.6]. After the beam has been properly focused, the electrons hit the sample contained on the specimen stage [2.6]. The excitation of the surface by the electrons causes the release of two different types of electrons: elastic, high-energy electrons called backscattered electrons and inelastic, low-energy electrons called secondary electrons [2.6]. Secondary electrons are very low energy and are often absorbed by adjacent electrons, with only those secondary electrons close to the surface able to escape [2.6]. The escaping secondary electrons are collected and converted to photons in a scintillator. These photons are carried via a light tube to a photocathode that converts the photons to photoelectrons [2.6]. These photoelectrons are then displayed on a cathode ray tube, with the brightness on the screen indicating where the most secondary

electrons were emitted [2.6]. Figure 2.8 shows the image collection system for the secondary electrons.

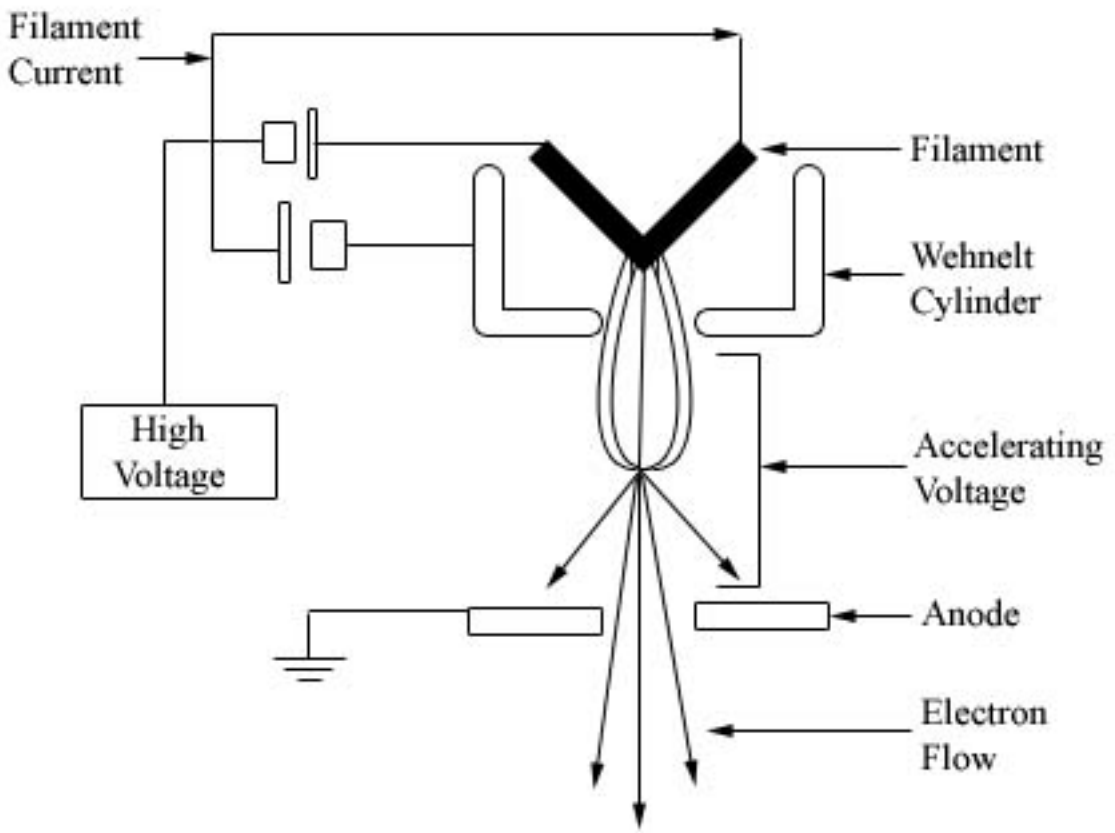

Figure 2.6. Flow of electrons from the excited, negatively-charged filament through the positively charged anode. Adapted from [2.6].

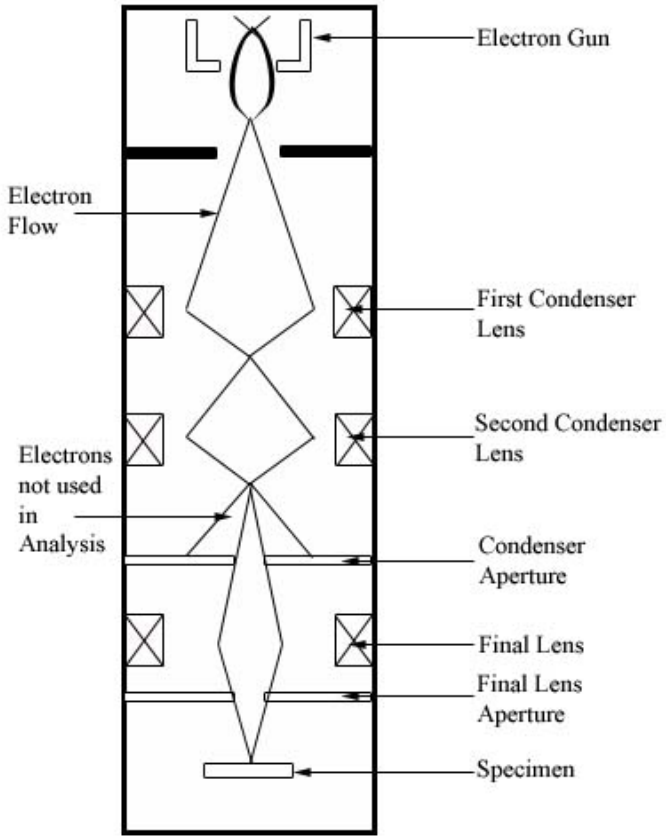

Figure 2.7. The electromagnetic lenses used to condense and focus the electron beam.

Adapted from [2.6].

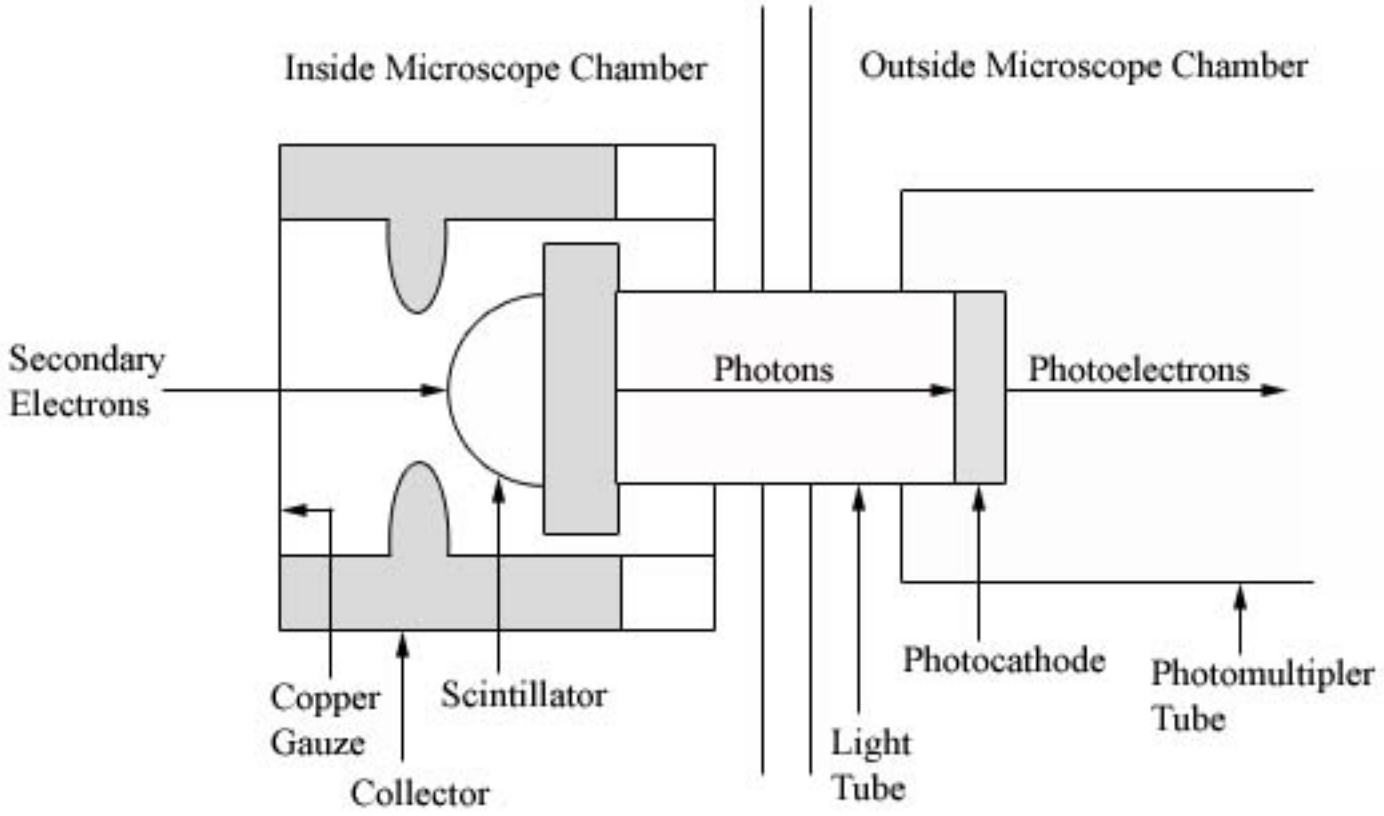

Figure 2.8. The image collection system for secondary electrons.

Adapted from [2.6].

At Mississippi State University, a special modification to the standard scanning electron microscope is used. In the standard scanning electron microscope, a filament is heated, "burning off" the electrons. In field-emission scanning electron microscopy, a crystal tungsten wire with a very sharp point, instead of a filament, is used [2.6]. The electrons are drawn out of the point by an electrical field, using an emission voltage of between 3 and 6 kV, as compared to the 10 – 50 kV used in a standard SEM [2.6]. Instead of one anode that helps create the accelerating voltage in a standard SEM, two anodes create the accelerating voltage in a field-emission SEM [2.6]. Figure 2.9 shows how the anodes work in a field-emission SEM.

As with the standard SEM, following the refinement of the anodes, the electron beam then passes through a series of electromagnetic lenses before hitting the specimen stage [2.6]. The secondary electrons, which are released, are collected, converted to photons, then converted to photoelectrons, and displayed on a screen, where the brightness indicates places where the most secondary electrons were emitted [2.6].

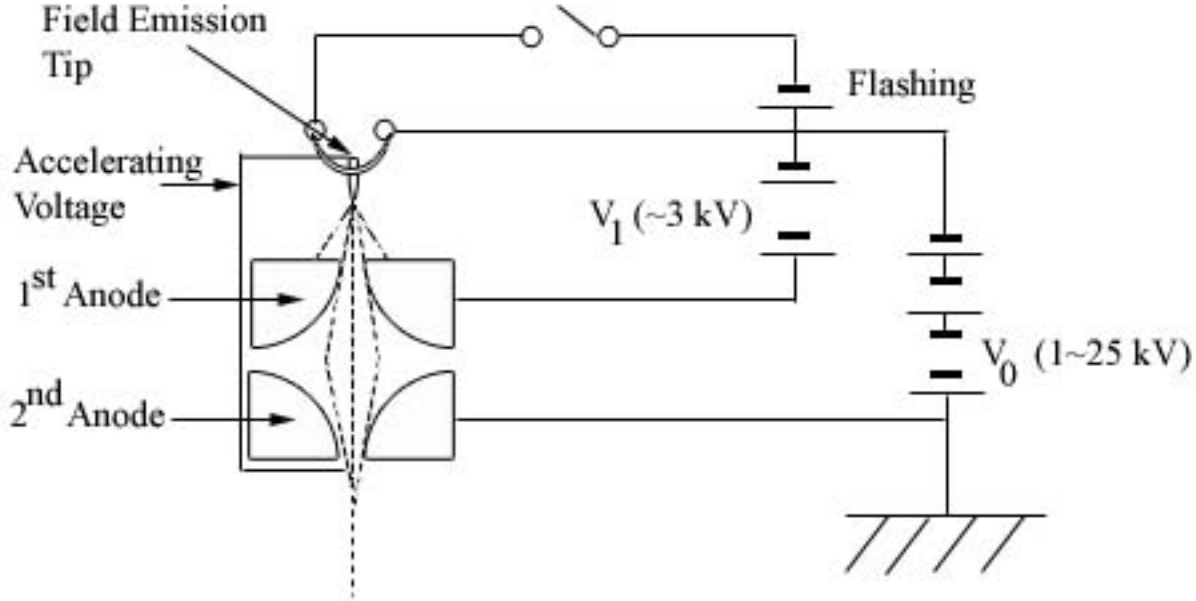

Figure 2.9. The electrical field produced in a field-emission SEM.

Adapted from [2.6].

Field-emission SEM is more desirable than standard SEM for several reasons. First, the number of secondary electrons that can be detected and the resulting brightness that can be displayed is 10^3 to 10^4 A/cm^2*ster times greater [2.6]. Second, the operating life for a field-emission SEM is more than 10 times that of the standard SEM [2.6]. Third, the spot diameter for a field-emission SEM is around 2 nm, while the theoretical spot diameter for a standard SEM is 4 – 8 nm [2.6]. While the machine cannot scan at 2 nm because the beam is teardrop shaped and not a single point, the smaller size does result in much higher resolution of the scanning location [2.6]. The one major disadvantage of field-emission SEM, however, is that the crystal tungsten wire requires an ultra-high vacuum, which is often incompatible with the specimens used in the microscope [2.6]. This issue was addressed through the use of ultra-high vacuum pumps in the gun chamber, which is shut off from the main chamber when samples are being loaded and unloaded, and turbo pumps, which maintain the pressure in the main chamber [2.6]. The gun chamber is opened to the main chamber only when the pressure within the main chamber has reached acceptable levels. Figure 2.13 shows a comparison between the standard SEM (a) and the field-emission SEM (b).

2.4.3 Nano-Indentation

Nano-indentation is a method to determine several properties of films. It is commonly used on thin films as a way to reduce, or remove, the effects of the underlying substrate, as the original hardness testers did not produce small enough indentations to account for just the overlying film. When using nano-indentation, the sample is loaded into the nano-indenter and locations for indentation are chosen using an optical

microscope [2.7]. Once the locations and parameters have been set, the machine is isolated to allow for a closed system [2.7]. Vibrations and temperature changes are minimized in order to obtain accurate data [2.7]. At Oak Ridge National Laboratory, the room temperature is maintained within ± 0.2^{o}C. The nano-indenter is placed on a high performance table to minimize vibrations [2.7]. This allows for resistance to the slight vibrations from the surrounding environment [2.7]. Once the machine is isolated, a load is applied to the sample through the use of an electrical current passing through a coil that sits within a circular magnet [2.7]. The indenter is pressed into the surface and the data is gathered by a series of three capacitors in the shape of circular disks [2.7]. Two of the three capacitors are attached to the outside of the machine head with a hole in the middle to accommodate the indenter shaft, while the third is attached to the indenter shaft [2.7]. As the indenter is pressed into the surface, the third capacitor moves with the shaft [2.7]. The difference in voltage between the center plate and one of the two outside capacitors is used to determine the position of the indenter, or the displacement into the surface [2.7]. Figure 2.10 shows the arrangement of the nano-indentation capacitors from the side and also the design of a fixed capacitor.

Nano-indentation can be used to determine the elastic modulus and hardness of a film. These values are calculated from the stiffness value, which is determined using the load applied to the surface and the displacement into the surface [2.7]. Based on this method, the elastic modulus and the hardness of the film can only be calculated when the load is removed or unloaded [2.7]. The inability to calculate the stiffness except during unloading is a problem for two reasons. The first reason is that the film may not be sufficiently thick and one would be unable to determine if the substrate properties were

included in the calculations when the load is removed [2.7]. Secondly, without the ability to calculate the stiffness except during unloading, the user would be unable to determine if the film properties change as a function of surface penetration [2.7].

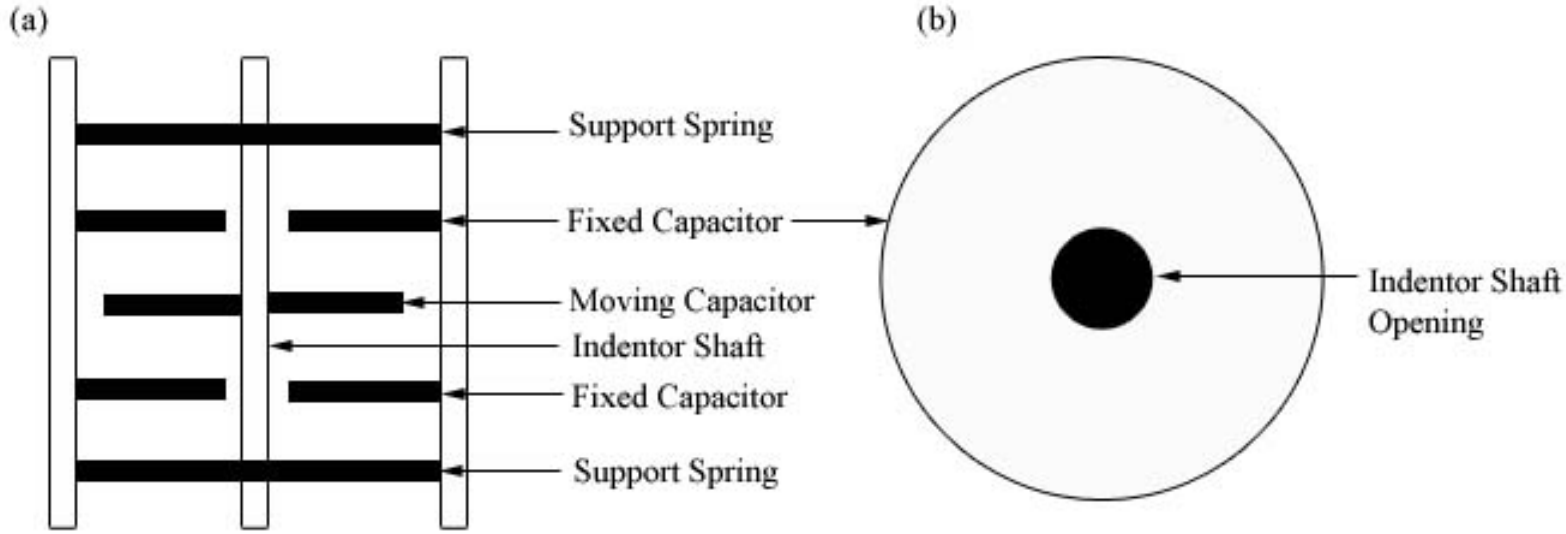

Figure 2.10. The Nano-Indenter XP's arrangement of capacitors.

(a) A side view of the discs. (b) A top view of a fixed disc. Adapted from [2.7].

In order to allow for changes due to either the substrate or the depth of penetration, a different method of gathering data is used. The continuous stiffness measurement (CSM) is a method used to gather information about the film behavior as the nano-indenter is being pressed into the surface. Using CSM, the nano-indenter is pressed into the surface and then a small oscillation is applied [2.8]. This small oscillation of around 2 nm for the Nano-Indenter XP, is enough of a load removal to allow for the calculation of stiffness throughout the entire penetration of the film [2.8]. With CSM, the user can obtain the elastic modulus and the hardness as a continuous function of film penetration [2.8]. This continuous collection of data allows the user to see the interaction between the substrate and the film if it exists. It also allows the user to determine if the film properties change as a function of depth or are time-dependent, two very important qualities when examining polymer films [2.8].

2.4.4 Scratch Testing

Scratch testing is a method to determine the reaction of the film to a stress. The equipment and procedure are the same with scratch testing as it is with nano-indentation. The positions are chosen with an optical microscope, an applied load and a constant strain rate are used, and vibrations and temperature changes are minimized [2.7]. As with nano-indentation, a load is applied to the sample by passing an electrical current through a coil in the magnet, with displacement measured by the change in voltage between the three capacitors [2.7]. Unlike nano-indentation, however, a drag velocity is specified [2.9]. A scratch is produced by moving the X – Y table at the specified drag velocity. Figure 2.10 shows the arrangement of the magnet and capacitors, while Figure 2.14

shows a schematic of the nano-indenter. Information can then be gathered about the film's deformation behavior and adhesion to the substrate from the resulting scratch [2.9].

Deformation of materials can occur in one of three ways: elastic – plastic, fracture, or visco – elastic [2.9]. For elastic – plastic behavior, the scratch produced is a groove with two lateral pile-up pads and the scratch looks exactly the same for the entire length [2.9]. For fracture behavior, pieces of the film are chipped out of the surface and cracks along the scratch may also occur [2.9]. Unlike elastic – plastic behavior, the scratch produced during fracture is very irregular and varies in appearance along the entire length of the scratch [2.9]. A scratch produced when the film is visco – elastic should be examined over an extended time period [2.9]. The scratch originally looks like that of an elastic – plastic scratch, with a deep grove and pile – up pads [2.9]. However, as time progresses, the groove produced by the scratch is filled by the pile – up pads moving back into place [2.9]. The type of deformation behavior is based on the type of film being investigated. For example, soft bulk metals will often deform in an elastic – plastic manner, while hard thin films, such as oxides, will fracture almost immediately due to their brittle nature [2.9].

Adhesion can be determined only if the film is separated from the substrate [2.10]. This allows the user to determine how much shear force is required to remove the film, which is necessary in this research to determine if the forces used in positioning an implant exceed the forces which the film can withstand. Also, the type of bonding, such as covalent, ionic, or hydrogen, affects how strongly the film is adhered and can be determined from scratch testing [2.11]. However, determination of adhesion and bond type both require that the film become separated from the substrate during testing.

2.4.5 Atomic Force Microscopy

AFM is a method used to determine the topography of surfaces. It is commonly used on films, specifically thin films, to determine if the method of applying the film results in a smooth surface or a rough surface [2.12]. When using AFM, a sample is loaded into the machine and locations are found using an optical microscope [2.12]. Once the locations and parameters, such as scan size and scan speed, have been set, the machine is then allowed to collect data [2.12]. A cantilever, with a very fine tip, moves across the surface of the sample [2.12]. A laser is aimed at a mirror on the top of cantilever [2.12]. As the cantilever tip encounters either valleys or peaks in the film, the cantilever bends slightly [2.12]. This bend is registered and analyzed by the computer software and displayed on a monitor [2.12]. Generally, brighter areas indicate peaks, while darker areas indicate valleys [2.12].

2.4.6 Bulk Adhesion

Bulk adhesion measurements are used to determine the bond strength of a film to a surface. In this research, bulk adhesion measurements are used to determine the bond strength of the chitosan film to one of the four treatment methods on commercially pure titanium grade 4. When using bulk adhesion, an aluminum cylindrical pin, with a diameter of 12.522 mm and a length of 26.254 mm, is glued to the film surface using Loctite Prism 454 Instant Gel Adhesive. The glue is allowed to cure for 24 hours before being placed in the machine. A tensile force is applied to the pin, causing stress to the glue and to the film. When the maximum load has been reached, a fracture will occur.

This fracture can take place in one of three locations: within the glue, within the film, or between the substrate surface and the film [2.13]. The fracture location allows the researcher to establish a lower number for the bond strength between the film and the substrate [2.13]. If the fracture occurs within the glue, then the researcher knows that the bond strength between the film and the substrate is greater than the bond strength of the glue [2.13]. If the fracture occurs within the film, then the researcher knows that the bond strength between the film and the substrate is greater than the bond strength of the glue, but the bond strength between film molecules is not as great as the bond strength of the glue [2.13]. Finally, if the fracture occurs between the substrate and the film, then the researcher knows that the bond strength between the film and the substrate is less than the bond strength of the glue [2.13].

2.4.7 Contact Angle

Contact angle measurements are used to determine the wetting of a solid by a liquid. It is commonly used on films to determine the nature of the film's interaction with water, an indication of the hydrophilic or hydrophobic nature of the film [2.14]. When using the contact angle instrument, locations are chosen by hand, without the assistance of a microscope. The camera is focused on the tip of the syringe, so the sample is moved in front of the camera until the surface becomes focused. Once the sample surface is focused, a drop of liquid is released from the syringe; the surface and the liquid are allowed to equilibrate before a picture is taken. After the picture of the drop is taken, software is used to analyze the angle that is formed between the liquid

droplet and the surface, allowing the researcher to determine if the film is hydrophobic or hydrophilic.

Contact angle measurements allow the user to determine the wettability of the surface [2.14]. The angle formed between the surface of the material and the liquid drop results from a balancing of two major forces: the cohesive force of liquid molecules attracted to each other and the adhesive force of liquid molecules attracted to the molecules at the surface of the material [2.14]. When the attraction between the surface molecules and the liquid molecules is stronger than the attraction between liquid molecules, the material is considered wettable. A contact angle less than 90^{o} results and the surface is considered hydrophilic [2.15]. When the attraction between the surface molecules and the liquid molecules is weaker than the attraction between liquid molecules, the material is considered non-wettable. A contact angle greater than 90^{o} results and the surface is considered hydrophobic [2.15]. Figure 2.11 demonstrates the differences between a hydrophilic contact angle and a hydrophobic contact angle.

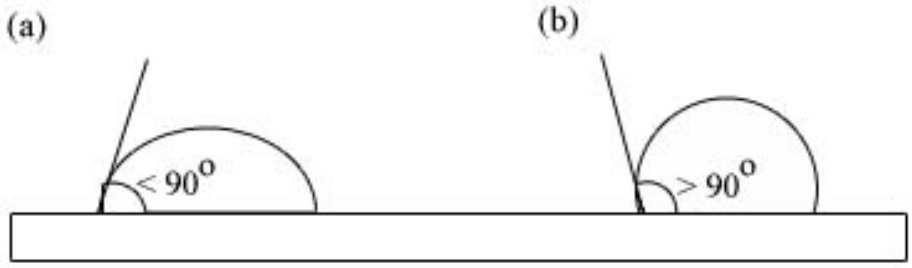

Figure 2.11. The difference in contact angles.

(a) A hydrophilic surface and (b) A hydrophobic surface.

2.5 Experimental Methodology

While the theory of the equipment used in this research has been explained previously, the actual use of the equipment, with the parameters needed for repeatability has not been given. The parameters used for this research, using each of the equipment described, are given in the following section.

2.5.1 X-Ray Photoelectron Spectroscopy

A PHI 1600 XPS Surface Analysis System (Physical Electronics, Eden Prairie, MN) incorporates a stainless steel chamber equipped with lead view ports in which to energize the x-ray source and collect data. The instrument uses a PHI 10-360 spherical capacitor energy analyzer to analyze the photoelectrons released from the sample surface. An Omni Focus II small-area lens is used to focus the incident source to produce an 800 μm diameter surface analysis area. The data was obtained using an achromatic MgK_{α} x-ray source operating at 300 W and 15 kV. Survey spectra were gathered using an average of 10 scans with a pass energy of 26.95 eV and running from 1100 eV to 0 eV. High-resolution spectra were gathered using an average of 15 scans with a pass energy of 23.5 eV and a step size of 0.1 eV. The incident sample angle was held constant at 45^{o}. The vacuum level for the reaction steps without the chitosan film was approximately $5x10^{-9}$ Torr, while the vacuum level for the chitosan film was approximately $3x10^{-8}$ Torr. For statistical analysis, three samples per treatment were used and three spots per sample were taken. Figure 2.12 shows a diagram of the PHI 1600 XPS machine.

2.5.2 Scanning Electron Microscopy

A JEOL JSM-6500F Field-Emission SEM (JEOL, Tokyo, Japan) incorporates a vacuum chamber equipped with infrared to view the samples. The instrument uses a cathode to produce an incident electron beam. An accelerating voltage of 1.0 kV was used and a vacuum of approximately $5x10^{-4}$ Pa was maintained. Magnifications of 900X and 1400X were used; an accelerating voltage any higher than 1.0 kV and magnifications greater than 1400X would cause the rapid degradation of the film. For statistical comparison, three samples per treatment were used and three spots per sample were taken. Figure 2.13 shows a diagram of both the standard SEM (a) and the field-emission SEM (b).

2.5.3 Nano-Indentation and Scratch Testing

Nano-Indentation and scratch testing were performed using a Nano-Indenter XP (NANO Instrument, Oak Ridge, TN). The instrument uses a Berkovich diamond indenter to produce triangle shaped indentation marks on the film surface. The instrument could apply a maximum load of 500 mN and used a 0.05 1/s constant strain rate. A 30 second hold time was used before the tip was removed from the sample. The maximum depth obtained using 500 mN was 20 μm. The data was collected using continuous stiffness measurement (CSM) and a Poisson's ratio of 0.3 was used for the calculations performed. For statistical analysis, three samples per treatment were used and three locations were chosen per sample. Five indentation marks were then made per location, for a total of fifteen indentations per sample. For scratch testing, a maximum load of 600 mN was applied. The scratch was produced using a 10 μm/sec scratch velocity and the length of

the scratch was set to 1000 μm. For statistical analysis, one sample per treatment was used and one location was chosen per sample. Five scratch marks were then made for each location. Figure 2.14 shows a schematic of the Nano-Indenter XP.

2.5.4 Atomic Force Microscopy

AFM was performed on a Park-M5AFM (Park Scientific Instruments, Sunnyvale, CA). The data was collected using a constant contact mode. The scans of the indentation marks were made using a scan size of 100 μm and a scan rate of 2.5 Hz. The scans of the pile – up surrounding the indentation mark and the film surface were made using a scan size of 25 μm and a scan rate of 1.5 Hz. The linearized displacement in the X and Y direction was a minimum of 90 μm while the linearized displacement in the Z direction was a maximum of 7.5 μm. For statistical comparison, three samples per treatment were used and one location per indentation series was chosen, for a total of three comparisons per sample. Figure 2.15 demonstrates how AFM data is collected.

2.5.5 Bulk Adhesion

An Instron 4465 (Instron Corporation, Norwood, MA) was loaded with the 5000 N load cell. Aluminum pins were glued to the film samples using Loctite Prism 454 Instant Gel Adhesive, placed under a load to ensure contact, and allowed to dry for 24 hours. The aluminum pins and samples were secured into the machine using a pin and then lowered to the stage and secured. The software was set to automatically zero the load at 5.0 N to ensure no compressive forces were included in the calculations. The machine exerted tensile forces, under load control, until failure was reached. For statistical analysis, three samples per treatment were used. To establish a baseline for the

glue, six samples were used on titanium. Figure 2.16 illustrates the design of the Instron 4465 Tensile Tester, while Figure 2.17 demonstrates how the metal samples were held down during the applied tensile load.

2.5.6 Contact Angle

A VCA Optima (AST Products, Inc., Billerica, MA) incorporates a syringe to produce a drop of liquid. Infrared lights and a camera capture the interaction between the liquid and the surface. The liquid used in these experiments was water, with a droplet volume of 1.0 μL. The picture of the water drop on the surface was taken after ten seconds to ensure that any spreading of the water across of the film surface had occurred. For statistical analysis, three samples per treatment were used and three locations were chosen per sample. Figure 2.18 demonstrates how data is collected for contact angle measurements.

2.5.7 Software

The XPS data was collected and averaged using PHI Surface Analysis Software, Version 3.0 (Physical Electronics, Eden Prairie, MN). The XPS data was then analyzed using the Spectral Data Processor (SDP), Version 4.0 (XPS International LLC, Mountain View, CA). The SEM pictures were taken using JEOL PC-SEM 3.5 (JEOL USA, Inc., Peabody, MA). The nano-indentation data and the scratch testing data were collected and analyzed using TestWorks, Version 4.0 (NTS Nanoinstruments, Oak Ridge, TN). The AFM pictures were taken and analyzed using ProScan Data Acquisition (Sunnyvale, CA). The Instron 4465 was controlled and measurements were taken using Bluehill, Version 2.0 (Instron Corporation, Norwood, MA). Contact angle pictures were taken and

measurements were made using VCA Optima XE (AST Products, Inc., Billerica, MA). Statistical analysis was performed using SAS, Version 9.1 (SAS Institute Inc., Cary, NC). Comparison of the individual reaction steps was performed using completely randomized design with subsampling while the comparison of the final films was performed using completely randomized design with a 2^2 factorial arrangement of treatments with subsampling.

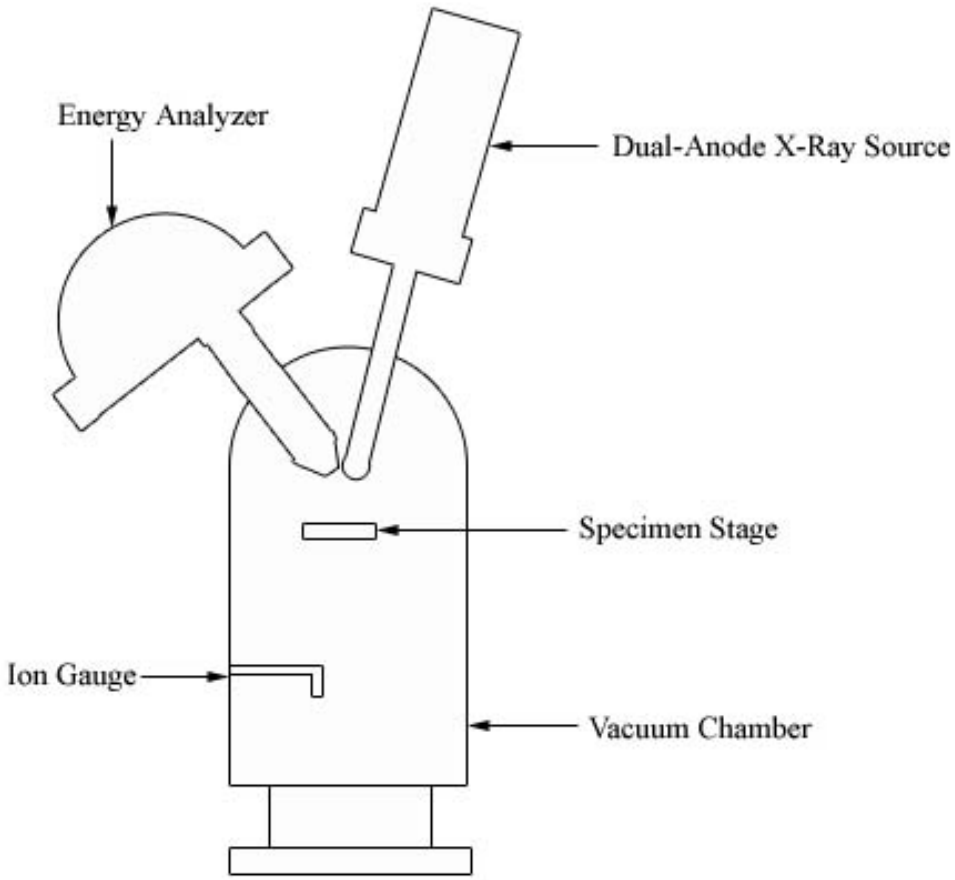

Figure 2.12. Diagram of the PHI 1600 XPS machine.

Adapted from [2.3].

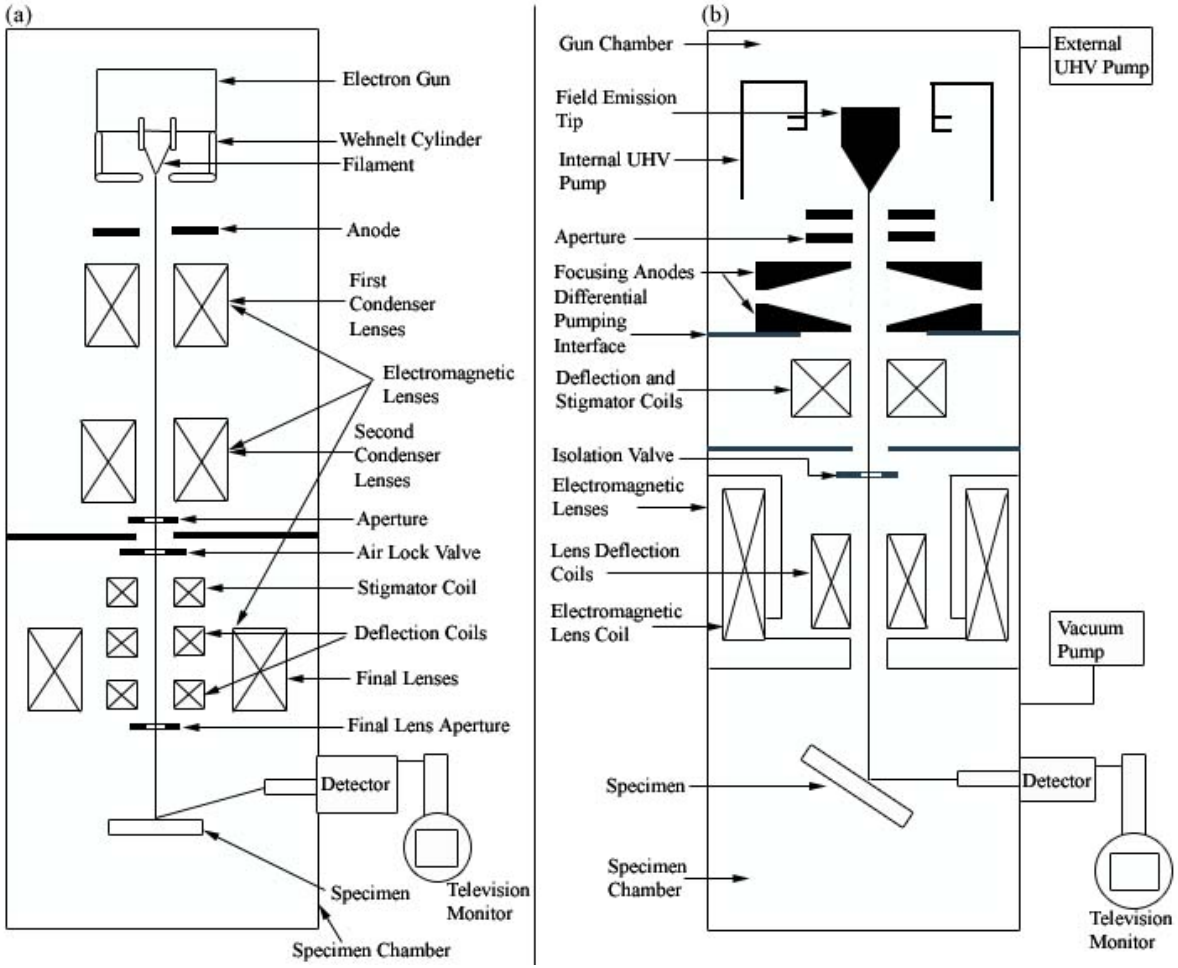

Figure 2.13. Diagram of the two types of SEM machines.

(a) Standard SEM machine (b) Field Emission SEM machine. Adapted from [2.6].

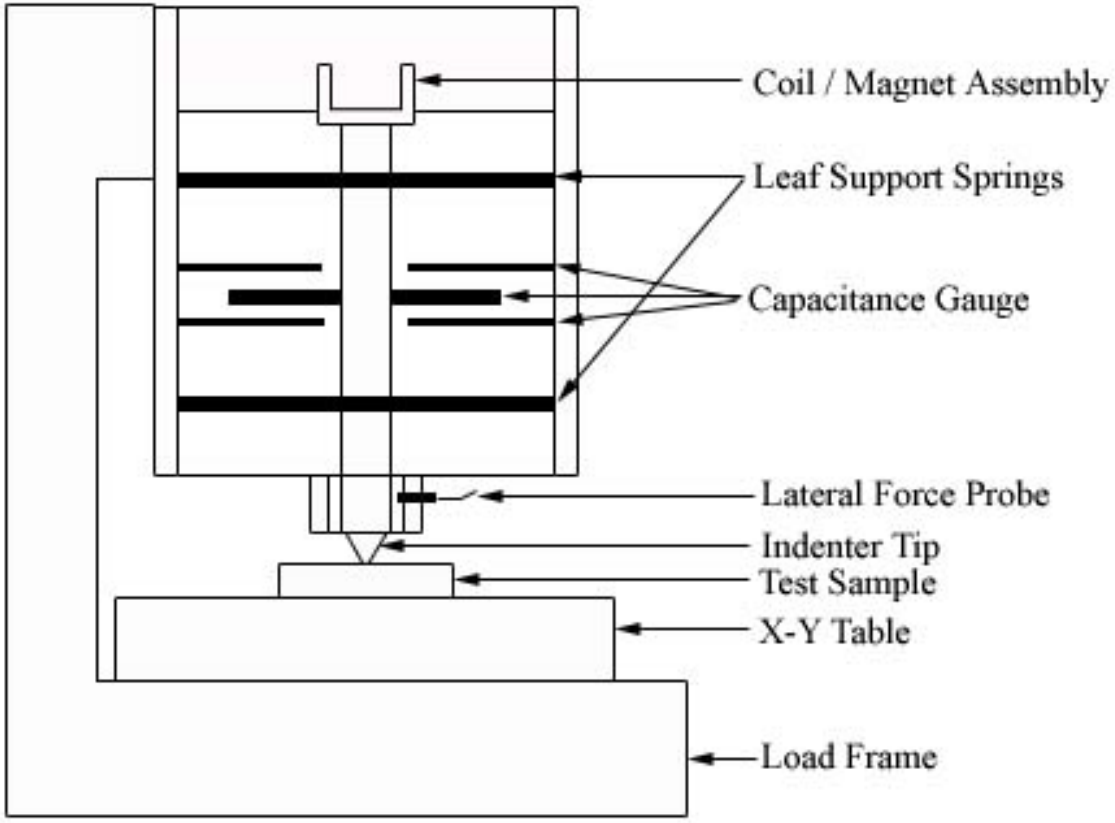

Figure 2.14. Schematic of the Nano-Indenter XP.

Adapted from [2.9].

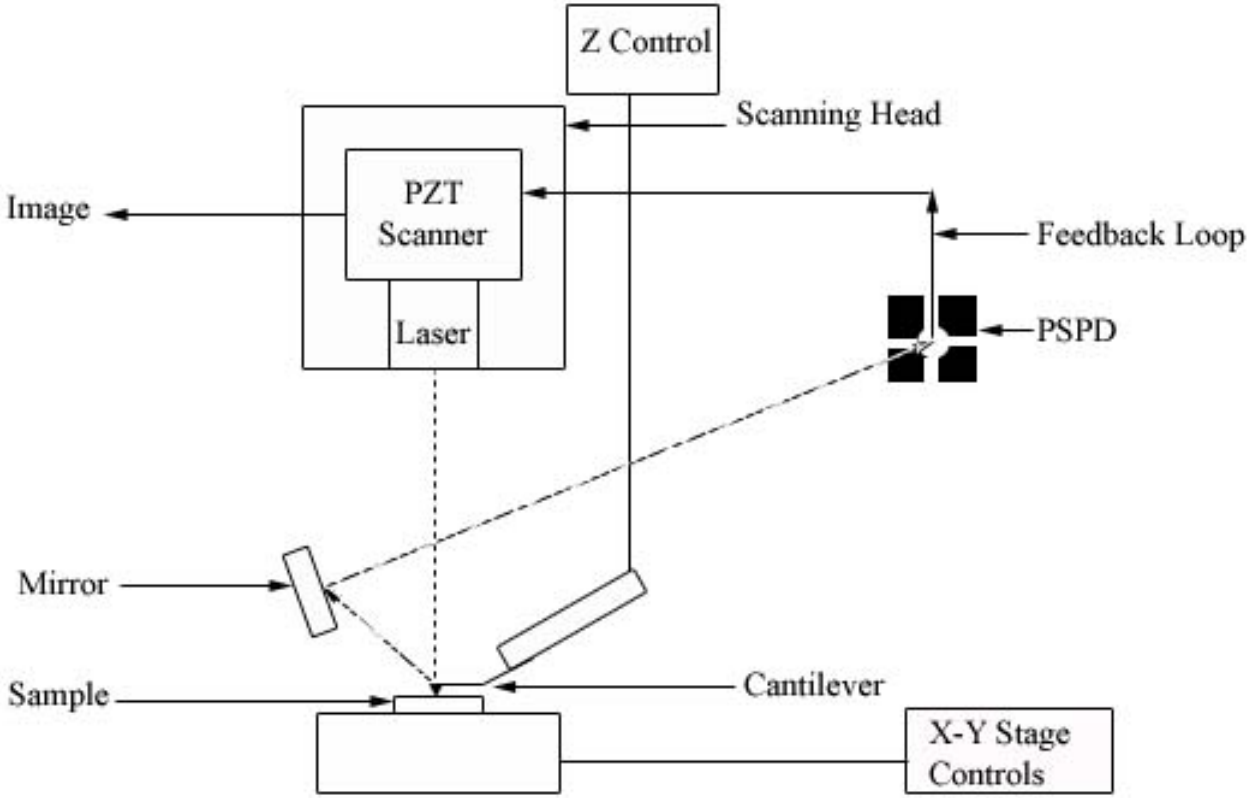

Figure 2.15. Schematic of AFM.

The laser beam is indicated by a dashed line. Adapted from [2.12].

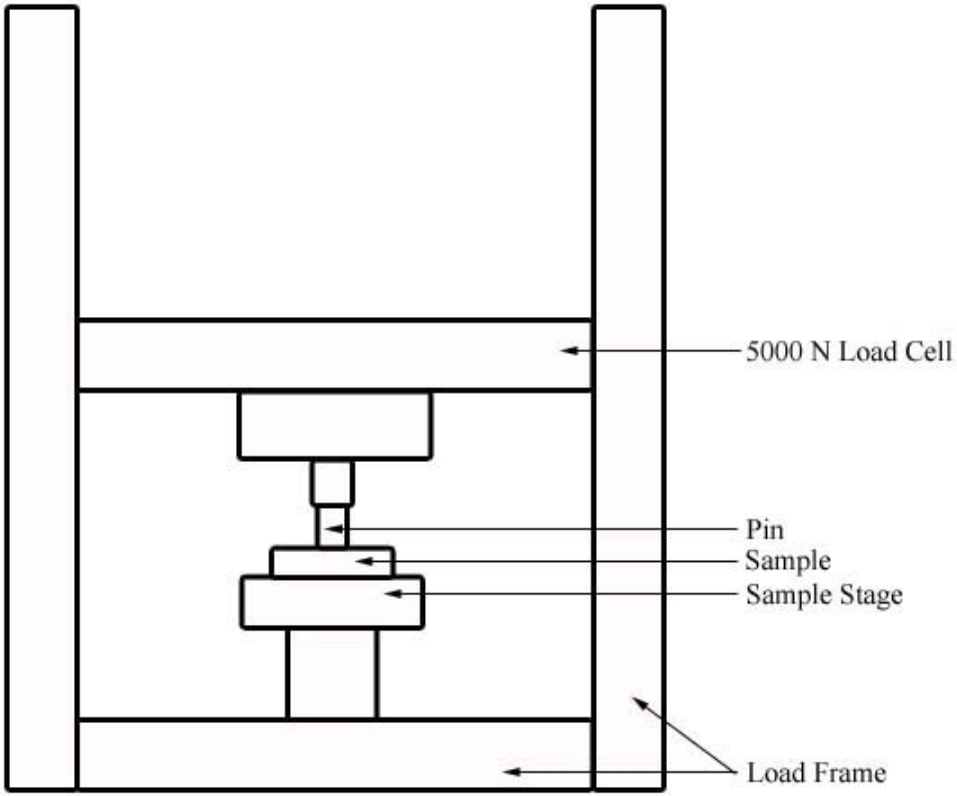

Figure 2.16. Schematic of the Instron 4465 Tensile Tester.

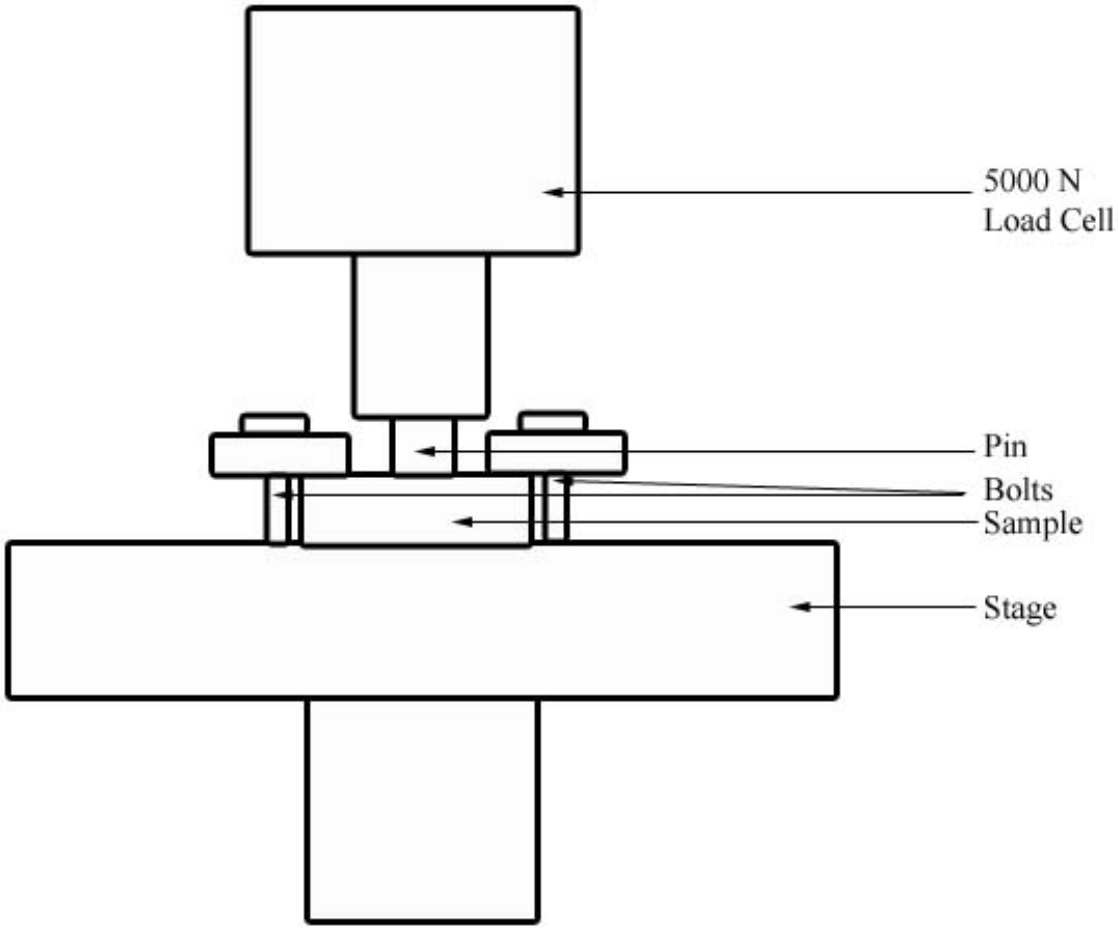

Figure 2.17. Close-up of the sample secured during tensile load testing.

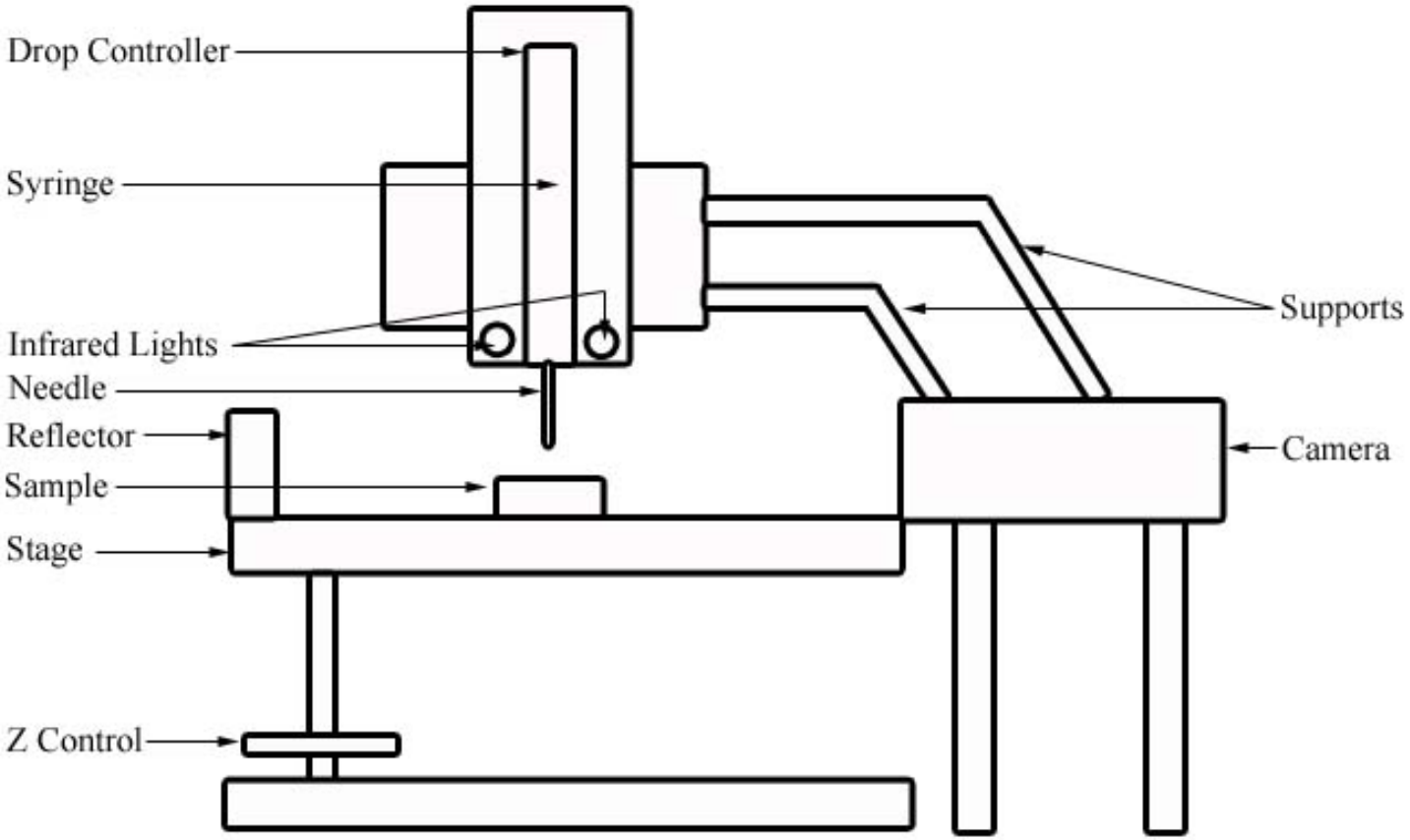

Figure 2.18. Schematic of the VCA Optima used to obtain contact angle readings.

2.6 Summary

The experimental methods used to collect data for this research were extremely varied. However, each of the methods used provided information about the film. XPS was used to provide information about the reaction series and binding the film to the metal substrate. SEM, AFM, bulk adhesion, and contact angles were used to provide information about the surface of the film, including appearance, roughness, reaction to stress, and wettability. Nano-indentation was used to provide information about surface properties, such as hardness and elastic modulus, and scratch testing was used to provide information about film behavior and adhesion properties. Using these methods, a thorough characterization of the films produced from the two metal treatments and two silane compounds was possible.

CHAPTER III

CHEMICAL ANALYSIS OF ISOCYANATOPROPYLTRIETHOXYSILANE

3.1 Introduction

Silanation reactions are commonly used to bind coatings to implant quality metals [3.1 – 3.3]. An initial reaction series was chosen that would allow chitosan to bind to commercially pure titanium grade 4. X-Ray Photoelectron Spectroscopy (XPS) was then used to document the surface reaction(s) occurring in each step.

3.2 Anticipated Surface Reaction

A published reaction series was initially used to bond chitosan to commercially pure titanium grade four [3.28]. The passivation metal treatment protocol was given in Chapter 2, Section 3.2, while the silane protocol was given in Chapter 2, Section 3.3.1. For each reaction step, one sample per metal treatment and five spots per sample were examined and the statistical analysis was performed using completely randomized design.

Changes in the amount of several chemical species on the reaction surfaces will indicate that the reactions are proceeding as anticipated. In order to bond silane molecules to the titanium surface, the presence of the highly reactive TiO species on the metal surface is preferred; the presence of the non-reactive TiO_2 is not desired. Following the reaction between the silane molecule and the titanium surface, a decrease

in the presence of TiO is expected. This occurs because the silane molecule binds to the TiO, and less of the titanium is now being probed due to the overlying silane layer, which prevents the release and detection of photoelectrons.

The presence of any silicon – oxygen compounds following the reaction between the silane molecule and titanium surface is advantageous, as this shows that the silane did bind to the metal surface. The presence of SiO indicates that the Si – O – C bond present in the silane is still occurring following the reaction with the surface, while the presence of SiO_3 indicates that the silane molecules are reacting with adjacent silane molecules to form a polysiloxane group that helps stabilize the silane molecules.

The presence of terminal end groups is also expected. The isocyanatopropyltriethoxysilane should produce a terminal group with nitrogen present, specifically a group containing C = N = O. The presence of this group would indicate that the silane molecule is binding to the titanium surface correctly, and that micelles, which may have formed during silane deposition, are not present. Therefore, changes in the amount of the TiO, SiO, SiO_3, and C = N = O peaks will allow us to determine if the reactions are occurring as anticipated.

3.3 Results

In order to determine the surface chemistry that occurred during each reaction step, XPS was performed. For each reaction step, survey scans were taken at five different locations. Following the survey scans, high resolution scans were taken of the major elements identified during the survey scans. The data gathered from running XPS must be analyzed to determine the elements and compounds present on the surface of the

material. The peak area of each of the functional groups is calculated by integrating the area underneath the peaks. For survey scans, the percentage is calculated by the following equation, where r is the number of elements present in the survey, I is the intensity of the elements, and S is the sensitivity factor that is dependent on the element:

$$A\% = \left(\frac{I_A / S_A}{\sum_r^1 I_r / S_r} \right) * 100 \qquad (3.1)$$

For high resolution scans, the percentage is calculated by the following equation, where r is the number of compound peaks present underneath the elemental peak and C is the composition of the peak:

$$A\% = \left(\frac{C_A}{\sum_r^1 C_r} \right) * 100 \qquad (3.2)$$

As one can see from the equations, especially for the high-resolution calculation, percentage is based not only on the area under each peak, but also, the number of peaks. If an element or chemical peak were missing, the percentage calculation would not be an accurate comparison between each of the reaction steps. In order to prevent erroneous comparisons, the statistical analysis was performed on both the peak areas and the percentages gathered from the XPS analysis. The statistical analysis for the peak areas and the percentages was then compared to determine if the trends present were similar or different.

The means and standard deviations of the five different elements for each of the reaction steps are shown in Table 3.1. Only two elements showed a significant change

based on the survey scans. Nitrogen, which was present in very small amounts on the passivated metal, increased significantly from 1 ± 1 % to 20 ± 1 % following reaction step 1, but did not significantly increase following reaction step 2. Silicon also increased significantly from 4 ± 1 % to 10 ± 1 % following reaction step 1 but returned to the original percentage of 4 ± 1 % following reaction step 2. Figure 3.1 shows the representative survey scans for each of the reaction steps. One can see that no change existed for the carbon, oxygen, and titanium peaks, while change did occur for the nitrogen and silicon peaks.

Following the survey scans, high-resolution scans of each of the elements were run and the chemicals present were identified. The means and standard deviations of the carbon peaks for each of the reaction steps are shown in Table 3.2, while the means and standard deviations of the nitrogen peaks are shown in Table 3.3. Table 3.4 displays the percentage means and standard deviations of the oxygen peaks, while Table 3.5 displays the functional group peak areas means and standard deviations. The percentage means and standard deviations of silicon are displayed in Table 3.6, while the functional group peak areas means and standard deviations are displayed in Table 3.7. Finally, the percentage means and standard deviations of the titanium peaks are shown in Table 3.8, while the functional group peak areas means and standard deviations are shown in Table 3.9.

Table 3.1. Elemental percentage based on XPS survey scans.

Reaction Step	Carbon	Nitrogen	Oxygen	Silicon	Titanium
Passivated	44 ± 2^{a} %	1 ± 1 %	40 ± 2^{c} %	4 ± 1^{d} %	9 ± 2^{e} %
Silane	44 ± 1^{a} %	20 ± 1^{b} %	37 ± 2^{c} %	10 ± 1 %	5 ± 1^{e} %
Gluteraldehyde	43 ± 2^{a} %	22 ± 1^{b} %	41 ± 2^{c} %	4 ± 1^{d} %	6 ± 1^{e} %

Values with the same superscript are not statistically different at the 5% significance level.

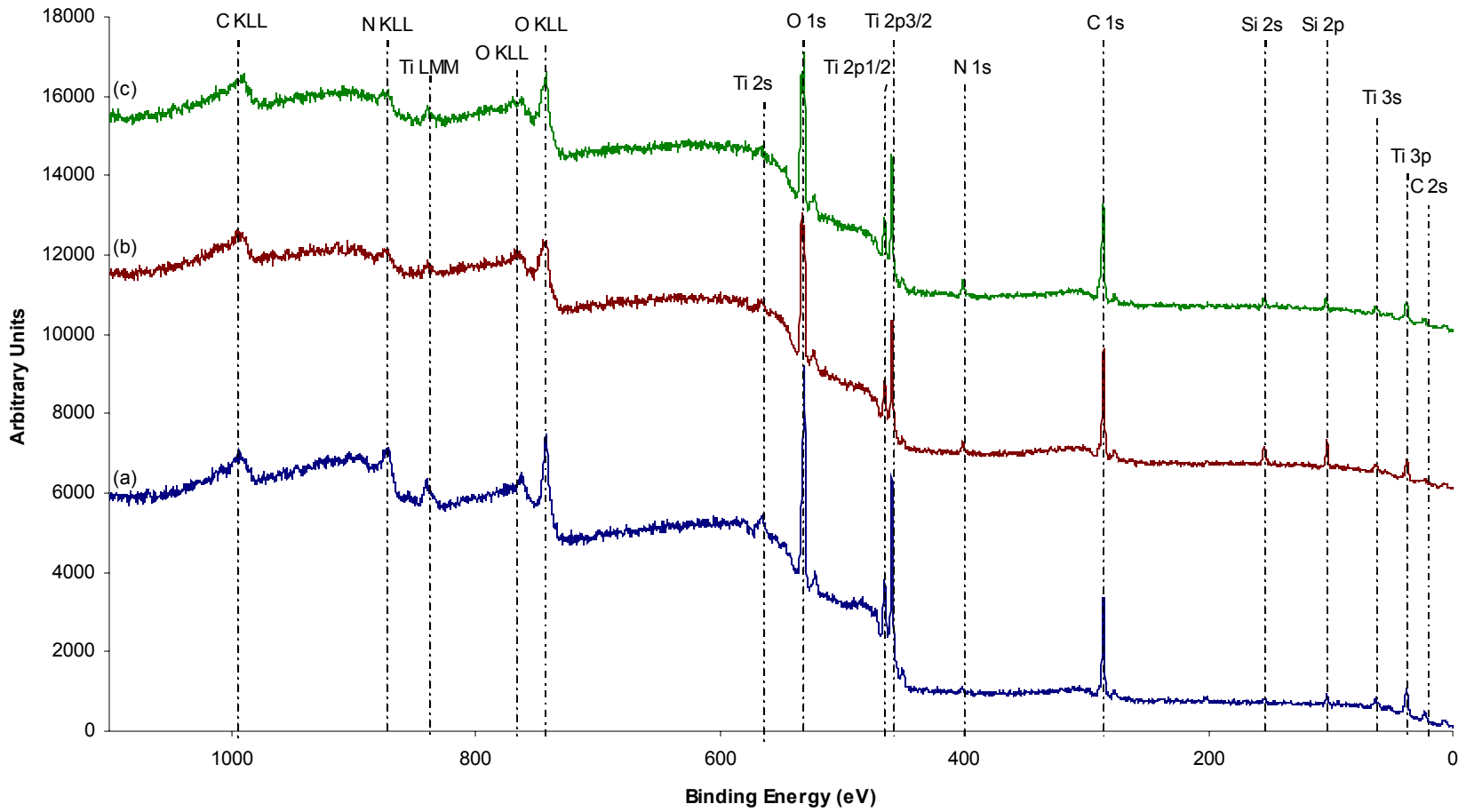

Figure 3.1. Representative survey scans of commercially pure titanium grade 4 following treatment.

(a) Passivation, (b) Isocyanatopropyltriethoxysilane, and (c) Gluteraldehyde.

Of the six different carbon compounds found on the surface of the isocyanatopropyltriethoxysilane reaction series, only two compounds were statistically unchanged through the reaction series: the hydrocarbon percentage and the O = C = O group. Elemental carbon was reduced from reaction step 1 to reaction step 2, as were the C – OH groups and the C = O groups. The COOH groups, when present, were not statistically different; however, COOH did not appear following reaction step 1. Figure 3.2 shows the changes occurred from the passivated metal through reaction step 1 to reaction step 2. The functional group peak areas numbers were examined and no trends were different as compared to the percentage trends.

The passivated metal did not indicate that nitrogen was present in any detectable form on the surface. While the survey scan indicated that 1 ± 1% existed, the intensity of the high-resolution scans was not enough to allow for accurate analysis. The peaks that were present following the other two steps of the reaction series were not statistically different. The changes that occurred in the nitrogen element between the reaction steps are shown in Figure 3.3. The functional group peak areas numbers were examined and no peak area trends were different as compared to the percentage trends.

Table 3.2. Carbon functional group percentages based on XPS high resolution scans.

	C [3.4]	C-C [3.5]	C-OH [3.6]	C=O [3.7]	COOH [3.8]	COO [3.9]
Reaction Step	284.6 ± 0.1 eV	285.4 ± 0.1 eV	286.5 ± 0.1 eV	287.7 ± 0.2 eV	288.7 ± 0.3 eV	289.4 ± 0.3 eV
Passivated	27 ± 6^{a} %	46 ± 5^{b} %	17 ± 1^{c} %	6 ± 1^{d} %	8 ± 1^{e} %	7 ± 1^{f} %
Silane	28 ± 5^{a} %	42 ± 3^{b} %	17 ± 2^{c} %	7 ± 1^{d} %	---	6 ± 1^{f} %
Gluteraldehyde	9 ± 3 %	37 ± 3^{b} %	25 ± 3 %	15 ± 1 %	8 ± 1^{e} %	8 ± 1^{f} %

Values with the same superscript are not statistically different at the 5% significance level.

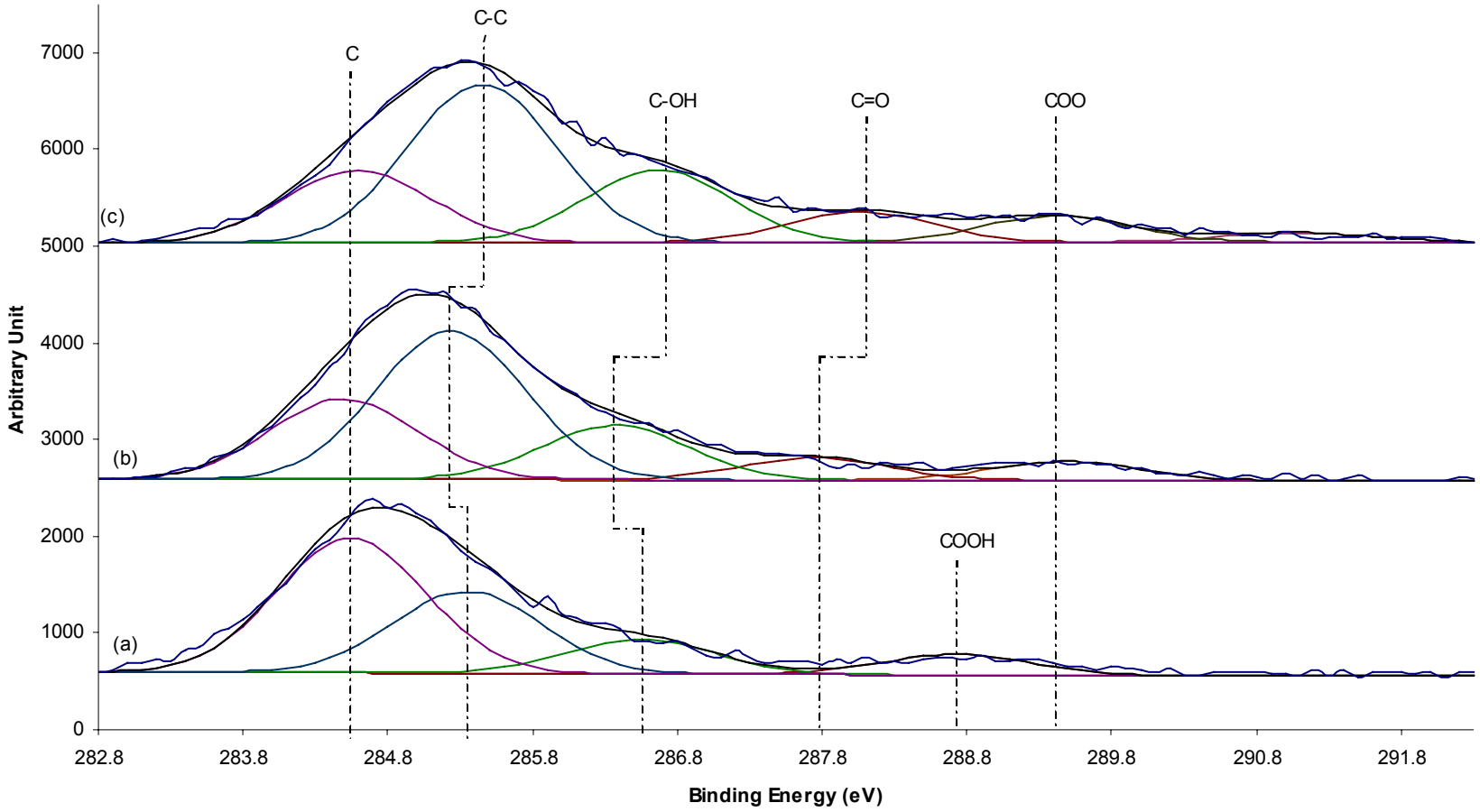

Figure 3.2. Representative carbon high resolution scans of commercially pure titanium grade 4 after treatment.

(a) Passivated, (b) Isocyanatopropyltriethoxysilane, and (c) Gluteraldehyde.

Table 3.3. Nitrogen functional group percentages based on XPS high resolution scans.

	N=C=O [3.10]	NO [3.11]	CN [3.12]
Reaction Step	399.4 ± 0.2 eV	400.5 ± 0.2 eV	401.6 ± 0.2 eV
Passivated	---	---	---
Silane	36 ± 6[a] %	45 ± 5[b] %	24 ± 2[c] %
Gluteraldehyde	26 ± 1[a] %	50 ± 4[b] %	29 ± 2[c] %

Values with the same superscript are not statistically different at the 5% significance level.

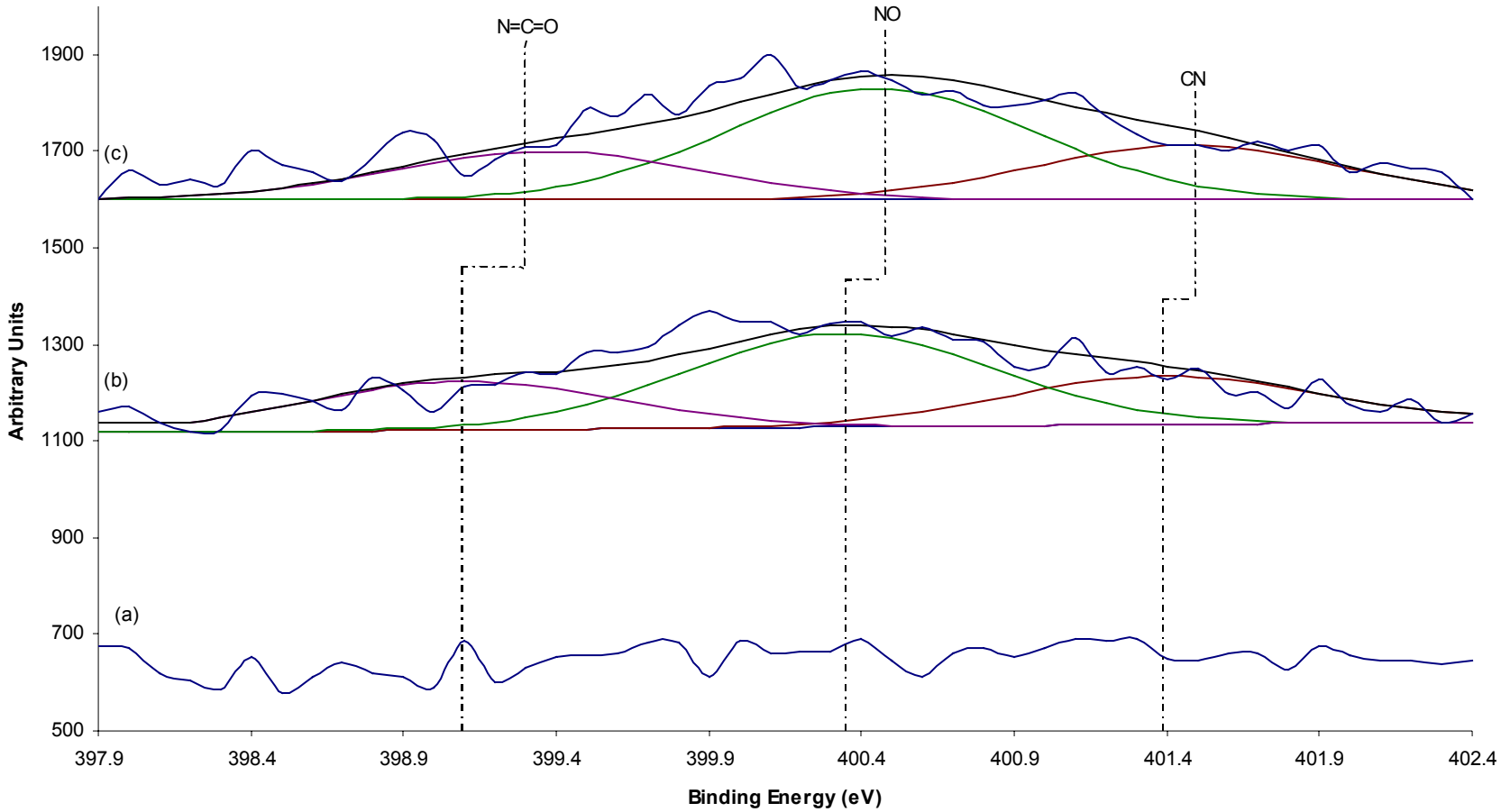

Figure 3.3. Representative nitrogen high resolution scans of commercially pure titanium grade 4 after treatment.

(a) Passivated, (b) Isocyanatopropyltriethoxysilane, and (c) Gluteraldehyde.

The oxygen peaks produced during the different reaction steps may or may not vary, depending on the functional group peak areas. Based on percentage, the TiO_2, TiO, and CO peaks varied between the passivated metal and reaction step 1, but did not vary between reaction step 1 and reaction step 2. However, these peaks were examined based on peak area, as well as percentage, because the SiO_x peak was missing for the passivated step. Based on peak area, the TiO_2 peak did not vary based on the reaction. The TiO peak showed a significant decrease from the passivated metal to reaction step 1, but a significant increase from reaction step 1 to reaction step 2, back to being statistically identical to the passivated metal. The CO peak was the only peak that showed a difference between the passivated metal and reaction step 1, but no change was seen between reaction step 1 and reaction step 2. The SiO peak showed a significant increase, both in peak area and in percentage, from the passivated metal to reaction step 1 and a significant decrease from reaction step 1 to reaction step 2; for the SiO peak, the difference between the passivated metal and reaction step 2 was statistically insignificant. The SiO_x peak did not appear on the passivated metal, but did appear following reaction step 1 and reaction step 2. Based on peak area, it showed a statistically significant increase from reaction step 1 to reaction step 2. The oxygen peak and the changes that occurred during each reaction step are shown in Figure 3.4.

Table 3.4. Oxygen functional group percentages based on XPS high resolution scans.

	TiO_2 [3.13]	TiO [3.14]	SiO [3.15]	CO [3.16]	SiO_x [3.17]
Reaction Step	530.2 ± 0.3 eV	531.2 ± 0.4 eV	532.3 ± 0.3 eV	533.3 ± 0.3 eV	534.4 ± 0.4 eV
Passivated	43 ± 4[a] %	22 ± 1 %	20 ± 2[d] %	8 ± 1 %	---
Silane	33 ± 3[b] %	18 ± 1[c] %	28 ± 3 %	16 ± 2[e] %	5 ± 1[f] %
Gluteraldehyde	35 ± 2[a,b] %	19 ± 1[c] %	21 ± 1[d] %	18 ± 2[e] %	7 ± 1[f] %

Values with the same superscript are not statistically different at the 5% significance level.

Table 3.5. Oxygen functional group peak areas based on XPS high resolution scans.

	TiO_2 [3.13]	TiO [3.14]	SiO [3.15]	CO [3.16]	SiO_x [3.17]
Reaction Step	530.2 ± 0.3 eV	531.2 ± 0.4 eV	532.3 ± 0.3 eV	533.3 ± 0.3 eV	534.4 ± 0.4 eV
Passivated	5460 ± 600[a]	2900 ± 220[b]	2540 ± 150[d]	1070 ± 80	---
Silane	4240 ± 570[a]	2280 ± 50[c]	3580 ± 260	2090 ± 190[e]	660 ± 70
Gluteraldehyde	4670 ± 350[a]	2550 ± 180[b,c]	2750 ± 160[d]	2360 ± 240[e]	970 ± 100

Values with the same superscript are not statistically different at the 5% significance level.

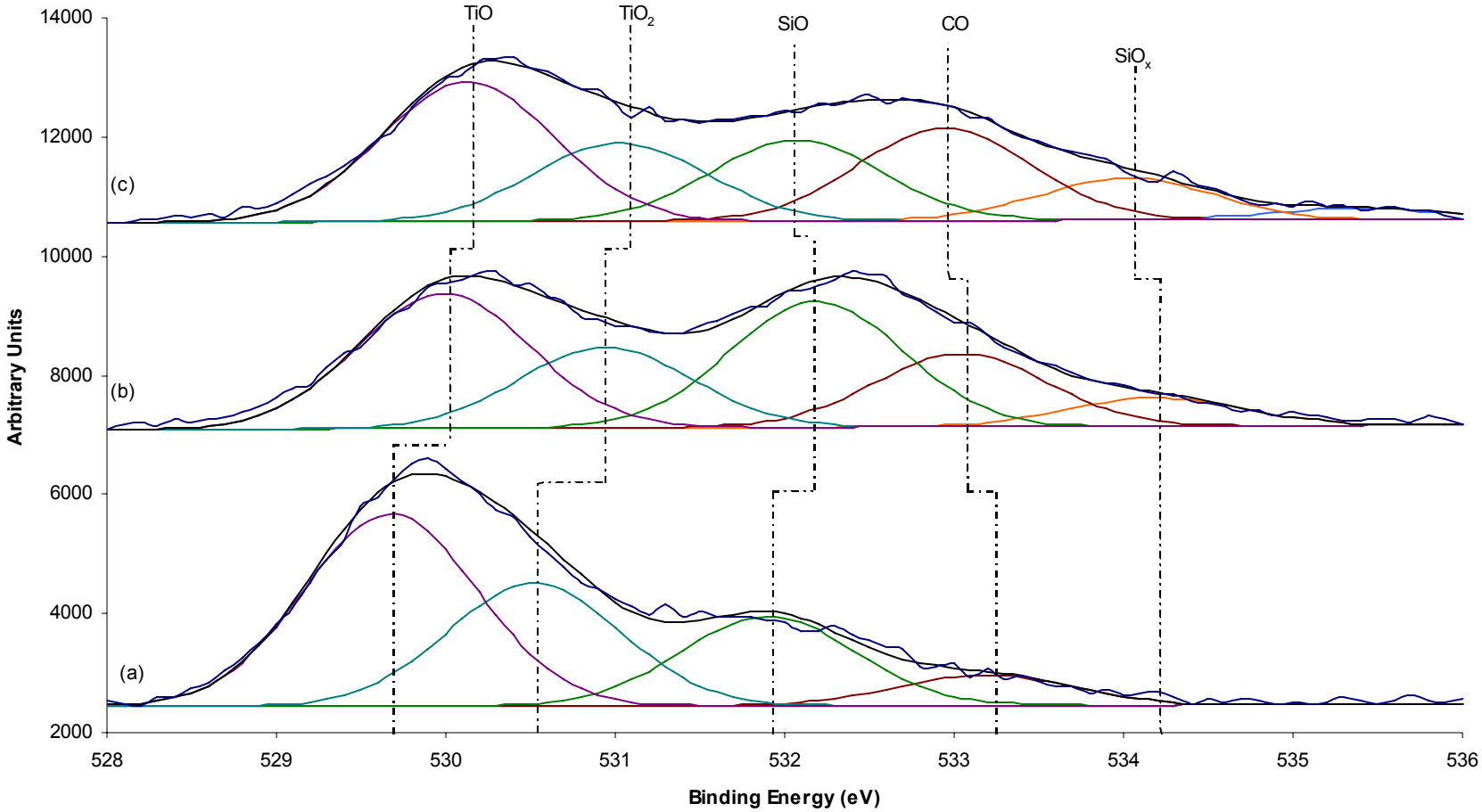

Figure 3.4. Representative oxygen high resolution scans of commercially pure titanium grade 4 after treatment.

(a) Passivated, (b) Isocyanatopropyltriethoxysilane, and (c) Gluteraldehyde.

The silicon high-resolution peak showed two forms of silicon present on the passivated metal, while a third form was added following reaction steps 1 and 2. Of the three silicon compounds present, only one compound showed any statistically significant change based on the percentage of each peak present; Si(III) was present in the highest amount on the passivated metal, while significantly decreasing following reaction step 1. However, since the SiO_x peak was missing from the passivated metal, the silicon peak area was also examined. Based on the peak area, Si(III) showed no significant change from the passivated metal through reaction steps 1 and 2. When examining the percentage, there was no significant change in the SiO peak between any of the reaction steps; however, examining the peak area did indicate a change in the SiO peak from the passivated metal to reaction step 1 followed by a change from reaction step 1 to reaction step 2. Interestingly, there was no significant change in the SiO peak when comparing the passivated metal with reaction step 2. Finally, there was no statistical difference, either in percentage or peak area, of the SiO_x peak that was present following reaction step 1. Figure 3.5 shows the differences in the silicon peaks between the different reaction steps.

Table 3.6. Silicon functional group percentages based on XPS high resolution scans.

	Si (III) [3.18]	Si-O [3.19]	SiO_x [3.20]
Reaction Step	101.6 ± 0.3 eV	102.5 ± 0.3 eV	103.5 ± 0.4 eV
Passivated	48 ± 2 %	64 ± 12[b] %	---
Silane	22 ± 8[a] %	48 ± 6[b] %	41 ± 12[c] %
Gluteraldehyde	23[a]* %	54 ± 4[b] %	63 ± 16[c] %

Values with the same superscript are not statistically different at the 5% significance level.
* Only one observation at given binding energy.

Table 3.7. Silicon functional group peak areas based on XPS high resolution scans.

	Si (III) [3.18]	Si-O [3.19]	SiO_x [3.20]
Reaction Step	101.6 ± 0.3 eV	102.5 ± 0.3 eV	103.5 ± 0.4 eV
Passivated	170 ± 0[a]	220 ± 30[b]	---
Silane	170 ± 60[a]	610 ± 120[c]	450 ± 140[d]
Gluteraldehyde	230[a]*	330 ± 30[b,c]	210 ± 30[d]

Values with the same superscript are not statistically different at the 5% significance level.
* Only one observation at given binding energy.

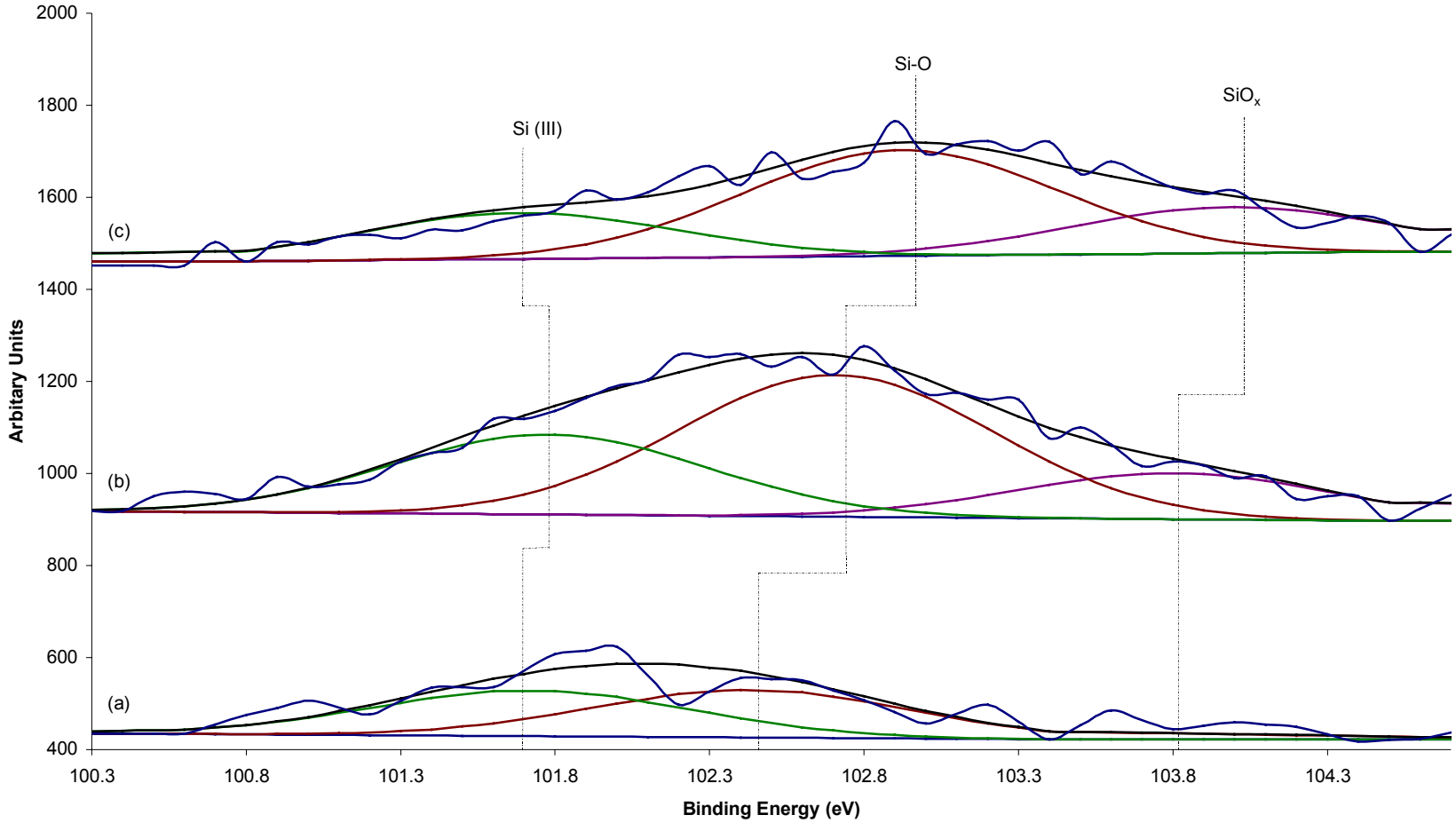

Figure 3.5. Representative silicon high resolution scans of commercially pure titanium grade 4 after treatment.

(a) Passivated, (b) Isocyanatopropyltriethoxysilane, and (c) Gluteraldehyde.

The titanium peak contained three different chemical compounds, of which only one did not vary statistically when examining the percentages. Based on percentage, TiOH, TiO and TiO_2 did not vary between the passivated metal and reaction step 1. However, when looking at reaction step 2, the TiOH peak has completely disappeared. Therefore, the titanium peak area must be examined. Based on peak area, the TiOH peak did not vary between the passivated metal and reaction step 1. However, by examining the peak area, the TiO peak did decrease significantly from the passivated metal to reaction step 1, while staying statistically the same following reaction step 2. The TiO_2 peak also decreased significantly from the passivated metal to reaction step 1; however, the TiO_2 peak then increased significantly from reaction step 1 to reaction step 2, reaching a statistically insignificant change between the passivated metal and reaction step 2. The titanium peak and the chemicals present are shown in Figure 3.6.

Table 3.8. Titanium functional group percentages based on XPS high resolution scans.

	TiOH [3.21]	**TiO [3.22]**	**TiO_2 [3.23]**
Reaction Step	457.8 ± 0.2 eV	458.7 ± 0.2 eV	459.6 ± 0.271 eV
Passivated	14 ± 3[a] %	71 ± 3[b] %	23 ± 6[c,d] %
Silane	21 ± 2[a] %	72 ± 1[b] %	15 ± 5[d] %
Gluteraldehyde	---	63 ± 6[b] %	44 ± 10[c] %

Values with the same superscript are not statistically different at the 5% significance level.

Table 3.9. Titanium functional group peak areas based on XPS high resolution scans.

	TiOH [3.21]	**TiO [3.22]**	**TiO_2 [3.23]**
Reaction Step	457.8 ± 0.2 eV	458.7 ± 0.2 eV	459.6 ± 0.3 eV
Passivated	110 ± 320[a]	4960 ± 390	1580 ± 400[c,d]
Silane	80 ± 90[a]	3400 ± 440[b]	790 ± 300[d]
Gluteraldehyde	---	3150 ± 330[b]	230 ± 680[c]

Values with the same superscript are not statistically different at the 5% significance level.

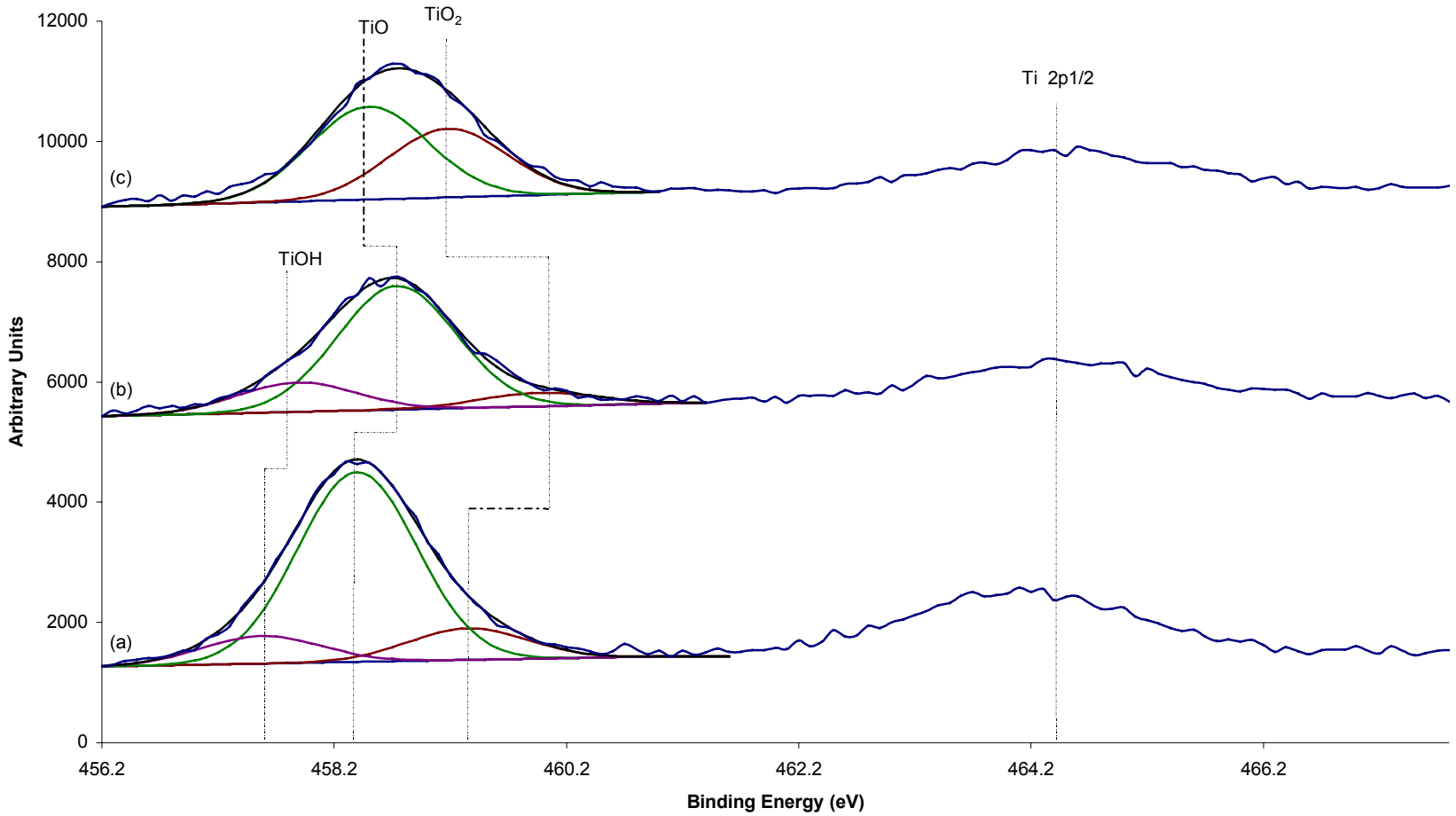

Figure 3.6. Representative titanium high resolution scans of commercially pure titanium, grade 4 after treatment.

(a) Passivated, (b) Isocyanatopropyltriethoxysilane, and (c) Gluteraldehyde.

3.4 Discussion

In the anticipated reaction pathway, the metal is first passivated and an oxide layer that covers the surface is formed. Following the passivation reaction, isocyanatopropyltriethoxysilane bonds to the titanium hydroxyl groups present on the surface of the metal; gluteraldehyde then bonds to the terminal group. Finally, the chitosan film attaches to the terminal group of the gluteraldehyde molecule. Five elements are present in the reaction and these elements should change as each step of the reaction proceeds.

XPS is a surface sensitive technique that allows a user to examine the top layers of a material. This surface analysis allows one to determine if the desired reaction is occurring in a step – wise manner. Because XPS can only penetrate the surface 5 – 100 Angstroms, certain elements will become "hidden" from the x-ray beam as the reaction occurs. Also, XPS can be used to determine the chemical compounds present, as the binding energies of the compounds are different. For example, when looking at the carbon peak on a survey scan, the binding energy appears to be 285. However, upon examining that same carbon peak using high-resolution, one can see that the carbon peak contains a range of binding energies, starting at 282.8 eV and continuing to 290.8 eV, as shown in Figure 3.2. The high-resolution peak then contains all of the compounds, which contain that element and appear within the top 5 – 100 Angstroms. Carbon, for example, contains up to five different compounds with binding energies contained with the range of 282.8 and 290.8 eV.

Using XPS, changes in the nitrogen and silicon peaks occur, as shown in Table 3.1 and Figure 3.1. However, no change occurs based on the survey scans for the carbon,

oxygen, and titanium peaks. While two elements do change based on the survey scans indicating a reaction may be proceeding, the lack of change in three of the elements is alarming. Furthermore, the chitosan films could not be examined using XPS, as the films did not stay attached in the ultra-high vacuum system. The lack of film attachment indicates that at least one reaction step is not occurring as anticipated. XPS was used to determine what reactions were occurring and where problems with the anticipated reaction pathway existed.

The bonding of films to a surface through the use of triethoxysilanes can present several major problems, two of which are the result of water in the system. Based on the Material Safety Data Sheet (MSDS), triethoxysilanes should not come in contact with water as this removes the terminal group in the form of a gas, such as hydrogen cyanide and nitrogen oxides [3.24]. Also, the presence of water combines with the triethoxysilane groups to form polysiloxanes, which do not allow the binding of the silane to the metal surface [3.25-3.27]. The third problem, and the first not related to water in the solution, is the result of the time that the metal samples spend in the silane solution during reaction step 1. A review of silane literature recommends allowing the substrate to sit in the silane solution for an extended period of time to promote the formation of a tightly packed monolayer. The procedure used placed the metal samples in the stirred silane solution for ten minutes, which did not allow for the proper formation of the silane monolayer [3.26]. A fourth problem arises based on the attraction of the terminal groups. The N = C = O group that is present on the end of isocyanatopropyltriethoxysilane may form micelles with the oxygens grouping together from either the N = C = O bonds or the O – Si bonds. These possibly formed micelles must be disrupted using sonication, which

was not performed on these samples. Without this disruption, the gluteraldehyde in reaction step 2 would be unable to reach the reactive terminal groups.

Each of the five elements present should show major changes with respect to the different chemical compounds present. These changes could be an increase or decrease in a certain compound or the conversion of one compound to a different compound. Our XPS results suggest that the reactions steps as outlined in Chapter 2, Figure 2.2 did not occur.

To begin with, a significant increase in the hydrocarbon peaks should be present if reaction steps 1 and 2 occur on the surface. Reaction step 1 introduced a propyl group, while reaction step 2 introduced a pentyl group. These two reactions should result in a net increase in the hydrocarbon group. However, no significant change was observed from the passivated metal through reaction step 2. The smaller C = O peak does increase from reaction step 1 to reaction step 2. This increase should occur as the two reaction steps proceed. During reaction step 2, the = C = O group is removed from the nitrogen present in the isocyanatopropyltriethoxysilane. Following the = C = O group's removal, the gluteraldehyde can bond to the nitrogen; the C = O peak would then increase, since the terminal group of gluteraldehyde is C = O. An increase in the C – OH peak is also seen from reaction step 1 to reaction step 2. Since gluteraldehyde is added to water, the reaction of the C = O group of gluteraldehyde to C – OH is expected. The COOH peak is present on the passivated metal, but does not appear on the surface following reaction step 1. However, the COOH peak does reappear following reaction step 2. This would indicate that the silane attempted to bond to the COOH present on the metal and was subsequently removed during reaction step 2. The COO peak does not change through

any of the reaction series. This would indicate that no reaction could take place with this group on the metal surface. The carbon peaks that should change based on the reaction include the hydrocarbon group and the C = O group. While the C = O group does change, slightly, the hydrocarbon group does not change at all.

Changes to the nitrogen surface species as measured by XPS were also not observed. Based on the anticipated reaction, the terminal group N = C = O should change to N during reaction step 2. However, as shown in Table 3.3 and Figure 3.3, no change occurs in the N = C = O group. This indicates that no reaction is occurring between isocyanatopropyltriethoxysilane and gluteraldehyde. Also, no change occurs in the N = O group between reaction steps 1 and 2. Finally, the only group that would allow for the binding of gluteraldehyde to the terminal group of the silane is CN, but that also does not change between reaction steps 1 and 2. The lack of change in the nitrogen surface species indicates that the terminal N = C = O groups still present following the addition of water do not convert to form terminal N groups following the addition of gluteraldehyde; without this conversion, no reaction can occur during reaction step 2. The few CN groups that do exist do not change following the addition of gluteraldehyde, also indicating that the anticipated reaction is not occurring.

Using data gathered from XPS, expected changes in the oxygen surface species were not observed. The TiO peak should change as the reactions occur. The passivated metal should have a small amount of TiO, which should then increase following reaction step 2, where Ti – OH is converted to TiO. After the gluteraldehyde reaction, the TiO peaks should be much smaller, as the isocyanatopropyltriethoxysilane – gluteraldehyde complex should cover the TiO signature. Instead, the TiO peak remains statistically the

same throughout the reaction series. The TiO_2 species does not change during any of the reaction steps, from the passivated metal to reaction step 1 or to reaction step 2. This is expected, as TiO_2 does not have a role to play in the binding of silane to the surface. Since TiO_2 makes up a majority of the surface, very little silane would be able to bind to the surface. The SiO peak shows a dramatic increase from the passivated metal to reaction step 1, as is expected. However, the SiO peak then shows a dramatic decrease following reaction step 2, which occurs because the silane is not properly bonded to the metal surface and micelles may also be present. The solution involved in reaction step 2 removes both the weakly bound silane and the possible micelles, thereby reducing the amount of SiO. The CO peak shows a significant increase from the passivated metal to reaction step 1. This is due to the addition of the isocyanato group from the silane. However, no change occurs between reaction step 1 and reaction step 2, due to the lack of bonding between the reactive terminal group on the silane and gluteraldehyde. Finally, the SiO_x peak shows a significant increase from the passivated metal, where it was not present, to reaction step 1. Because water is in the system, the existence of the SiO_x peak indicates that polysiloxanes may have formed. The increase between reaction steps 1 and 2 further shows that polysiloxane formation occurred as a higher amount of water was introduced into the system, in the form of the aqueous gluteraldehyde solution.

The silicon peaks should show the most dramatic changes through the entire reaction series and give a strong indication of the actual surface chemistry. The survey scans, as shown in Table 3.1 and Figure 3.1, show change occurring in the amount of silicon present following reaction step 1. However, the survey scan indicates that following reaction step 2, the amount of silicon is the same for both the passivated metal

and reaction step 2. This drop in silicon is possibly due to the micelle formation surrounding the N = C = O groups. Once the metals were added to the solution for reaction step 2, and stirring took place, if micelles were present, they were broken up, removing large quantities of the silicon that was present. Since this took place in water, the removal of the terminal groups was also possible. Si(III) is the major peak of silicon present on the passivated metal and is due to the silicon dioxide sand paper used for polishing. Si(III) remains unchanged as a function of peak area, which indicates that the Si(III) is not removed in any of the reaction steps. SiO does vary from the passivated metal to reaction step 1 and from reaction step 2 to reaction step 3. However, the passivated metal and reaction step 2 are considered statistically equivalent. The SiO present following passivation is the result of the silicon from the sand paper reacting with one of the solvents used in the passivation of the metal. The SiO present from reaction step 1 is the result of the triethoxysilane groups present in isocyanatopropyltriethoxysilane, while the SiO groups present following reaction step 2 is the result of the lack of binding between the N group of the isocyanatopropyltriethoxysilane and gluteraldehyde. SiO_x, which is present following both reaction steps 1 and 2, is the result of the triethoxysilane groups reacting with water to form polysiloxanes. Since these groups will react with themselves, the removal of the isocyanatopropyl group can occur. These groups then react with the titanium substrate, forming a polysiloxane layer without the ability to bind gluteraldehyde.

The titanium peak should show a statistically significant decrease through each step of the reaction series and would indicate that a film is growing on the surface. Because XPS can only reach a depth of up to 100 Angstroms, the titanium peak would be

reduced as reaction step 1 followed by reaction step 2 created the gluteraldehyde – isocyanatopropyltriethoxysilane – titanium complex. Since no change is seen in the survey scans, there are strong indications that only a very small reaction is occurring, if, in fact, a reaction is actually occurring. When looking at the high-resolution scan results, one sees a very small amount of Ti – OH present. Since reaction step 1 requires an OH ending group to bond the silane, this is the first step to the reaction. Without a large amount of Ti – OH present, only a small silanation reaction could occur. Following the silanation reaction, the same amount of Ti – OH is present, which indicates that only a slight reaction occurred, as the Ti – OH group would be converted to TiO. The TiO peak, according the percentage, is not changed through any of the reaction series. However, the peak area does indicate that the TiO peak is the largest for the passivated metal. The TiO peak is statistically the same for reaction steps 1 and 2. If a major reaction was occurring, the TiO peak should be much larger following reaction step 1, and would almost disappear following reaction step 2, as the peak would be fully covered by the two reactions. The TiO_2 peak is present due to the passivation of the metal surface and is one of several peaks that form the passive oxide layer, a desirable quality for implant quality metals. While the TiO_2 peak is reduced following reaction step 1, the peak returns to the statistically identical percentage as the passivated metal following reaction step 2, suggesting that reaction step 2 removed the isocyanatopropyltriethoxysilane that was loosely attached to TiO_2.

3.5 XPS Supported Surface Reaction

The analysis of the data gathered from XPS indicates that the anticipated reaction pathway is not occurring. The lack of Ti – OH on the surface of the substrate was the first indication that a problem may occur with the reaction. Since the isocyanatopropyltriethoxysilane could not bond in large amounts to the metal, there could be no further film growth. During reaction step 1, small amounts of isocyanatopropyltriethoxysilane would bind with the small amounts of Ti – OH present. Water in the silane solution also created two problems. The water reacted with both the reactive terminal group, releasing it as a gas, and with the triethoxysilane part of the molecule, causing the formation of polysiloxanes. During reaction step 1, the terminal groups were removed and polysiloxanes were formed. Finally, the possible formation of micelles could be a major problem when using this method from previous research. The possible formation of micelles prevented gluteraldehyde from reaching the reactive terminal group, if it was still present, and thereby prevented a further reaction. During reaction step 1, micelles may have been formed. During reaction step 2, the possible micelles were removed, due to the stirring of the solution. Figure 3.7 shows the proposed surface chemistry following reaction steps 1 and 2, based on the XPS data.

As one can see in Figure 3.7, there are very few open oxygens. Without the oxygens available, the chitosan molecule cannot bind to the surface; the resulting chitosan film could easily be removed when any stress, such as ultra-high vacuum, was applied.

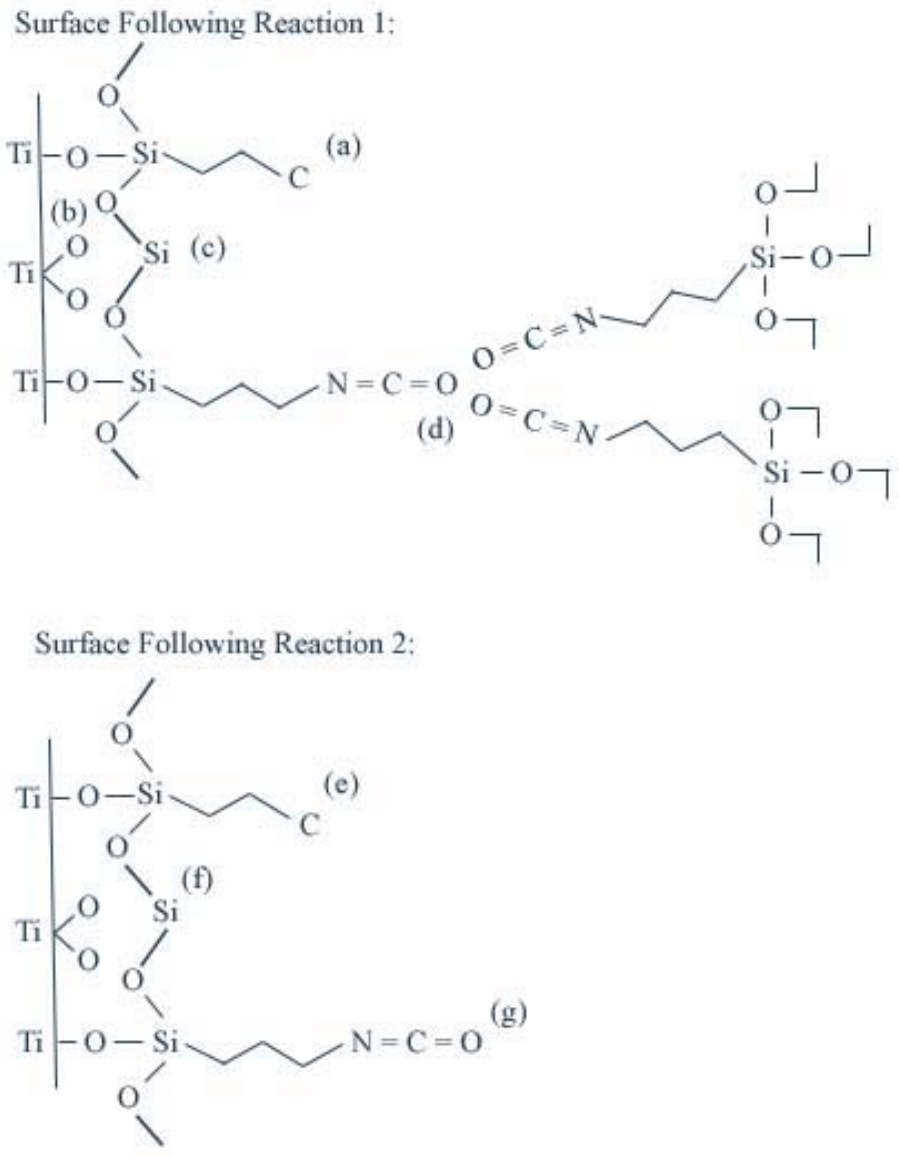

Figure 3.7. XPS supported surface chemistry.

The surface following reaction 1 demonstrates the four major features present: (a) the removal of the terminal group, (b) the presence of TiO_2, (c) the creation of polysiloxanes, and (d) the possible formation of micelles.

The surface following reaction 2 demonstrates the inability of gluteraldehyde to bond to the silane molecule because of (e) the removal of the terminal group, (f) the creation of polysiloxanes, and (g) the presence of the N = C = O group, with the removal of polysiloxanes.

3.6 Summary

Based on the XPS data, the theoretical reactions did not occur. Several problems need to be addressed in order to produce the best quality film possible. The problems include a lack of Ti – OH groups, removal of the reactive terminal groups, formation of polysiloxanes, an inability to form a silane monolayer, possible formation of silane micelles, and failure to remove the = C = O group, which does not allow the gluteraldehyde to bond to the nitrogen group.

In order to address the lack of Ti – OH groups, the surface needs to be treated in a manner that allows the creation of Ti – OH. Currently, passivation is the method to treat the metal surface, which promotes the formation of a passive oxide layer and includes TiO, TiO_2, and Ti_2O_3. Two of these three titanium oxide complexes are extremely stable and do not react. A metal treatment, such as the use of piranha, needs to be investigated as a means to increase the amount of Ti – OH groups present on the surface of the metal.

The formation of polysiloxanes, removal of the terminal group, and inability to form a silane monolayer can easily be addressed by the type of solution used and the amount of time during which the samples are left in the silane solution. Instead of using water as part of the silane solution, an organic solvent, such as toluene, is commonly used in silanation reactions [3.5 – 3.7]. The removal of water, in the form of a different solvent, will help prevent the formation of polysiloxanes and the removal of the terminal group. It also allows the formation of a silane monolayer, as no competition for the triethoxysilane groups occurs. Also, by increasing the time from ten minutes to twenty – four hours, the chance to form a silane monolayer greatly increases.

The fifth problem that needs to be addressed is the possible formation of micelles. The previous research was performed without using sonication, so if micelles were present, they were not removed or were removed during reaction step 2, which would not allow for that reaction step to occur. By sonicating the samples multiple times in a clean solvent, the micelles, which may have formed, would be disrupted.

Finally, the last problem to be addressed is the selection and use of the correct silane. Since isocyanatopropyltriethoxysilane has an additional = C = O that prevents the nitrogen group from bonding with the gluteraldehyde group, it is recommended that a silane be chosen which removes the extraneous = C = O. Aminopropyltriethoxysilane is commonly used in biomedical studies [3.25 – 3.27] and should serve well for this research. Also, another silane should be chosen which removes the linker molecule. The linker molecule provides for a longer chain, which could more easily be broken by stressing the surface. Triethoxsilylbutyraldehyde is a silane that has a terminal aldehyde group, which is the same group created by adding gluteraldehyde to the aminopropyltriethoxysilane group. These two silanes, combined with the other recommendations, should improve the adhesion and quality of the chitosan films on the titanium surface.

CHAPTER IV

CHEMICAL ANALYSIS OF THE FOUR TREATMENT COMBINATIONS

4.1 Introduction

One major issue with the isocyanatopropyltriethoxysilane reaction was the inability of the chitosan films to remain bonded to the implant metal when subjected to a vacuum. In order to improve the adhesion of the film to the metal, several changes where made, which resulted in four treatment combinations. The samples after each of the treatment combinations were examined using X-Ray Photoelectron Spectroscopy (XPS) and the results were analyzed to determine the statistical similarities and differences between the similar treatment combinations.

4.2 Anticipated Surface Reactions

In order to determine the best method to bond chitosan to commercially pure titanium, four treatment combinations were created, utilizing one of two metal treatments and one of two silane treatments. The metal treatment protocol was given in Chapter 2, Section 3.2, while the silane protocol was given in Chapter 2, Sections 3.3.2 – 3.3.3. For each reaction step, three samples per metal treatment and three spots per sample were examined and the statistical analysis was performed using completely randomized design with subsampling. The chitosan films were examined using three samples per treatment

and three spots per sample; the statistical analysis was performed using a 2^2 factorial arrangement of treatments with subsampling.

Changes in the amount of several chemical species on the reaction surfaces will indicate that the reactions are proceeding as anticipated. In order to bond silane molecules to the titanium surface, the presence of the highly reactive TiO species on the metal surface is preferred; the presence of the non-reactive TiO_2 is not desired. Following the reaction between the silane molecule and the titanium surface, a decrease in the presence of TiO is expected. This occurs because the silane molecule binds to the TiO and less of the titanium is now being probed due to the over-lying silane layer, preventing the release and detection of photoelectrons.

The presence of any silicon – oxygen compounds following the reaction between the silane molecule and titanium surface is advantageous, as this shows that the silane did bind to the metal surface. The presence of SiO indicates that the Si – O – C bond present in the silane is still occurring following the reaction with the surface, while the presence of SiO_3 indicates that the silane molecules are reacting with adjacent silane molecules to form a polysiloxane group that helps stabilize the silane molecules.

The presence of terminal end groups is also expected and based on the silane used, clear differences between the types of silanes should be seen. The aminopropyltriethoxysilane should produce a terminal group with nitrogen present, specifically a group containing C – N – H. The presence of this group would indicate that the silane molecule is binding to the titanium surface correctly, and that any micelles possibly formed during silane deposition are not present. The triethoxsilylbutyraldehyde compound should produce a terminal group with oxygen present, so an increase in the

oxygen content following deposition should occur. This increase should be seen in an increase of the C = O peak, from the aldehyde terminal group, and possibly the COOH peak, since the aldehyde could react with the ethanol used to rinse toluene off the metal surface. Therefore, changes in the amounts of TiO, SiO, SiO_3, C – N – H, C = O, and COOH will allow us to determine if the reactions are occurring as anticipated.

If the metal treatments do not affect the chemical structure of the chitosan chains, the chemical analysis of the chitosan films should be significantly similar, as chitosan films are produced using powder with the same degree of deacetylation. Small differences between the carbon, nitrogen, oxygen, and silicon peaks should be seen, as this would determine the arrangement of the chains in the chitosan films.

4.3 Results

The results for this chapter are divided into several different groups. To begin with, the two metal treatments were examined to determine if the surface composition changed as a result of the passivation or piranha treatment. Each of the silane reactions were examined based on metal treatment and on the reaction series. Finally, the chitosan films were examined based on reaction series, metal treatment, and silane treatment.

4.3.1 Metal Treatments

The means and standard deviations from the survey scans of the metal treatments are shown in Table 4.1. There were no statistical similarities when looking at the metal surface treated by either the passivation protocol or the piranha protocol. The carbon peak was much larger for the passivated peak as compared to the piranha peak, with values of 65 ± 3 % and 40 ± 2 % respectively. The oxygen peak was also dramatically

different, with values of 30 ± 2 % and 45 ± 1 % for passivated and piranha treated metals, respectively. Finally, the titanium peak was noticeably larger for the piranha treated metals, with a value of 15 ± 2 %, as compared to 6 ± 2 % for the passivated metal. Figure 4.1 shows the representative survey scans of the passivated metal compared to the piranha treated metal.

Table 4.1. Elemental percentage based on XPS survey scans of the metal treatments.

Metal Treatment	**Carbon**	**Oxygen**	**Titanium**
Passivated	65 ± 3 %	30 ± 2 %	6 ± 2%
Piranha	40 ± 2 %	45 ± 1 %	15 ± 2 %

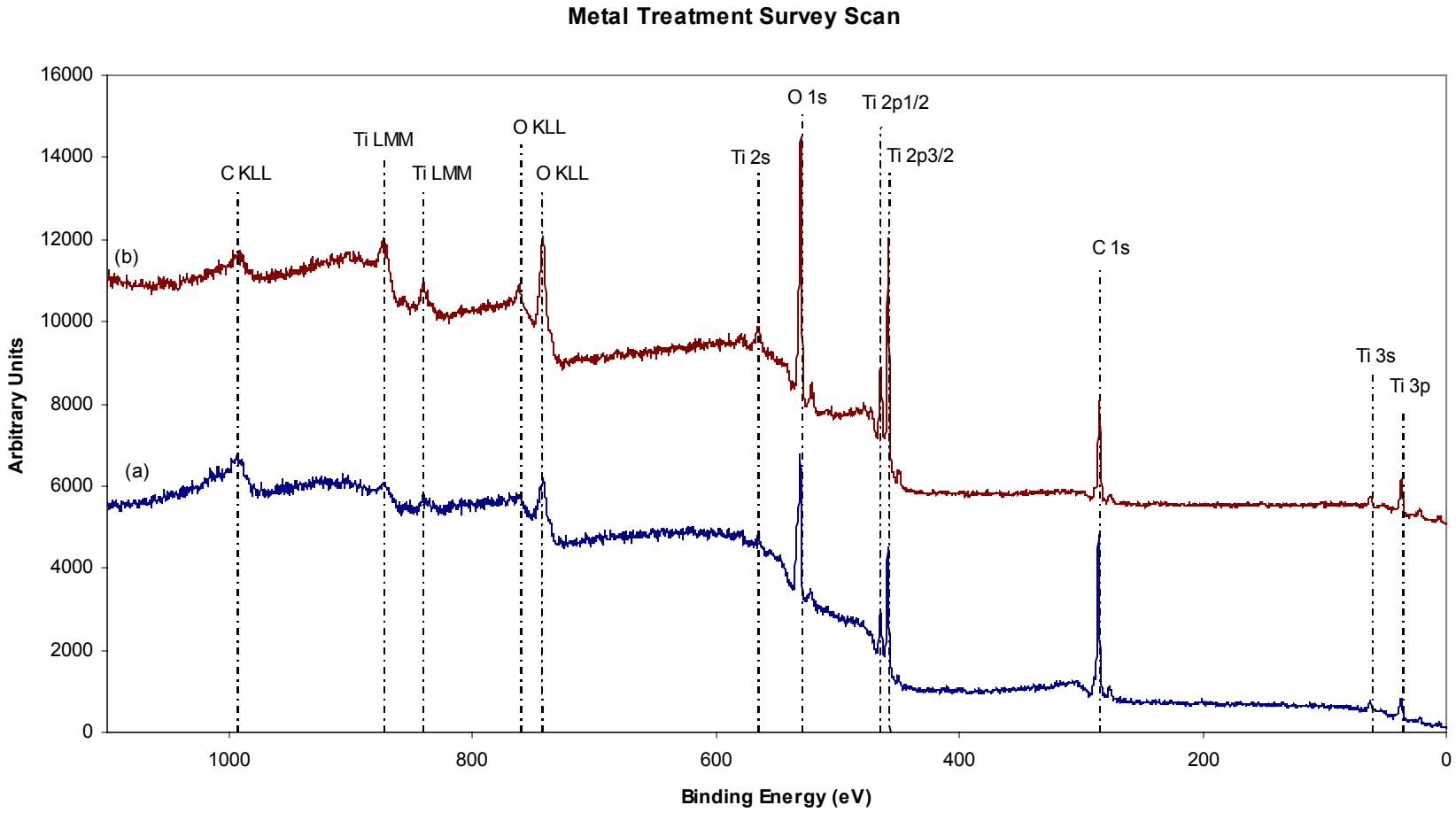

Figure 4.1. Representative survey scans of commercially pure titanium grade 4.

The passivated treatment is labeled (a), while the piranha treatment is labeled (b).

The means and standard deviations from the high resolution scans are shown in Tables 4.2 – 4.4. Table 4.2 shows the peak areas of the four peaks present on both metal treated surfaces as determined from the carbon high resolution scans. There were no statistical similarities for any of the four carbon peaks, with the peak areas on the passivated metal being substantially larger than the peak areas on the piranha metal. Figure 4.2 illustrates the differences in peak areas between the piranha treated and passivated metal surface.

Table 4.3 shows the peak areas of the four peaks present on both metal treated surfaces as determined from the oxygen high resolution scans. Only the C – O peak was not statistically different for the two metal treatments, with values of 2160 ± 290 per unit area for the passivated metal and 2120 ± 350 per unit area for the piranha treated metal. The remaining four peaks were all significantly different based on the metal treatment. TiO and – OH peaks were significantly higher on the piranha treated metal as compared with the passivated metal; peak areas for the TiO and the – OH peaks for the piranha treated metal were more than twice the peak areas of the passivated metal. The $-(OH)_3^{-3}$ peak area on the passivated metal was twice the peak area of the piranha treated metal, while C = O peak was only present on the passivated metal. The differences in oxygen peaks are graphically illustrated in Figure 4.3.

Table 4.4 shows the peak areas of the three peaks present on both metal treated surfaces as determined from the titanium high resolution scans. Only the TiO_2 peak was statistically similar between the two treatments, with values of 1060 ± 150 per unit area for the passivated metal compared with 1010 ± 350 per unit area for the piranha treated metal. The TiO peak area of the piranha treated metal was almost twice the TiO peak

area of the passivated metal, with values of 6860 ± 460 per unit area and 2640 ± 560 per unit area, respectively. There was also a significant difference in the peak area of TiC, with values of 430 per unit area for the passivated metal and 750 ± 170 per unit area for the piranha treated metal. Figure 4.4 illustrates the differences in the peak areas of the titanium peaks.

By looking at the XPS results from the different metal treatments, the piranha treatment significantly decreased the amount of carbon present. It also significantly increased the amount of oxygen and titanium present, both of which are needed for the silane molecule to bind to the titanium surface.

Table 4.2. Carbon functional group peak areas based on XPS high resolution scans of metal treatments.

	C [4.1]	C-C [4.2]	C-O [4.3]	COOH [4.4]
Metal Treatment	284.8 ± 0.1 eV	285.7 ± 0.1 eV	287.0 ± 0.2 eV	289.3 ± 0.1 eV
Passivated	1590 ± 640[a]	4140 ± 300	1350 ± 250	590 ± 50
Piranha	1270 ± 270[a]	2590 ± 230	670 ± 60	370 ± 30

Values with the same superscript are not statistically different at the 5% significance level.

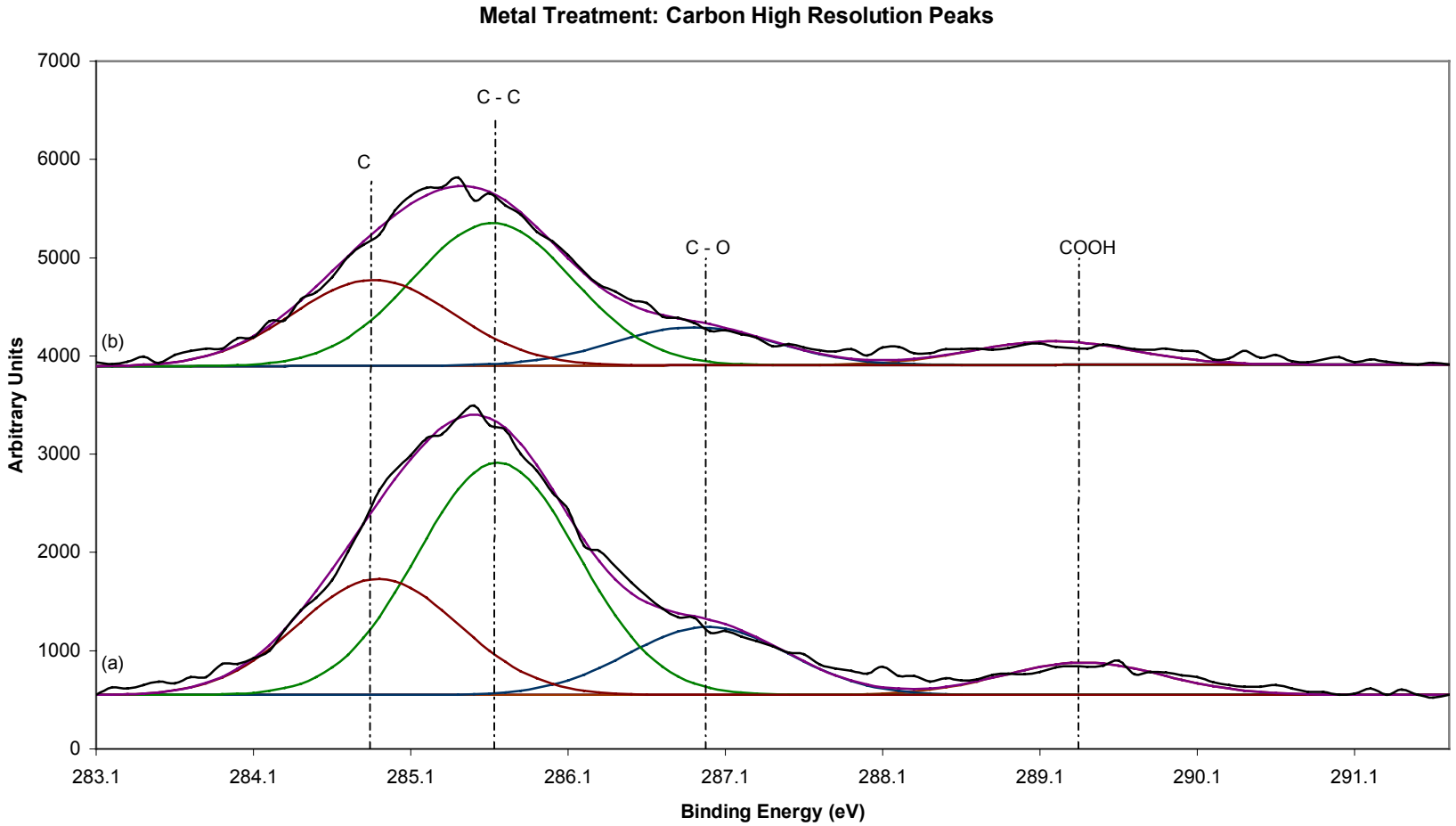

Figure 4.2. Representative carbon high resolution scans of commercially pure titanium.

The passivated treatment is labeled (a), while the piranha treatment is labeled (b).

Table 4.3. Oxygen functional group peak areas based on XPS high resolution scans of metal treatments.

	TiO [4.12]	-OH [4.13]	C-O [4.14]	$-(OH)_3^{-3}$ [4.15]	C=O [4.16]
Metal Treatment	530.4 ± 0.1eV	531.4± 0.1eV	532.6± 0.1 eV	533.7 ± 0.1 eV	534.9 ± 0.1 eV
Passivated	3330 ± 790	190 ± 200	2160 ± 290[a]	1650 ± 270	570 ± 130
Piranha	6970 ± 250	380 ± 350	2120 ± 350[a]	850 ± 40	---

Values with the same superscript are not statistically different at the 5% significance level.

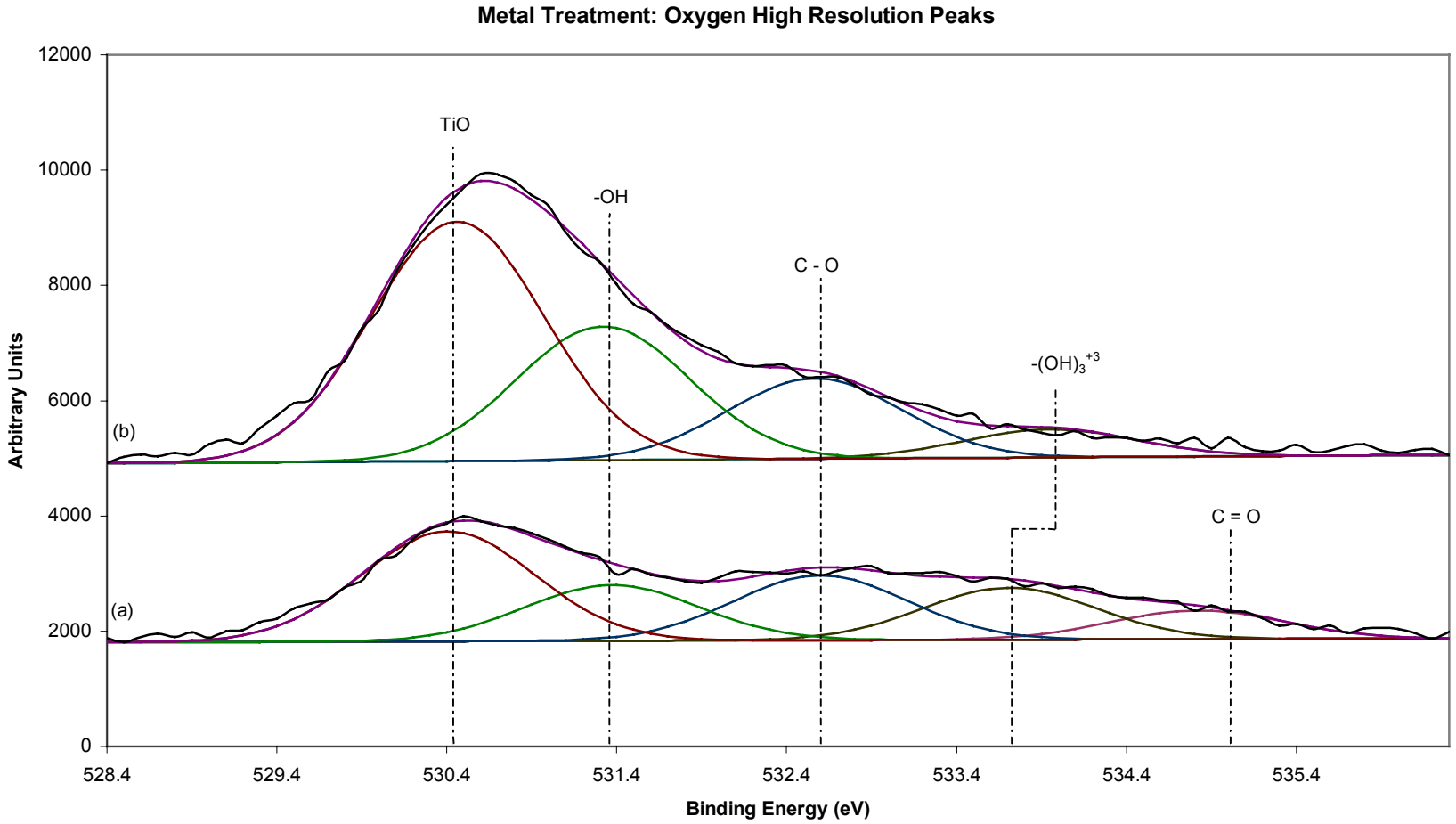

Figure 4.3. Representative oxygen high resolution scans of commercially pure titanium.

The passivated treatment is labeled (a), while the piranha treatment is labeled (b).

Table 4.4. Titanium functional group peak areas based on XPS high resolution scans of metal treatments.

	TiO_2 [4.23]	TiO [4.24]	TiC [4.25]
Metal Treatment	458.4 ± 0.2 eV	459.2 ± 0.1 eV	460.3 ± 0.2 eV
Passivated	1060 ± 150[a]	2640 ± 560	430
Piranha	1010 ± 350[a]	6860 ± 460	750 ± 170

Values with the same superscript are not statistically different at the 5% significance level.
*Only one observation at given binding energy.

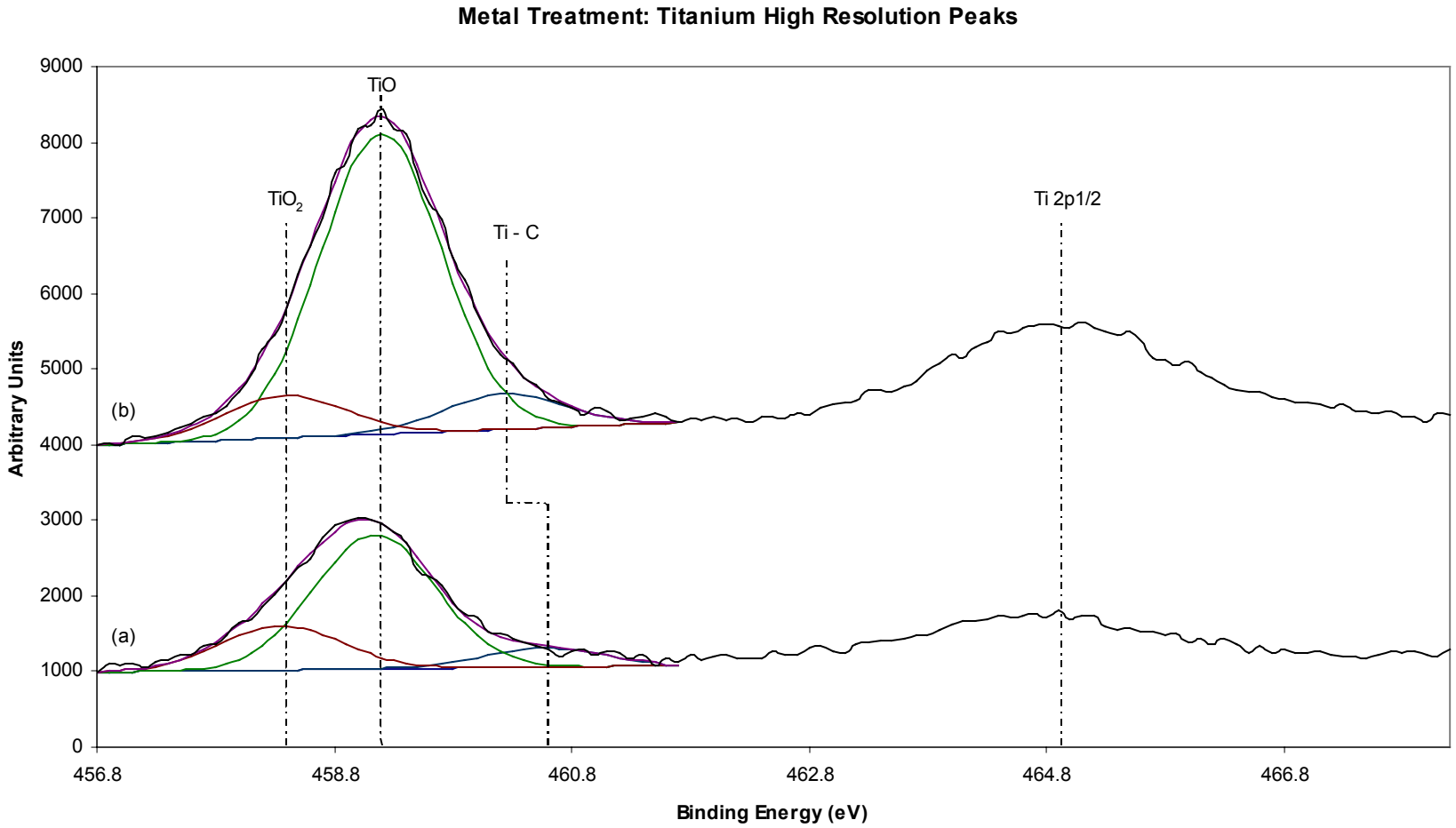

Figure 4.4. Representative titanium high resolution scans of commercially pure titanium.

The passivated treatment is labeled (a), while the piranha treatment is labeled (b).

4.3.2 Aminopropyltriethoxysilane Results

Two of the four treatment combinations involved aminopropyltriethoxysilane (Amino); the results produced were compared in two different methods. The first method was to compare each of the metal treatments with respect to each reaction step, while the second method compared each step of the reaction with respect to the metal treatment. The chitosan comparison will be performed in Section 4.3.4.

4.3.2.1 Silane Reaction Step 1a: Comparing Metal Treatments

The percentage means and standard deviations calculated from the survey scans of the two metal treatments for the first reaction step are shown in Table 4.5. The nitrogen and titanium percentages were the only two values that are statistically different. The nitrogen percentage was smaller for the passivated step than for the piranha step, with amounts of 7 ± 1 % and 8 ± 1% respectively, while the titanium percentage was larger for the passivated step than for the piranha step, with amounts of 2 ± 1 % and 1 ± 1 % respectively.

The peak area means and standard deviations calculated from the survey scans of the two metal treatments for the first reaction step are shown in Table 4.6. Unlike the percentages table, the carbon and silicon peak areas were statistically different; the nitrogen and titanium peak areas remained statistically different. The piranha treatment resulted in higher peak areas of carbon, nitrogen, and silicon and a lower peak area of titanium than the passivated metal treatment. Figure 4.5 illustrates representative survey scans of the passivated metal and piranha treated metal for the first reaction step.

Table 4.5. Elemental percentages based on XPS survey scans of the amino treatments, silane step (reaction step 1a).

Metal Treatment	Carbon	Oxygen	Nitrogen	Silicon	Titanium
Passivated	52 ± 3^{a} %	26 ± 3^{b} %	7 ± 1 %	13 ± 2^{c} %	2 ± 1 %
Piranha	54 ± 1^{a} %	22 ± 1^{b} %	8 ± 1 %	14 ± 1^{c} %	1 ± 1 %

Values with the same superscript are not statistically different at the 5% significance level.

Table 4.6. Elemental peak areas based on XPS survey scans of the amino treatments, silane step (reaction step 1a).

Metal Treatment	Carbon	Oxygen	Nitrogen	Silicon	Titanium
Passivated	17320 ± 1000	21450 ± 2400[a]	3790 ± 560	3910 ± 560	5350 ± 2060
Piranha	20380 ± 380	20600 ± 650[a]	5050 ± 480	4870 ± 260	2370 ± 1180

Values with the same superscript are not statistically different at the 5% significance level.

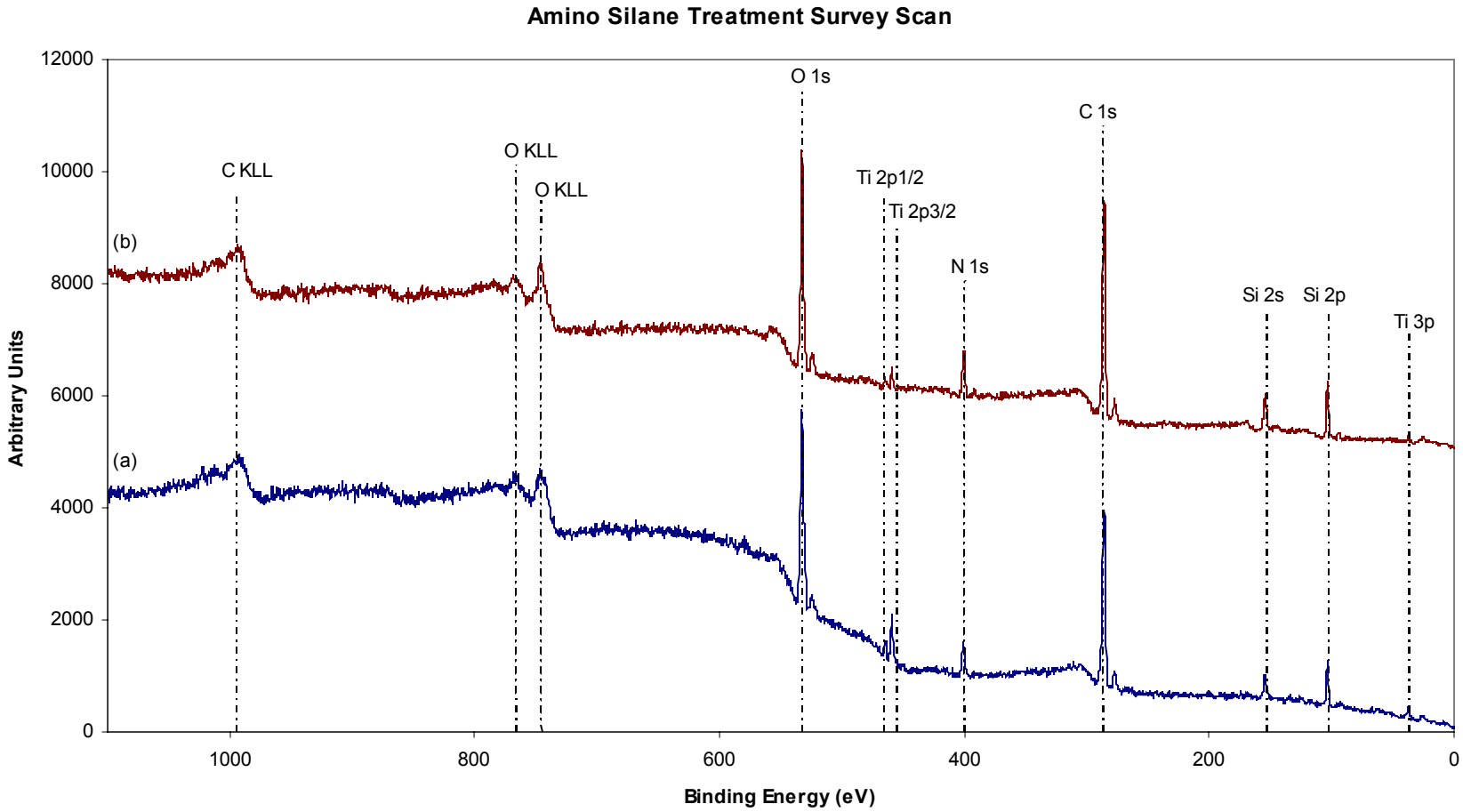

Figure 4.5. Representative survey scans of the amino treatment, silane step, on the two metal treatments.

The passivated treatment is labeled (a), while the piranha treatment is labeled (b).

The means and standard deviations of the high resolutions scans are shown in Tables 4.7 – 4.11. Table 4.7 shows the peak areas of the five peaks present on both metal treated surfaces as determined from the carbon high resolution scans. Only two of the five peaks were statistically different, while the peaks indicative of C – C, C = O, and N – C showed no statistical differences. The peaks indicative of C – O and C – N – H were statistically different; the piranha treatment had higher peak areas of 3890 ± 340 per unit area for C – O and 1610 ± 260 per unit area for C – N - H, while the passivated treatments had lower peak areas of 2940 ± 470 per unit area for C – O and 1220 ± 240 per unit area for C – N – H. Figure 4.6 illustrates the difference in peak areas of the surface following the silanation step on each of the two metal treatments.

The means and standard deviations calculated from the high resolution scans of oxygen are shown in Table 4.8. Five peaks were present on both metal surfaces; only two of the five peaks were statistically different. The peaks identified as TiO and SiO_2 were significantly different, with the piranha treated surface having lower peak areas of both peaks as compared to the passivated surface. The differences between the two surfaces are illustrated in Figure 4.7.

Table 4.9 contains the means and standard deviations from the high resolution scans of nitrogen. Three peaks were present on both of the metal treatments, while the last peak, identified as NO_2, was only present on the passivated surface. Only the peak identified as NH_4^+ was statistically similar; the other two peaks, N – C and C – N – H, were statistically higher on the piranha treated surface than on the passivated surface. Figure 4.8 shows the high resolution peak area differences of the nitrogen peak between the two metal surfaces.

The means and standard deviations of the high resolution scans of silicon are listed in Table 4.10. Two peaks were present on both treatment surfaces, while one additional peak, SiO_2, was present on the piranha treated surface. The two peaks identified were statistically different; the piranha treated surface had a much lower peak area of SiO than the passivated surface, while the piranha treated surface had a much higher peak area of SiO_3 than the passivated surface. The peak area differences between the two metal surfaces are shown graphically in Figure 4.9.

The titanium means and standard deviations from the high resolution scans are shown in Table 4.11. Three peaks were present, but only one peak, TiO, was present on both surfaces. TiO_2 was only present on the passivated surface, while Ti – C was present only on the piranha treated surface. The one peak present on both surfaces, TiO, was statistically different, with the peak area on the piranha treated surface significantly less than the peak area on the passivated surface. Figure 4.10 shows the titanium peaks on the two metal surfaces.

After examining the different high resolution peaks, it appeared that more amino silane was bound per unit area by the piranha treated surface than by the passivated surface. The more numerous amino silane molecules present on the piranha treated surface were most strongly demonstrated by the significantly lower amount of TiO, the significantly higher amount of C – N – H, and the significantly higher amounts of SiO, SiO_2, and SiO_3.

Table 4.7. Carbon functional group peak areas based on XPS high resolution scans of the amino treatments, silane step (reaction step 1a).

	C-C [4.2]	C-O [4.3]	C-N-H [4.9]	C=O [4.10]	N-C [4.11]
Metal Treatment	285.4 ± 0.1 eV	286.3 ± 0.1 eV	287.4 ± 0.2 eV	288.7 ± 0.3 eV	289.9 ± 0.4 eV
Passivated	2420 ± 670[a]	2940 ± 470	1220 ± 240	390 ± 80[b]	210 ± 30[c]
Piranha	2240 ± 610[a]	3890 ± 340	1610 ± 260	450 ± 80[b]	260 ± 80[c]

Values with the same superscript are not statistically different at the 5% significance level.

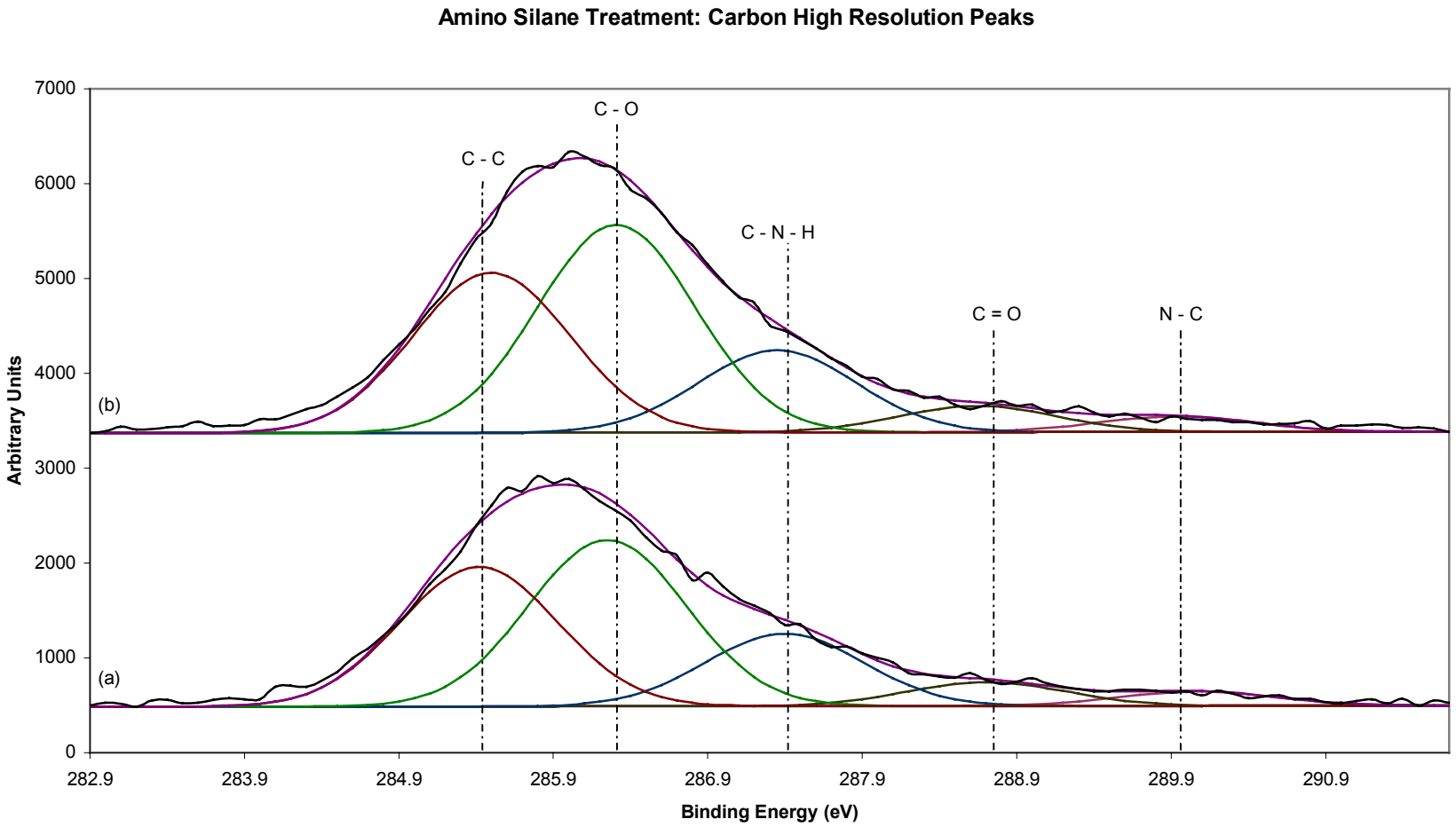

Figure 4.6. Representative carbon high resolution scans of the amino treatment, silane step, on the two metal treatments. The passivated treatment is labeled (a), while the piranha treatment is labeled (b).

Table 4.8. Oxygen functional group peak areas based on XPS high resolution scans of the amino treatments, silane step (reaction step 1a).

	TiO [4.12]	**SiO [4.17]**	**SiO_x [4.18]**	**SiO_2 [4.19]**	**NO [4.22]**
Metal Treatment	530.5 ± 0.1 eV	531.6 ± 0.2 eV	532.8 ± 0.2 eV	533.6 ± 0.1 eV	534.8 ± 0.2 eV
Passivated	1370 ± 300	1190 ± 230[a]	2900 ± 420[b]	2790 ± 550	610 ± 120[c]
Piranha	600 ± 200	890 ± 210[a]	2500 ± 450[b]	3960 ± 480	730 ± 300[c]

Values with the same superscript are not statistically different at the 5% significance level.

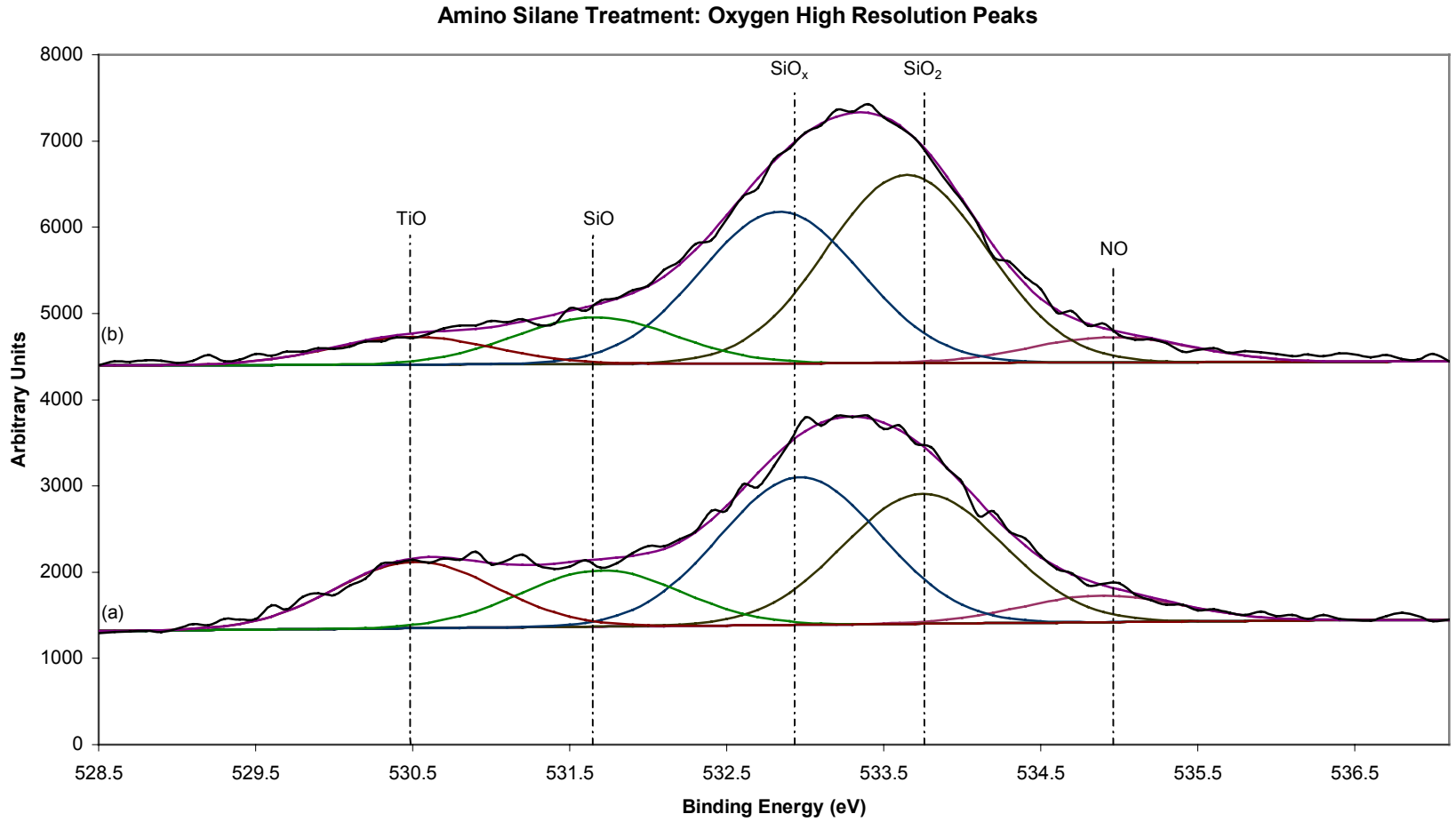

Figure 4.7. Representative oxygen high resolution scans of the amino treatment, silane step, on the two metal treatments. The passivated treatment is labeled (a), while the piranha treatment is labeled (b).

Table 4.9. Nitrogen functional group peak areas based on XPS high resolution scans of the amino treatments, silane step (reaction step 1a).

	N-C [4.32]	C-N-H [4.33]	NH_4^+ [4.34]	NO_2^- [4.35]
Metal Treatment	399.6 ± 0.2 eV	400.7 ± 0.2 eV	401.9 ± 0.2 eV	403.2 ± 0.3 eV
Passivated	400 ± 90	650 ± 90	450 ± 70[a]	190 ± 20
Piranha	660 ± 60	950 ± 100	440 ± 50[a]	---

Values with the same superscript are not statistically different at the 5% significance level.

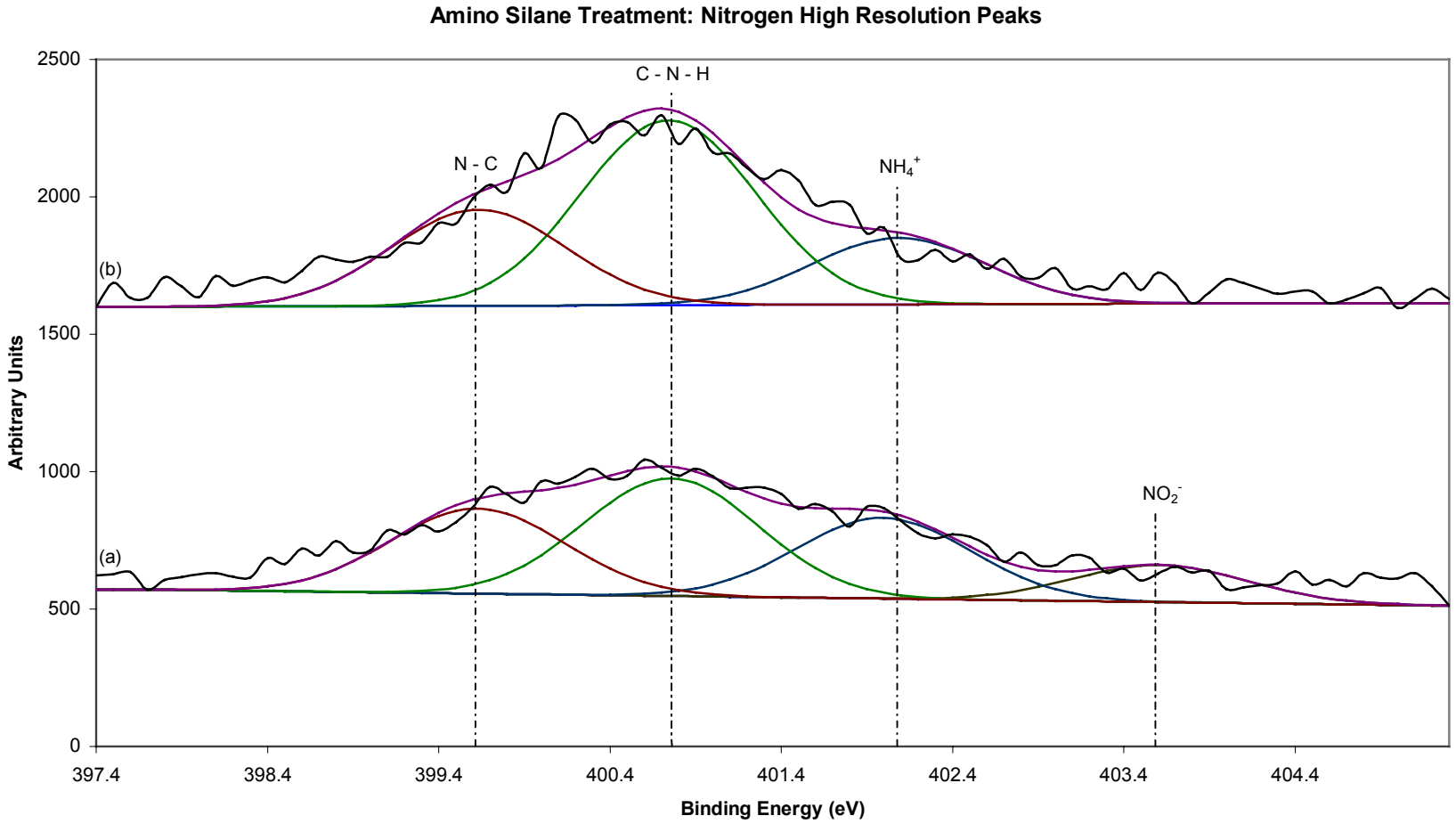

Figure 4.8. Representative nitrogen high resolution scans of the amino treatment, silane step, on the two metal treatments. The passivated treatment is labeled (a), while the piranha treatment is labeled (b).

Table 4.10. Silicon functional group peak areas based on XPS high resolution scans of the amino treatments, silane step (reaction step 1a).

	SiO [4.28]	**SiO_3 [4.29]**	**SiO_2 [4.30]**
Metal Treatment	102.9 ± 0.3 eV	103.8 ± 0.3 eV	104.5 ± 0.1 eV
Passivated	740 ± 140	670 ± 140	---
Piranha	420 ± 130	1150 ± 60	390 ± 60

Values with the same superscript are not statistically different at the 5% significance level.

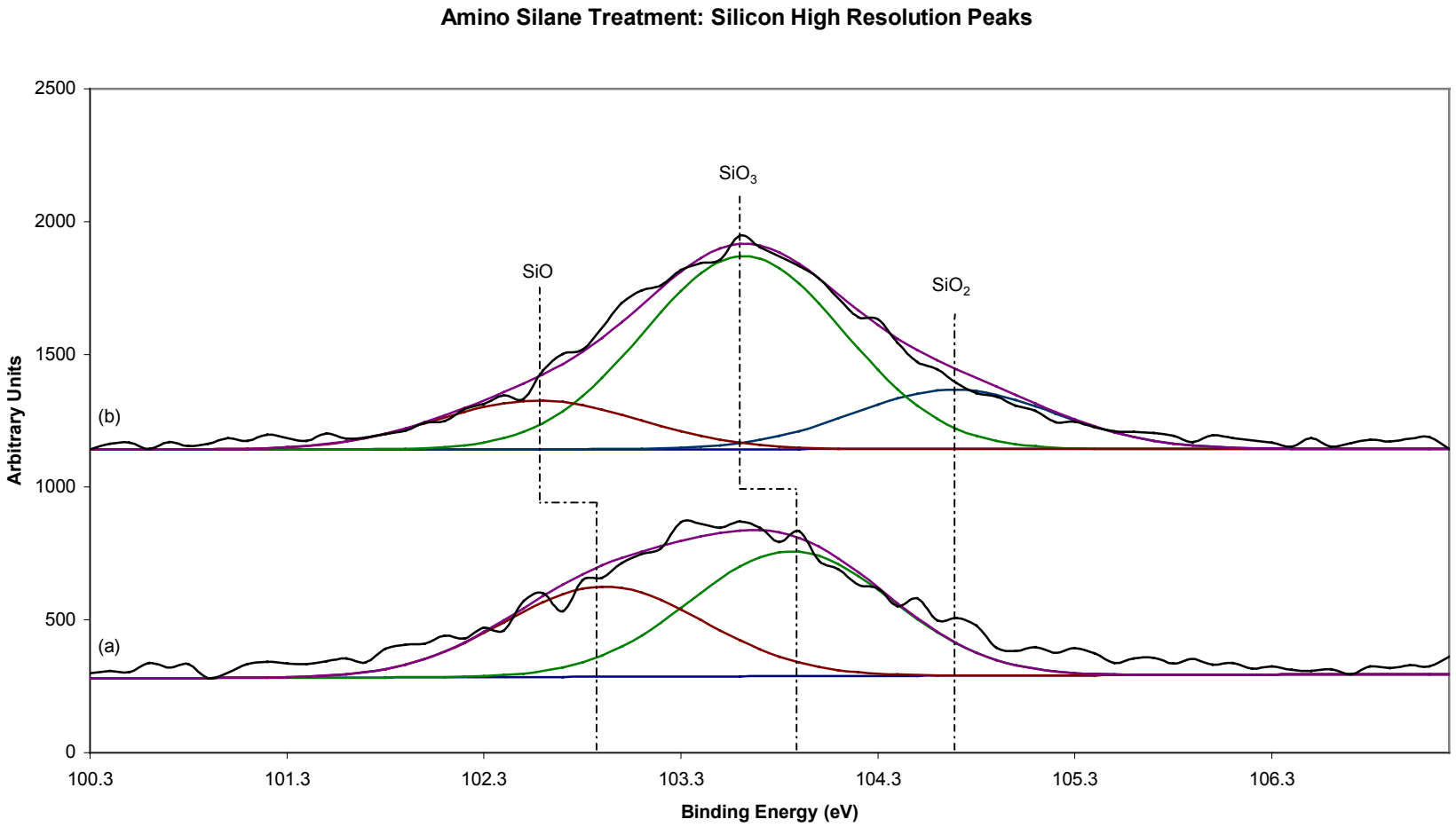

Figure 4.9. Representative silicon high resolution scans of the amino treatment, silane step, on the two metal treatments. The passivated treatment is labeled (a), while the piranha treatment is labeled (b).

Table 4.11. Titanium functional group peak areas based on XPS high resolution scans of the amino treatments, silane step (reaction step 1a).

	TiO_2 [4.23]	TiO [4.24]	TiC [4.25]
Metal Treatment	458.7 ± 0.2 eV	459.6 ± 0.2 eV	460.4 ± 0.1 eV
Passivated	830 ± 390	750 ± 160	---
Piranha	---	550 ± 150	260 ± 10

Values with the same superscript are not statistically different at the 5% significance level.

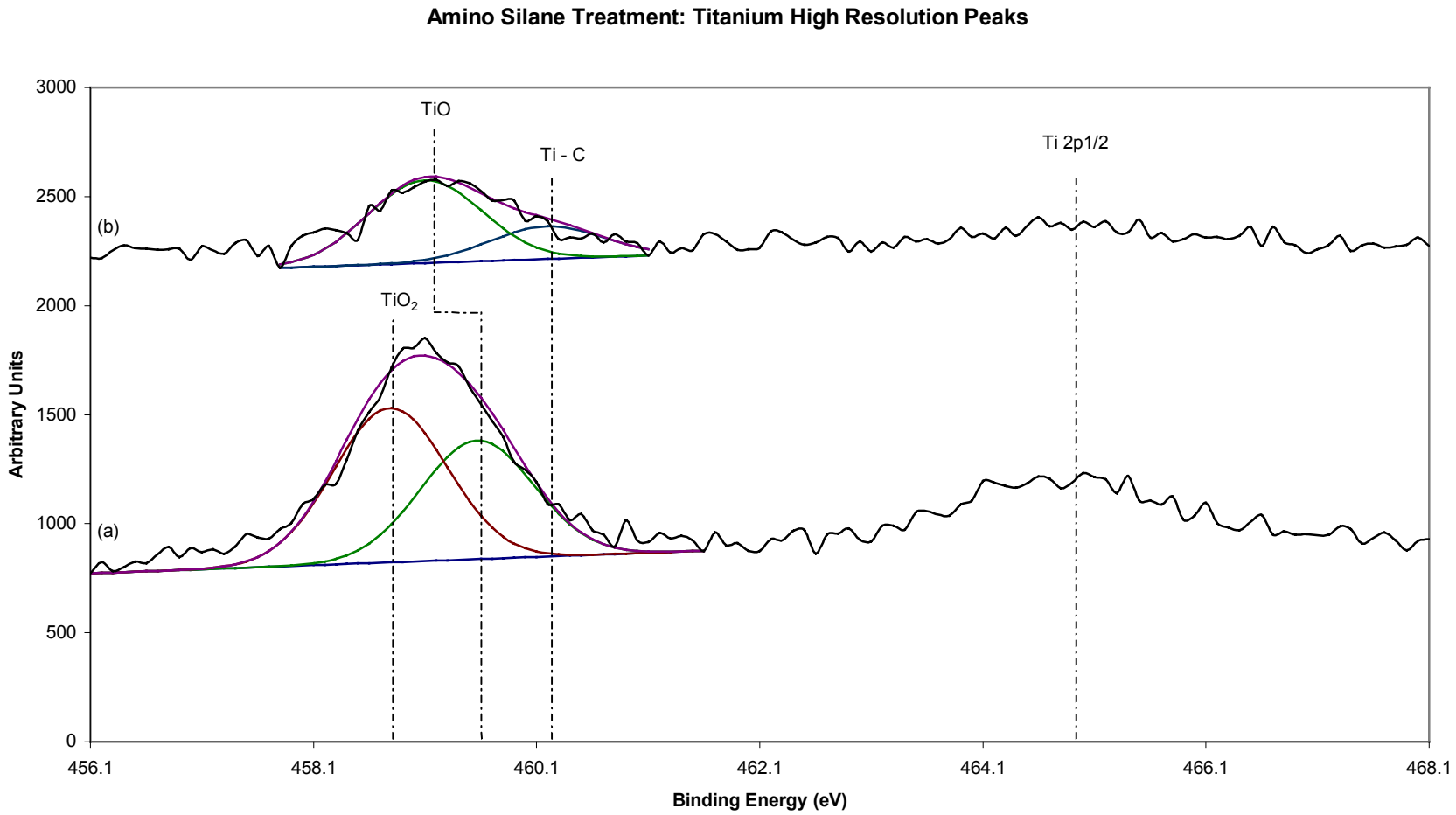

Figure 4.10. Representative titanium high resolution scans of the amino treatment, silane step, on the two metal treatments. The passivated treatment is labeled (a), while the piranha treatment is labeled (b).

4.3.2.2 Gluteraldehyde Reaction Step 2a: Comparing Metal Treatments

The compositional percentage means and standard deviations calculated from the survey scans of the two metal treatments for the second reaction step are shown in Table 4.12. Based on the percentages, the two different metal treatments did not display any significant differences for the five elements present. In order to determine if the percentages were correct, the peak area means and standard deviations were determined for the second reaction step and are shown in Table 4.13. The peak areas of oxygen, silicon, and titanium were not statistically different for the two metal treatments. However, the peak areas of carbon and nitrogen were statistically different. The piranha treated metal showed higher peak areas of carbon and nitrogen, with values of 23460 ± 1010 per unit area and 3850 ± 810 per unit area, respectively, as compared to the passivated metal, which had a peak area of 21290 ± 760 per unit area for carbon and a peak area of 2640 ± 460 per unit area for nitrogen. The representative survey scans of the passivated metal and the piranha treated metal for the second reaction step are shown in Figure 4.11.

Table 4.12. Elemental percentage based on XPS survey scans of the amino treatments, gluteraldehyde step (reaction step 2a).

Metal Treatment	Carbon	Oxygen	Nitrogen	Silicon	Titanium
Passivated	62 ± 2^{a} %	23 ± 1^{b} %	5 ± 1^{c} %	9 ± 1^{d} %	1 ± 0.5^{e} %
Piranha	62 ± 2^{a} %	22 ± 1^{b} %	6 ± 1^{c} %	9 ± 1^{d} %	1 ± 1^{e} %

Values with the same superscript are not statistically different at the 5% significance level.

Table 4.13. Elemental peak areas based on XPS survey scans of the amino treatments, gluteraldehyde step (reaction step 2a).

Metal Treatment	Carbon	Oxygen	Nitrogen	Silicon	Titanium
Passivated	21290 ± 760	18960 ± 1180[a]	2640 ± 460	2940 ± 370[b]	2120 ± 950[c]
Piranha	23460 ± 1010	20680 ± 1270[a]	3850 ± 810	2900 ± 400[b]	1160 ± 1700[c]

Values with the same superscript are not statistically different at the 5% significance level.

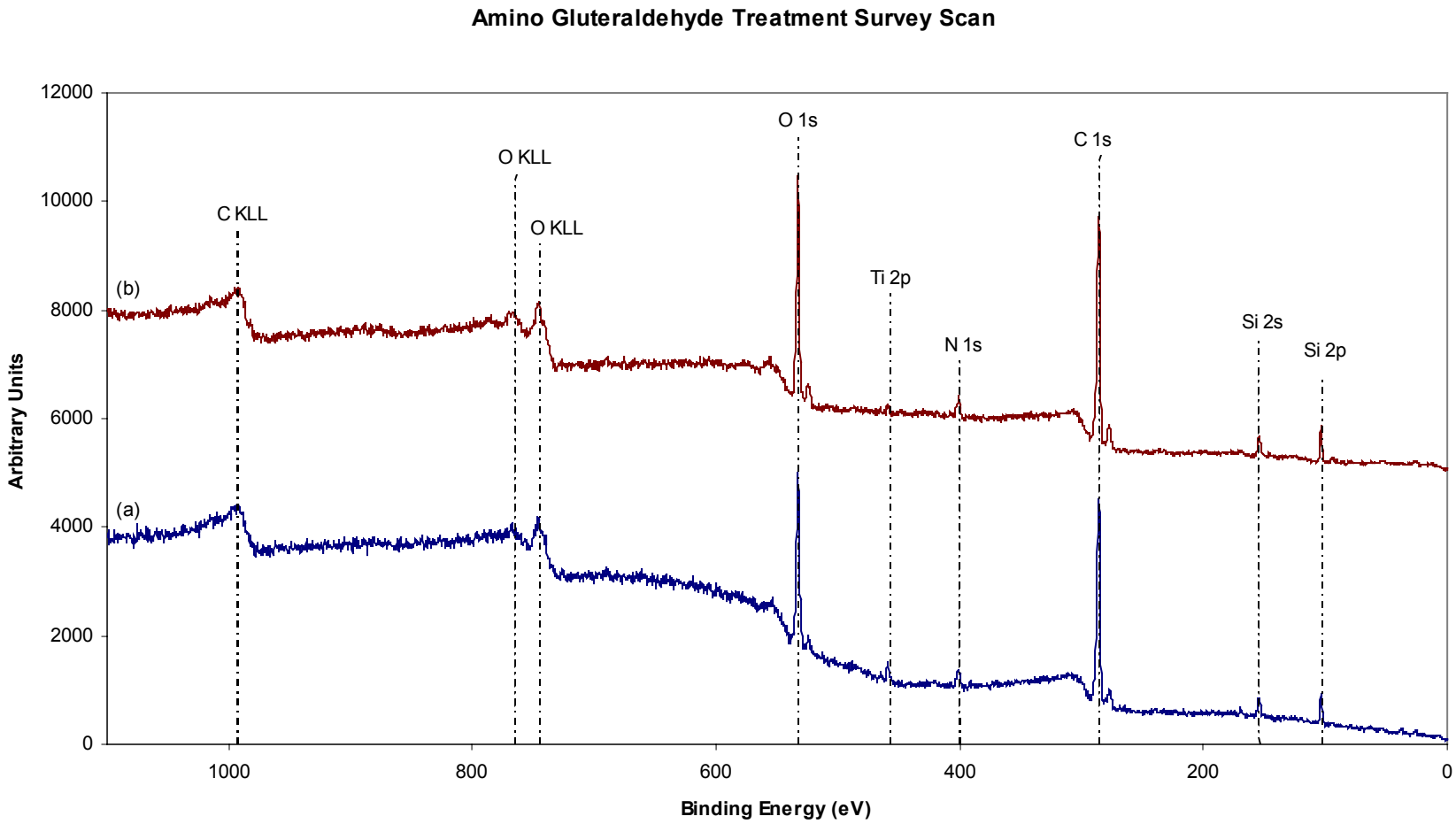

Figure 4.11. Representative survey scans of the amino treatment, gluteraldehyde step, on the two metal treatments.

The passivated treatment is labeled (a), while the piranha treatment is labeled (b).

The means and standard deviations of the high resolutions scans are shown in Tables 4.14 – 4.20. Tables 4.14 – 4.15 show the peaks from the high resolutions scans of carbon; there were six carbon peaks on both metal treatments. Only one of the six peaks was statistically different, while the peaks indicative of C – C, C – N – H, C = O, N – C, and CO_3^{-2} showed no statistical differences. The peak indicative of C – O was statistically different; the piranha treatment had higher peak area of 4180 ± 240 per unit area, as compared to the passivated treatment which had a peak area of 3660 ± 200 per unit area. Figure 4.12 illustrates the difference in peak areas of carbon following the gluteraldehyde step on each of the two metal treatments.

The means and standard deviations calculated from the high resolution scans of oxygen are shown in Tables 4.16 – 4.17. Six peaks were present on both metal surfaces; only one of the six peaks was statistically different. The peak identified as SiO_2 was significantly different, with the piranha treated surface having a higher peak area as compared to the passivated surface, with values of 3660 ± 410 per unit area and 3280 ± 270 per unit area, respectively. The differences in peak areas between the two surfaces are illustrated in Figure 4.13.

Table 4.18 contains the means and standard deviations from the high resolution scans of nitrogen. Five peaks were present on both of the metal treatments, with two of the five peaks being statistically different. The peaks identified as N – C and C – N – H were statistically different, with the piranha treated surface having a higher peak area of both peaks as compared to the passivated surface. Figure 4.14 shows the high resolution peak area differences of the nitrogen peak between the two metal surfaces treated with gluteraldehyde.

The means and standard deviations of the high resolution scans of silicon are listed in Table 4.19. Three peaks were present on both treatment surfaces, with only one peak being statistically different. The SiO_3 was higher on the piranha treated surface than on the passivated surface, with values of 750 ± 50 per unit area and 630 ± 50 per unit area, respectively. The peak area differences between the two metal surfaces are shown graphically in Figure 4.15.

The titanium means and standard deviations from the high resolution scans are shown in Table 4.20. Three peaks are present, but only one peak, TiO, was present on both surfaces, while the peak of Ti – C was present on both surfaces only once out of nine locations scanned. TiO_2 was only present on the passivated surface. The one peak present on both surfaces, TiO, was not statistically different. Figure 4.16 shows the titanium peaks on the two metal surfaces treated with gluteraldehyde.

By looking at the two different surfaces following the gluteraldehyde reaction, it appeared that more gluteraldehyde was bound per unit area to the piranha treated surface than to the passivated surface, as there were more terminal amine ends on piranha treated surface. The higher amount of gluteraldehyde on the piranha treated surface was most strongly demonstrated by the significantly higher amounts of the C – O, C – N – H, and SiO_3 peaks.

Table 4.14. Carbon functional group peak areas based on XPS high resolution scans of the amino treatments, gluteraldehyde step (reaction step 2a).

	C-C [4.2]	C-O [4.3]	C-N-H [4.9]	C=O [4.10]
Metal Treatment	285.3 ± 0.1 eV	286.2 ± 0.1 eV	287.2 ± 0.1 eV	288.3 ± 0.2 eV
Passivated	2180 ± 290[a]	3660 ± 200	1810 ± 170[b]	700 ± 90[c]
Piranha	2190 ± 340[a]	4180 ± 240	1980 ± 200[b]	730 ± 90[c]

Values with the same superscript are not statistically different at the 5% significance level.

Table 4.15. Carbon functional group peak areas based on XPS high resolution scans of the amino treatments, gluteraldehyde step (reaction step 2a).

	N-C [4.11]	**CO_3^{-2} [4.8]**
Metal Treatment	289.4 ± 0.2 eV	290.5 ± 0.2 eV
Passivated	350 ± 110[d]	180 ± 10[e]
Piranha	310 ± 80[d]	220 ± 50[e]

Values with the same superscript are not statistically different at the 5% significance level.

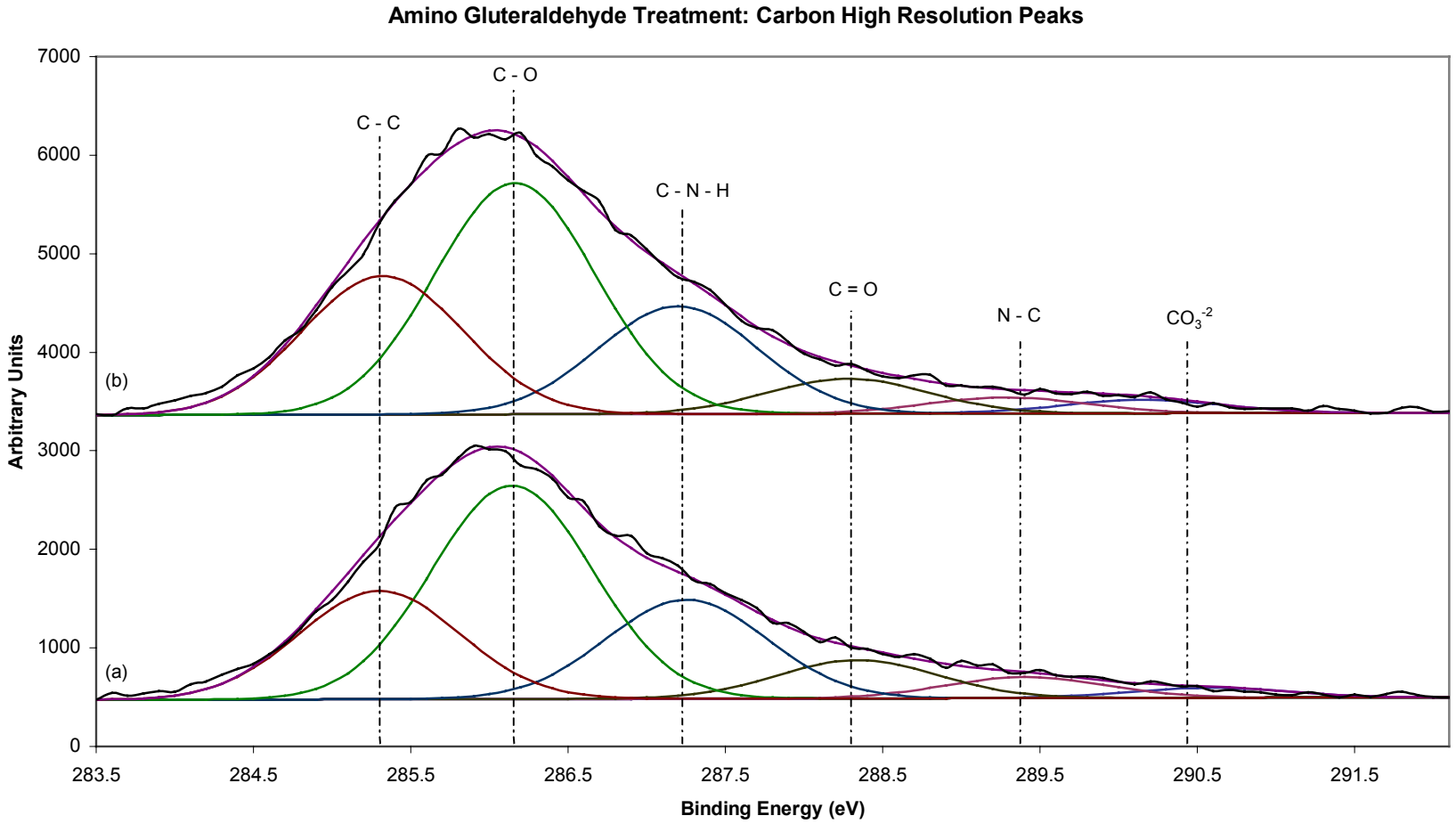

Figure 4.12. Representative carbon high resolution scans of the amino treatment, gluteraldehyde step, on the two metal treatments. The passivated treatment is labeled (a), while the piranha treatment is labeled (b).

Table 4.16. Oxygen functional group peak areas based on XPS high resolution scans of the amino treatments, gluteraldehyde step (reaction step 2a).

	TiO [4.12]	**SiO [4.17]**	**SiO_x [4.18]**	**SiO_2 [4.19]**
Metal Treatment	530.4 ± 0.1 eV	531.4 ± 0.2 eV	532.5 ± 0.2 eV	533.4 ± 0.2 eV
Passivated	510 ± 180[a]	840± 210	1950 ± 400[c]	3280 ± 270
Piranha	620 ± 300[a]	760± 110	2030 ± 560[c]	3660 ± 410

Values with the same superscript are not statistically different at the 5% significance level.

Table 4.17. Oxygen functional group peak areas based on XPS high resolution scans of the amino treatments, gluteraldehyde step (reaction step 2a).

	NO [4.22]	C=O [4.21]
Metal Treatment	534.4 ± 0.2 eV	535.6 ± 0.4 eV
Passivated	1330 ± 320[d]	340 ± 100[e]
Piranha	1450 ± 420[d]	430 ± 120[e]

Values with the same superscript are not statistically different at the 5% significance level.

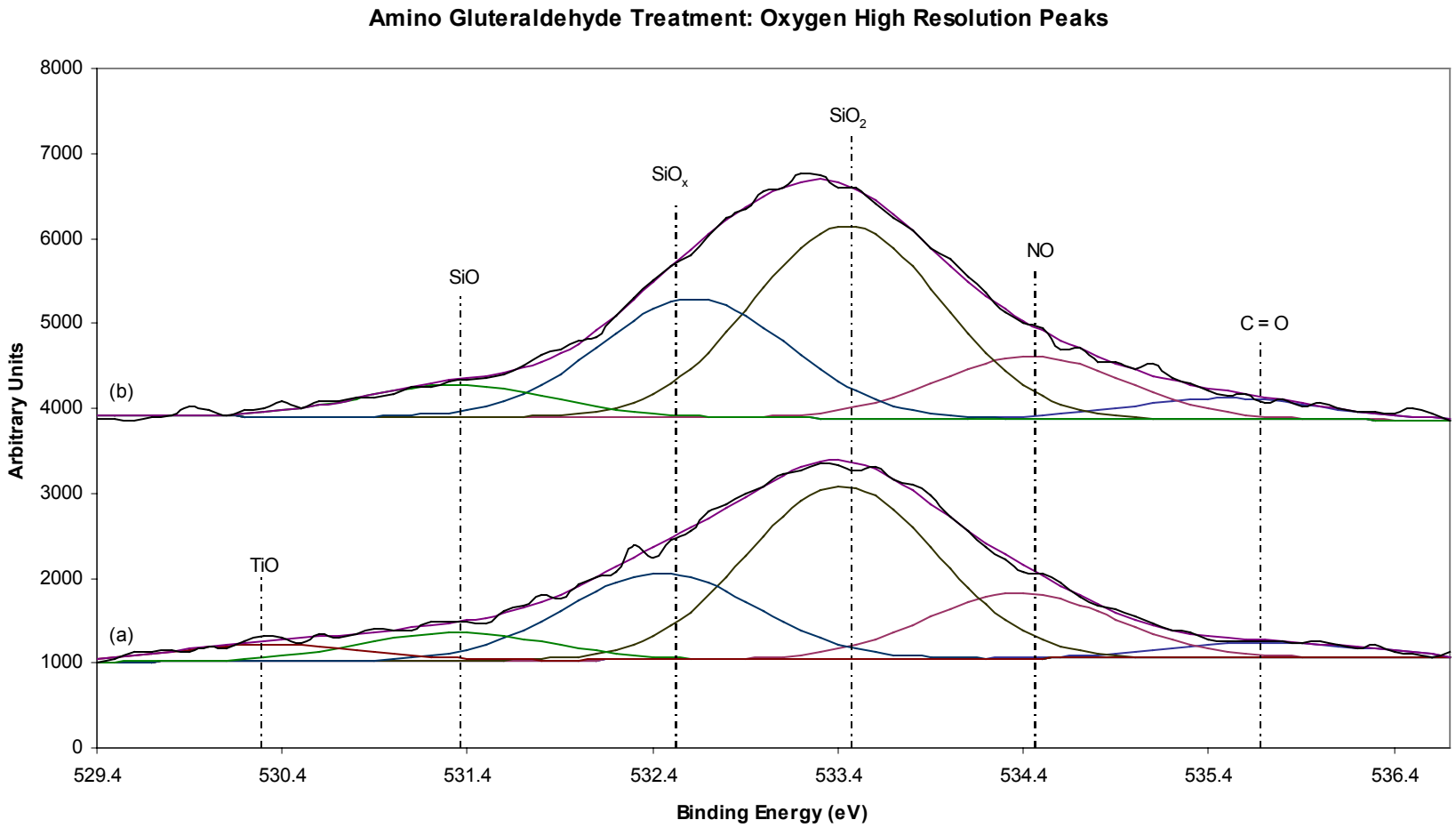

Figure 4.13. Representative oxygen high resolution scans of the amino treatment, gluteraldehyde step, on the two metal treatments. The passivated treatment is labeled (a), while the piranha treatment is labeled (b).

Table 4.18. Nitrogen functional group peak areas based on XPS high resolution scans of the amino treatments, gluteraldehyde step (reaction step 2a).

	N-C [4.32]	C-N-H [4.33]	NH_4^+ [4.34]	NO [4.36]	NO_2^- [4.35]
Metal Treatment	399.5 ± 0.4 eV	400.6 ± 0.4 eV	401.7 ± 0.3 eV	402.8 ± 0.4 eV	403.8 ± 0.3 eV
Passivated	200 ± 40	380 ± 70	350 ± 30[a]	230 ± 60[b]	200 ± 50[c]
Piranha	370 ± 100	490 ± 80	310 ± 90[a]	260 ± 20[b]	210 ± 40[c]

Values with the same superscript are not statistically different at the 5% significance level.

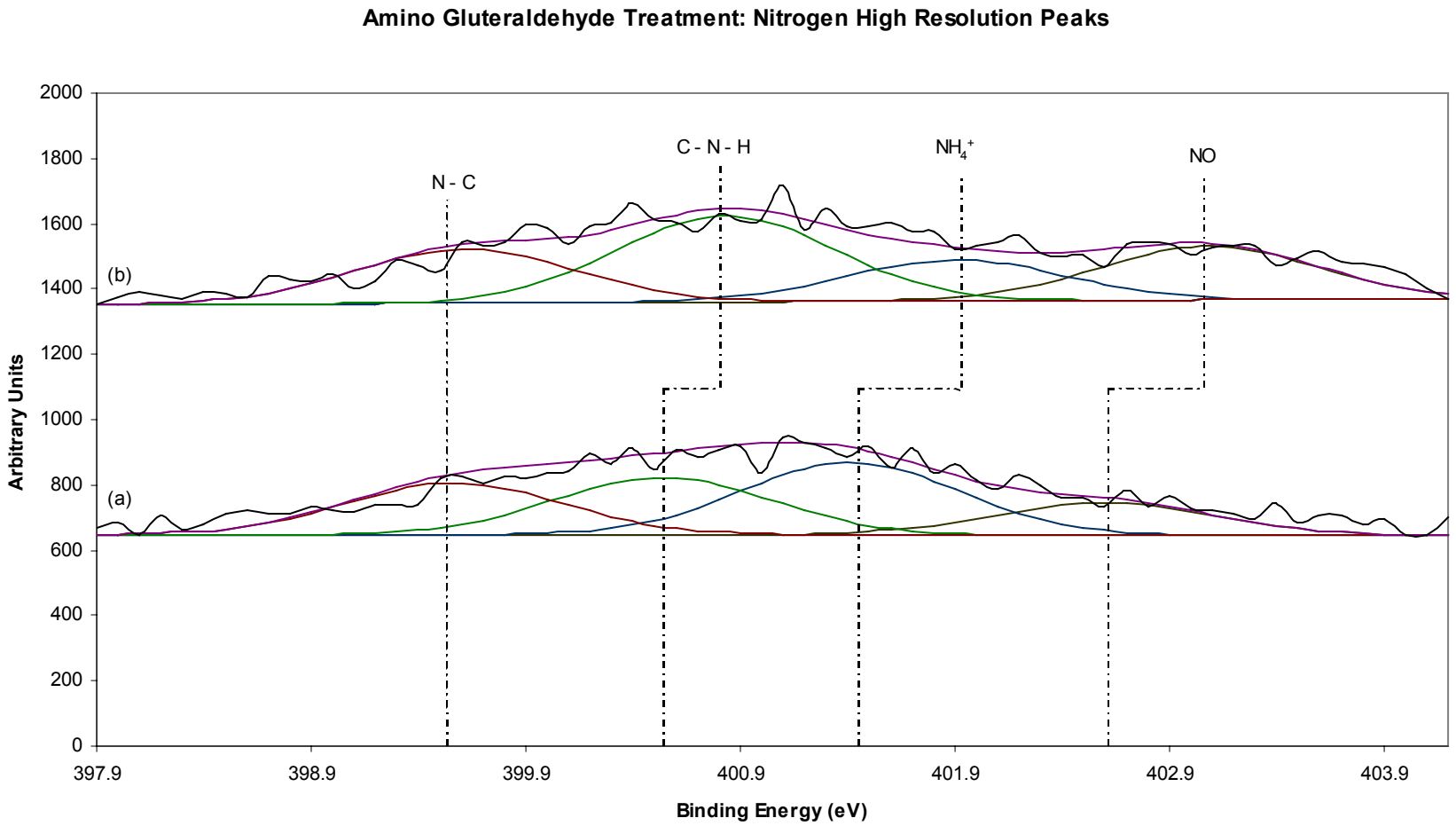

Figure 4.14. Representative nitrogen high resolution scans of the amino treatment, gluteraldehyde step, on the two metal treatments.

The passivated treatment is labeled (a), while the piranha treatment is labeled (b).

Table 4.19. Silicon functional group peak areas based on XPS high resolution scans of the amino treatments, gluteraldehyde step (reaction step 2a).

	SiO [4.28]	**SiO_3 [4.29]**	**SiO_2 [4.30]**
Metal Treatment	102.5 ± 0.1 eV	103.4 ± 0.1 eV	104.5 ± 0.2 eV
Passivated	240 ± 50[a]	630 ± 50	240 ± 70[b]
Piranha	270 ± 60[a]	750 ± 50	200 ± 30[b]

Values with the same superscript are not statistically different at the 5% significance level.

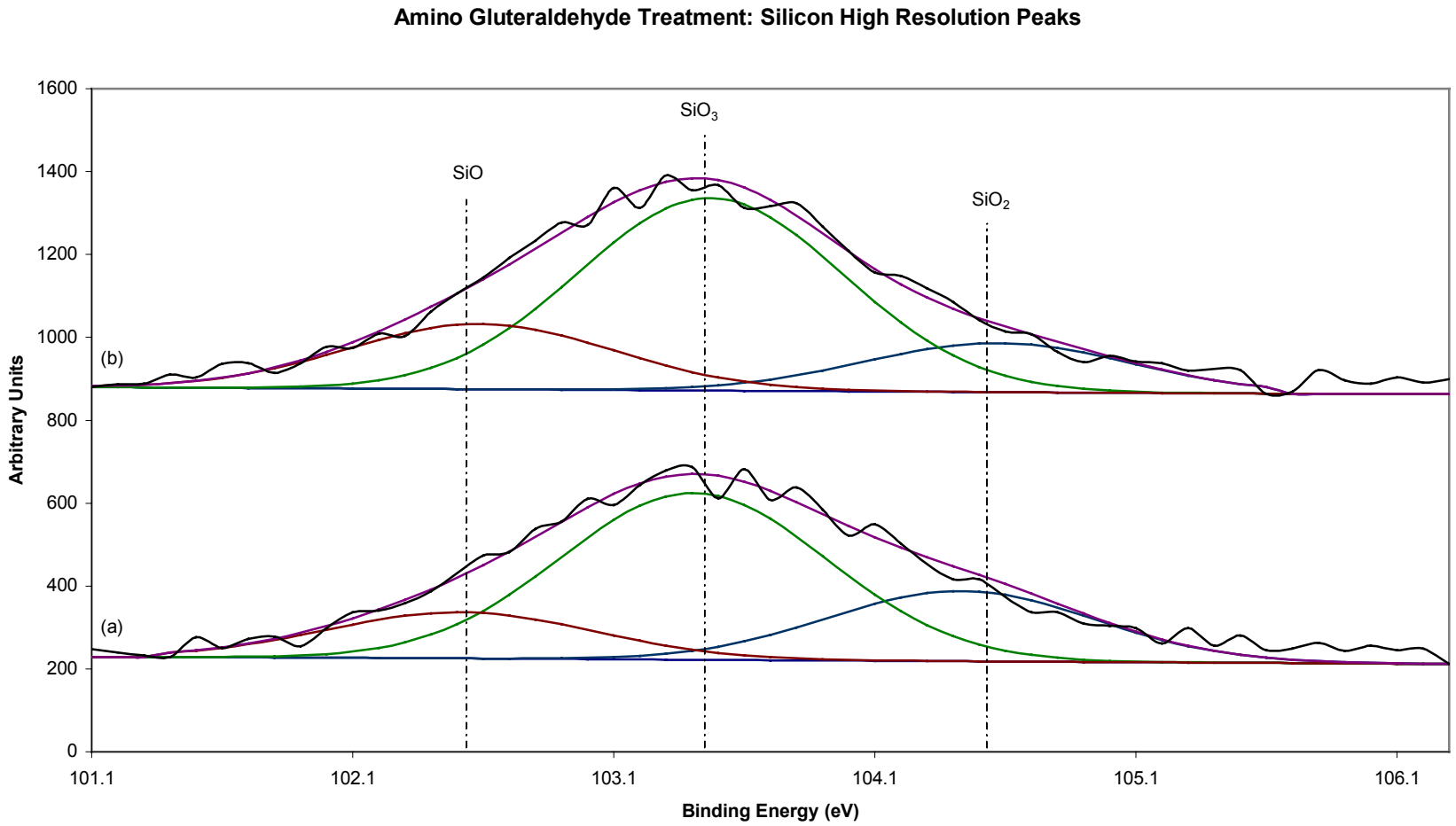

Figure 4.15. Representative silicon high resolution scans of the amino treatment, gluteraldehyde step, on the two metal treatments. The passivated treatment is labeled (a), while the piranha treatment is labeled (b).

Table 4.20. Titanium functional group peak areas based on XPS high resolution scans of the amino treatments, gluteraldehyde step (reaction step 2a).

	TiO_2 [4.23]	TiO [4.24]	TiC [4.25]
Metal Treatment	458.2 ± 0.2 eV	459.1 ± 0.1 eV	460.4 ± 0.3 eV
Passivated	190 ± 30	490 ± 100[a]	170*
Piranha	---	260 ± 340[a]	170*

Values with the same superscript are not statistically different at the 5% significance level.
*Only one observation at given binding energy.

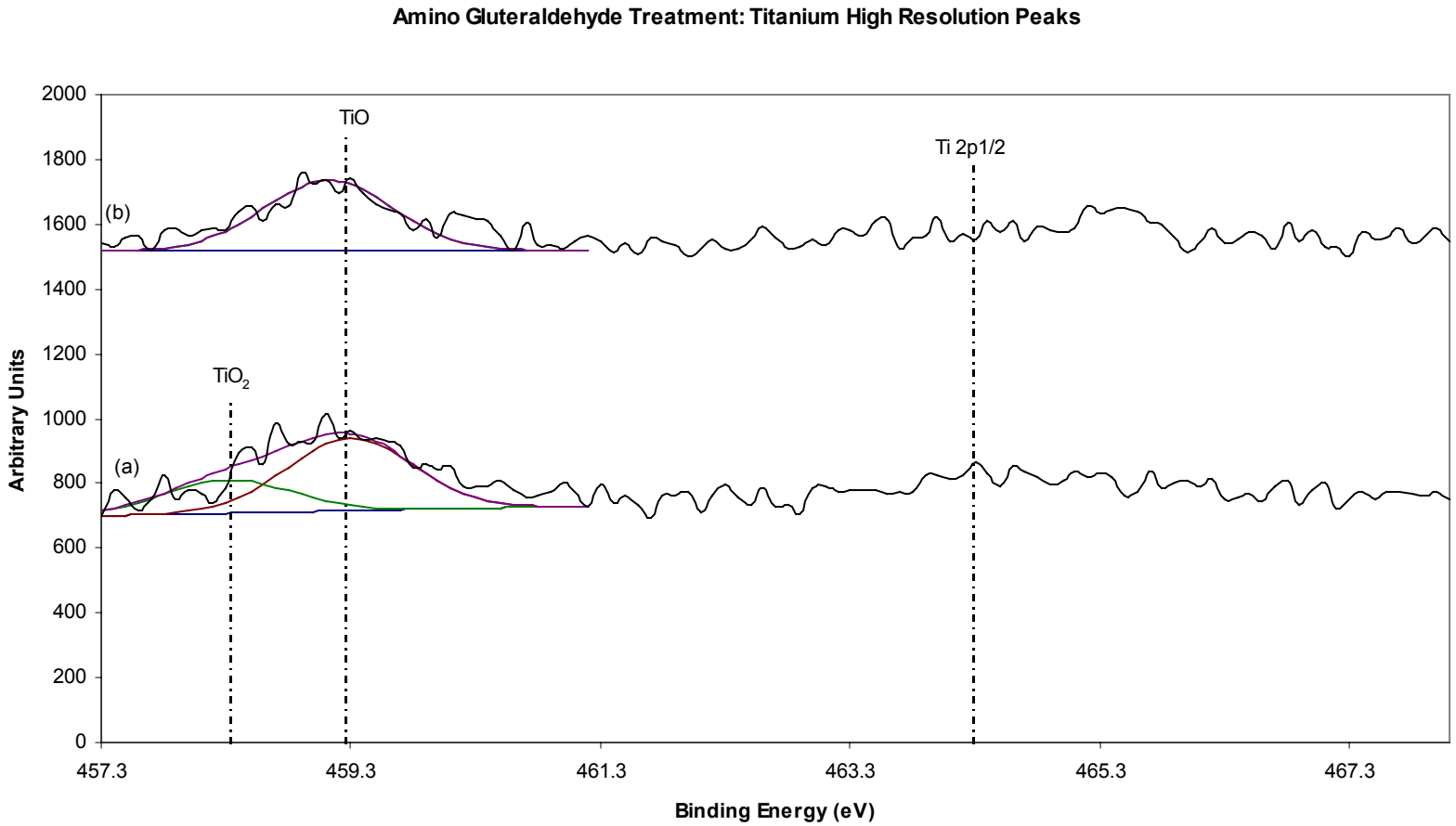

Figure 4.16. Representative titanium high resolution scans of the amino treatment, gluteraldehyde step, on the two metal treatments. The passivated treatment is labeled (a), while the piranha treatment is labeled (b).

4.3.2.3 Passivated Metal Treatment: Comparing Reaction Steps

The percentage means and standard deviations calculated from the survey scans of each step of the amino reaction series on passivated metal are shown in Table 4.21, while the peak area means and standard deviations are shown in Table 4.22. Figure 4.17 shows representative survey scans of each of the reaction steps. By examining the reaction series, several trends were seen. The percentage of carbon showed a statistical decrease from the passivated step to the amino step, with values of 65 ± 3 % and 52 ± 3 %, respectively. A statistical increase was seen from the amino step to the gluteraldehyde step, which was not statistically different from the passivated step. The peak area of carbon showed no statistical similarities, with the amino reaction step significantly less than the other steps and the chitosan reaction step significantly more than the other steps.

The percentage of oxygen showed a statistical decrease from the amino step to the gluteraldehyde step, with values of 26 ± 3 % and 23 ± 1 %, respectively. A statistical increase was seen from the gluteraldehyde step to the chitosan step, which was not statistically different from the passivated step or the amino step. The peak area of oxygen showed a decrease from the amino step to the gluteraldehyde step, followed by an increase to the chitosan step. The passivated step, amino step, and the chitosan step were not statistically different.

Nitrogen was not present on the passivated step. After reaction step 1, a significant increase in nitrogen of 7 ± 1 % was seen; a significant decrease was seen following reaction step 2, to a value of 5 ± 1 %. There was no statistical difference between the gluteraldehyde step (reaction step 2a) and the chitosan film (reaction step

3a). Looking at peak area, there was also a significant decrease between the amino reaction step (1a) and the gluteraldehyde reaction step (2a). The chitosan step was not statistically different from either reaction step.

Silicon was also not present on the passivated step. After the amino reaction (reaction step 1a), a significant increase was seen in both percentage and peak area, to values of 13 ± 2 % and 3910 ± 560 per unit area, respectively. A significant decrease was seen in the silicon percentage following the gluteraldehyde step (reaction step 2a) and the chitosan step (reaction step 3a), to percentage values of 9 ± 1 % and 1 ± 1 %, respectively. A significant decrease in the silicon peak area was also seen following the gluteraldehyde step and the chitosan step.

Titanium was not present in the chitosan step, but was present on the passivated surface and following the other two reaction steps (reaction steps 1a and 2a). A significant decrease from the passivated surface to the amino reaction step (1a) was seen, with values of 6 ± 2 % to 2 ± 1 %, respectively. There was not a statistical difference between the amino reaction and the gluteraldehyde reaction, with respect to percentage or peak area.

Table 4.21. Elemental percentage based on XPS survey scans of passivated metal using amino silane.

Reaction Step	Carbon	Oxygen	Nitrogen	Silicon	Titanium
Passivated	$65 \pm 3^{a,b}$ %	30 ± 2^{a} %	---	---	6 ± 2 %
Amino (1a)	52 ± 3 %	26 ± 3^{b} %	7 ± 1 %	13 ± 2 %	2 ± 1^{d} %
Gluteraldehyde (2a)	62 ± 2^{b} %	23 ± 1 %	5 ± 1^{c} %	9 ± 1 %	1 ± 1^{d} %
Chitosan (3a)	66 ± 1^{a} %	$28 \pm 1^{a,b}$ %	6 ± 1^{c} %	1 ± 1 %	---

Values with the same superscript are not statistically different at the 5% significance level.

Table 4.22. Elemental peak areas based on XPS survey scans of passivated metal using amino silane.

Reaction Step	Carbon	Oxygen	Nitrogen	Silicon	Titanium
Passivated	19480 ± 1410	21920 ± 1590[a]	---	---	11780 ± 4660
Amino (1a)	17320 ± 1000	21450 ± 2400[a]	3790 ± 560[c]	3910 ± 560	5350 ± 2060[e]
Gluteraldehyde (2a)	21290 ± 760	18960 ± 1180	2640 ± 460[d]	2940 ± 370	2130 ± 950[e]
Chitosan (3a)	22730 ± 680	23500 ± 1200[a]	3220 ± 600[c,d]	50 ± 160	---

Values with the same superscript are not statistically different at the 5% significance level.

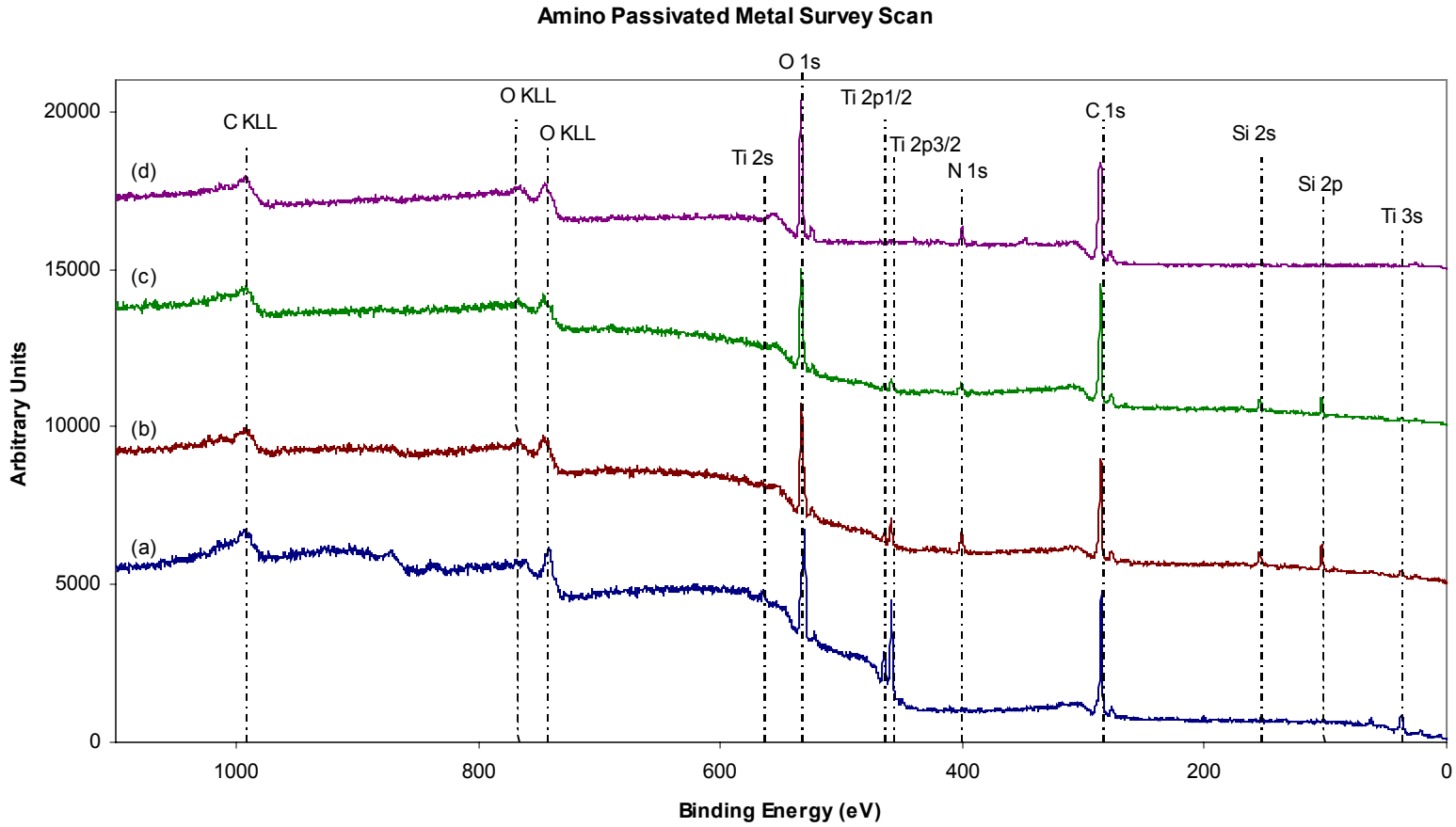

Figure 4.17. Representative survey scans of the amino reaction series on passivated metal.

The passivated metal is labeled (a). The amino silane reaction (reaction step 1a) is labeled (b). The gluteraldehyde reaction (reaction step 2a) is labeled (c). The chitosan reaction (reaction step 3a) is labeled (d).

The means and standard deviations of the high resolutions scans are shown in Tables 4.23 – 4.29. Tables 4.23 – 4.24 show the peak areas of the seven peaks present following each reaction step as determined from the carbon high resolution scans. Of the seven peaks present, only three of the peaks were present in all four reactions. The C peak, located at 284.9 ± 0.1 eV, was present on both the passivated metal and on the chitosan surface; it was not statistically different. The C – C peak, located at 285.8 ± 0.2 eV, dropped significantly from the passivated step to the amino reaction step (1a), from 4140 ± 300 per unit area to 2420 ± 670 per unit area, respectively. There were no statistical differences between reaction steps 1a, 2a, and 3a. The C – O peak, located at 286.5 ± 0.3 eV, was not present on the passivated surface; it increased significantly from the amino reaction (1a), with a value of 2940 ± 470 per unit area, to the gluteraldehyde reaction (2a), with a value of 3660 ± 200 per unit area, before dropping significantly following the chitosan reaction (3a), to a value of 2640 ± 520 per unit area. The peak located at 287.4 ± 0.3 eV was identified as C = O on the passivated metal and C – N – H following the three reaction steps. There was a significant increase from the amino reaction step to the gluteraldehyde reaction step, as well as a significant increase from the gluteraldehyde reaction step to the chitosan reaction step. The C = O peak, located at 288.7 ± 0.3 eV, was not present on the passivated surface and it increased significantly through each of the reaction steps, with a starting value of 390 ± 90 per unit area in the amino reaction step (1a) to a final value of 1120 ± 100 per unit area in the chitosan reaction step (3a). The peak located at 289.8 ± 0.4 eV was identified as CO_3^{+2} on the passivated metal and N – C following the three reaction steps. A significant increase was

seen between the amino reaction step and the gluteralderaldehyde reaction step, from values of 210 ± 30 per unit area to 350 ± 110 per unit area, respectively, while no significant changes were seen between the gluteraldehyde reaction and the chitosan reaction step. The last remaining peak, CO_3^{-2}, was present only on the gluteraldehyde reaction surface (2a) and was located at 290.6 ± 0.2 eV. Figure 4.18 shows the differences of the peaks areas following the four reaction steps on the passivated metal surface.

Table 4.23. Carbon functional group peak areas based on XPS high resolution scans of passivated metal using amino silane.

	C [4.1]	C-C [4.2]	C-O [4.3]	C=O [4.5] / C-N-H [4.9]
Metal Treatment	284.9 ± 0.1 eV	285.8 ± 0.2 eV	286.5 ± 0.3 eV	287.4 ± 0.3 eV
Passivated	1590 ± 640[a]	4140 ± 300	---	1350 ± 250[d,e]
Amino (1a)	---	2420 ± 670[b]	2940 ± 470[c]	1220 ± 240[e]
Gluteraldehyde (2a)	---	2180 ± 290[b]	3660 ± 200	1810 ± 170[d]
Chitosan (3a)	820 ± 80[a]	2540 ± 1100[b]	2640 ± 510[c]	2430 ± 820

Values with the same superscript are not statistically different at the 5% significance level.

Table 4.24. Carbon functional group peak areas based on XPS high resolution scans of passivated metal using amino silane.

	C=O [4.10]	CO_3^{+2} [4.7] / N-C [4.11]	CO_3^{-2} [4.8]
Metal Treatment	288.7 ± 0.3 eV	289.8 ± 0.4 eV	290.6 ± 0.2 eV
Passivated	---	590 ± 50[f]	---
Amino (1a)	390 ± 90	210 ± 30[g]	---
Gluteraldehyde (2a)	700 ± 90	350 ± 110[f]	180 ± 10
Chitosan (3a)	1120 ± 100	400 ± 210[f,g]	---

Values with the same superscript are not statistically different at the 5% significance level.

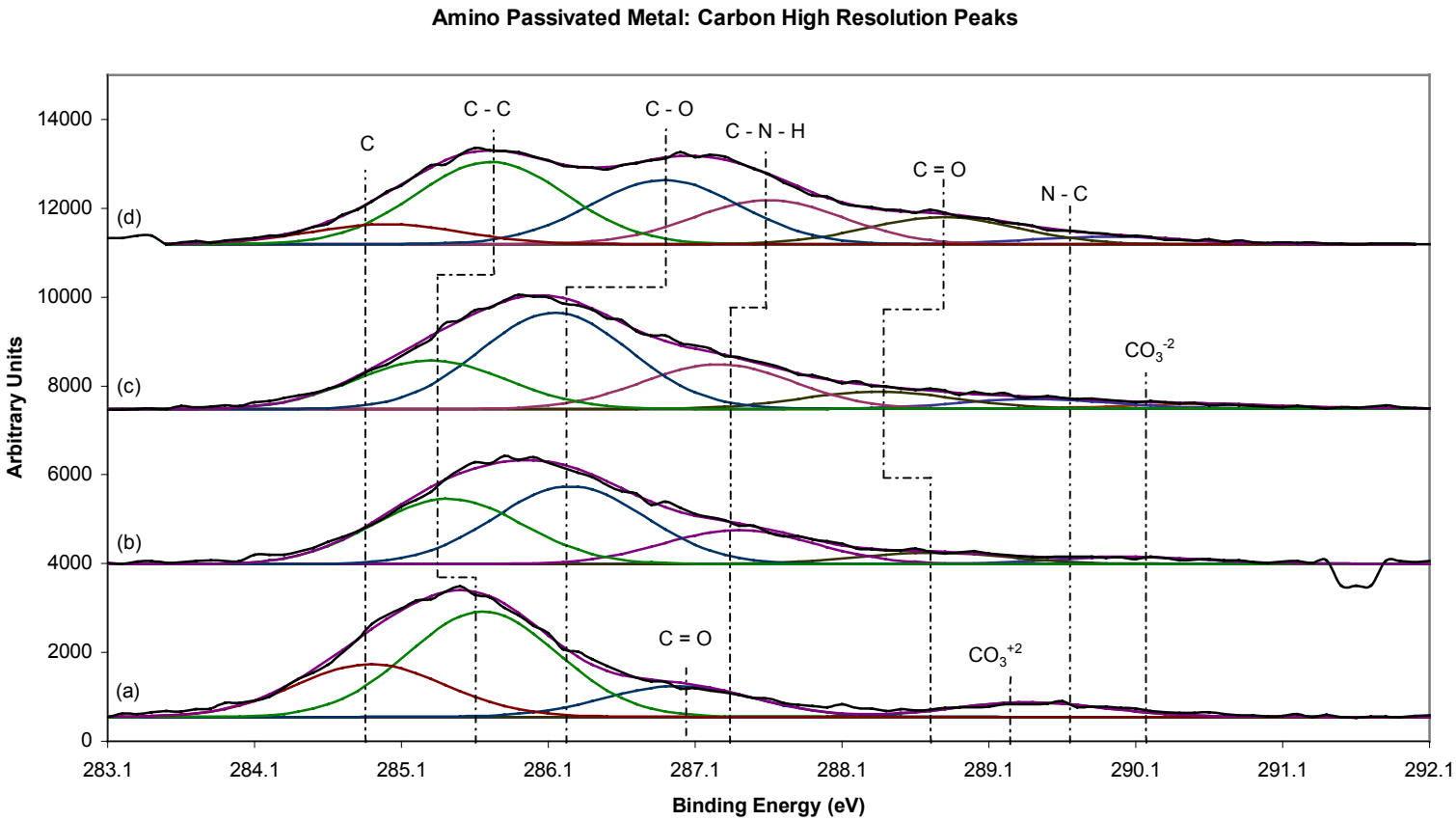

Figure 4.18. Representative carbon high resolution scans of the amino reaction series on passivated metal.

The passivated metal is labeled (a). The amino silane reaction (reaction step 1a) is labeled (b). The gluteraldehyde reaction (reaction step 2a) is labeled (c). The chitosan reaction (reaction step 3a) is labeled (d).

Tables 4.25 – 4.26 show the peaks from the high resolutions scans of oxygen; there were six oxygen peaks present, with only four of the peaks present in all four reactions. The peak located at 530.4 ± 0.1 eV and identified as TiO, showed a significant decrease from the passivated step through the amino reaction step (1a) and the gluteraldehyde step (2a). The TiO peak is not present following the chitosan reaction step (3a). There were statistical similarities between the four peaks that were present on the four surfaces; however, the identities of the peaks were different for the passivated surface as compared to the reaction steps. For the peak located at 531.5 ± 0.2 eV, the identity of the peak on the passivated surface was – OH, while the peak for the other three reaction steps was SiO. The SiO peak dropped significantly from the first reaction step (1a), with a value of 1190 ± 220 per unit area, to the last reaction step (3a), with a value of 650 ± 340 per unit area. The peak located at 532.7 ± 0.2 eV was identified as C – O for the passivated step and SiO_x for the other three reaction steps. Following the gluteraldehyde reaction (2a), there was a significant decrease from a value 2890 ± 420 per unit area in the amino reaction to a value of 1950 ± 400 per unit area. There was no significant difference between the gluteraldehyde reaction and the chitosan reaction (3a). The peak located at 533.7 ± 0.2 eV was identified as $-(OH)_3^{-3}$ on the passivated surface and SiO_2 following the three reaction steps. There was no statistical differences between the amino step (1a) and the gluteraldehyde step (2a), while there was a significant increase from the gluteraldehyde step, with a value of 3280 ± 270 per unit area, to the chitosan step (3a), with a value of 4230 ± 990 per unit area. The fifth peak was identified as C – O on the passivated surface and NO following the reaction steps and was located

at 534.7 ± 0.3 eV. There were no statistical differences between any of the reaction steps; however, the peak area following the amino reaction and the peak area following the chitosan reaction were statistically different, with values of 610 ± 120 per unit area and 2410 ± 1130 per unit area, respectively. The last peak was not present on the passivated surface or the amino treated surface (1a), but was present following the gluteraldehyde step (2a) and the chitosan step (3a). The peak identified as C = O was located at 535.7 ± 0.3 eV and did not vary significantly between the two reactions. Figure 4.19 shows the differences in the peak areas of the oxygen peaks on the surface following the four reaction steps on the passivated metal surface.

Table 4.25. Oxygen functional group peak areas based on XPS high resolution scans of passivated metal using amino silane.

	TiO [4.12]	-OH [4.13] / SiO [4.17]	C-O [4.14] / SiO_x [4.18]	$-(OH)_3^{-3}$ [4.15] / SiO_2 [4.19]
Metal Treatment	530.4 ± 0.1 eV	531.5 ± 0.2 eV	532.7 ± 0.2 eV	533.7 ± 0.2 eV
Passivated	3330 ± 790	1920 ± 200	2160 ± 290[c]	1650 ± 270
Amino (1a)	1370 ± 300	1190 ± 230[a]	2890 ± 420	2790 ± 550[d]
Gluteraldehyde (2a)	510 ± 180	840 ± 210[a,b]	1950 ± 400[c]	3280 ± 270[d]
Chitosan (3a)	---	650 ± 340[b]	1860 ± 640[c]	4230 ± 990

Values with the same superscript are not statistically different at the 5% significance level.

Table 4.26. Oxygen functional group peak areas based on XPS high resolution scans of passivated metal using amino silane.

	C-O [4.16] / NO [4.22]	C=O [4.21]
Metal Treatment	534.7 ± 0.3 eV	535.7 ± 0.3 eV
Passivated	570 ± 130[a]	---
Amino (1a)	610 ± 120[a]	---
Gluteraldehyde (2a)	1330 ± 320[a,b]	340 ± 100[c]
Chitosan (3a)	2410 ± 1130[b]	560 ± 380[c]

Values with the same superscript are not statistically different at the 5% significance level.

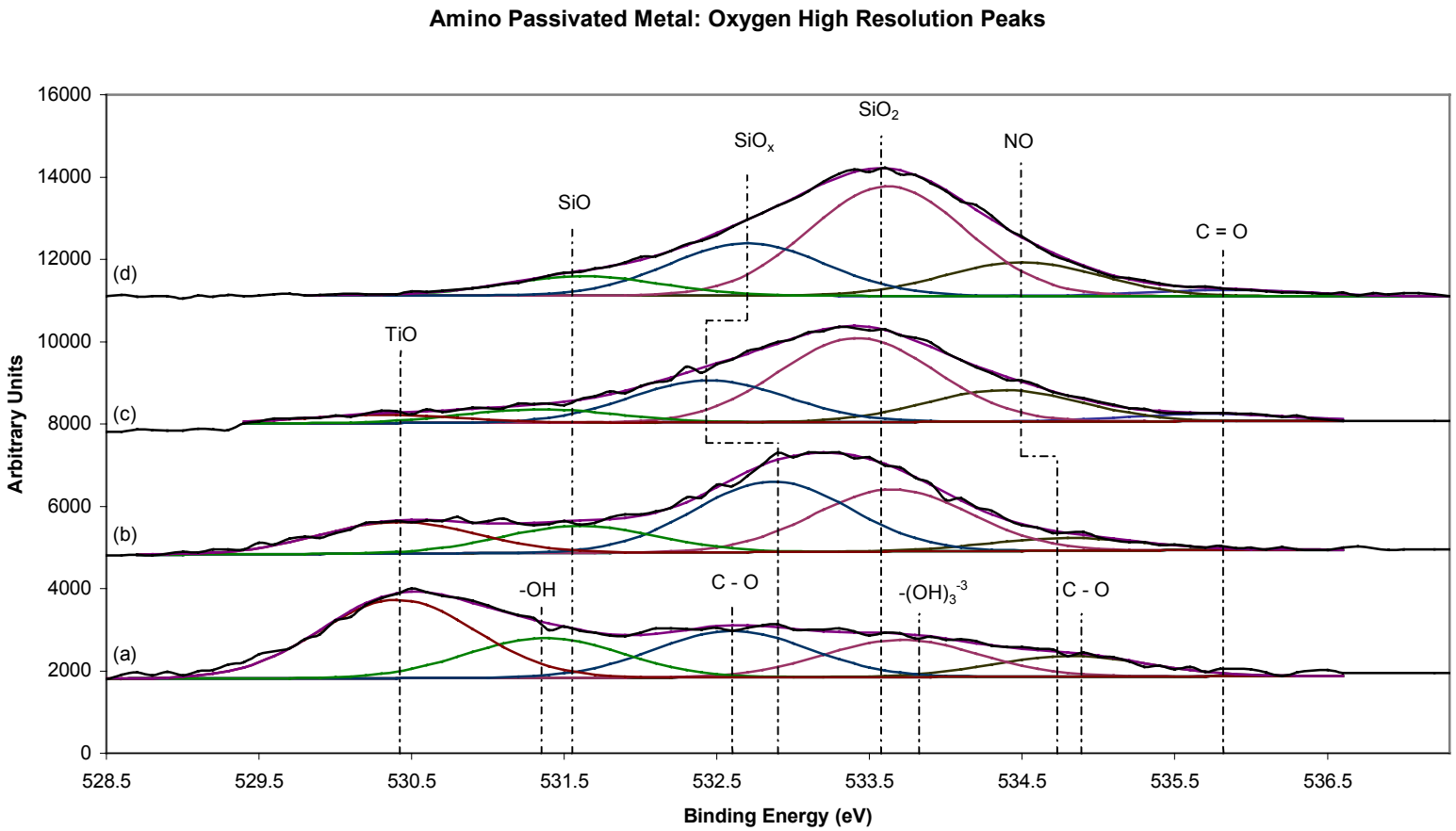

Figure 4.19. Representative oxygen high resolution scans of the amino reaction series on passivated metal.

The passivated metal is labeled (a). The amino silane reaction (reaction step 1a) is labeled (b). The gluteraldehyde reaction (reaction step 2a) is labeled (c). The chitosan reaction (reaction step 3a) is labeled (c).

Table 4.27 shows the peaks from the high resolution scans of nitrogen; there were no nitrogen peaks present on the passivated surface, while there were five peaks present, with three of the peaks present on all of the reaction surfaces. The peak located at 399.6 ± 0.4 eV was identified as N – C and was not statistically different from the amino reaction step to the gluteraldehyde step; a statistically significant increase was seen from the gluteraldehyde step to the chitosan step. The peak identified as C – N – H and located at 400.6 ± 0.3 eV showed a significant decrease between the amino treated step (1a) and the gluteraldehyde step (2a) from a value of 650 ± 90 per unit area to a value of 380 ± 70 per unit area, while a significant increase was seen between the gluteraldehyde step (2a) and the chitosan step (3a), with a final value of 630 ± 120 per unit area. The peak located at 401.6 ± 0.3 eV, and identified as NH_4^+, was not present on the chitosan surface. It decreased significantly from the amino reaction (1a) to the gluteraldehyde reaction (2a). NO, located at 402.8 ± 0.4 eV, was present on all three of the reaction surfaces. It did not significantly change from the amino reaction step to the gluteraldehyde reaction step, nor did it change significantly from the gluteraldehyde step to the chitosan step. The last peak, NO_2^-, located at 403.7 ± 0.3 eV, was present only following the amino reaction step, with a value of 200 ± 50 per unit area; it was no longer present following the gluteraldehyde reaction. Figure 4.20 shows the differences in the peak areas of nitrogen on the surface following the three reaction steps on the passivated metal surface; the passivated surface was not shown, as no nitrogen was present.

Table 4.27. Nitrogen functional group peak areas based on XPS high resolution scans of passivated metal using amino silane.

	N-C [4.32]	C-N-H [4.33]	NH_4^+ [4.34]	NO [4.36]	NO_2^- [4.35]
Metal Treatment	399.6 ± 0.4 eV	400.6 ± 0.3 eV	401.6 ± 0.2 eV	402.8 ± 0.4 eV	403.7 ± 0.3 eV
Passivated	---	---	---	---	---
Amino (1a)	400 ± 90[a,b]	650 ± 90[c]	450 ± 70	190 ± 20[d]	200 ± 50
Gluteraldehyde (2a)	200 ± 40[a]	380 ± 70	350 ± 30	230 ± 60[d,e]	---
Chitosan (3a)	540 ± 230[b]	630 ± 120[c]	---	270 ± 40[e]	---

Values with the same superscript are not statistically different at the 5% significance level.

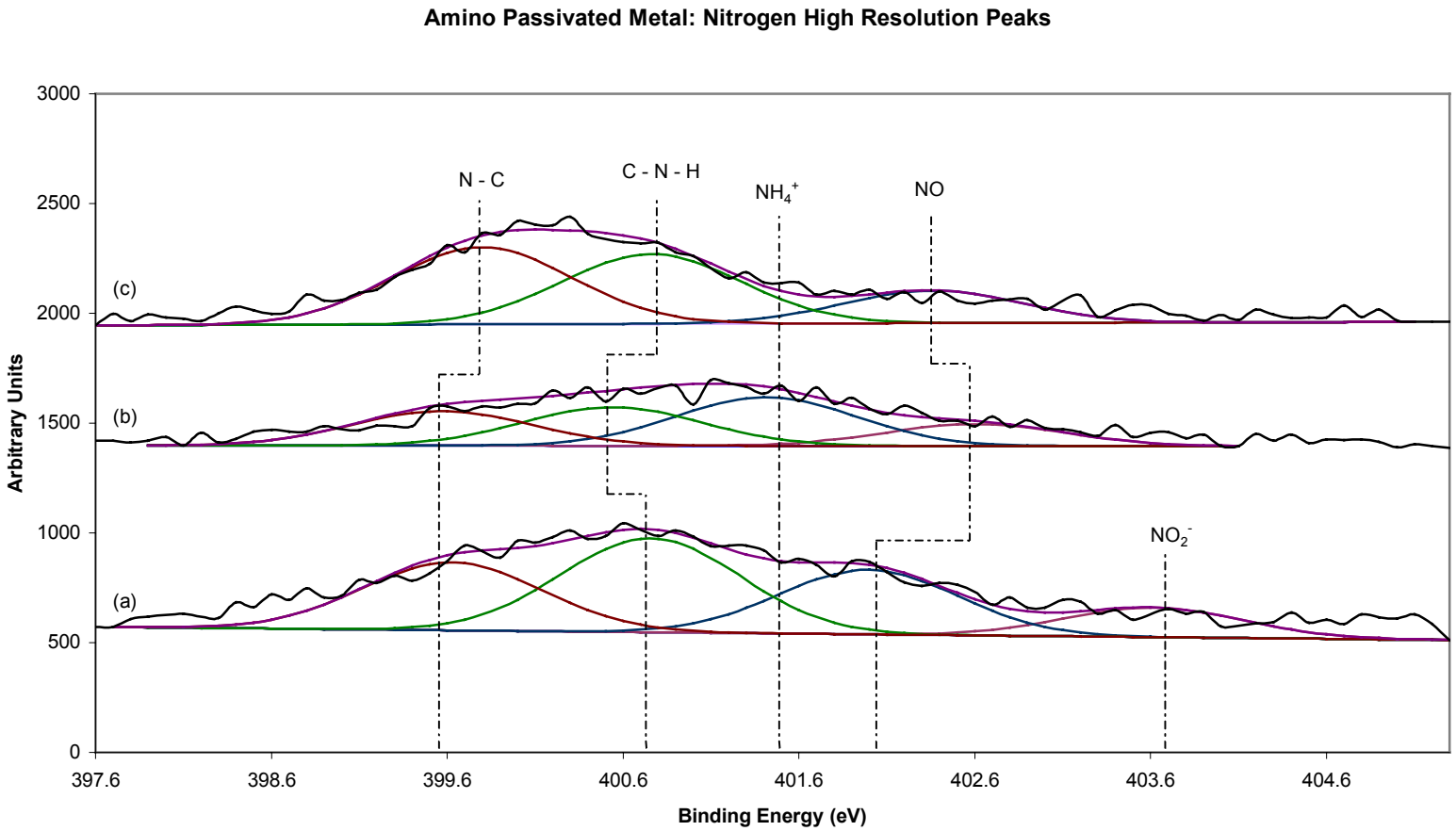

Figure 4.20. Representative nitrogen high resolution scans of the amino reaction series on passivated metal.

The amino silane reaction (reaction step 1a) is labeled (a). The gluteraldehyde reaction (reaction step 2a) is labeled (b). The chitosan reaction (reaction step 3a) is labeled (c).

Table 4.28 shows the peak areas of the three peaks present following the four reaction steps as determined from the silicon high resolution scans; there were no silicon peaks present on the passivated surface. Of the three peaks present, only one of the peaks was present on all of the reaction surfaces. The peak located at 102.8 ± 0.3 eV was identified as SiO and dropped significantly following each of the reaction steps, from an initial value of 740 ± 140 per unit area following the amino reaction step to a value of 20 ± 60 per unit area following the chitosan reaction step. The peak identified as SiO_3 was not present on the chitosan surface, but was present following the amino reaction step and the gluteraldehyde reaction step; there were no statistical differences between the reaction steps however. The final peak, identified as SiO_2 and located at 104.5 ± 0.2 eV, was present only following the gluteraldehyde reaction. Figure 4.21 illustrates the differences of the silicon peak following the three reaction steps on the passivated metal; the passivated metal was not shown, as there was no silicon present.

Table 4.28. Silicon functional group peak areas based on XPS high resolution scans of passivated metal using amino silane.

	SiO [4.28]	**SiO_3 [4.29]**	**SiO_2 [4.30]**
Metal Treatment	102.8 ± 0.3 eV	103.7 ± 0.3 eV	104.5 ± 0.2 eV
Passivated	---	---	---
Amino (1a)	740 ± 140	670 ± 140[a]	---
Gluteraldehyde (2a)	240 ± 50	630 ± 50[a]	240 ± 70
Chitosan (3a)	20 ± 60	---	---

Values with the same superscript are not statistically different at the 5% significance level.

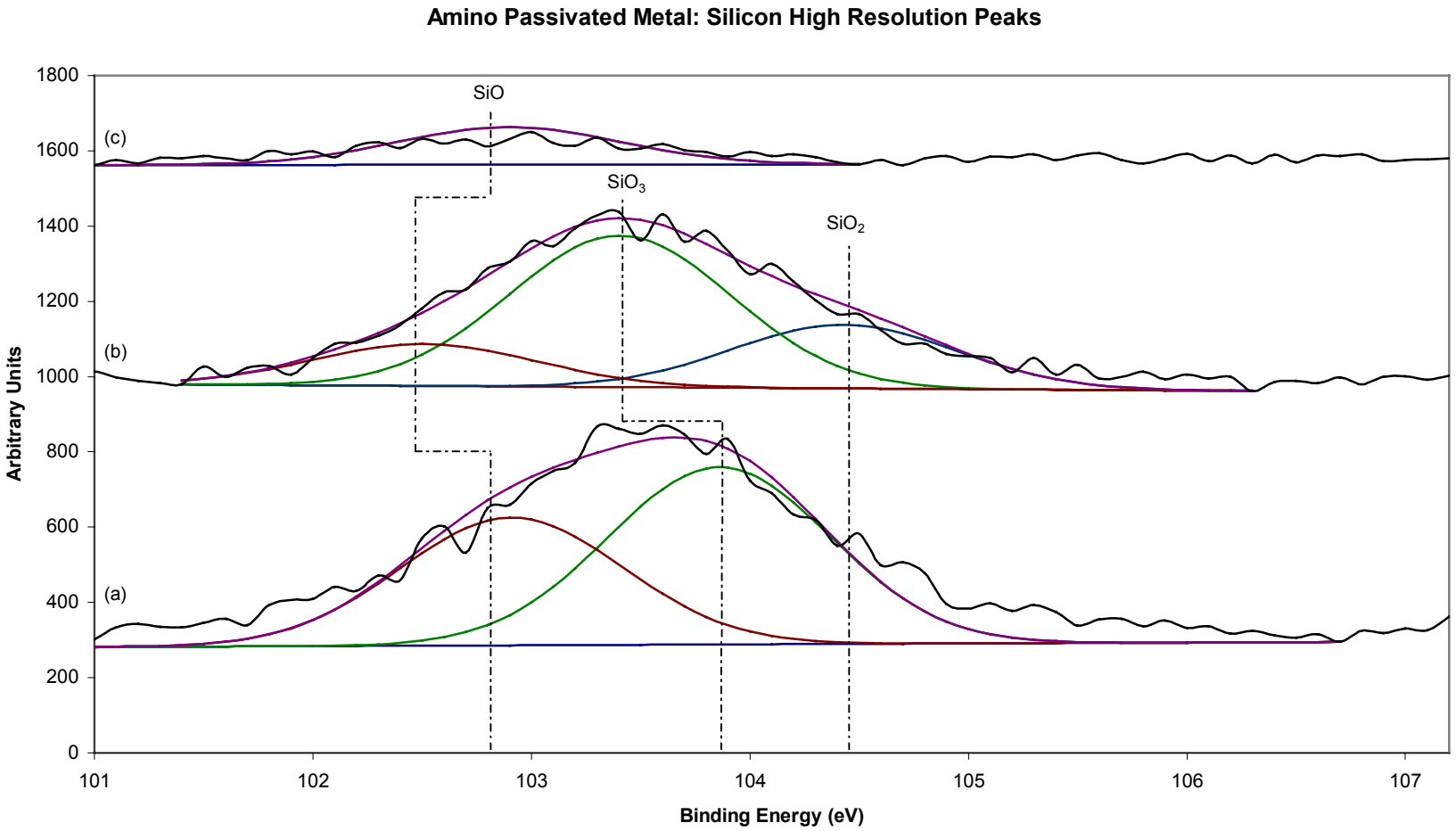

Figure 4.21. Representative silicon high resolution scans of the amino reaction series on passivated metal.

The amino silane reaction (reaction step 1a) is labeled (b). The gluteraldehyde reaction (reaction step 2a) is labeled (c). The chitosan reaction (reaction step 3a) is labeled (c).

Table 4.29 shows the peaks from the high resolution scans of titanium; there were no titanium peaks present following the chitosan reaction step. There were three peaks present, with one peak located on only the passivated surface and following the gluteraldehyde reaction step. The peak located at 458.5 ± 0.2 eV was identified as TiO_2. There was no significant change between the passivated surface and the amino reaction step, nor was there a significant change between the amino reaction step and the gluteraldehyde step. However, there was a significant decrease from the passivated surface to the gluteraldehyde step, with values of 1060 ± 150 per unit area and 190 ± 30 per unit area, respectively. The peak located at 459.3 ± 0.2 eV was identified as TiO; a significant decrease between the passivated surface and the amino reaction step was seen, with values of 2650 ± 560 per unit area and 750 ± 160 per unit area, respectively. No significant change was seen between the amino reaction step and the gluteraldehyde reaction step. The last peak, located at 460.4 ± 0.3 eV, was identified as TiC; the peak was seen in only one scan of the passivated surface and one scan of the gluteraldehyde surface. Figure 4.22 illustrates the differences of the titanium peak following the three reaction steps on the passivated metal; the chitosan reaction step was not shown, as there was no titanium present.

By looking at the three different surfaces on the passivated metal surface, significant changes between the reaction species were seen. An overall increase of the C = O peak indicated that the gluteraldehyde molecule did bind to the amino silane molecule, while an overall decrease of the TiO peak further indicated that the anticipated surface reactions had occurred. The anticipated reaction was further proven by the initial increase of the C – N – H group, followed by a decrease after the gluteraldehyde reaction,

showing that the gluteraldehyde molecule did bond with the terminal amine group. The presence of SiO, SiO_2, and SiO_3 further proved that the anticipated reaction between the passivated surface and the amino silane did occur.

Table 4.29. Titanium functional group peak areas based on XPS high resolution scans of passivated metal using amino silane.

	TiO_2 [4.23]	TiO [4.24]	TiC [4.25]
Metal Treatment	458.5 ± 0.2 eV	459.3 ± 0.2 eV	460.4 ± 0.3 eV
Passivated	1060 ± 150[a]	2650 ± 560	420*
Amino (1a)	840 ± 390[a,b]	750 ± 160[c]	---
Gluteraldehyde (2a)	190 ± 30[b]	490 ± 100[c]	170*
Chitosan (3a)	---	---	---

Values with the same superscript are not statistically different at the 5% significance level.
*Only one observation at given binding energy.

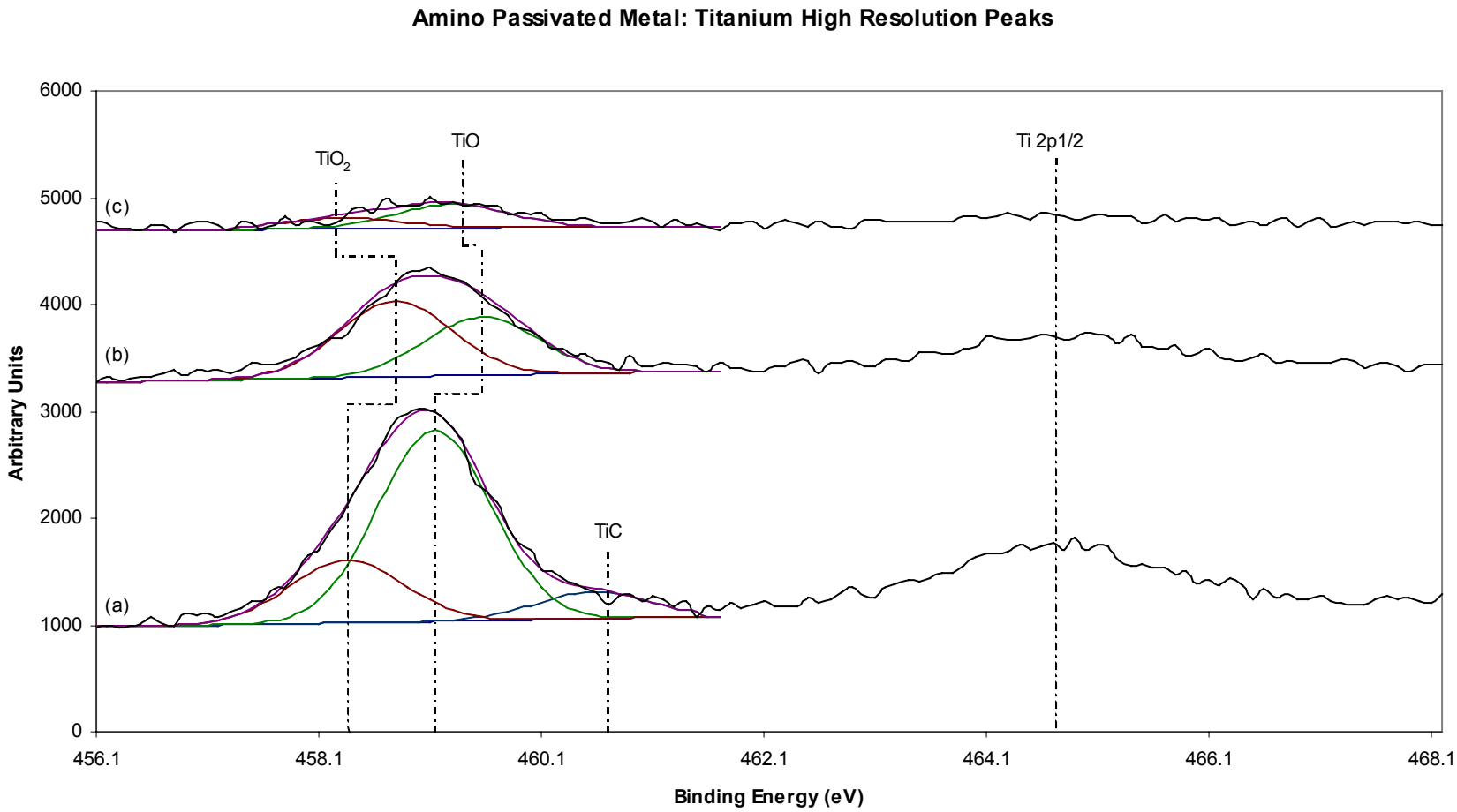

Figure 4.22. Representative titanium high resolution scans of the amino reaction series on passivated metal.

The passivated metal is labeled (a). The amino silane reaction (reaction step 1a) is labeled (b). The gluteraldehyde reaction (reaction step 2a) is labeled (c).

4.3.2.4 Piranha Treated Metal: Comparing Reaction Steps

The percentage means and standard deviations calculated from the survey scans of each step of the amino reaction series on piranha treated metal are shown in Table 4.30, while the peak area means and standard deviations are shown in Table 4.31. Figure 4.23 shows representative survey scans of each of the reaction steps. By examining the reaction series, several trends were seen. The carbon percentage showed a statistical increase between every step, from the piranha treated metal through to the chitosan reaction step (3a); the carbon percentage started at 40 ± 2 % for the piranha treated metal and ended at 68 ± 1 % for the chitosan reaction step. The peak area of carbon showed a statistical increase from the piranha metal through to the gluteraldehyde reaction step (2a); the gluteraldehyde reaction step and the chitosan reaction step (3a) were not statistically different.

The percentage of oxygen showed a statistical decrease from the piranha treated metal to the amino reaction step (1a), with values of 45 ± 1 % and 22 ± 1 %, respectively. No statistical differences exist between the amino reaction step and the gluteraldehyde step (2a); however, there was a statistical increase from the gluteraldehyde step to the chitosan step (3a), with values of 22 ± 2 % and 25 ± 1 %, respectively. The peak area of oxygen showed a decrease from the piranha treated metal to the amino reaction step; there was no statistical difference between the amino reaction step, the gluteraldehyde reaction step, and the chitosan reaction step.

Nitrogen was not present on the piranha treated metal. After reaction step 1, a significant increase in nitrogen of 8 ± 1 % was seen; a significant decrease was seen

following reaction step 2, to a value of 6 ± 1 %. There was no statistical difference between the gluteraldehyde step (reaction step 2a) and the chitosan film (reaction step 3a). Looking at the peak areas, there was also a significant decrease between the amino reaction step (1a) and the gluteraldehyde reaction step (2a) and a significant decrease between the gluteraldehyde reaction step and the chitosan reaction step (3a).

Silicon was also not present on the piranha treated metal. After the amino reaction (reaction step 1a), a significant increase was seen in both percentage and peak area, to values of 14 ± 1 % and 4870 ± 260 per unit area, respectively. A significant decrease was seen in the silicon percentage following the gluteraldehyde step (reaction step 2a) and the chitosan step (reaction step 3a), to percentage values of 9 ± 1 % and 1 ± 1 %, respectively. A significant decrease was seen in the silicon peak area following the gluteraldehyde step and the chitosan step, as well.

Titanium was not present in the chitosan step, but was present on the piranha treated surface and following the other two reaction steps (reaction steps 1a and 2a). A significant decrease from the piranha treated surface to the amino reaction step (1a) was seen, with values of 15 ± 2 % to 1 ± 1 %, respectively. There was not a statistical difference between the amino reaction and the gluteraldehyde reaction, with respect to percentage or peak area.

Table 4.30. Elemental percentage based on XPS survey scans of piranha treated metal using amino silane.

Reaction Step	Carbon	Oxygen	Nitrogen	Silicon	Titanium
Piranha	40 ± 2 %	45 ± 1 %	---	---	15 ± 2 %
Amino (1a)	54 ± 1 %	22 ± 1[a] %	8 ± 1 %	14 ± 1 %	1 ± 1[c] %
Gluteraldehyde (2a)	62 ± 2 %	22 ± 2[a] %	6 ± 1[b] %	9 ± 1 %	1 ± 1[c] %
Chitosan (3a)	68 ± 1 %	25 ± 1 %	5 ± 1[b] %	1 ± 1 %	---

Values with the same superscript are not statistically different at the 5% significance level.

Table 4.31. Elemental peak area based on XPS survey scans of piranha treated metal using amino silane.

Reaction Step	Carbon	Oxygen	Nitrogen	Silicon	Titanium
Piranha	12430 ± 380	34410 ± 1340	---	---	33400 ± 5640
Amino (1a)	20380 ± 670	20600 ± 650[b]	5050 ± 480	4870 ± 260	2370 ± 1180[e]
Gluteraldehyde (2a)	23460 ± 1010[a]	20680 ± 1270[b]	3850 ± 810	2900 ± 400	1160 ± 1700[e]
Chitosan (3a)	23110 ± 460[a]	20470 ± 1240[b]	2900 ± 290	260 ± 230	---

Values with the same superscript are not statistically different at the 5% significance level.

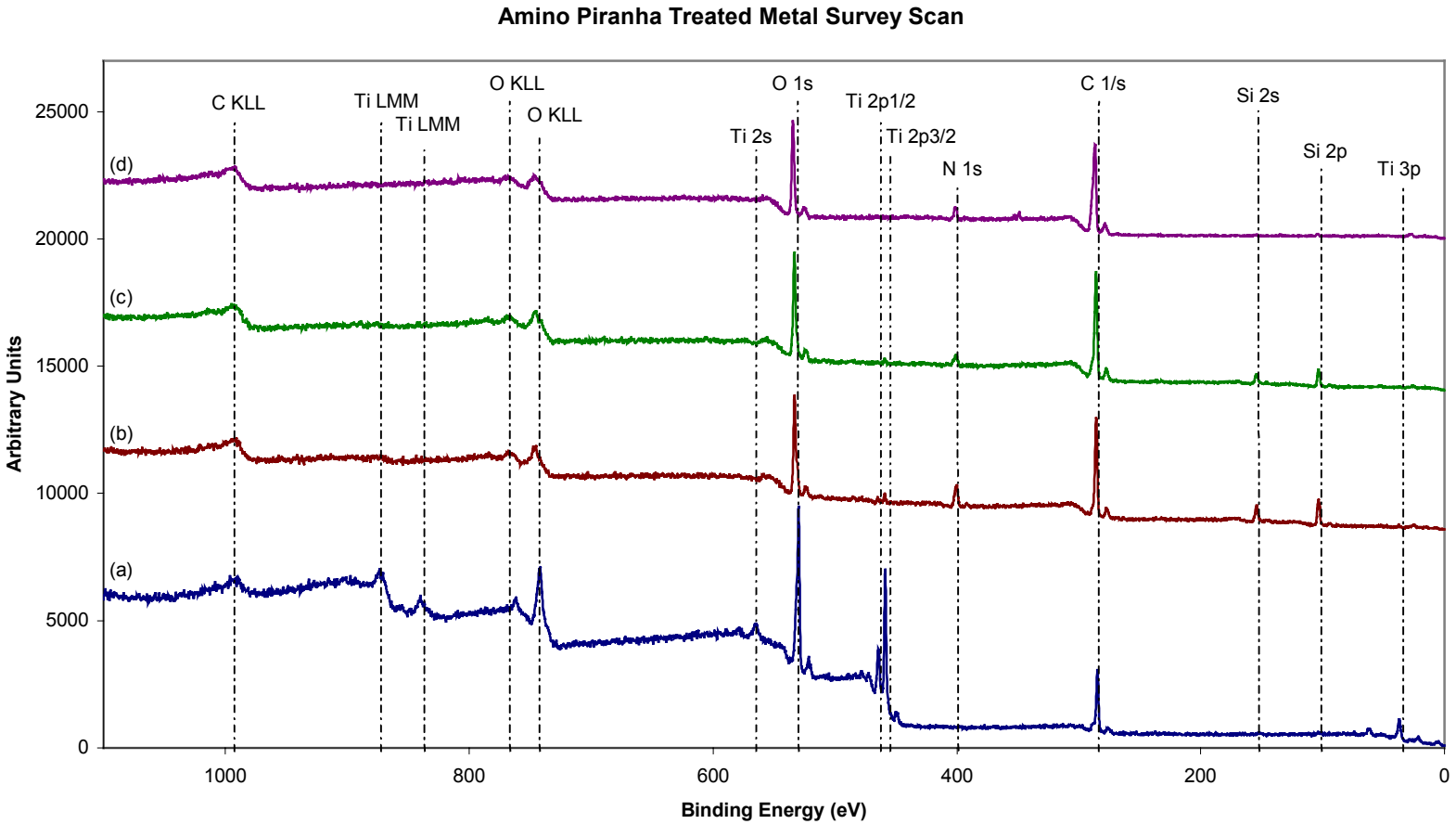

Figure 4.23. Representative survey scans of the amino reaction series on piranha treated metal.

The piranha treated metal is labeled (a). The amino silane reaction (reaction step 1a) is labeled (b). The gluteraldehyde reaction (reaction step 2a) is labeled (c). The chitosan reaction (reaction step 3a) is labeled (d).

The means and standard deviations of the high resolutions scans are shown in Tables 4.32 – 4.38. Tables 4.32 – 4.33 show the peaks from the high resolutions scans of carbon; there were seven carbon peaks present, only three of the peaks were present in all four reactions. Each of the three peaks present showed some statistical differences. The C peak, located at 284.8 ± 0.1 eV was present only on the piranha treated metal. The C – C peak, located at 285.5 ± 0.2 eV, did not significantly change between the piranha treated surface and the three reaction steps. The peak located at 286.4 ± 0.3 eV and identified as C – O was not present on the piranha treated metal. There was no significant change between the amino reaction step and the gluteraldehyde reaction step; a significant decrease was seen between the gluteraldehyde reaction step and the chitosan reaction step, with peak area values of 4180 ± 240 per unit area and 3690 ± 160 per unit area, respectively. The peak located at 287.3 ± 0.4 eV was identified as C = O on the piranha treated surface and C – N – H following the reaction series. There was a significant increase of the C – N – H peak following each of the three reaction steps, from an initial value of 1610 ± 260 per unit area following the amino reaction step to a final value of 2580 ± 380 per unit area following the chitosan reaction step. The peak located at 288.5 ± 0.3 eV was identified as C = O; it was not present on the piranha treated surface. A significant increase was seen from the amino reaction step through to the chitosan reaction step, with an initial value of 450 ± 80 per unit area to a final value of 1660 ± 420 per unit area. On the piranha treated surface, the peak located at 289.5 ± 0.3 eV was identified as CO_3^{+2}, while the peak following the reaction series was identified as N – C. There was no statistical difference between the amino reaction step and the

gluteraldehyde reaction step; however, a significant increase was seen between the gluteraldehyde reaction step and the chitosan reaction step, from a value of 310 ± 80 per unit area to a value of 950 ± 90 per unit area, respectively. The last remaining peak, CO_3^{-2}, was present following the gluteraldehyde reaction surface (2a) and the chitosan reaction surface (3a); it was located at 290.5 ± 0.4 eV. A significant decrease between the gluteraldehyde reaction step and the chitosan reaction step was seen, from a value of 1960 ± 50 per unit area to a value of 870 ± 30 per unit area, respectively. Figure 4.24 shows the differences in the peak areas of carbon on the surface following the four reaction steps on the piranha treated metal surface.

Table 4.32. Carbon functional group peak areas based on XPS high resolution scans of piranha treated metal using amino silane.

	C [4.1]	C-C [4.2]	C-O [4.3]	C=O [4.5] / C-N-H [4.9]
Metal Treatment	284.8 ± 0.1 eV	285.5 ± 0.2 eV	286.4 ± 0.3 eV	287.3 ± 0.4 eV
Piranha	1270 ± 270	2590 ± 230[a]	---	670 ± 60
Amino (1a)	---	2240 ± 620[a]	3890 ± 340[b,c]	1610 ± 260
Gluteraldehyde (2a)	---	2190 ± 340[a]	4180 ± 240[b]	1980 ± 200
Chitosan (3a)	---	530 ± 220	3690 ± 160[c]	2580 ± 380

Values with the same superscript are not statistically different at the 5% significance level.

Table 4.33. Carbon functional group peak areas based on XPS high resolution scans of piranha treated metal using amino silane.

	C=O [4.10]	CO_3^{+2} [4.7] / N-C [4.11]	CO_3^{-2} [4.8]
Metal Treatment	288.5 ± 0.3 eV	289.5 ± 0.3 eV	290.5 ± 0.4 eV
Piranha	---	370 ± 30[a]	---
Amino (1a)	450 ± 80	260 ± 80[b]	---
Gluteraldehyde (2a)	730 ± 90	310 ± 80[a,b]	1960 ± 50
Chitosan (3a)	1660 ± 420	950 ± 90	870 ± 30

Values with the same superscript are not statistically different at the 5% significance level.

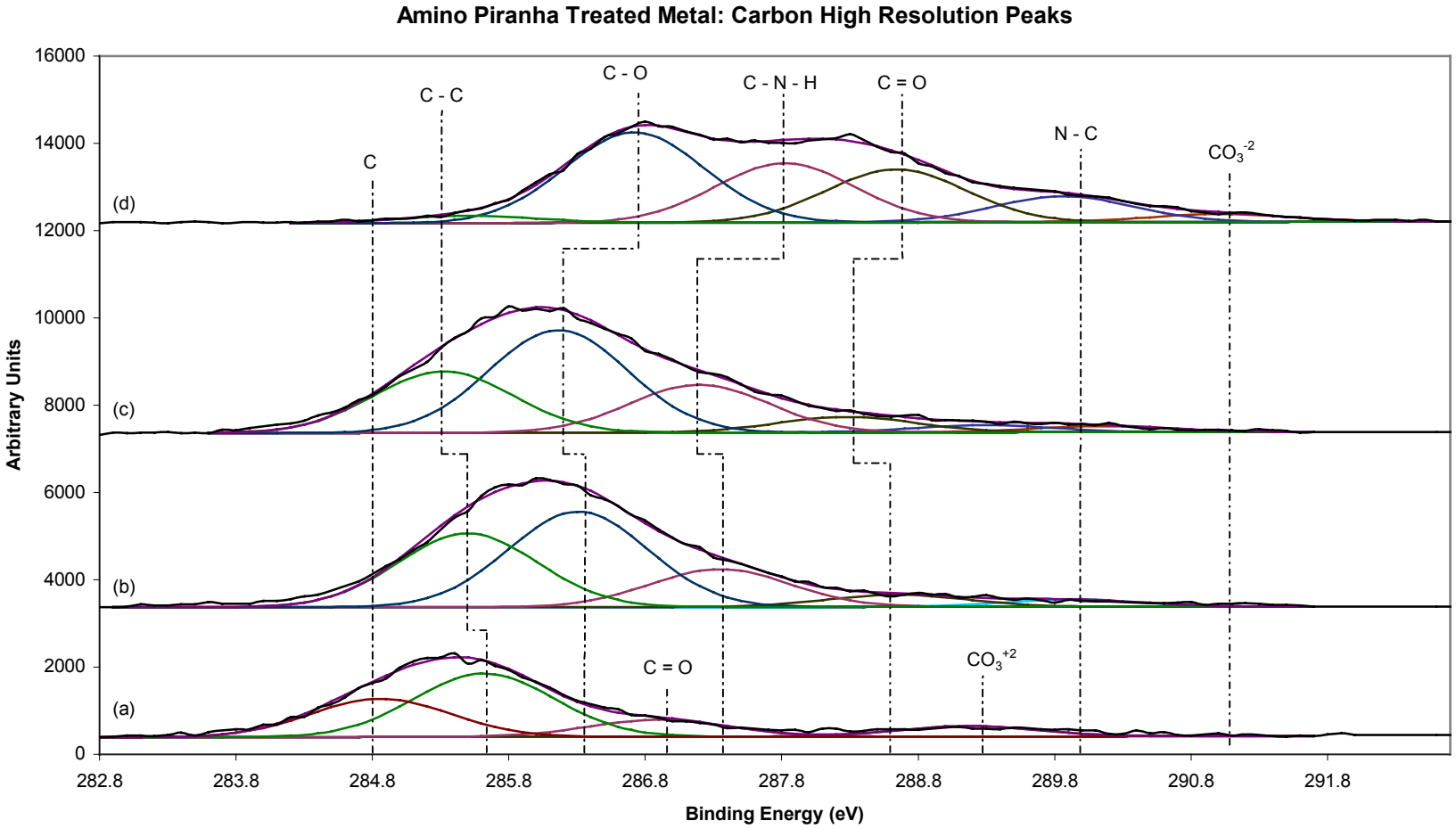

Figure 4.24. Representative carbon high resolution scans of the amino reaction series on piranha treated metal.

The piranha treated metal is labeled (a). The amino silane reaction (reaction step 1a) is labeled (b). The gluteraldehyde reaction (reaction step 2a) is labeled (c). The chitosan reaction (reaction step 3a) is labeled (d).

Tables 4.34 – 4.35 show the peaks from the high resolutions scans of oxygen; there were six oxygen peaks present, with only three of the peaks present in all four reactions. The peak located at 530.5 ± 0.1 eV and identified as TiO showed a significant decrease from the piranha reaction step to the amino reaction step (1a); there was no statistical change between the amino reaction step and the gluteraldehyde step (2a). The TiO peak was not present following the chitosan reaction step (3a). For the peak located at 531.4 ± 0.2 eV, the identity of the peak on the piranha surface was – OH, while the peak for the other three reaction steps was SiO. The SiO peak did not show a statistical change between the amino reaction step and the gluteraldehyde reaction step; however, a significant decrease between the gluteraldehyde step and the chitosan reaction was seen, with values of 760 ± 110 per unit area and 200 ± 20 per unit area, respectively. The peak located at 532.6 ± 0.2 eV was identified as C – O for the piranha treated step and SiO_x for the other three reaction steps. A significant decrease was seen between the amino reaction step and the gluteraldehyde reaction step, from a value of 2500 ± 450 per unit area to a value of 2030 ± 560 per unit area, respectively. A significant decrease was also seen between the gluteraldehyde reaction step and the chitosan reaction step, with a final value of 1010 ± 160 per unit area. The peak located at 533.6 ± 0.2 eV was identified as $-(OH)_3^{-3}$ on the piranha treated surface and SiO_2 following the three reaction steps. There was a significant decrease between the amino reaction step (1a) and the gluteraldehyde reaction step (2a), as well as a significant decrease between the gluteraldehyde reaction step to the chitosan reaction step (3a), with an initial value of 3960 ± 480 per unit area and a final value of 2690 ± 340 per unit area. The fifth peak

was not present on the piranha treated surface and was identified as NO following the reaction steps; it was located at 534.6 ± 0.3 eV. There was significant increase between the amino reaction step and the gluteraldehyde reaction step, along with a significant increase between the gluteraldehyde reaction step to the chitosan reaction step, with an initial value of 730 ± 300 per unit area to a final value of 3930 ± 370 per unit area. The last peak was not present on the piranha treated surface or the amino treated surface (1a), but was present following the gluteraldehyde step (2a) and the chitosan step (3a). The peak identified as C = O was located at 535.6 ± 0.3 eV and did increase significantly from the gluteraldehyde reaction step to the chitosan reaction step, with values of 430 ± 120 per unit area and 890 ± 250 per unit area. Figure 4.25 shows the differences in the peak areas of oxygen on the surface following the four reaction steps on the piranha treated metal surface.

Table 4.34. Oxygen functional group peak areas based on XPS high resolution scans of piranha treated metal using amino silane.

	TiO [4.12]	-OH [4.13] / SiO [4.17]	C-O[4.14] / SiO_x [4.18]	$-(OH)_3^{-3}$ [4.15] / SiO_2 [4.19]
Metal Treatment	530.5 ± 0.1 eV	531.4 ± 0.2 eV	532.6 ± 0.2 eV	533.6 ± 0.2 eV
Piranha	6970 ± 250	3830 ± 350	2120 ± 350[c,d]	850 ± 40
Amino (1a)	600 ± 200[a]	890 ± 210[b]	2500 ± 450[c]	3960 ± 480
Gluteraldehyde (2a)	620 ± 300[a]	760 ± 110[b]	2030 ± 560[d]	3660 ± 410
Chitosan (3a)	---	200 ± 20	1010 ± 160	2690 ± 340

Values with the same superscript are not statistically different at the 5% significance level.

Table 4.35. Oxygen functional group peak areas based on XPS high resolution scans of piranha treated metal using amino silane.

	C-O [4.16] / NO [4.22]	C=O [4.21]
Metal Treatment	534.6 ± 0.3 eV	535.6 ± 0.3 eV
Piranha	---	---
Amino (1a)	730 ± 300	---
Gluteraldehyde (2a)	1450 ± 420	430 ± 120
Chitosan (3a)	3920 ± 370	890 ± 250

Values with the same superscript are not statistically different at the 5% significance level.

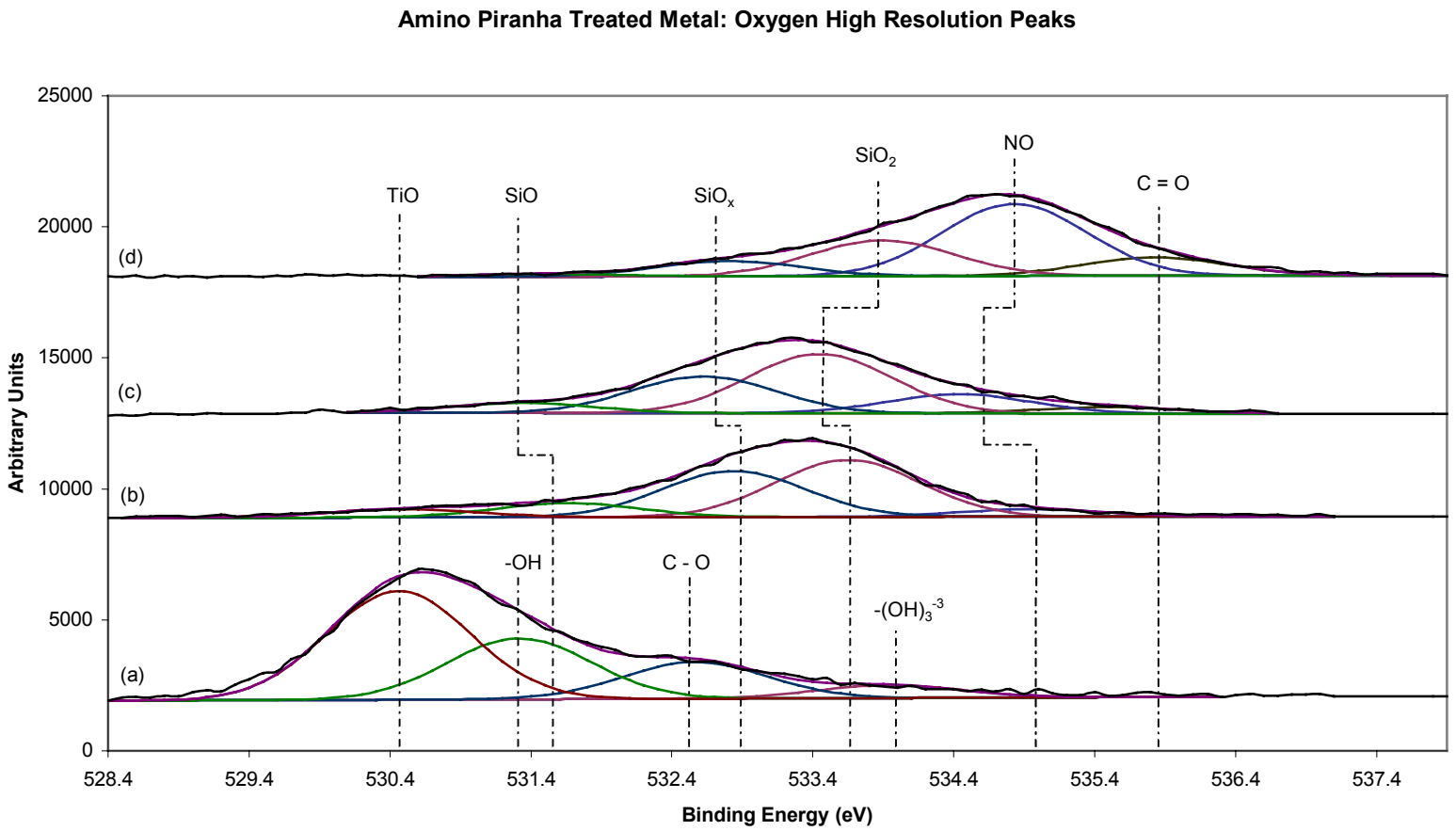

Figure 4.25. Representative oxygen high resolution scans of the amino reaction series on piranha treated metal.

The piranha treated metal is labeled (a). The amino silane reaction (reaction step 1a) is labeled (b). The gluteraldehyde reaction (reaction step 2a) is labeled (c). The chitosan reaction (reaction step 3a) is labeled (d).

Table 4.36 shows the peaks from the high resolution scans of nitrogen; there were no nitrogen peaks present on the piranha treated surface, while there were five peaks present, with two of the peaks present on all of the reaction surfaces. The peak located at 399.8 ± 0.2 eV was identified as N – C; the peak significantly decreased between the three reaction steps, with an initial value of 660 ± 60 per unit area and a final value of 190 ± 10 per unit area. The peak identified as C – N – H and located at 400.9 ± 0.3 eV showed a significant decrease from the amino treated step (1a) to the gluteraldehyde step (2a) from a value of 950 ± 100 per unit area to a value of 490 ± 80 per unit area, while a significant increase was seen from the gluteraldehyde step (2a) to the chitosan step (3a), with a final value of 760 ± 60 per unit area. The peak located at 402.0 ± 0.2 eV, and identified as NH_4^+, was not present on the chitosan surface. It decreased significantly from the amino reaction (1a) to the gluteraldehyde reaction (2a). NO, located at 402.7 ± 0.5 eV, was not present on the amino reaction surface. There was not a significant change between the gluteraldehyde reaction step and the chitosan reaction step. The last peak, NO_2^-, located at 403.8 ± 0.4 eV, was present only following the amino reaction step, with a value of 210 ± 40 per unit area; it was no longer present following the gluteraldehyde reaction. Figure 4.26 shows the differences in the peak areas of nitrogen on the surface following the three reaction steps on the piranha treated metal surface; the piranha treated surface was not shown, as no nitrogen was present.

Table 4.36. Nitrogen functional group peak areas based on XPS high resolution scans of piranha treated metal using amino silane.

	N-C [4.32]	C-N-H [4.33]	NH_4^+ [4.34]	NO [4.36]	NO_2^- [4.35]
Metal Treatment	399.8 ± 0.2 eV	400.9 ± 0.3 eV	402 ± 0.2 eV	402.7 ± 0.5 eV	403.8 ± 0.4 eV
Piranha	---	---	---	---	---
Amino (1a)	660 ± 60	950 ± 100	440 ± 50	---	210 ± 40
Gluteraldehyde (2a)	370 ± 100	490 ± 80	310 ± 90	260 ± 20[a]	---
Chitosan (3a)	190 ± 10	760 ± 60	---	340 ± 70[a]	---

Values with the same superscript are not statistically different at the 5% significance level.

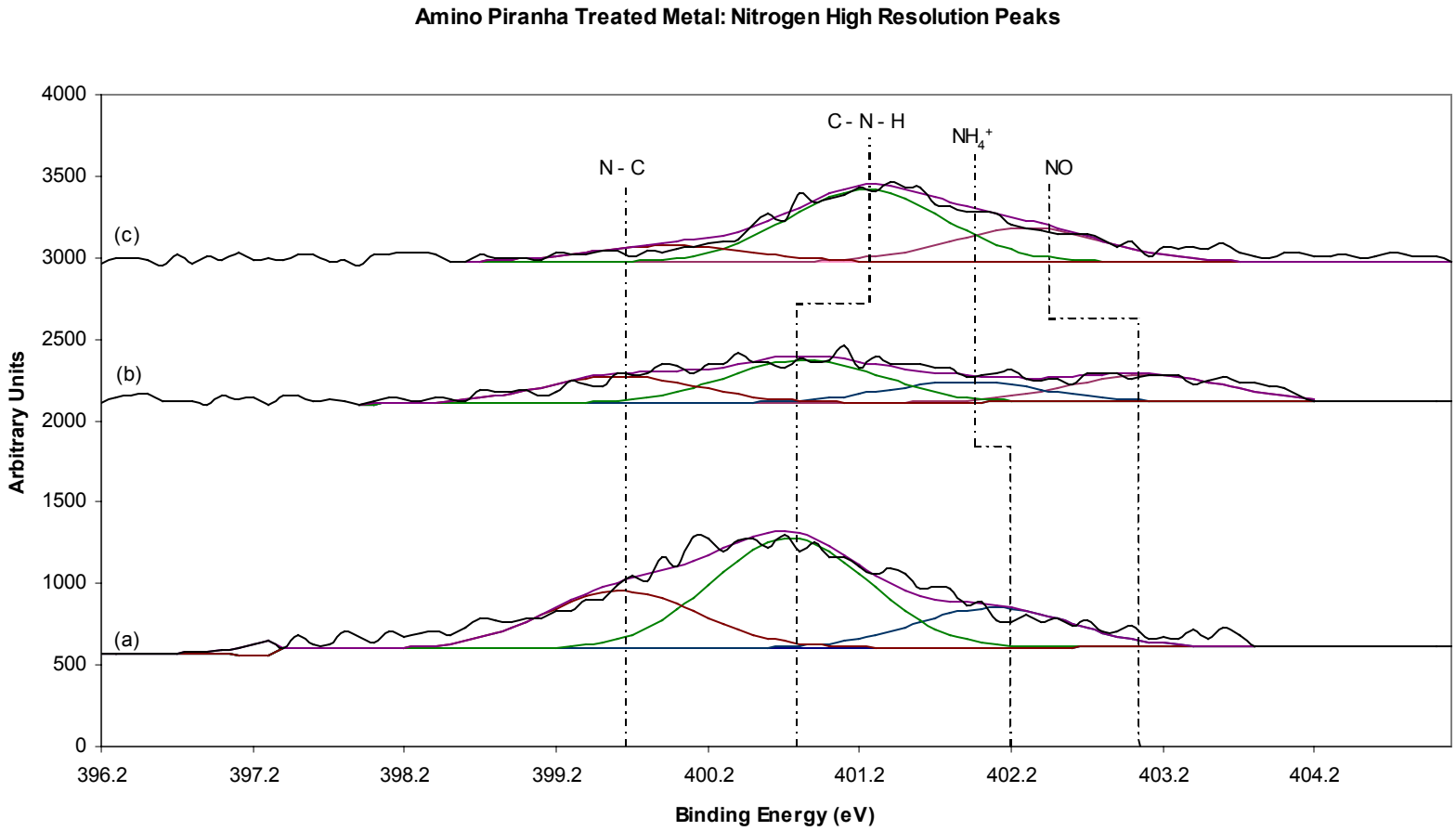

Figure 4.26. Representative nitrogen high resolution scans of the amino reaction series on piranha treated metal.

The amino silane reaction (reaction step 1a) is labeled (a). The gluteraldehyde reaction (reaction step 2a) is labeled (b). The chitosan reaction (reaction step 3a) is labeled (c).

Table 4.37 shows the peaks from the high resolution scans of silicon; there were no silicon peaks present on the piranha treated surface, while there were three peaks present, with only one of the peaks present on all of the reaction surfaces. The peak located at 102.6 ± 0.1 eV was identified as SiO; there was no significant change between the amino reaction step and the gluteraldehyde step, while the peak was not present following the chitosan reaction step. The second peak identified as SiO_3 was located at 103.6 ± 0.2 eV; it was present following all three reaction steps. A significant decrease was seen between the amino reaction step and the gluteraldehyde reaction step; the peak area also significantly decreased between the gluteraldehyde reaction step and the chitosan reaction step, with an initial value following the amino reaction step of 1150 ± 60 per unit area and a final value following the chitosan reaction step of 60 ± 90 per unit area. The third peak, identified as SiO_2, was located at 104.5 ± 0.1 eV. A significant decrease was seen between the amino reaction step and the gluteraldehyde reaction step, while the peak was not present following the chitosan reaction step. Figure 4.27 illustrates the differences of the silicon peak following the three reaction steps on the piranha treated metal; the piranha treated metal was not shown as there was no silicon present.

Table 4.37. Silicon functional group peak areas based on XPS high resolution scans of piranha treated metal using amino silane.

	SiO [4.28]	**SiO_3 [4.29]**	**SiO_2 [4.30]**
Metal Treatment	102.5 ± 0.1 eV	103.6 ± 0.2 eV	104.5 ± 0.1 eV
Piranha	---	---	---
Amino (1a)	420 ± 130[a]	1150 ± 60	390 ± 60
Gluteraldehyde (2a)	270 ± 60[a]	750 ± 50	200 ± 30
Chitosan (3a)	---	60 ± 90	---

Values with the same superscript are not statistically different at the 5% significance level.

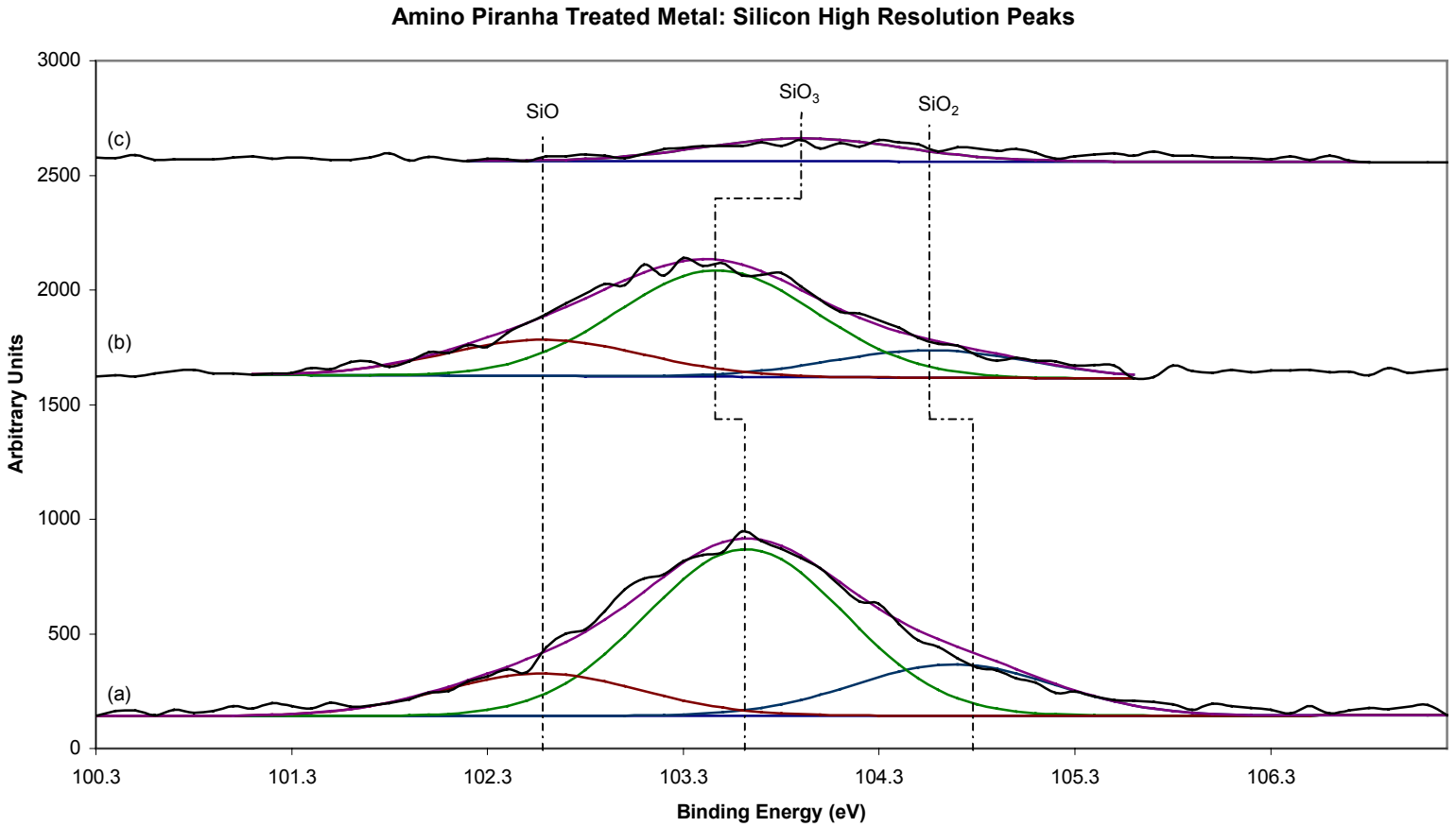

Figure 4.27. Representative silicon high resolution scans of the amino reaction series on piranha treated metal.

The amino silane reaction (reaction step 1a) is labeled (a). The gluteraldehyde reaction (reaction step 2a) is labeled (b). The chitosan reaction (reaction step 3a) is labeled (c).

Table 4.38 shows the peaks from the high resolution scans of titanium; there were no titanium peaks present following the chitosan reaction step. There were three peaks present, with one peak present on only the piranha treated surface. The peak located at 458.3 ± 0.3 eV was identified as TiO_2. It was present only on the piranha treated surface. The peak located at 459.2 ± 0.1 eV was identified as TiO; a significant decrease between the piranha treated surface and the amino reaction step was seen, with values of 6860 ± 460 per unit area and 550 ± 150 per unit area, respectively. No significant change was seen between the amino reaction step and the gluteraldehyde reaction step. The last peak, located at 460.3 ± 0.2 eV, was identified as TiC; there was a significant decrease between the piranha treated surface and the amino treated surface, from an initial value of 750 ± 170 per unit area to a value following the amino reaction of 260 ± 10 per unit area. Only one scan of the gluteraldehyde surface indicated the presence of the TiC peak, which was not statistically different from the peak following the amino reaction step. Figure 4.28 illustrates the differences of the titanium peak following the three reaction steps on the piranha treated metal; the chitosan reaction step was not shown as there was no titanium present.

By looking at the three different surfaces on the piranha treated metal surface, significant changes between the reaction species were seen. An overall increase of the C = O peak indicated that the gluteraldehyde molecule did bind to the amino silane molecule, while an overall decrease of the TiO peak further indicated that the anticipated surface reactions had occurred. The anticipated reaction was further proven by the initial increase of the C – N – H group, followed by a decrease after the gluteraldehyde reaction,

showing that the gluteraldehyde molecule did bond with the terminal amine group. The presence of SiO, SiO_2, and SiO_3 further proved that the anticipated reaction between the piranha treated surface and the amino silane was occurring.

Table 4.38. Titanium functional group peak areas based on XPS high resolution scans of piranha treated metal using amino silane.

	TiO_2 [4.23]	TiO [4.24]	TiC [4.25]
Metal Treatment	458.3 ± 0.3 eV	459.2 ± 0.1 eV	460.3 ± 0.2 eV
Piranha	1010 ± 350	6860 ± 460	750 ± 170
Amino (1a)	---	550 ± 150[b]	260 ± 10[c]
Gluteraldehyde (2a)	---	260 ± 340[b]	170[c]*
Chitosan (3a)	---	---	---

Values with the same superscript are not statistically different at the 5% significance level.
*Only one observation at given binding energy.

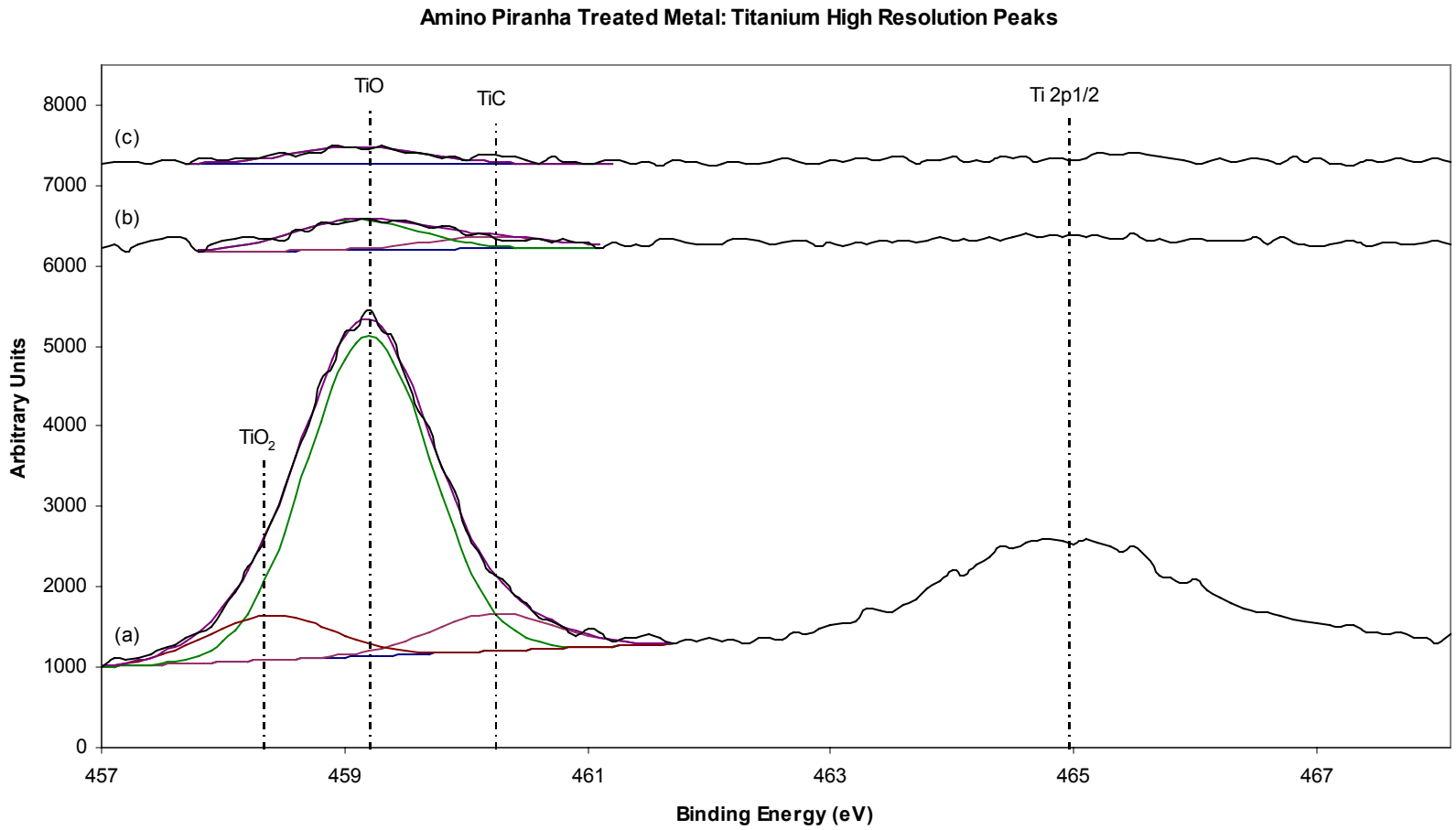

Figure 4.28. Representative titanium high resolution scans of the amino reaction series on piranha treated metal.

The piranha treated metal is labeled (a). The amino silane reaction (reaction step 1a) is labeled (b). The gluteraldehyde reaction (reaction step 2a) is labeled (c).

4.3.3 Triethoxsilylbutyraldehyde Results

Two of the four treatment combinations involved triethoxsilylbutyraldehyde (Aldehyde); the results produced were compared in two different methods. The first method was to compare each metal treatment with respect to each reaction step, while the second method compared each step of the reaction with respect to the metal treatment. The chitosan comparison will be performed in Section 4.3.4.

4.3.3.1 Silane Reaction Step 1b: Comparing Metal Treatments

The percentage means and standard deviations calculated from the survey scans of the two metal treatments for the first reaction step are shown in Table 4.39. Unlike the amino reaction series, which had five elements present, there were only four elements present using the aldehyde reaction step; based on the percentages, there were no statistical differences between any of the elements present. The peak area means and standard deviations table was not given, as the metal treatment peak areas were not statistically different, as shown in Table 4.39. Figure 4.29 shows the representative surface scans of the aldehyde reaction step (1b) on the two treated metals.

Table 4.39. Elemental percentage based on XPS survey scans of the aldehyde treatments, silane step (reaction step 1b).

Metal Treatment	Carbon	Oxygen	Silicon	Titanium
Passivated	50 ± 3^{a} %	32 ± 4^{b} %	17 ± 1^{c} %	1 ± 1^{d} %
Piranha	53 ± 3^{a} %	30 ± 3^{b} %	16 ± 1^{c} %	0 ± 1^{d} %

Values with the same superscript are not statistically different at the 5% significance level.

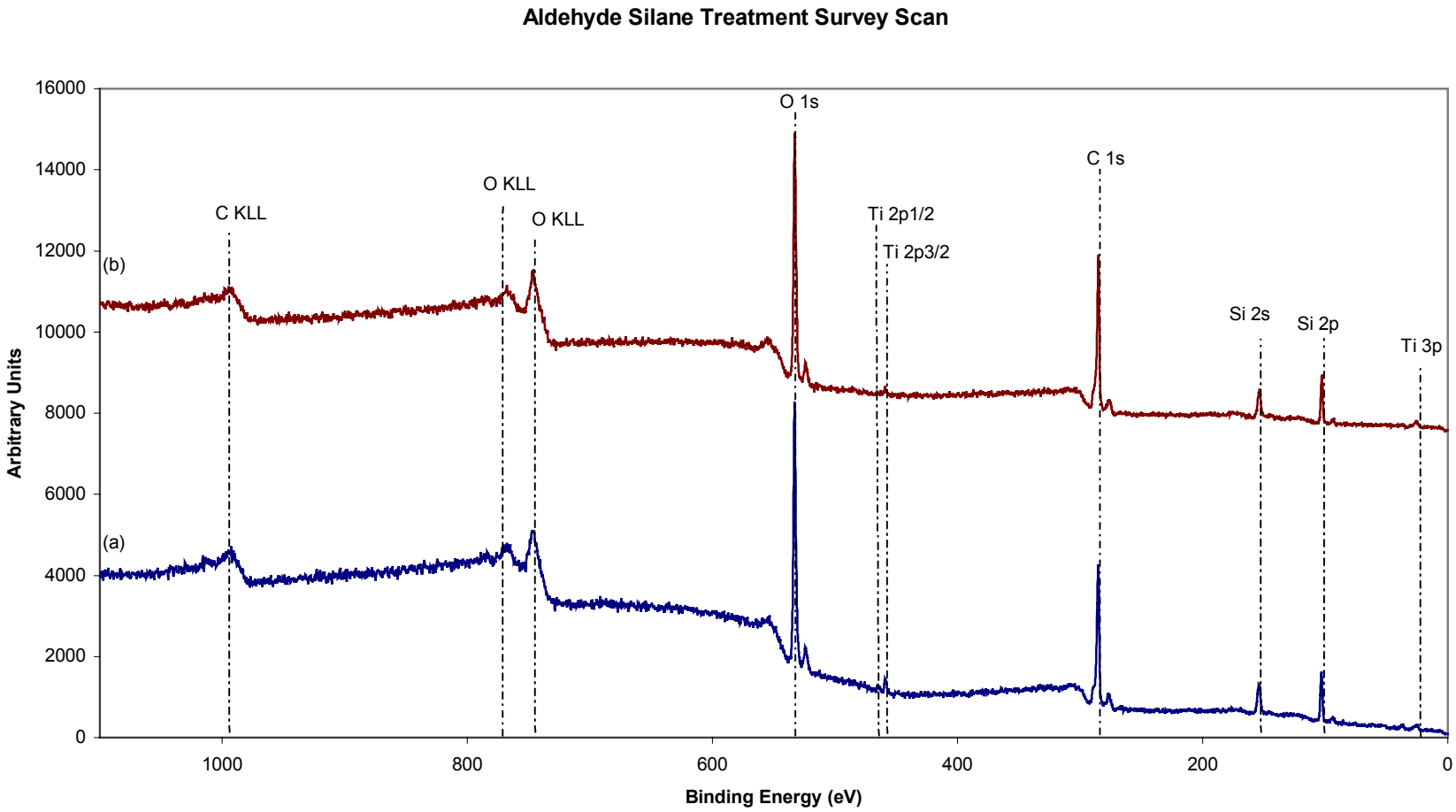

Figure 4.29. Representative survey scans of the aldehyde treatment, silane step, on the two metal treatments.

The passivated treatment is labeled (a), while the piranha treatment is labeled (b).

The means and standard deviations of the high resolutions scans are shown in Tables 4.40 – 4.45. Tables 4.40 – 4.41 show the peaks from the high resolutions scans of carbon; there were seven carbon peaks present on the metal treatments. None of the peaks present were statistically different between the two metal treatments. Figure 4.30 shows the carbon high resolution peaks present on the two metal surfaces.

Table 4.42 – 4.43 show the peaks from the high resolution scans of oxygen; there were six oxygen peaks present on the metal treatments. Of the six peaks present, one peak was not present on both surfaces; the SiO peak, located at 531.9 ± 0.5 eV, was not present on the passivated surface. The SiO_2 peak, located at 533.6 ± 0.3 eV, was the only one of two peaks to show a significant change; the peak area of SiO_2 was significantly less on the piranha treated surface than on the passivated surface, with values of 3420 ± 730 per unit area and 5430 ± 800 per unit area, respectively. The other peak that showed a significant change was the peak located at 535.5 ± 0.2 eV, identified as C = O; however, while the passivated surface was significantly less than the piranha treated surface, there was only one scan that indicated the C = O peak was present on the piranha treated surface. Figure 4.31 shows the oxygen high resolution peaks present on the two metal surfaces.

Table 4.44 shows the peaks from the high resolution scans of silicon; there were five silicon peaks present on the metal treatments. Of the five peaks present, one peak was not present on both surfaces; the SiO_x peak, located at 101.6 ± 0.1 eV was not present on the passivated surface. The other four peaks did not show a significant

difference between the two metal treatments. Figure 4.32 shows the silicon high resolution peaks present on the two metal surfaces.

Table 4.45 shows the peaks from the high resolution scans of titanium; there were four titanium peaks present on the metal treatments. Of the four peaks present, two peaks were not present on both surfaces. The TiO_2 peak, located at 457.6 ± 0.3 eV, was not present on the piranha treated surface, while the TiC peak, located at 460.2 ± 0.2 eV, was not present on the passivated surface. The other two peaks did not show a significant difference. Figure 4.33 shows the titanium high resolution peaks present on the two metal surfaces.

By looking at the two different surfaces following the aldehyde silane reaction, it appeared likely that more aldehyde silane was bound to the piranha treated surface than to the passivated surface, as there was an equal amount of TiO following the silane reaction, but more TiO before the reaction. The attraction of the aldehyde silane reaction was likely best characterized by the significant amount of SiO_3 present on both metal surfaces.

Table 4.40. Carbon functional group peak areas based on XPS high resolution scans of the aldehyde treatments, silane step (reaction step 1b).

	C [4.1]	C-C [4.2]	C-O [4.3]	C=O [4.5]
Metal Treatment	284.8 ± 0.2 eV	285.6 ± 0.2 eV	286.5 ± 0.2 eV	287.6 ± 0.2 eV
Passivated	1580 ± 440[a]	3570 ± 330[b]	1490 ± 210[c]	720 ± 120[d]
Piranha	1830 ± 1050[a]	3240 ± 370[b]	1730 ± 890[c]	860 ± 410[d]

Values with the same superscript are not statistically different at the 5% significance level.

Table 4.41. Carbon functional group peak areas based on XPS high resolution scans of the aldehyde treatments, silane step (reaction step 1b).

	COOH [4.6]	**CO_3^{+2} [4.7]**	**CO_3^{-2} [4.8]**
Metal Treatment	288.8 ± 0.3 eV	289.9 ± 0.2 eV	290.9 ± 0.5 eV
Passivated	460 ± 90[e]	400 ± 100[f]	210 ± 40[g]
Piranha	460 ± 120[e]	330 ± 80[f]	230 ± 70[g]

Values with the same superscript are not statistically different at the 5% significance level.

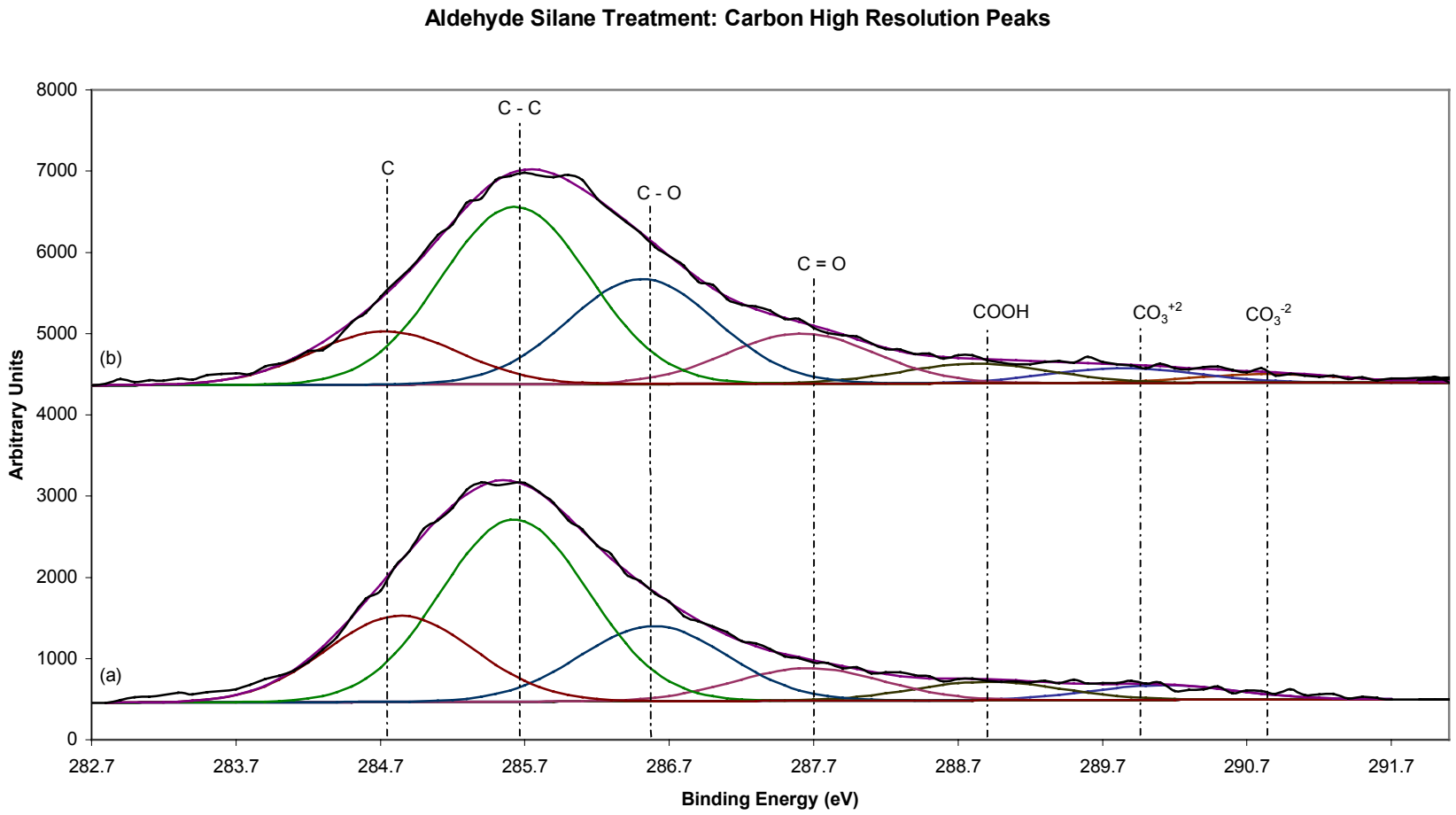

Figure 4.30. Representative carbon high resolution scans of the aldehyde treatment, silane step, on the two metal treatments. The passivated treatment is labeled (a), while the piranha treatment is labeled (b).

Table 4.42. Oxygen functional group peak areas based on XPS high resolution scans of the aldehyde treatments, silane step (reaction step 1b).

	TiO [4.12]	**SiO [4.17]**	**SiO_x [4.18]**	**SiO_2 [4.19]**
Metal Treatment	530.8 ± 0.2 eV	531.9 ± 0.5 eV	532.9 ± 0.2 eV	533.6 ± 0.3 eV
Passivated	840 ± 470[a]	---	4000 ± 1160[b]	5430 ± 800
Piranha	500 ± 90[a]	1650 ± 830	5160 ± 2290[b]	3420 ± 730

Values with the same superscript are not statistically different at the 5% significance level.

Table 4.43. Oxygen functional group peak areas based on XPS high resolution scans of the aldehyde treatments, silane step (reaction step 1b).

	C-O [4.20]	C=O [4.21]
Metal Treatment	534.6 ± 0.3 eV	535.5 ± 0.2 eV
Passivated	1680 ± 450[c]	370 ± 90
Piranha	1310 ± 1360[c]	1190*

Values with the same superscript are not statistically different at the 5% significance level.
* Only one observation at given binding energy.

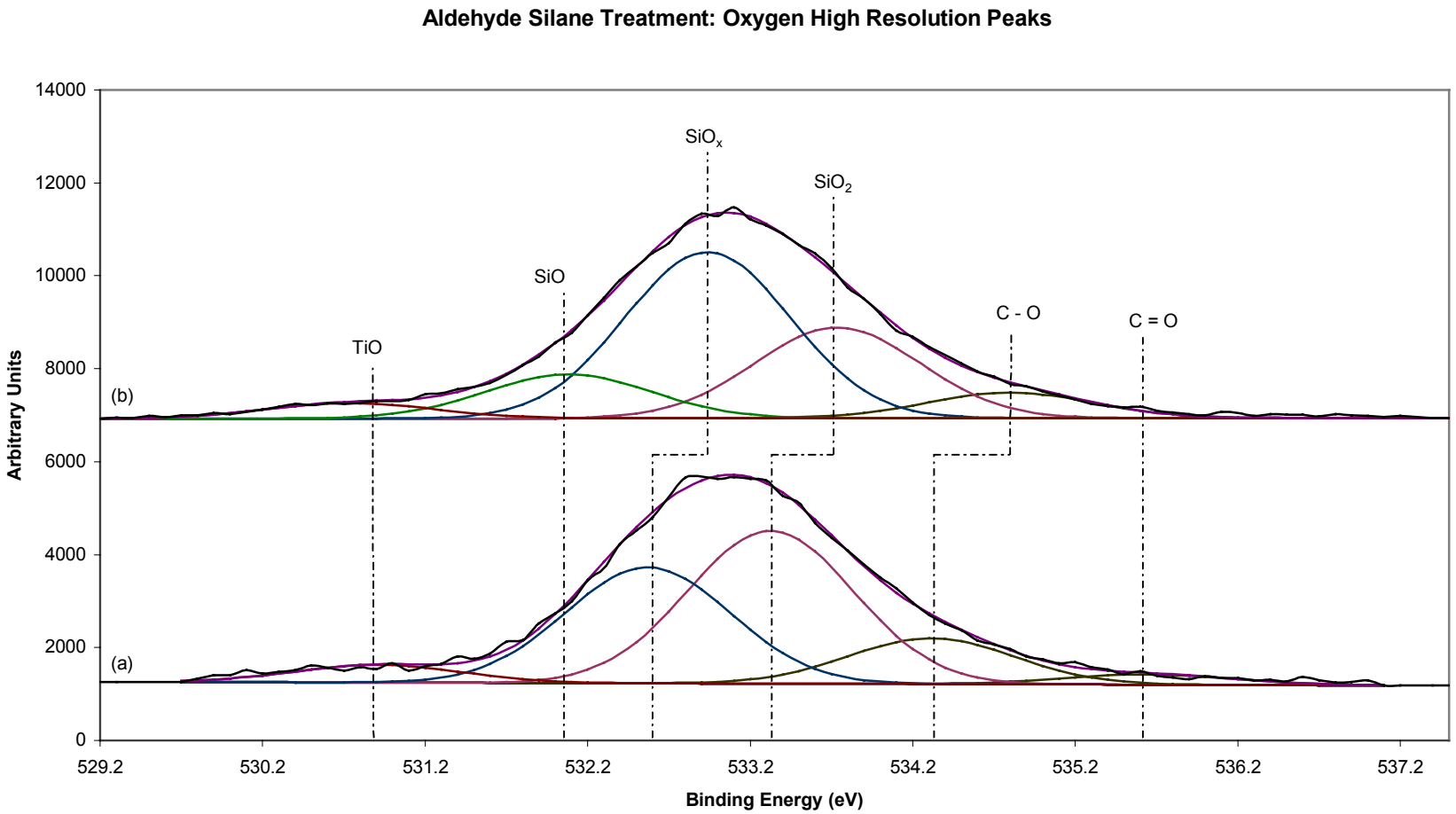

Figure 4.31. Representative oxygen high resolution scans of the aldehyde treatment, silane step, on the two metal treatments. The passivated treatment is labeled (a), while the piranha treatment is labeled (b).

Table 4.44. Silicon functional group peak areas based on XPS high resolution scans of the aldehyde treatments, silane step (reaction step 1b).

	SiO_x [4.27]	**SiO [4.28]**	**SiO_3 [4.29]**	**SiO_2 [4.30]**	**SiO_2 [4.31]**
Metal Treatment	101.6 ± 0.1 eV	102.6 ± 0.2 eV	103.5 ± 0.3 eV	104.5 ± 0.3 eV	105.4 ± 0.3 eV
Passivated	---	710 ± 380[a]	1150 ± 180[b]	530 ± 280[c]	120 ± 50[d]
Piranha	170 ± 0	1010 ± 410[a]	960 ± 160[b]	420 ± 350[c]	240 ± 100[d]

Values with the same superscript are not statistically different at the 5% significance level.

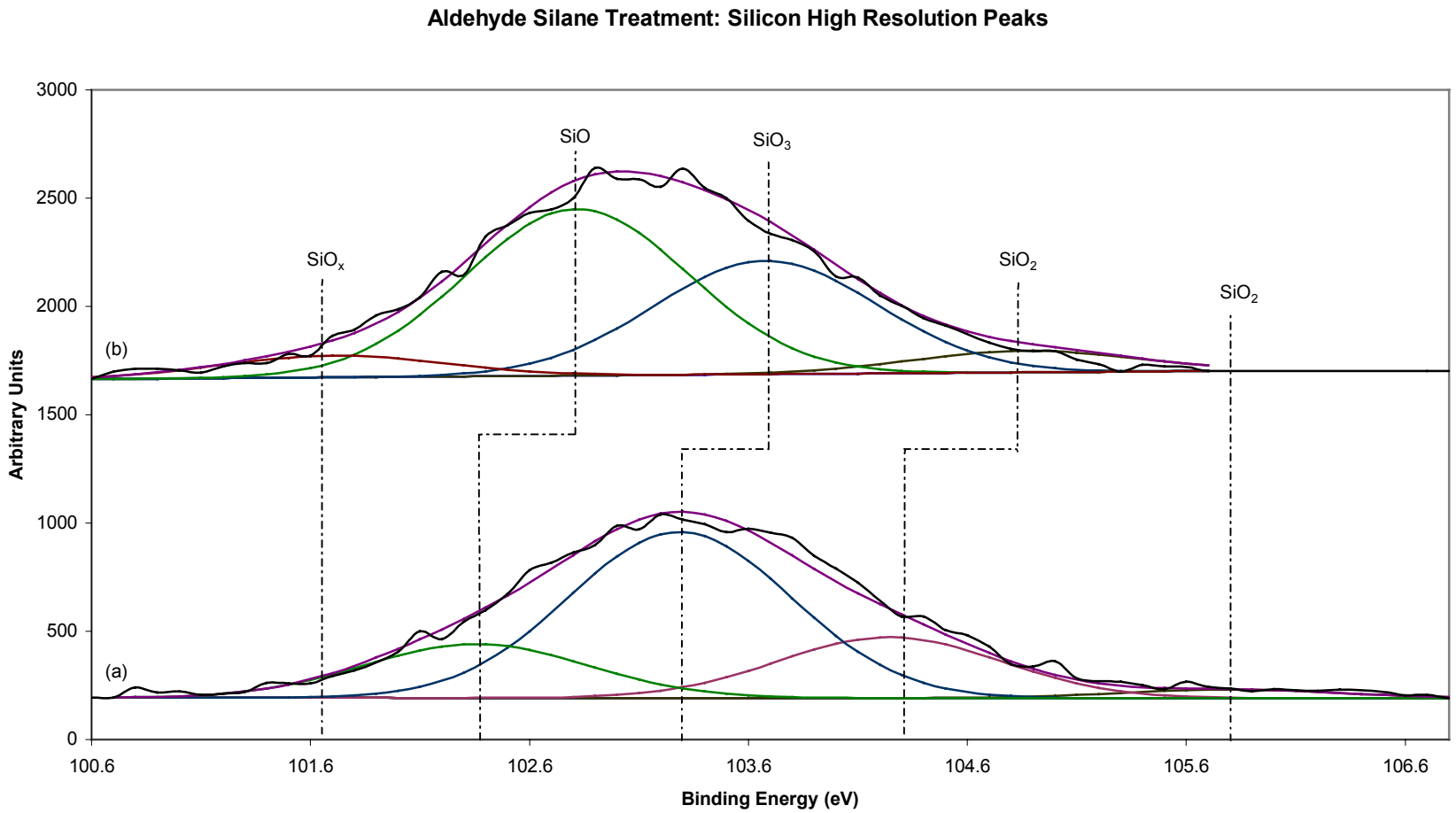

Figure 4.32. Representative silicon high resolution scans of the aldehyde treatment, silane step, on the two metal treatments. The passivated treatment is labeled (a), while the piranha treatment is labeled (b).

Table 4.45. Titanium functional group peak areas based on XPS high resolution scans of the aldehyde treatments, silane step (reaction step 1b).

	TiO_2 [4.23]	TiO [4.24]	TiO_2 [4.26]	TiC [4.25]
Metal Treatment	457.6 ± 0.3 eV	458.8 ± 0.2 eV	459.9 ± 0.3 eV	460.2 ± 0.2 eV
Passivated	150 ± 40	500 ± 300[a]	200 ± 90[b]	---
Piranha	---	180 ± 150[a]	120 ± 90[b]	750 ± 170

Values with the same superscript are not statistically different at the 5% significance level.

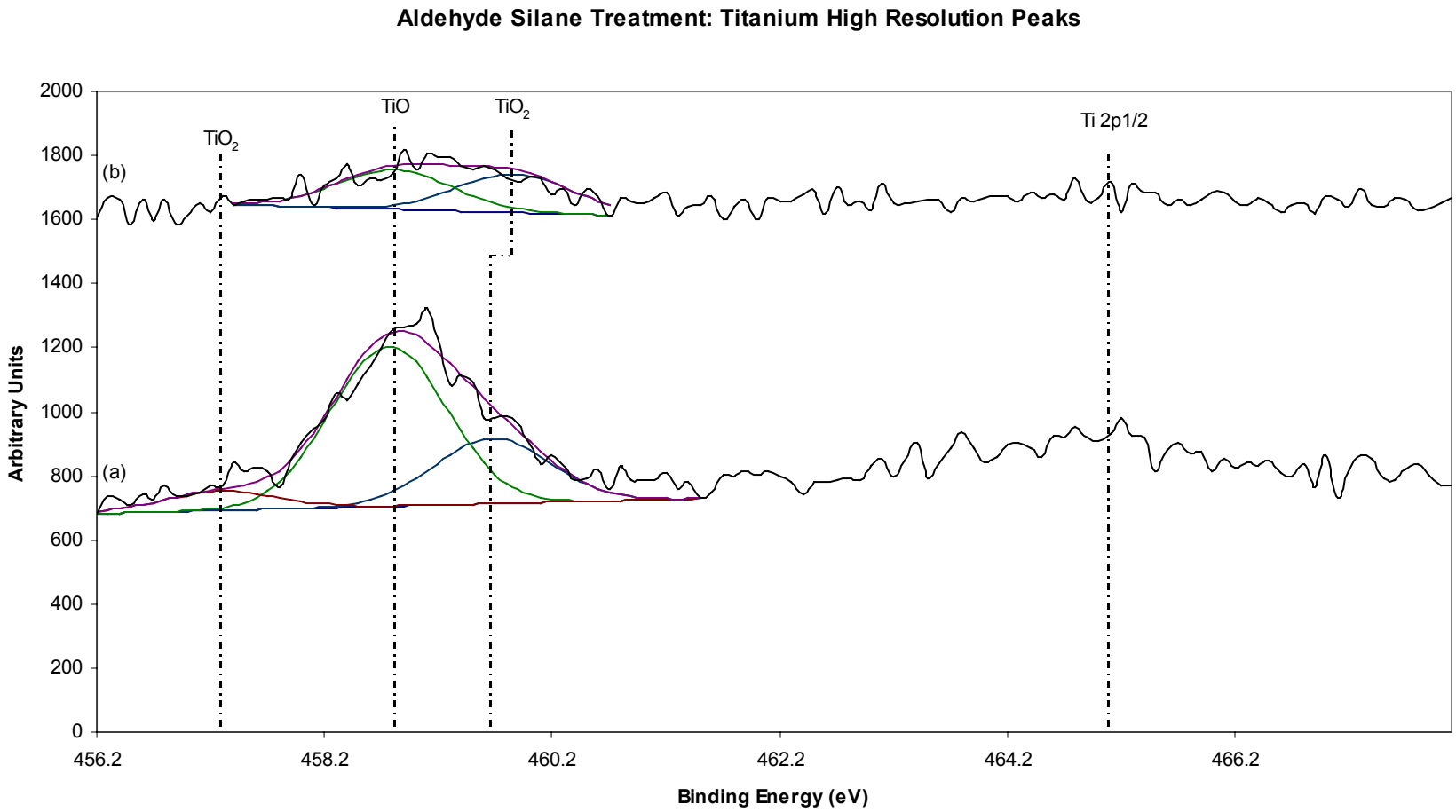

Figure 4.33. Representative titanium high resolution scans of the aldehyde treatment, silane step, on the two metal treatments. The passivated treatment is labeled (a), while the piranha treatment is labeled (b).

4.3.3.2 Passivated Metal Treatment: Comparing Reaction Steps

The percentage means and standard deviations calculated from the survey scans of each step of the aldehyde reaction series on passivated metal are shown in Table 4.46, while the peak area means and standard deviations are shown in Table 4.47. Figure 4.34 shows representative survey scans of each of the reaction steps. By examining the reaction series, several trends were seen. The percentage of carbon initially showed a statistical decrease from the passivated step to the aldehyde step, with values of 65 ± 3 % and 50 ± 3 %, respectively. A statistical increase was then seen from the aldehyde step to the chitosan step, with a final value of 63 ± 3 %. The peak area of carbon showed a different trend; there was no statistical difference between the passivated step and the aldehyde step, while there was a significant increase between the aldehyde step and the chitosan step, with values of 19570 ± 1320 per unit area and 23910 ± 1140 per unit area, respectively.

The percentage of oxygen showed no significant change between the passivated step and the aldehyde step, while there was a significant decrease from the aldehyde step to the chitosan step, with values of 32 ± 4 % and 25 ± 2 %, respectively. The peak area of oxygen showed a different trend; there was a significant increase in peak area between the passivated step and the aldehyde reaction step, with values of 21920 ± 1590 per unit area and 30740 ± 3120 per unit area. However, a significant decrease from the aldehyde reaction step to the chitosan reaction step did still exist, with a final value of 23270 ± 1840 per unit area.

Silicon was not present on the surface of the passivated metal. After the aldehyde reaction step (1b), a significant increase of silicon was seen in both the percentage and peak area, with values of 17 ± 2 % and 5860 ± 580 per unit area, respectively. A significant decrease was seen in both the percentage and peak area following the chitosan reaction step, with values of 6 ± 2 % and 2030 ± 560 per unit area, respectively.

Titanium was not present on the surface of the chitosan film, but was present on the passivated surface and following the aldehyde reaction step (reaction step 1b). A significant decrease from the passivated surface to the aldehyde reaction step was seen, with values of 6 ± 2 % and 1 ± 1 %, respectively. The peak area of titanium showed the same decreasing trend, with values of 11780 ± 4660 per unit area and 2220 ± 1410 per unit area, respectively.

Table 4.46. Elemental percentage based on XPS survey scans of passivated metal using aldehyde silane.

Reaction Step	Carbon	Oxygen	Titanium	Silicon
Passivated	65 ± 3 %	30 ± 2[a] %	6 ± 2 %	---
Aldehyde (1b)	50 ± 3 %	32 ± 4[a] %	1 ± 1 %	17 ± 2 %
Chitosan (2b)	63 ± 3 %	25 ± 2 %	---	6 ± 2 %

Values with the same superscript are not statistically different at the 5% significance level.

Table 4.47. Elemental peak areas based on XPS survey scans of passivated metal using aldehyde silane.

Reaction Step	Carbon	Oxygen	Titanium	Silicon
Passivated	19480 ± 1140[a]	21920 ± 1590	11780 ± 4660	---
Aldehyde (1b)	19570 ± 1320[a]	30740 ± 3120	2220 ± 1410	5860 ± 580
Chitosan (2b)	23910 ± 1140	23270 ± 1840	---	2030 ± 560

Values with the same superscript are not statistically different at the 5% significance level.

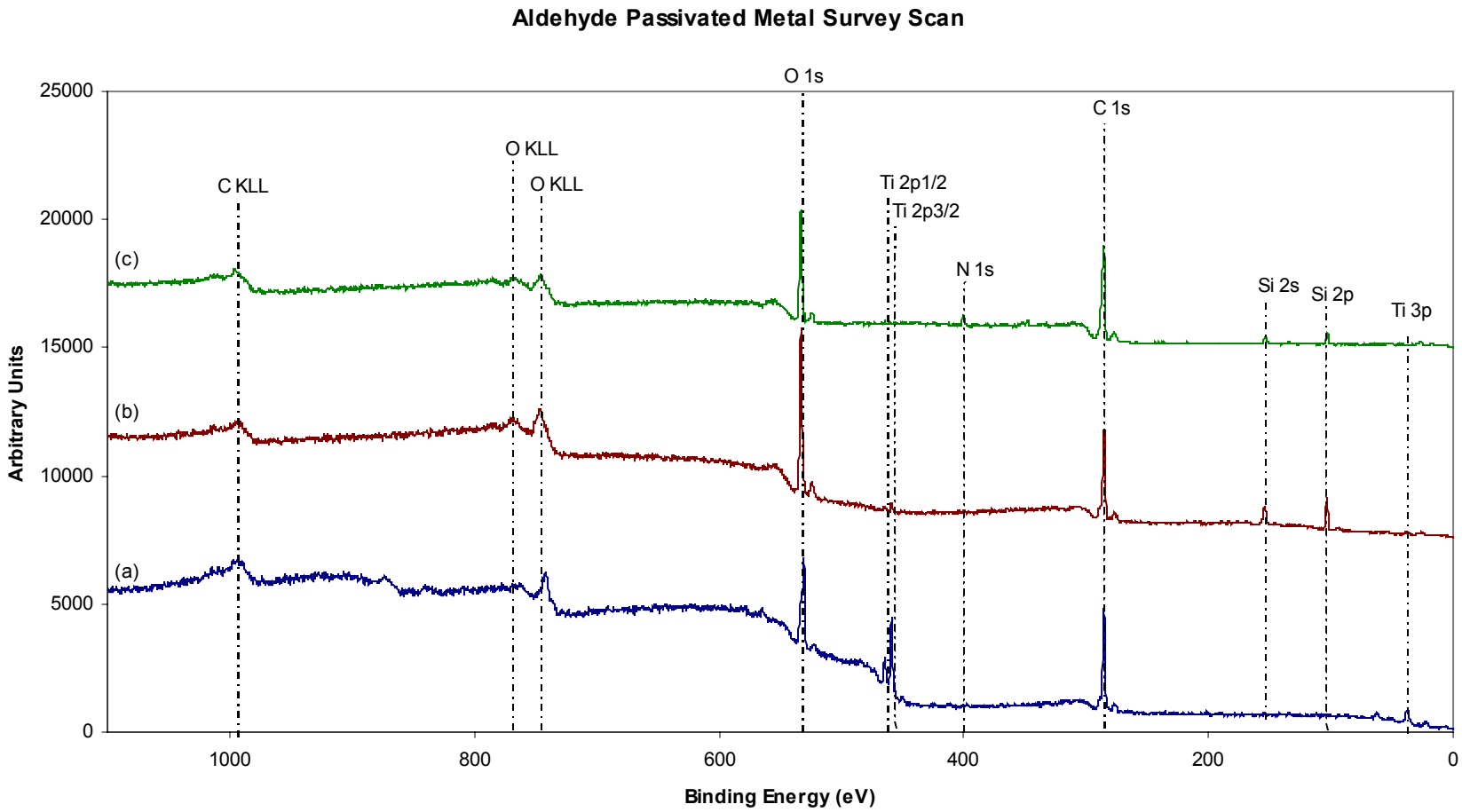

Figure 4.34. Representative survey scans of the aldehyde reaction series on passivated metal.

The passivated metal is labeled (a). The aldehyde silane reaction (reaction step 1b) is labeled (b). The chitosan reaction (reaction step 2b) is labeled (c).

The means and standard deviations of the high resolutions scans are shown in Tables 4.48 – 4.53. Tables 4.48 – 4.49 show the peaks from the high resolutions scans of carbon; there were seven carbon peaks present, only three of the peaks were present in all three reactions. The C peak, located at 284.8 ± 0.2 eV, was present on both the passivated surface and following the aldehyde reaction surface; it was not statistically different. The C – C peak, located at 285.5 ± 0.2 eV, dropped significantly from the passivated metal to the aldehyde reaction step (1b), from 4140 ± 300 per unit area to 3570 ± 330 per unit area, respectively. There were no statistical differences between reaction steps 1b and 2b. The C – O peak, located at 286.3 ± 0.2 eV, was not present on the passivated surface; it increased significantly from the aldehyde reaction (1b), with a value of 1490 ± 210 per unit area, to the chitosan reaction (2b), with a value of 2030 ± 500 per unit area. The peak located at 287.2 ± 0.3 eV was identified as C = O. There was a significant decrease from the passivated metal to the aldehyde reaction step (1b), as well as a significant increase from the aldehyde reaction step to the chitosan reaction step (2b). The COOH peak, located at 288.6 ± 0.2 eV, was not present on the passivated surface; it increased significantly from the aldehyde reaction step to the chitosan reaction step, with a starting value of 460 ± 90 per unit area to a final value of 1020 ± 100 per unit area. The peak located at 290 ± 0.3 eV was identified as CO_3^{+2}. A significant decrease was seen between the passivated surface and the aldehyde reaction step, with values of 590 ± 40 per unit area and 400 ± 100 per unit area, respectively, while no significant changes were seen between the aldehyde reaction step and the chitosan reaction step. The last remaining peak, CO_3^{-2}, was present only on the aldehyde reaction surface (1b)

and was located at 290.7 ± 0.4 eV. Figure 4.35 shows the differences in the peak areas of carbon on the surface following the three reaction steps on the passivated metal surface.

Table 4.48. Carbon functional group peak areas based on XPS high resolution scans of passivated metal using aldehyde silane.

	C [4.1]	C-C [4.2]	C-O [4.3]	C=O [4.5]
Reaction Step	284.8 ± 0.2 eV	285.5 ± 0.2 eV	286.3 ± 0.2 eV	287.3 ± 0.3 eV
Passivated	1590 ± 630[a]	4140 ± 300	---	1350 ± 250
Aldehyde (1b)	1580 ± 440[a]	3570 ± 330[b]	1490 ± 210	720 ± 120
Chitosan (2b)	---	3720 ± 310[b]	2030 ± 500	2460 ± 310

Values with the same superscript are not statistically different at the 5% significance level.

Table 4.49. Carbon functional group peak areas based on XPS high resolution scans of passivated metal using aldehyde silane.

	COOH [4.6]	**CO_3^{+2} [4.7]**	**CO_3^{-2} [4.8]**
Reaction Step	288.6 ± 0.2 eV	289.6 ± 0.3 eV	290.7 ± 0.4 eV
Passivated	---	590 ± 40	---
Aldehyde (1b)	460 ± 90	400 ± 100[c]	210 ± 40
Chitosan (2b)	1020 ± 100	340 ± 40[c]	---

Values with the same superscript are not statistically different at the 5% significance level.

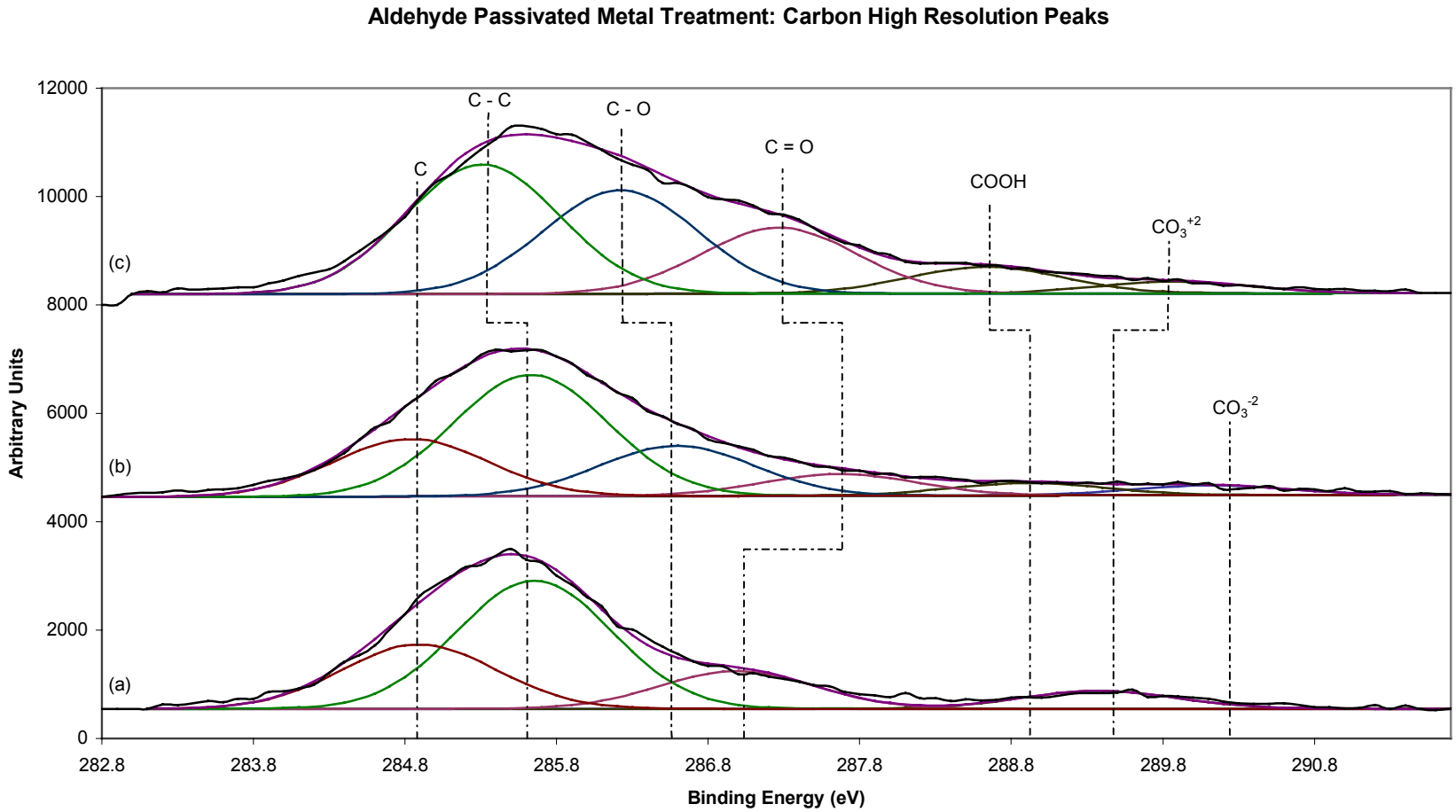

Figure 4.35. Representative carbon high resolution scans of the aldehyde reaction series on passivated metal.

The passivated metal is labeled (a). The aldehyde silane reaction (reaction step 1b) is labeled (b). The chitosan reaction (reaction step 2b) is labeled (c).

Tables 4.50 – 4.51 show the peaks from the high resolutions scans of oxygen; there were six oxygen peaks present, with only three of the peaks present in all three reactions. The peak located at 530.6 ± 0.3 eV, identified as TiO, shows a significant decrease from the passivated step through the aldehyde reaction step (1b) and was not present following the chitosan reaction step (2b). The peak located at 531.4 ± 0.1 eV was identified as – OH on the passivated surface and SiO following the chitosan reaction step; it was not present following the aldehyde reaction. The peak located at 532.6 ± 0.1 eV was identified as C – O on the passivated surface and SiO_x following the aldehyde reaction and the chitosan reaction. A significant decrease was seen from the aldehyde reaction step to the chitosan reaction step, with values of 4000 ± 1160 per unit area and 2500 ± 520 per unit area, respectively. The peak identified as $-(OH)_3^{-3}$ on the passivated surface and SiO_2 following the aldehyde reaction and the chitosan reaction was located at 533.5 ± 0.2 eV. A significant decrease was seen from the aldehyde reaction to the chitosan surface, with values of 5430 ± 800 per unit area and 4000 ± 330 per unit area, respectively. The peak located at 534.5 ± 0.3 eV was identified as C – O; a significant increase was seen from the passivated surface to the aldehyde reaction surface, with values of 570 ± 130 per unit area and 1680 ± 450 per unit area, respectively. There was no significant change between the aldehyde reaction step and the chitosan reaction step. The last peak, identified as C = O and located at 535.5 ± 0.2 eV, was not present on the passivated surface. There was also no significant change between the aldehyde reaction step and the chitosan reaction step. Figure 4.36 shows the differences in the peak areas of oxygen on the surface following the three reaction steps on the passivated metal surface.

Table 4.50. Oxygen functional group peak areas based on XPS high resolution scans of passivated metal using aldehyde silane.

	TiO [4.12]	**-OH [4.13] / SiO [4.17]**	**C-O [4.14] / SiO_x [4.18]**	**$-(OH)_3^{-3}$ [4.15] / SiO_2 [4.19]**
Reaction Step	530.6 ± 0.3 eV	531.4 ± 0.1 eV	532.6 ± 0.1 eV	533.5 ± 0.2 eV
Passivated	3330 ± 790	1920 ± 200	2160 ± 290	1650 ± 270
Aldehyde (1b)	840 ± 470	---	4000 ± 1160	5430 ± 800
Chitosan (2b)	---	720 ± 220	2500 ± 520	4000 ± 330

Values with the same superscript are not statistically different at the 5% significance level.

Table 4.51. Oxygen functional group peak areas based on XPS high resolution scans of passivated metal using aldehyde silane.

	C-O [4.20]	C=O [4.21]
Reaction Step	534.5 ± 0.3 eV	535.5 ± 0.2 eV
Passivated	570 ± 130	---
Aldehyde (1b)	1680 ± 450[a]	370 ± 90[b]
Chitosan (2b)	1860 ± 460[a]	280 ± 80[b]

Values with the same superscript are not statistically different at the 5% significance level.

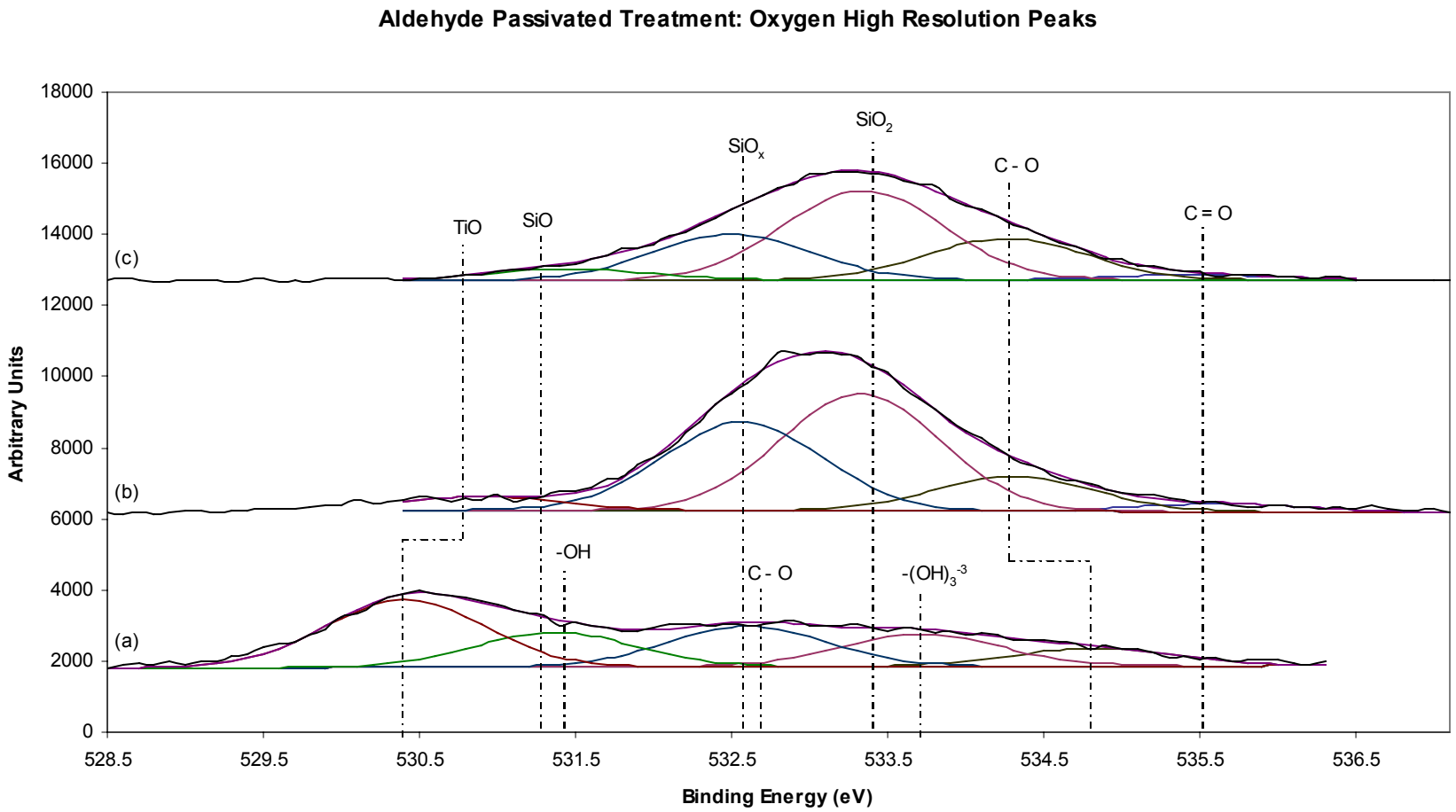

Figure 4.36. Representative oxygen high resolution scans of the aldehyde reaction series on passivated metal.

The passivated metal is labeled (a). The aldehyde silane reaction (reaction step 1b) is labeled (b). The chitosan reaction (reaction step 2b) is labeled (c).

Table 4.52 shows the peaks from the high resolution scans of silicon; there were no silicon peaks present on the passivated surface, while there were five peaks present, with two of the peaks present on the two reaction surfaces. The peak located at 101.9 eV was identified as SiO_x; only one scan out of nine indicated the presence of this peak on the chitosan surface. The peak located at 102.5 ± 0.2 eV was identified as SiO and was present on both the aldehyde reaction surface and the chitosan reaction surface; there was no significant change between the two reaction steps. The next peak, identified as SiO_3, was located at 103.5 ± 0.2 eV; a significant decrease was seen between the aldehyde reaction step and the chitosan reaction step, with a value of 1150 ± 180 per unit area and 210 ± 90 per unit area, respectively. The fourth peak, identified as SiO_2 and located at 104.3 ± 0.3 eV, was not present on the chitosan reaction step; the fifth peak, identified as SiO_2 and located at 105.4 ± 0.3 eV, was also not present on the chitosan reaction step. Figure 4.37 illustrates the differences of the silicon peak following the two reaction steps on the passivated metal; the passivated metal was not shown as there was no silicon present.

Table 4.52. Silicon functional group peak areas based on XPS high resolution scans of passivated metal using aldehyde silane.

	SiO_x [4.27]	**SiO [4.28]**	**SiO_3 [4.29]**	**Si(IV) [4.30]**	**SiO_2 [4.31]**
Reaction Step	101.8* eV	102.5 ± 0.2 eV	103.5 ± 0.2 eV	104.3 ± 0.3 eV	105.4 ± 0.3 eV
Passivated	---	---	---	---	---
Aldehyde (1b)	---	710 ± 380[a]	1150 ± 180	530 ± 280	120 ± 50
Chitosan (2b)	170*	510 ± 120[a]	210 ± 90	---	---

Values with the same superscript are not statistically different at the 5% significance level.
*Only one observation at given binding energy.

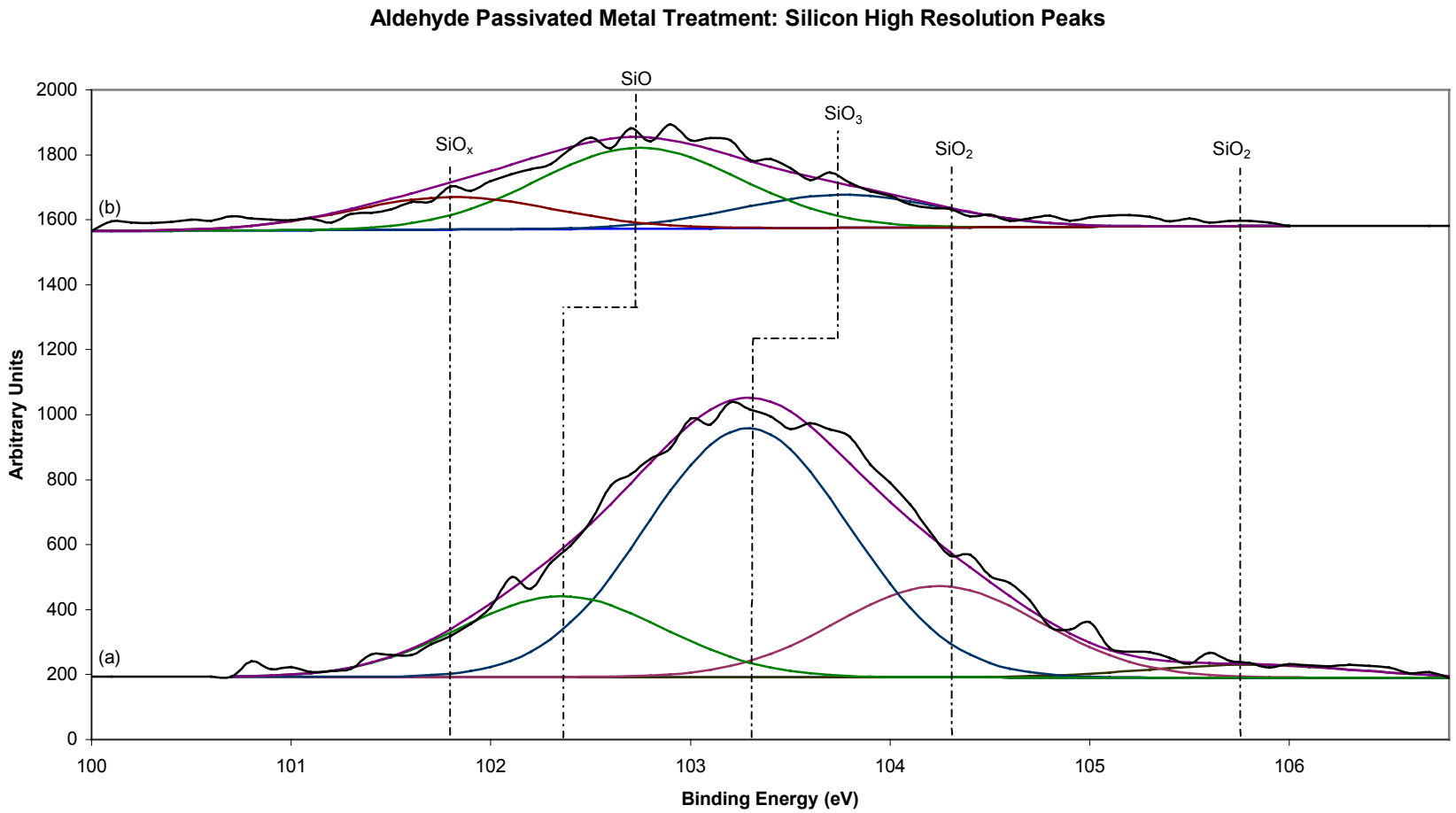

Figure 4.37. Representative silicon high resolution scans of the aldehyde reaction series on passivated metal.

The aldehyde silane reaction (reaction step 1b) is labeled (a). The chitosan reaction (reaction step 2b) is labeled (b).

Table 4.53 shows the peaks from the high resolution scans of titanium; there were no titanium peaks present following the chitosan reaction step. There were four peaks present, with one peak located on only the passivated surface and one peak located only on the surface of the metal following the aldehyde reaction step. The peak located at 457.6 ± 0.3 eV was identified as TiO_2, it was present only following the aldehyde reaction step. The peak located at 458.6 ± 0.2 eV was identified as TiO. A significant decrease was seen from the passivated surface to the aldehyde reaction, with values of 1060 ± 150 per unit area and 500 ± 300 per unit area, respectively. The third peak, located at 459.6 ± 0.4 eV, was identified as TiO_2; a significant decrease from the passivated surface to the aldehyde reaction was seen, with values of 2640 ± 560 per unit area and 200 ± 90 per unit area, respectively. The last peak, located at 460.6 eV, was identified as TiC; it was present only on the passivated surface and was only present in one scan out of nine scans. Figure 4.38 illustrates the differences of the titanium peak following the two reaction steps on the passivated metal; the chitosan reaction step was not shown as there was no titanium present.

By looking at the two different surfaces on the passivated metal surface, significant changes between the reaction species were seen. An overall increase of the C = O peak indicated that the aldehyde silane molecule did bind to the passivated metal surface, while an overall decrease of the TiO peak further indicated that the anticipated surface reactions had occurred. The presence of SiO, SiO_2, and SiO_3 further proved that the anticipated reaction between the passivated surface and the aldehyde silane occurred as expected.

Table 4.53. Titanium functional group peak areas based on XPS high resolution scans of passivated metal using aldehyde silane.

	TiO_2 [4.23]	TiO [4.24]	TiO_2 [4.26]	TiC [4.25]
Reaction Step	457.6 ± 0.3 eV	458.6 ± 0.2 eV	459.6 ± 0.4 eV	460.6* eV
Passivated	---	1060 ± 150	2640 ± 560	420*
Aldehyde (1b)	150 ± 40	500 ± 300	200 ± 90	---
Chitosan (2b)	---	---	---	---

Values with the same superscript are not statistically different at the 5% significance level.
*Only one observation at given binding energy.

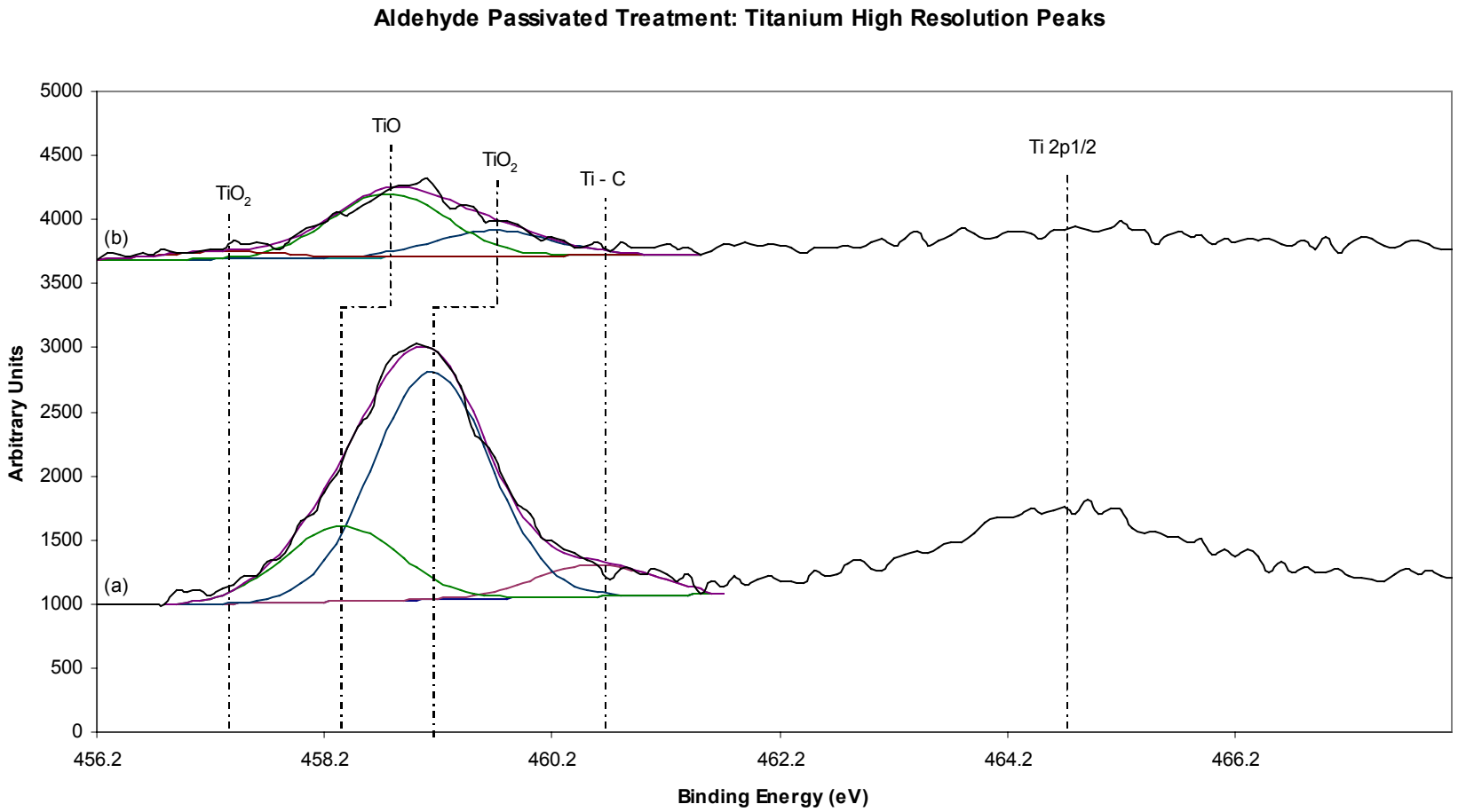

Figure 4.38. Representative titanium high resolution scans of the aldehyde reaction series on passivated metal.

The passivated metal is labeled (a). The aldehyde silane reaction (reaction step 1b) is labeled (b).

4.3.3.3 Piranha Treated Metal: Comparing Reaction Steps

The percentage means and standard deviations calculated from the survey scans of each step of the aldehyde reaction series on the piranha treated metal are shown in Table 4.54, while the peak area means and standard deviations are shown in Table 4.55. Figure 4.39 shows representative survey scans of each of the reaction steps. By examining the reaction series, several trends were seen. The percentage of carbon initially showed a statistical increase from the piranha treated metal to the aldehyde step (1b), with values of 40 ± 1 % and 53 ± 3 %, respectively. Another statistical increase was seen from the aldehyde step to the chitosan step (2b), with a final value of 65 ± 1 %. The peak area of carbon showed the same trend, with a statistical increase from the piranha treated metal through the aldehyde reaction step to the final chitosan reaction step.

The percentage of oxygen showed a significant decrease from the piranha treated surface to the aldehyde reaction step, with values of 45 ± 1 % and 30 ± 3 %, respectively. Another significant decrease was seen from the aldehyde reaction step to the chitosan reaction step, ending with a final value of 26 ± 1 %. The same trend was seen in the oxygen peak area; a significant decrease in the amount of oxygen occurred between the piranha treated metal and the aldehyde reaction step, along with a significant decrease between the aldehyde reaction step and the chitosan reaction step.

Silicon was not present on the piranha treated surface, but was present following the aldehyde reaction step (1b) and the chitosan reaction step (2b). After the aldehyde reaction step, a significant increase of silicon was seen in both the percentage and peak area, with values of 16 ± 1 % and 5640 ± 280 per unit area, respectively. A significant

decrease was seen in both the percentage and peak area following the chitosan reaction step, with values of 2 ± 2 % and 770 ± 530 per unit area, respectively.

Titanium was not present on the surface of the chitosan film, but was present on the piranha treated surface and following the aldehyde reaction step (1b). A significant decrease from the piranha treated surface to the aldehyde reaction step was seen, with values of 15 ± 2 % and 0 ± 1 %, respectively. The peak area of titanium showed the same decreasing trend, with values of 3340 ± 5640 per unit area and 760 ± 920 per unit area, respectively.

Table 4.54. Elemental percentage based on XPS survey scans of piranha treated metal using aldehyde silane.

Reaction Step	Carbon	Oxygen	Titanium	Silicon
Piranha	40 ± 1 %	44 ± 1 %	15 ± 2 %	---
Aldehyde (1b)	53 ± 3 %	30 ± 3 %	0 ± 1 %	16 ± 1 %
Chitosan (2b)	64 ± 1 %	26 ± 1 %	---	2 ± 2 %

Values with the same superscript are not statistically different at the 5% significance level.

Table 4.55. Elemental peak areas based on XPS survey scans of piranha treated metal using aldehyde silane.

Reaction Step	Carbon	Oxygen	Titanium	Silicon
Piranha	12430 ± 660	34410 ± 1340	33400 ± 5640	---
Aldehyde (1b)	20310 ± 970	28480 ± 2780	760 ± 920	5640 ± 280
Chitosan (2b)	24790 ± 730	24750 ± 1050	---	770 ± 530

Values with the same superscript are not statistically different at the 5% significance level.

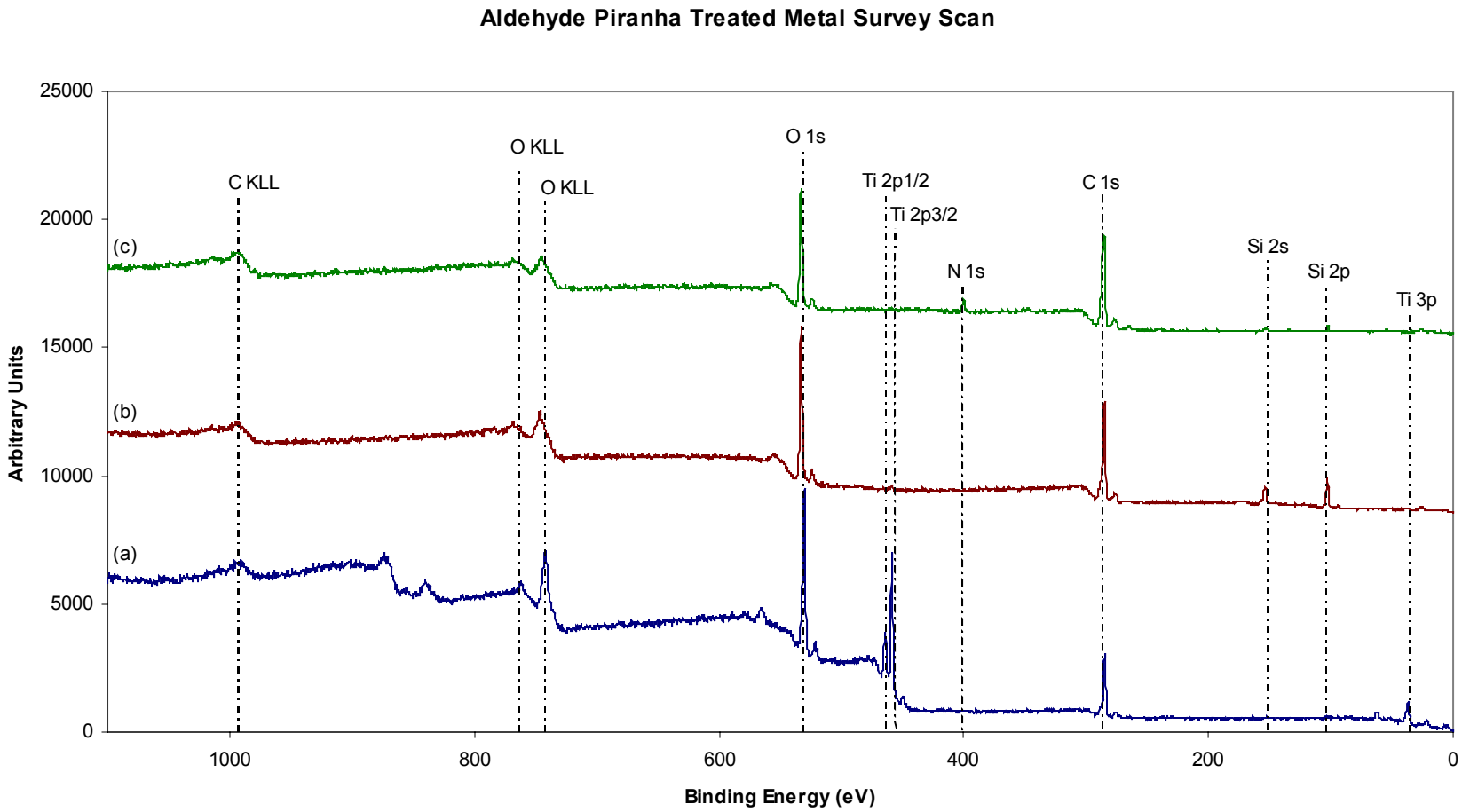

Figure 4.39. Representative survey scans of the aldehyde reaction series on the piranha treated metal.

The piranha treated metal is labeled (a). The aldehyde silane reaction (reaction step 1b) is labeled (b). The chitosan reaction (reaction step 2b) is labeled (c).

The means and standard deviations of the high resolutions scans are shown in Tables 4.56 – 4.61. Tables 4.56 – 4.57 show the peaks from the high resolutions scans of carbon; there were seven carbon peaks present, only four of the peaks were present in all three reactions. The first peak, identified as C and located at 284.8 ± 0.1 eV, was present on all three reaction surfaces; there were no statistical differences between the three reaction steps. The C – C peak, located at 285.6 ± 0.1 eV, also showed no statistical differences between the three reaction steps. The C – O peak, located at 286.6 ± 0.2 eV, was not present on the piranha treated surface. It increased significantly from the piranha treated surface to the aldehyde reaction surface, while there were no significant changes between the aldehyde reaction surface and the chitosan reaction surface. The fourth peak, located at 287.3 ± 0.4 eV, was identified as C = O. There was a no significant change between the piranha treated surface and the aldehyde reaction surface; however, there was a significant increase from the aldehyde reaction step to the chitosan reaction step, with values of 860 ± 410 per unit area and 2490 ± 690 per unit area, respectively. The COOH peak, located at 288.8 ± 0.2 eV, was not present on the piranha treated surface; it increased significantly from the aldehyde reaction step to the chitosan reaction step, with a starting value of 460 ± 120 per unit area to a final value of 1120 ± 90 per unit area. The peak located at 289.6 ± 0.4 eV was identified as CO_3^{+2}. There were no significant changes between the three reaction steps. The last remaining peak, CO_3^{-2}, was not present on the piranha treated surface; it was located at 290.8 ± 0.5 eV. The amount present was not statistically different between the aldehyde reaction step and the chitosan

reaction step. Figure 4.40 shows the differences in the peak areas of carbon on the surface following the three reaction steps on the piranha treated metal surface.

Table 4.56. Carbon functional group peak areas based on XPS high resolution scans of piranha treated metal using aldehyde silane.

	C [4.1]	C-C [4.2]	C-O [4.3]	C=O [4.5]
Reaction Step	284.8 ± 0.1 eV	285.6 ± 0.1 eV	286.6 ± 0.2 eV	287.3 ± 0.4 eV
Piranha	1270 ± 270[a]	2590 ± 230[b]	---	670 ± 60[d]
Aldehyde (1b)	1830 ± 1050[a]	3240 ± 350[b]	1730 ± 890[c]	860 ± 410[d]
Chitosan (2b)	750 ± 160[a]	3030 ± 1250[b]	2660 ± 650[c]	2490 ± 690

Values with the same superscript are not statistically different at the 5% significance level.

Table 4.57. Carbon functional group peak areas based on XPS high resolution scans of piranha treated metal using aldehyde silane.

	COOH [4.6]	CO_3^{+2} [4.7]	CO_3^{-2} [4.8]
Reaction Step	288.8 ± 0.2 eV	289.6 ± 0.4 eV	290.8 ± 0.5 eV
Piranha	---	370 ± 30[e]	---
Aldehyde (1b)	460 ± 120	330 ± 80[e]	230 ± 70[f]
Chitosan (2b)	1120 ± 90	540 ± 340[e]	230 ± 40[f]

Values with the same superscript are not statistically different at the 5% significance level.

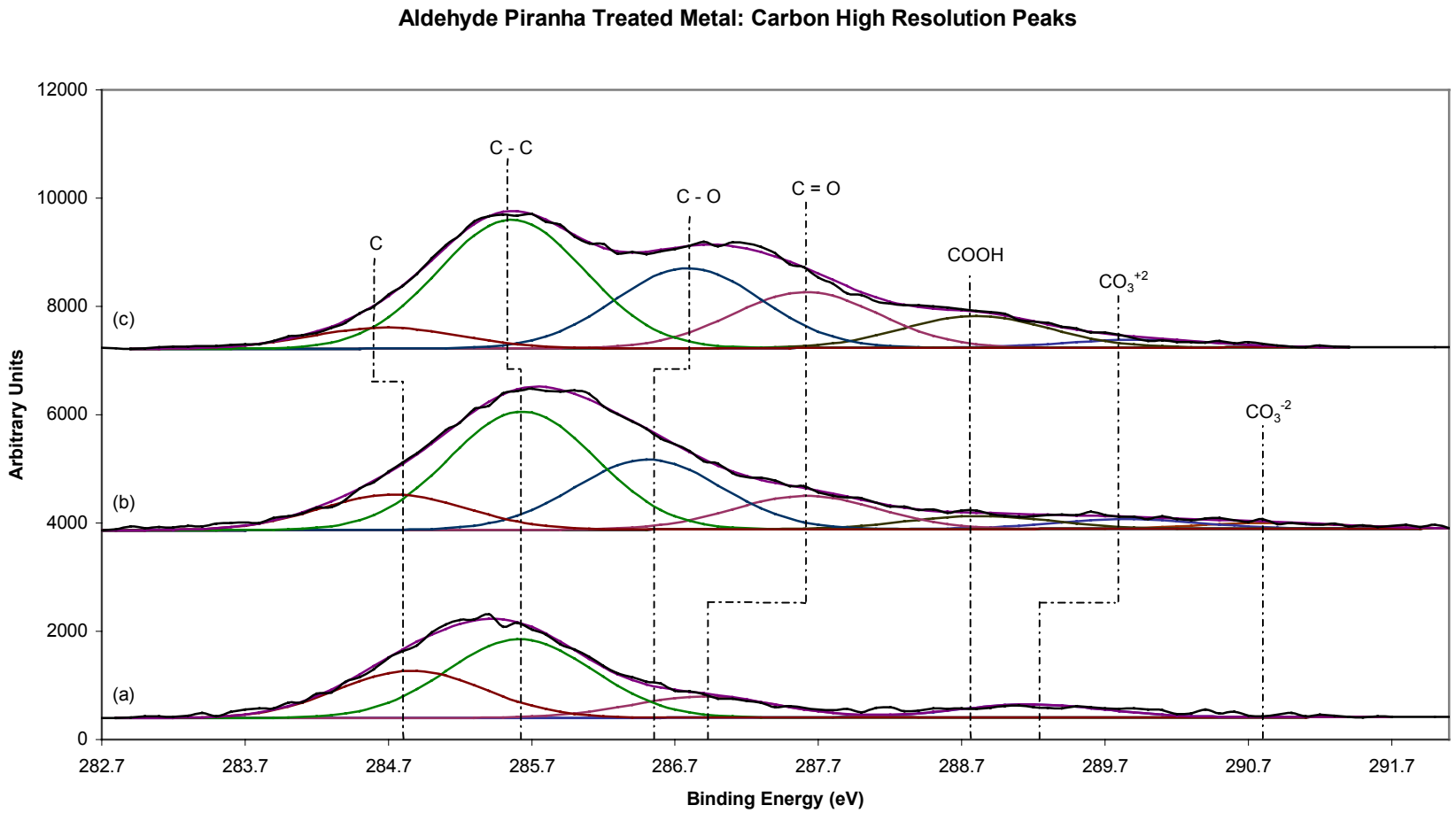

Figure 4.40. Representative carbon high resolution scans of the aldehyde reaction series on the piranha treated metal.

The piranha treated metal is labeled (a). The aldehyde silane reaction (reaction step 1b) is labeled (b). The chitosan reaction (reaction step 2b) is labeled (c).

Tables 4.58 – 4.59 show the peaks from the high resolutions scans of oxygen; there were six oxygen peaks present, with only two of the peaks present in all three reactions. The peak located at 530.5 ± 0.2 eV and identified as TiO showed a significant decrease from the piranha treated metal through the aldehyde reaction step (1b) and was not present following the chitosan reaction step (2b). The peak located at 531.5 ± 0.4 eV was identified as – OH on the piranha treated surface and SiO following the aldehyde reaction step; it was not present following the chitosan reaction. The peak located at 532.4 ± 0.4 eV was identified as C – O on the piranha treated surface and SiO_x following the aldehyde reaction and the chitosan reaction. A significant decrease was seen from the aldehyde reaction step to the chitosan reaction step, with values of 5160 ± 2290 per unit area and 1600 ± 530 per unit area, respectively. The peak identified as $-(OH)_3^{-3}$ on the piranha treated surface and SiO_2 following the aldehyde reaction and the chitosan reaction was located at 533.5 ± 0.3 eV. There was no significant change between the aldehyde reaction and the chitosan reaction. The peak located at 534.5 ± 0.4 eV was identified as C – O and was not present on the piranha treated surface; no significant changes were seen between the aldehyde reaction and the chitosan reaction. However, the peak was seen only once out of nine scans on the aldehyde reaction surface. The last peak, identified as C = O and located at 535.3 ± 0.2 eV, was not present on the passivated surface. There was also no significant change between the aldehyde reaction step and the chitosan reaction step, although there was only one scan out of nine that showed the peak following the aldehyde reaction surface. Figure 4.41 shows the differences in the peak

areas of oxygen on the surface following the three reaction steps on the piranha treated metal surface.

Table 4.58. Oxygen functional group peak areas based on XPS high resolution scans of piranha treated metal using aldehyde silane.

	TiO [4.12]	**-OH [4.13] / SiO [4.17]**	**C-O [4.14] / SiO_x [4.18]**	**$-(OH)_3^{-3}$ [4.15] / SiO_2 [4.19]**
Reaction Step	530.5 ± 0.2 eV	531.5 ± 0.4 eV	532.4 ± 0.4 eV	533.5 ± 0.3 eV
Piranha	6970 ± 250	3830 ± 350	2120 ± 350	850 ± 40
Aldehyde (1b)	500 ± 90	1650 ± 830	5160 ± 2290	3420 ± 730[a]
Chitosan (2b)	---	---	1600 ± 530	3950 ± 910[a]

Values with the same superscript are not statistically different at the 5% significance level.

Table 4.59. Oxygen functional group peak areas based on XPS high resolution scans of piranha treated metal using aldehyde silane.

	C-O [4.20]	C=O [4.21]
Reaction Step	534.5 ± 0.4 eV	535.3 ± 0.2 eV
Piranha	---	---
Aldehyde (1b)	1310 ± 1360[b]	1190[c]*
Chitosan (2b)	3740 ± 1020[b]	790 ± 480[c]

Values with the same superscript are not statistically different at the 5% significance level.
*Only one observation at given binding energy.

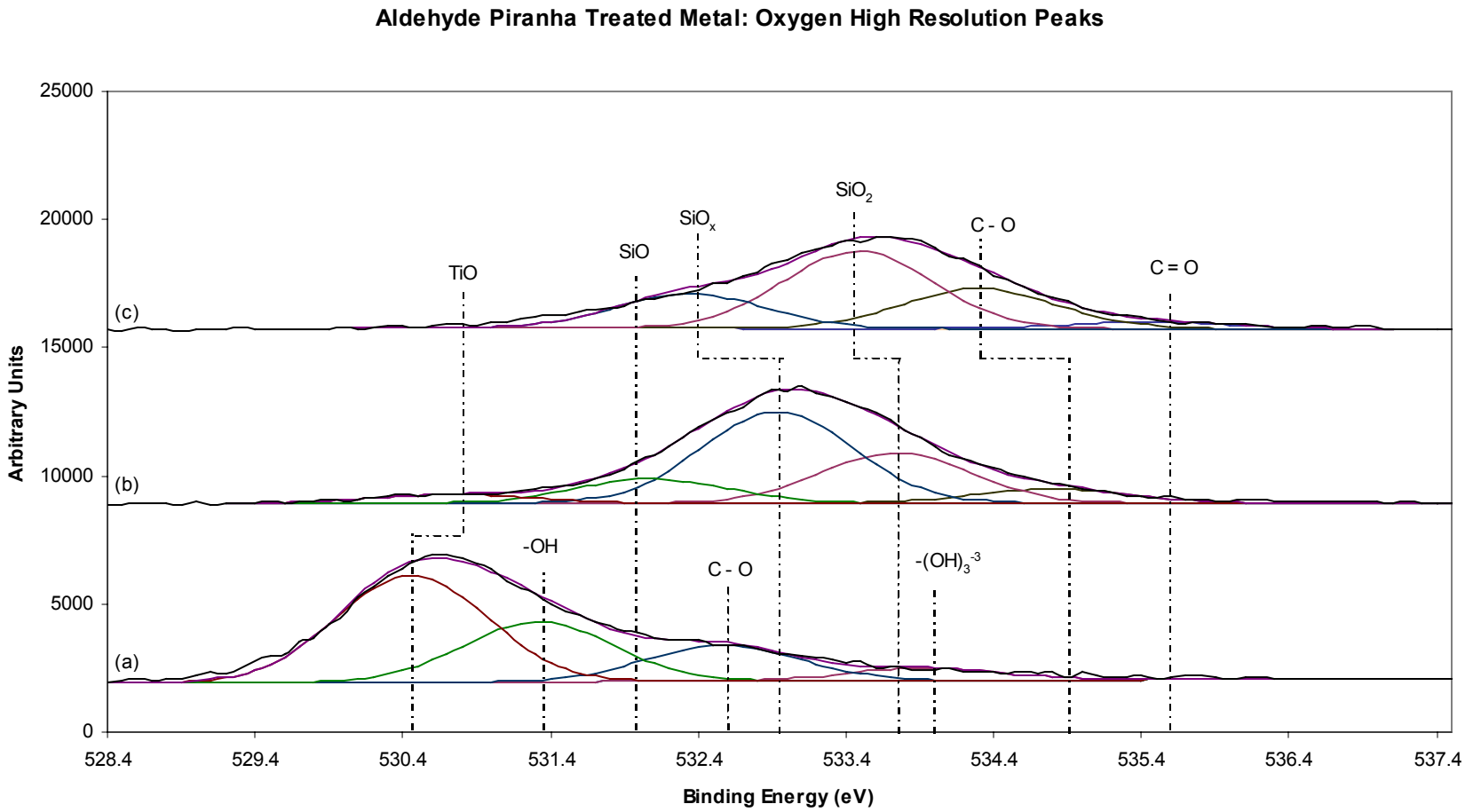

Figure 4.41. Representative oxygen high resolution scans of the aldehyde reaction series on the piranha treated metal.

The piranha treated metal is labeled (a). The aldehyde silane reaction (reaction step 1b) is labeled (b). The chitosan reaction (reaction step 2b) is labeled (c).

Table 4.60 shows the peaks from the high resolution scans of silicon; there were no silicon peaks present on the piranha treated surface, while there were five peaks present, with three of the peaks present on the two reaction surfaces. The peak located at 102.0 ± 0.3 eV was identified as SiO_x; only one scan out of nine indicated the presence of this peak on the aldehyde surface; there were no statistical differences between the aldehyde surface and the chitosan surface. The peak located at 102.8 ± 0.3 eV was identified as SiO and was present on both the aldehyde reaction surface and the chitosan reaction surface; there was a significant decrease between the aldehyde surface and the chitosan surface, with values of 1010 ± 410 per unit area and 260 ± 120 per unit area, respectively. The next peak, identified as SiO_3, was located at 103.7 ± 0.2 eV; a significant decrease was seen between the aldehyde reaction step and the chitosan reaction step, with values of 960 ± 160 per unit area and 150 ± 50 per unit area, respectively. The fourth peak, identified as SiO_2 and located at 104.7 ± 0.3 eV, was not present on the chitosan reaction step; the fifth peak, identified as SiO_2 and located at 105.6 ± 0.2 eV, was also not present on the chitosan reaction step. Figure 4.42 illustrates the differences of the silicon peak following the two reaction steps on the piranha treated metal; the passivated metal was not shown as there was no silicon present.

Table 4.60. Silicon functional group peak areas based on XPS high resolution scans of piranha treated metal using aldehyde silane.

	SiO_x [4.27]	**SiO [4.28]**	**SiO_3 [4.29]**	**SiO_2 [4.30]**	**SiO_2 [4.31]**
Reaction Step	102.0 ± 0.3 eV	102.8 ± 0.3 eV	103.7 ± 0.2 eV	104.7 ± 0.3 eV	105.6 ± 0.2 eV
Piranha	---	---	---	---	---
Aldehyde (1b)	170[a]*	1010 ± 410	960 ± 160	420 ± 340	240 ± 100
Chitosan (2b)	130 ± 100[a]	260 ± 120	150 ± 50	---	---

Values with the same superscript are not statistically different at the 5% significance level.
*Only one observation at given binding energy.

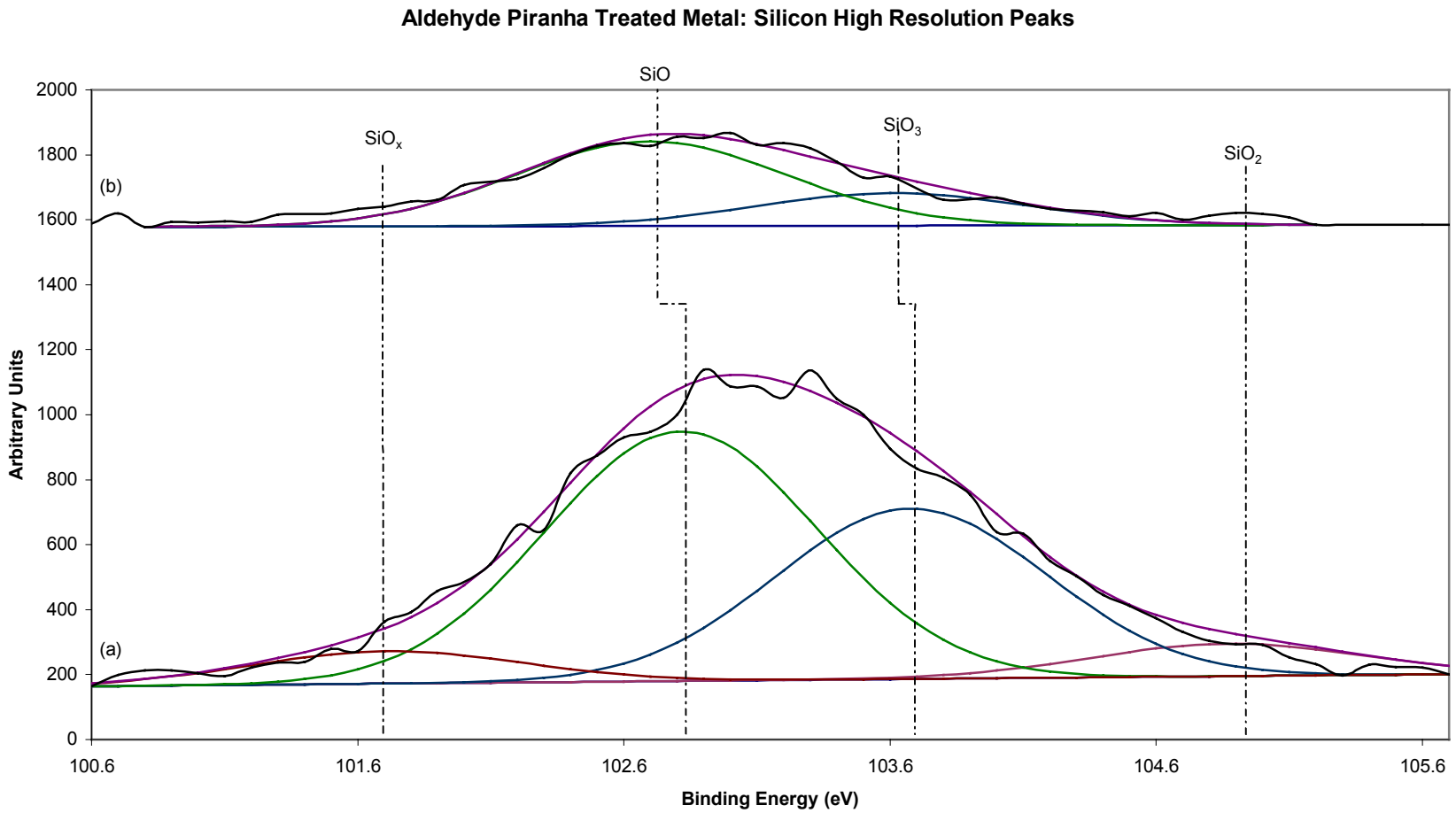

Figure 4.42. Representative silicon high resolution scans of the aldehyde reaction series on the piranha treated metal. The aldehyde silane reaction (reaction step 1b) is labeled (a). The chitosan reaction (reaction step 2b) is labeled (b).

Table 4.61 shows the peaks from the high resolution scans of titanium; there were no titanium peaks present following the chitosan reaction step. There were three peaks present, with one peak located on only the piranha treated surface. The peak located at 458.5 ± 0.33 eV was identified as TiO_2. A significant decrease was seen from the piranha treated surface to the aldehyde reaction, with values of 1010 ± 350 per unit area and 180 ± 150 per unit area, respectively. The third peak, located at 459.5 ± 0.4 eV, was identified as TiO; a significant decrease from the piranha treated surface to the aldehyde reaction was seen, with values of 6860 ± 460 per unit area and 120 ± 90 per unit area, respectively. The last peak, located at 460.2 ± 0.2 eV, was identified as TiC; it was present only on the piranha treated surface. Figure 4.43 illustrates the differences of the titanium peak following the two reaction steps on the piranha treated metal; the chitosan reaction step was not shown as there was no titanium present.

By looking at the two different surfaces on the piranha treated metal surface, significant changes between the reaction species were seen. The presence of the COOH peak indicated that the aldehyde silane was deposited on the surface and then possibly reacted with the ethanol rinse. An overall decrease of the TiO peak further indicated that the anticipated surface reactions had occurred. The presence of SiO, SiO_2, and SiO_3 further proved that the anticipated reaction between the passivated surface and the amino silane had occurred.

Table 4.61. Titanium functional group peak areas based on XPS high resolution scans of piranha treated metal using aldehyde silane.

	TiO_2 [4.23]	**TiO [4.24]**	**TiC [4.25]**
Reaction Step	458.5 ± 0.3 eV	459.5 ± 0.4 eV	460.2 ± 0.2 eV
Piranha	1010 ± 350	6860 ± 460	750 ± 170
Aldehyde (1b)	180 ± 150	120 ± 90	---
Chitosan (2b)	---	---	---

Values with the same superscript are not statistically different at the 5% significance level.

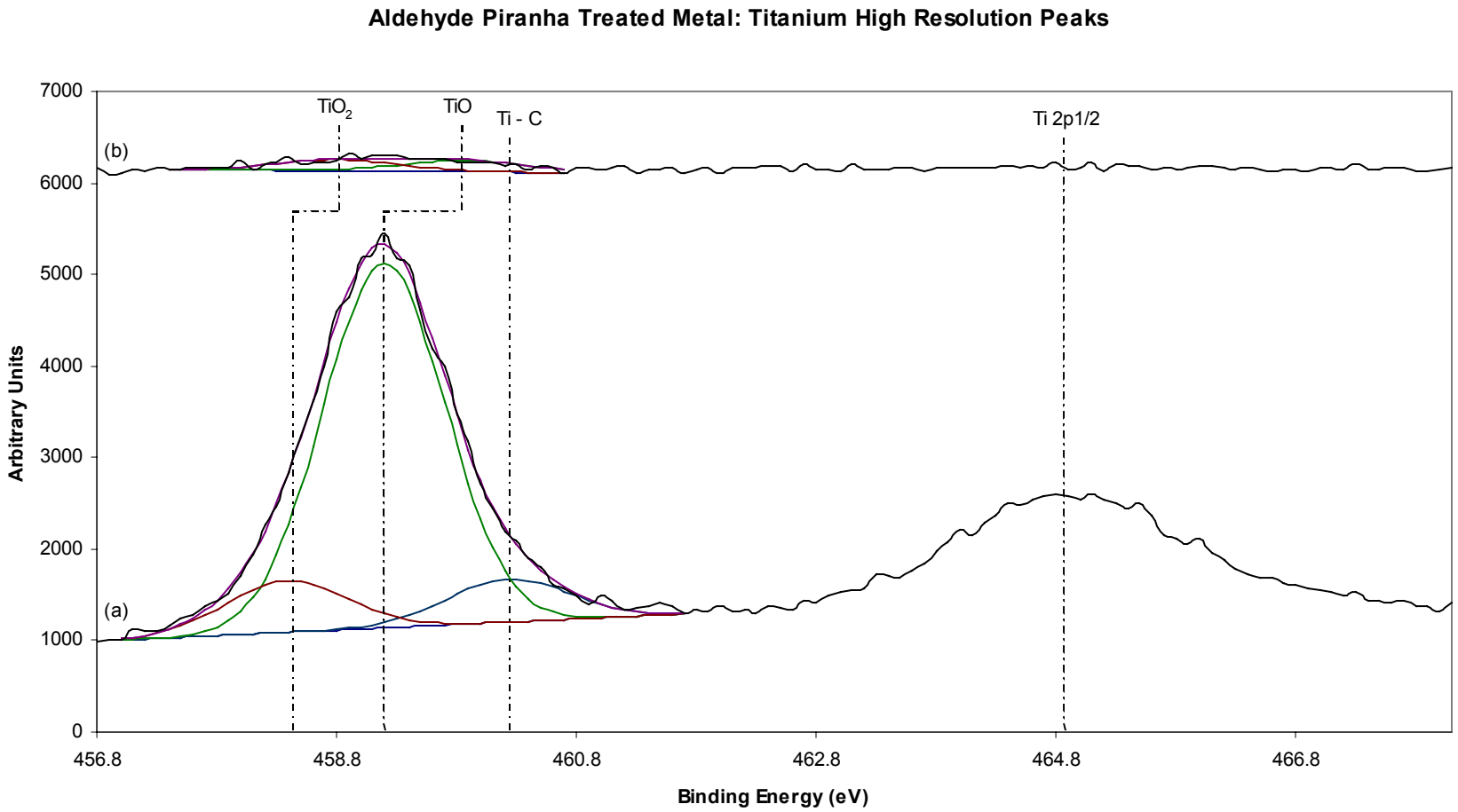

Figure 4.43. Representative titanium high resolution scans of the aldehyde reaction series on the piranha treated metal. The piranha treated metal is labeled (a). The aldehyde silane reaction (reaction step 1b) is labeled (b).

4.3.4 Chitosan Results

The results between the reactions steps could not be compared, since the silanes end in two different terminal groups. However, the chitosan films can be compared based on the silane used. Therefore, the chitosan results were analyzed in three different ways. The first method compared the films with respect to both the metal treatment and the silane treatment. The second method evaluated the films with respect to the metal treatment, while the third method compared the films based to the silane treatment.

4.3.4.1 Chitosan Film Analysis based on Metal Treatment and Silane Treatment

The means and standard deviations from the survey scans of the chitosan films on the four different treatment combinations based on percentage are shown in Table 4.62. The peak areas of the four chitosan films are shown in Tables 4.63 and 4.64. In order to keep track of the different treatment combinations, the following abbreviations were used: Passivated Metal combined with Aldehyde Silane – PaAl, Piranha Treated Metal combined with Aldehyde Silane – PiAl, Passivated Metal combined with Amino Silane – PaAm, Piranha Treated Metal combined with Amino Silane – PiAm.

Based on percentage, the PiAm was significantly higher than the other three treatments, PaAl, PaAm, and PiAl. The peak area of carbon, however, shows that PaAm and PiAm were statistically similar, while the peak areas of carbon present on PaAl and PiAl were significantly higher; the peak area of carbon on the PaAl film was 23910 ± 1140 per unit area while the peak area of carbon on the PiAl film was 24790 ± 730 per unit area, which were both significantly higher than either PaAm or PiAm. The percentage of oxygen indicated no statistical change between PaAl and the PiAm. The

other two treatment combinations were statistically higher, with PiAl significantly higher than PaAm.

The amount of nitrogen present was not significantly different between the four treatment combinations, based on both the percentage and the peak area. Calcium was also not statistically different between the four treatment combinations based on percentage and peak area.

The amount of silicon was not statistically different between PaAm and PiAm based on both percentage and peak area; however, PaAl was significantly higher than either PaAm or PiAm, with a value of 6 ± 2 % as compared to 0 ± 1 %, respectively. The amount of silicon on PiAl, based on both percentage and peak area, was also significantly higher than either PaAm or PiAl. The percentage and peak area of phosphorous was not significantly different between the four treatment combinations. Figure 4.44 shows the surface scans of the chitosan films based on the four treatment combinations.

Table 4.62. Elemental percentage based on XPS survey scans of the chitosan films.

Metal Treatment	Carbon	Oxygen	Nitrogen	Calcium	Silicon	Phosphorous
Passivated, Aldehyde	63 ± 3^{b} %	25 ± 2^{c} %	5 ± 1^{d} %	1 ± 1^{e} %	6 ± 2 %	1 ± 1^{g} %
Passivated, Amino	65 ± 1^{a} %	28 ± 1 %	6 ± 1^{d} %	1 ± 1^{e} %	0 ± 1^{f} %	0 ± 1^{g} %
Piranha, Aldehyde	$64 \pm 1^{a,b}$ %	26 ± 1 %	5 ± 1^{d} %	1 ± 1^{e} %	2 ± 2 %	1 ± 1^{g} %
Piranha, Amino	68 ± 1 %	25 ± 1^{c} %	5 ± 1^{d} %	1 ± 1^{e} %	1 ± 1^{f} %	0 ± 1^{g} %

Values with the same superscript are not statistically different at the 5% significance level.

Table 4.63. Elemental peak areas based on XPS survey scans of the chitosan films.

Metal Treatment	Carbon	Oxygen	Nitrogen
Passivated, Aldehyde	23910 ± 1140	23270 ± 1840[b]	2930 ± 820[c]
Passivated, Amino	22730 ± 680[a]	23490 ± 1200[b]	3220 ± 600[c]
Piranha, Aldehyde	24790 ± 730	24750 ± 1050	3230 ± 450[c]
Piranha, Amino	23110 ± 460[a]	20470 ± 1240	2890 ± 290[c]

Values with the same superscript are not statistically different at the 5% significance level.

Table 4.64. Elemental peak areas based on XPS survey scans of the chitosan films.

Metal Treatment	Calcium	Silicon	Phosphorous
Passivated, Aldehyde	1750 ± 630[d]	2030 ± 560	330 ± 170[f]
Passivated, Amino	1200 ± 1000[d]	50 ± 160[e]	160 ± 220[f]
Piranha, Aldehyde	2190 ± 740[d]	770 ± 530	420 ± 210[f]
Piranha, Amino	1590 ± 610[d]	210 ± 230[e]	120 ± 180[f]

Values with the same superscript are not statistically different at the 5% significance level.

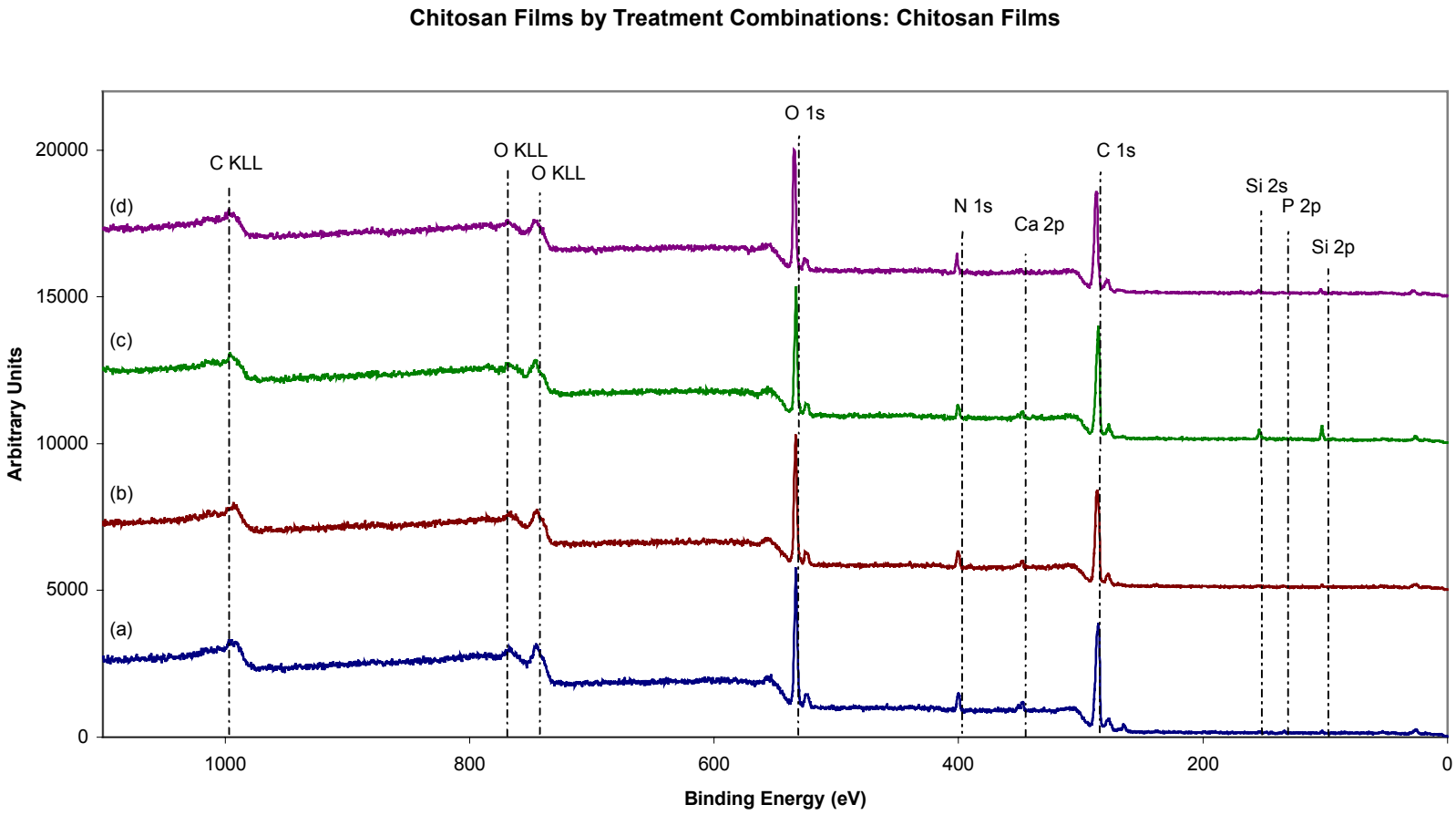

Figure 4.44. Representative survey scans of the chitosan films by treatment combination.

The treatment combination of passivated metal and aldehyde silane (PaAl) is labeled (a), passivated metal and amino silane (PaAm) is labeled (b), piranha treated metal and aldehyde silane (PiAl) is labeled (c), and the piranha treated metal and amino silane (PiAm) is labeled (d).

Tables 4.65 – 4.70 show the high resolution scans of five of the six elements present. The scan of phosphorous could not be analyzed as the peak area was too small to analyze accurately. Tables 4.65 – 4.66 show the peaks from the high resolution scans of carbon; there were seven peaks present, of which all but two of the peaks were present on all of the chitosan films. The first peak, located at 284.8 ± 0.2 eV, was identified as C; it was not present on PaAl or PiAm. The C peak was present on both the PaAm and PiAl surfaces, with no statistical difference between the two combinations. The second peak, located at 285.6 ± 0.2 eV, was identified as C – C; the peak was present on all four films, but no significant change was seen between PaAl, PaAm, and PiAl. A significant decrease was seen when examining the PiAm surface. The peak located at 286.6 ± 0.3 eV was identified as C – O; the PaAm surface and the PiAl surface were not significantly different. The PaAl surface was significantly less than the PaAm and PiAl surfaces, with a value of 2030 ± 500 per unit area compared to 2640 ± 510 per unit area, while the PiAm surface was significantly higher, with a value of 3690 ± 165 per unit area. The C – N – H peak, located at 287.6 ± 0.3 eV, was not significantly different between the four treatment combinations. The fifth peak, located at 288.7 ± 0.2 eV and identified as C = O, was not statistically different between the PaAl, PaAm, and PiAl surfaces. The PiAm surface was significantly higher than the other three surfaces, with a value of 1660 ± 420 per unit area compared to 1120 ± 90 per unit area, respectively. The $CaCO_3$ peak, located at 289.9 ± 0.2 eV, was not significantly different when comparing the PaAl, PaAm, and PiAl surfaces; however, the PiAm surface had a significantly higher peak area than the three other films, with a value of 950 ± 90 per unit area compared to 540 ± 340

per unit area, respectively. The final peak, located at 290.8 ± 0.3 eV, was not present on PaAl or PaAm; the two surfaces, PiAl and PiAm, were not statistically different. Figure 4.45 shows the differences of the high resolution scans of carbon for each of the four treatment combinations.

Table 4.65. Carbon functional group peak areas based on XPS high resolution scans of the chitosan films.

	C [4.1]	C-C [4.2]	C-O [4.3]	C-N-H [4.9]
Metal Treatment	284.8 ± 0.2 eV	285.6 ± 0.2 eV	286.6 ± 0.3 eV	287.6 ± 0.3 eV
Passivated, Aldehyde	---	3720 ± 310[b]	2030 ± 500	2460 ± 310[d]
Passivated, Amino	820 ± 80[a]	2540 ± 1100[b]	2640 ± 510[c]	2430 ± 820[d]
Piranha, Aldehyde	750 ± 160[a]	3030 ± 1250[b]	2660 ± 650[c]	2490 ± 680[d]
Piranha, Amino	---	530 ± 220	3690 ± 160	2580 ± 380[d]

Values with the same superscript are not statistically different at the 5% significance level.

Table 4.66. Carbon functional group peak areas based on XPS high resolution scans of the chitosan films.

	C=O [4.10]	$CaCO_3$ [4.37]	N-C [4.11]
Metal Treatment	288.7 ± 0.2 eV	289.9 ± 0.2 eV	290.8 ± 0.3 eV
Passivated, Aldehyde	1020 ± 100[e]	340 ± 40[f]	---
Passivated, Amino	1120 ± 100[e]	400 ± 210[f]	---
Piranha, Aldehyde	1120 ± 90[e]	540 ± 340[f]	230 ± 40[g]
Piranha, Amino	1660 ± 420	950 ± 90	290 ± 20[g]

Values with the same superscript are not statistically different at the 5% significance level.

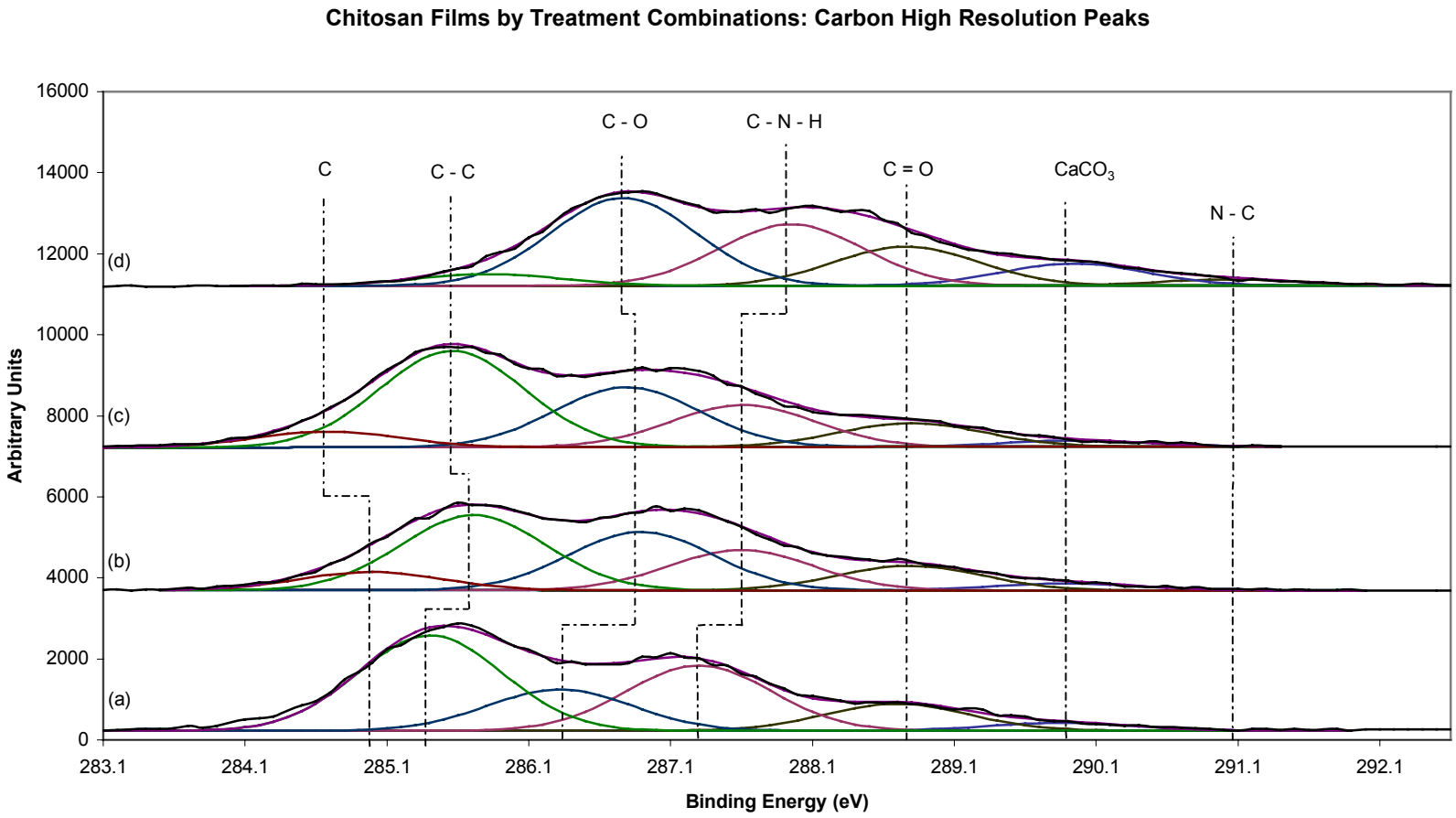

Figure 4.45. Representative carbon high resolution scans of the chitosan films by treatment combination.

The treatment combination of passivated metal and aldehyde silane (PaAl) is labeled (a), passivated metal and amino silane (PaAm) is labeled (b), piranha treated metal and aldehyde silane (PiAl) is labeled (c), and the piranha treated metal and amino silane (PiAm) is labeled (d).

Table 4.67 shows the peaks from the high resolution scans of oxygen; there were five peaks present, with all but one of the peaks present on all four films produced by the treatment combinations. The first peak, located at 531.6 ± 0.2 eV and identified as $CaCO_3$, was not present on the PiAl surface. It was present on the PaAl, PaAm, and PiAm surfaces, but there were not significant differences between the three films. The CaO peak, located at 532.5 ± 0.4 eV, was present on all four surfaces. There were no statistical differences between the PaAl and PaAm surfaces, while there was a significant decrease seen between the PaAl and PiAl surfaces, with values of 2500 ± 520 per unit area and 1600 ± 530 per unit area, respectively. There also were no significant changes seen between the PiAl and PiAm surfaces, while there was a significant decrease seen between the PaAm and PiAm surfaces, with values of 1860 ± 640 per unit area and 1010 ± 160 per unit area, respectively. The third peak, identified as SiO_2 and located at 533.5 ± 0.3 eV, showed no significant change between PaAl, PaAm, and PiAl, while a significant decrease was seen between PiAl and PiAm, with values of 3950 ± 910 per unit area and 2690 ± 340 per unit area, respectively. The NO peak, located at 534.4 ± 0.3 eV, was not significantly different between the PaAl and PaAm surfaces, nor was it significantly different between the PaAm, PiAl, and PiAm surfaces; however, there was a significant increase seen between the PaAl and PiAl surfaces, with values of 1860 ± 460 per unit area and 3740 ± 1020 per unit area, respectively. The final peak, located at 535.5 ± 0.3 eV and identified as C = O, was not significantly different between the four film surfaces. Figure 4.46 shows the differences of the high resolution scans of oxygen for each of the four treatment combinations.

Table 4.67. Oxygen functional group peak areas based on XPS high resolution scans of the chitosan films.

	$CaCO_3$ [4.38]	CaO [4.39]	SiO_2 [4.19]	NO [4.22]	C=O [4.21]
Metal Treatment	531.6 ± 0.2 eV	532.5 ± 0.4 eV	533.5 ± 0.3 eV	534.4 ± 0.3 eV	535.5 ± 0.3 eV
Passivated, Aldehyde	730 ± 220[a]	2500 ± 520[a]	4000 ± 330[d]	1860 ± 460[e]	280 ± 80[g]
Passivated, Amino	650 ± 340[a]	1860 ± 640[a,b]	4230 ± 1000[d]	2410 ± 1130[e,f]	560 ± 380[g]
Piranha, Aldehyde	---	1600 ± 530[b,c]	3950 ± 910[d]	3740 ± 1020[f]	790 ± 480[g]
Piranha, Amino	200 ± 20[a]	1010 ± 160[c]	2690 ± 340	3920 ± 370[f]	890 ± 250[g]

Values with the same superscript are not statistically different at the 5% significance level.

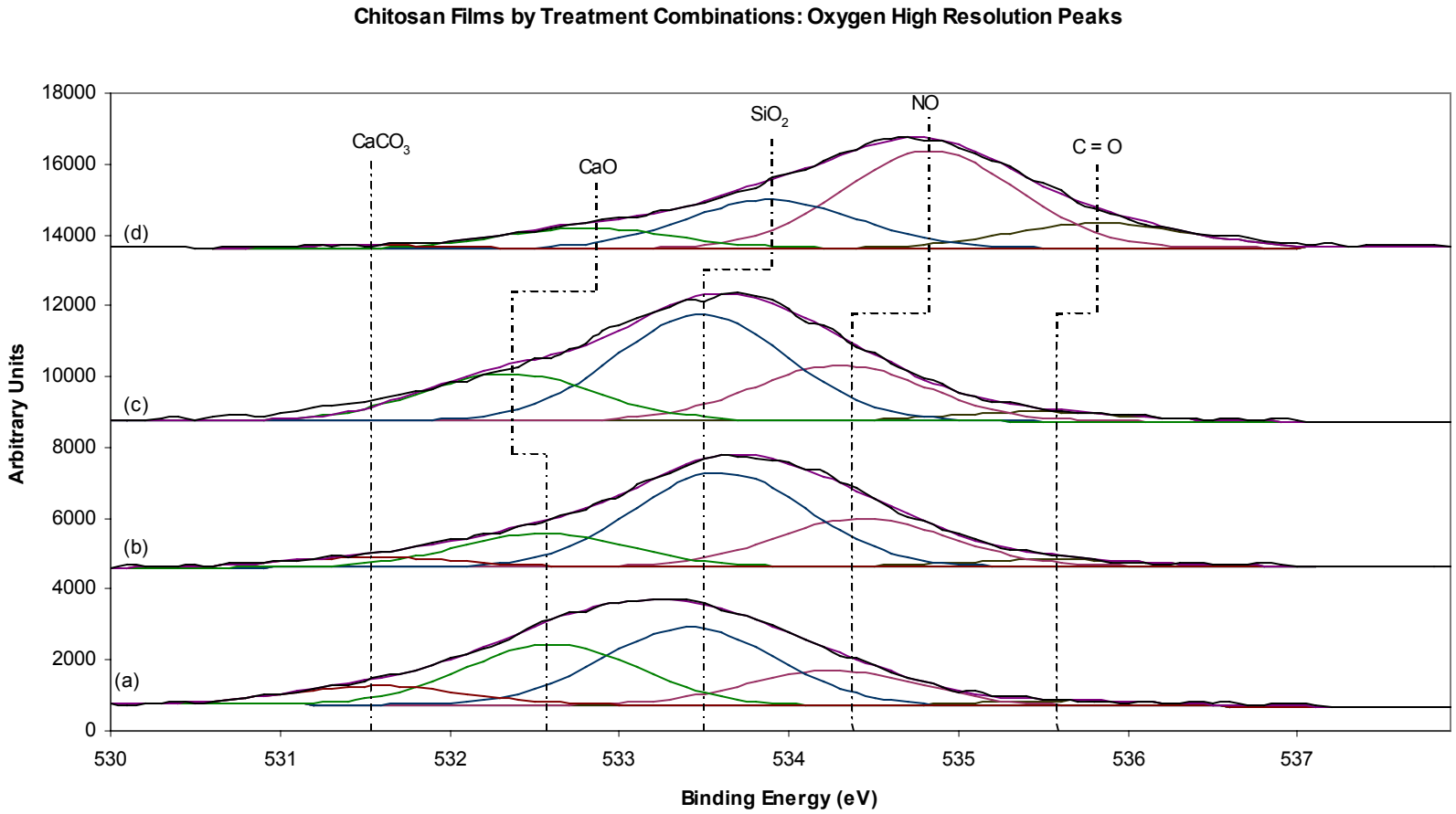

Figure 4.46. Representative oxygen high resolution scans of the chitosan films by treatment combination.

The treatment combination of passivated metal and aldehyde silane (PaAl) is labeled (a), passivated metal and amino silane (PaAm) is labeled (b), piranha treated metal and aldehyde silane (PiAl) is labeled (c), and the piranha treated metal and amino silane (PiAm) is labeled (d).

Table 4.68 shows the peaks from the high resolution scans of calcium; there were three peaks present, with only one peak present on all four films. The first peak, identified as CaO and located at 347.8 ± 0.2 eV, was not present on the PiAm surface; it also did not show any significant changes between the PaAl, PaAm, and PiAl surfaces. The second peak, located at 348.7 ± 0.3 eV and identified as $CaHPO_4$, was present on all four films, but was not significantly different between the four treatment combinations. The final peak, identified as $CaCO_3$ and located at 349.4 ± 0.3 eV, was not present on the PaAl surface; it was not significantly different between the PaAm, PiAl, and PiAm surfaces. Figure 4.47 illustrates the differences of the high resolution scans of oxygen based on the four treatment combinations.

Table 4.68. Calcium functional group peak areas based on XPS high resolution scans of the chitosan films.

	CaO [4.40]	**$CaHPO_4$ [4.41]**	**$CaCO_3$ [4.42]**
Metal Treatment	347.8 ± 0.2 eV	348.7 ± 0.3 eV	349.4 ± 0.3 eV
Passivated, Aldehyde	280 ± 70[a]	150 ± 90[b]	---
Passivated, Amino	210 ± 190[a]	230 ± 190[b]	140 ± 240[c]
Piranha, Aldehyde	240 ± 80[a]	290 ± 60[b]	250 ± 40[c]
Piranha, Amino	---	280 ± 80[b]	300 ± 20[c]

Values with the same superscript are not statistically different at the 5% significance level.

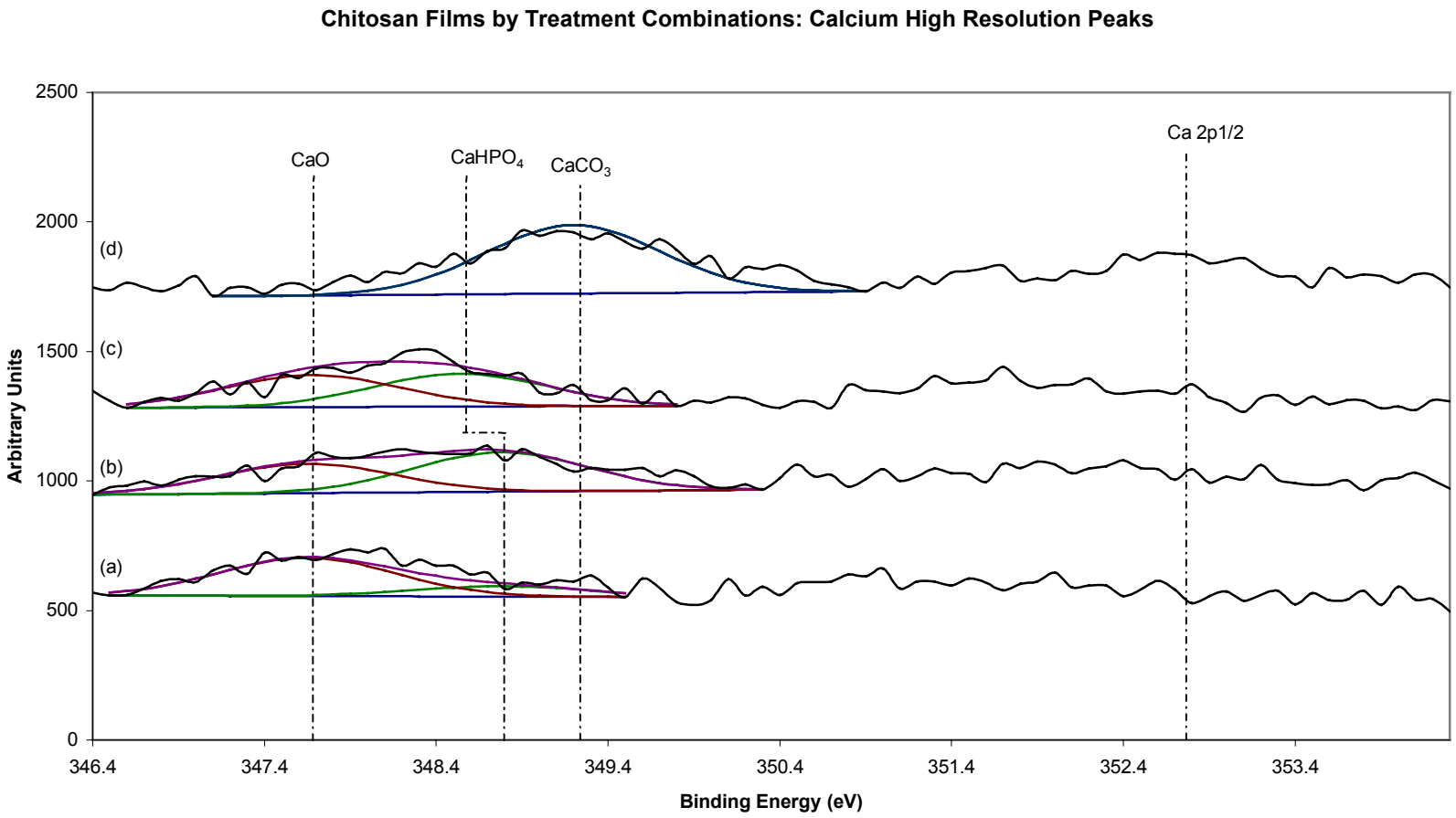

Figure 4.47. Representative calcium high resolution scans of the chitosan films by treatment combination.

The treatment combination of passivated metal and aldehyde silane (PaAl) is labeled (a), passivated metal and amino silane (PaAm) is labeled (b), piranha treated metal and aldehyde silane (PiAl) is labeled (c), and the piranha treated metal and amino silane (PiAm) is labeled (d).

Table 4.69 shows the peaks from the high resolution scans of nitrogen; there were four peaks present, with two of the peaks present on all four film surfaces. The N – C peak, located at 399.8 ± 0.2 eV, was not significantly different between PaAl, PaAm, and PiAl. There also were no statistical differences between the PaAl, PiAl, and PiAm peaks. However, a significant increase was seen between the PaAm and PiAm peaks, with values of 540 ± 230 per unit area and 750 ± 10 per unit area, respectively. The second peak, located at 400.0 ± 0.2 eV and identified as C – N – H, was not statistically different between PaAl and PiAl; it was also not significantly different between PaAm, PiAl, and PiAm. However, a significant increase was seen between PaAl and PaAm, with values of 460 ± 100 per unit area and 630 ± 120 per unit area, respectively. A significant increase between PaAl and PiAm was also seen, with values of 460 ± 100 per unit area and 760 ± 60 per unit area, respectively. The third peak, identified as NH_4^+ and located at 401.9 ± 0.2 eV, was present only on the PiAl and PiAm surfaces; there were no significant differences between the two surfaces. The final peak, located at 402.4 ± 0.2 eV and identified as NO, was present only on PaAl and PaAm surfaces, with no statistical differences seen between the two surfaces. Figure 4.48 shows the differences between the high resolution scans of nitrogen based on the four treatment combinations.

Table 4.69. Nitrogen functional group peak areas based on XPS high resolution scans of the chitosan films.

	N-C [4.32]	C-N-H [4.33]	NH_4^+ [4.34]	NO [4.36]
Metal Treatment	399.8 ± 0.2 eV	400.9 ± 0.2 eV	401.9 ± 0.2 eV	402.4 ± 0.2 eV
Passivated, Aldehyde	440 ± 70[a,b]	460 ± 100[c]	---	210 ± 40[f]
Passivated, Amino	540 ± 230[a]	630 ± 120[d]	---	280 ± 110[f]
Piranha, Aldehyde	400 ± 140[a,b]	610 ± 120[c,d]	270 ± 40[e]	---
Piranha, Amino	750 ± 10[b]	760 ± 60[d]	340 ± 70[e]	---

Values with the same superscript are not statistically different at the 5% significance level.

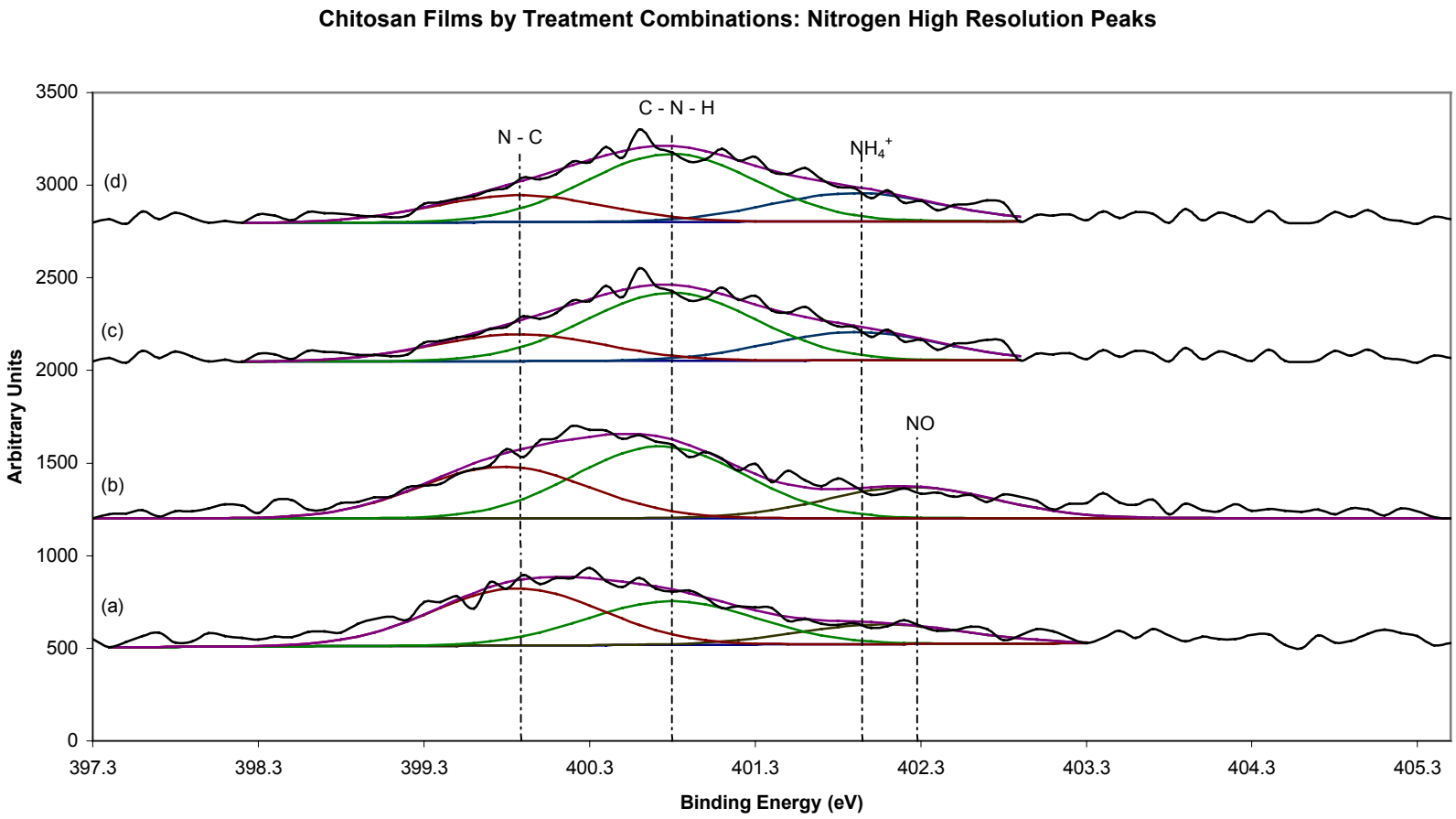

Figure 4.48. Representative nitrogen high resolution scans of the chitosan films by treatment combination.

The treatment combination of passivated metal and aldehyde silane (PaAl) is labeled (a), passivated metal and amino silane (PaAm) is labeled (b), piranha treated metal and aldehyde silane (PiAl) is labeled (c), and the piranha treated metal and amino silane (PiAm) is labeled (d).

Table 4.70 shows the peaks from the high resolution scans of silicon; there were three peaks present, but none of the peaks were present on all four film surfaces. The first peak, located at 102.0 ± 0.2 eV and identified as SiO_x, was not present on the PaAm or PiAm surfaces. Only one scan out of nine scans indicated the presence of the peak on the PaAl surface, which was not statistically different from the PiAl surface. The SiO peak, located at 102.8 ± 0.2 eV, was not present on the PiAm surface. All four surfaces were significantly different. A major decrease occurred between the PaAl surface and the PaAm surface, with values of 510 ± 120 per unit area and 20 ± 60 per unit area, respectively, while a significant increase occurred between the PaAm and PiAl surfaces, with a final value of 260 ± 120 per unit area. The PaAl and PiAl surfaces were also not statistically similar. The final peak, identified as SiO_3 and located at 103.7 ± 0.2 eV, was not present on the PaAm surface. It was also not significantly different between the PaAl and PiAl surface, nor was it significantly different between the PiAl and PiAm surfaces. However, a significant decrease was seen between the PaAl and PiAm surfaces, with values of 210 ± 93 per unit area and 60 ± 90 per unit area, respectively. Figure 4.49 illustrates the differences between the high resolution scans of silicon based on the four treatment combinations.

By comparing the films produced by using the four treatment combinations, some minor changes were noticed. Most of these changes, including changes to the C – O, C = O, and C – N – H peaks, were likely caused by the arrangement of the chitosan chains, which was caused by the polar nature of the amine group positioning itself to be with the polar water molecules. The other changes, including the changes in the peak

areas of $CaCO_3$ and SiO_2, were likely the result of incomplete demineralization, possibly caused by the different amounts of the compounds taken in by the different shellfish used to create the chitosan powder. All of the changes were minimal, showing the four treatment combinations did not affect the chemical structure of the chitosan.

Table 4.70. Silicon functional group peak areas based on XPS high resolution scans of the chitosan films.

	SiO_x [4.27]	**SiO [4.28]**	**SiO_3 [4.29]**
Metal Treatment	102.0 ± 0.2 eV	102.8 ± 0.2 eV	103.7 ± 0.2 eV
Passivated, Aldehyde	170[a]*	510 ± 120	210 ± 90[a]
Passivated, Amino	---	20 ± 60	---
Piranha, Aldehyde	130 ± 100[a]	260 ± 120	150 ± 50[a,b]
Piranha, Amino	---	---	60 ± 90[b]

Values with the same superscript are not statistically different at the 5% significance level.
*Only one observation at given binding energy.

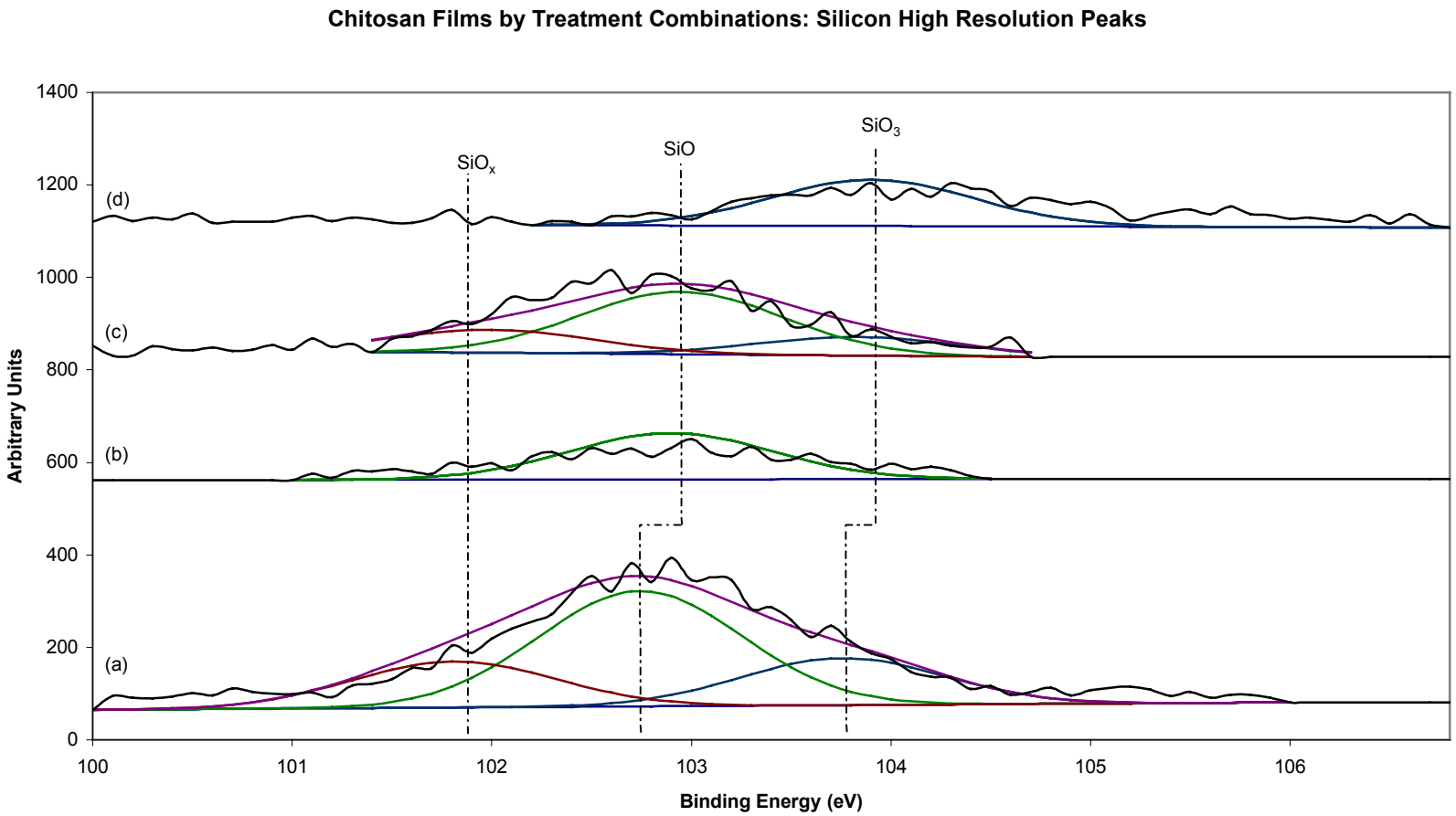

Figure 4.49. Representative silicon high resolution scans of the chitosan films by treatment combination.

The treatment combination of passivated metal and aldehyde silane (PaAl) is labeled (a), passivated metal and amino silane (PaAm) is labeled (b), piranha treated metal and aldehyde silane (PiAl) is labeled (c), and the piranha treated metal and amino silane (PiAm) is labeled (d).

Based on the statistical analysis, there were several elements that were not statistically different. Therefore, analysis was performed on the metal treatment and the silane treatment in order to determine if there were any changes that were related to one of the two treatments that were not present when examining the four treatment combinations.

4.3.4.2 Chitosan Film Analysis based on Metal Treatment

The means and standard deviations from the survey scans of the chitosan films based on the two metal treatments are shown in Table 4.71 and are based on percentage. The peak areas of the chitosan films based on metal treatment are shown in Tables 4.72 and 4.73. Based on percentage, the carbon peak on the passivated metal was significantly lower than the carbon peak on the piranha treated metal, with values of 64 ± 2 % and 66 ± 2 %. The peak area of the carbon indicated the same trend, with a significantly lower amount present on the passivated metal as compared to the piranha treated metal.

The oxygen peak on the passivated metal was significantly higher than the piranha treated metal, based on percentage, with values of 26 ± 2 % and 25 ± 1 %, respectively. The peak area of the oxygen, however, did not match the percentage trend; there was no significant change between the two metals.

Based on percentage and peak area, there were no significant changes of the nitrogen peak between the two metal treatments. The calcium peak also did not show any significant change between the two metal treatments, based on percentage and peak area.

Based on percentage, a significant decrease in the presence of silicon occurred on the passivated metal as compared to the piranha treated metal, with values of 3 ± 3 % and

1 ± 1 %, respectively. The peak area supported this trend, with values of 1040 ± 1090 per unit area and 490 ± 490 per unit area, respectively. Based on percentage and peak area, there were no significant changes between the two metal treatments for phosphorous. Figure 4.50 shows the surface scans of the chitosan films based on metal treatments.

Table 4.71. Elemental percentage based on XPS survey scans of the chitosan films based on metal treatment.

Metal Treatment	Carbon	Oxygen	Nitrogen	Calcium	Silicon	Phosphorous
Passivated	64 ± 2 %	26 ± 2 %	5 ± 1[a] %	1 ± 1[b] %	3 ± 3 %	1 ± 1[c] %
Piranha	66 ± 2 %	25 ± 1 %	5 ± 1[a] %	1 ± 1[b] %	1 ± 1 %	1 ± 1[c] %

Values with the same superscript are not statistically different at the 5% significance level.

Table 4.72. Elemental peak areas based on XPS survey scans of the chitosan films based on metal treatment.

Metal Treatment	Carbon	Oxygen	Nitrogen
Passivated	23320 ± 1090	23380 ± 1510[a]	3070 ± 710[b]
Piranha	23950 ± 1050	22610 ± 2470[a]	3060 ± 410[b]

Values with the same superscript are not statistically different at the 5% significance level.

Table 4.73. Elemental peak areas based on XPS survey scans of the chitosan films based on metal treatment.

Metal Treatment	Calcium	Silicon	Phosphorous
Passivated	1480 ± 860^{c}	1040 ± 1090	250 ± 210^{d}
Piranha	1890 ± 730^{c}	490 ± 490	270 ± 240^{d}

Values with the same superscript are not statistically different at the 5% significance level.

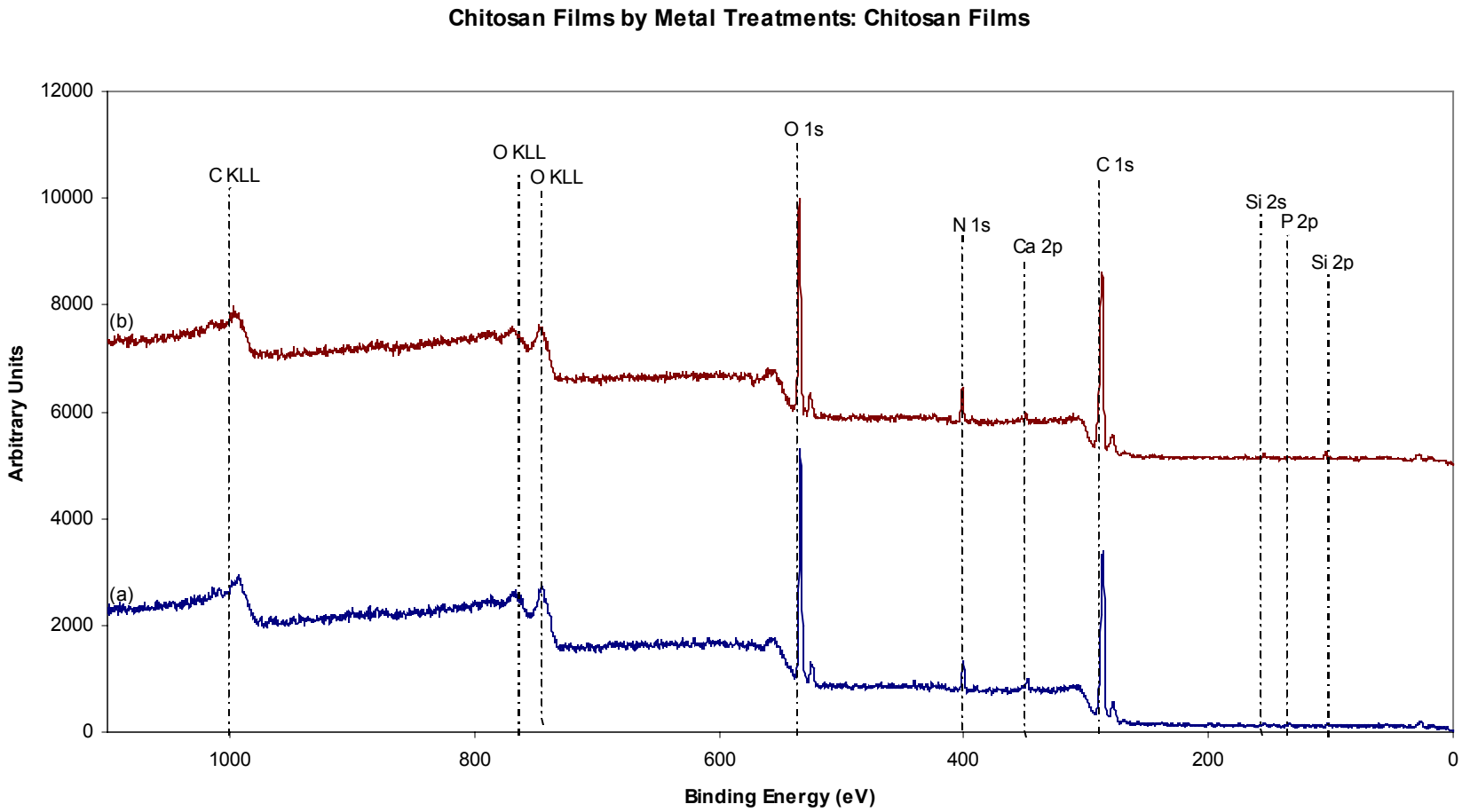

Figure 4.50. Representative survey scans of the chitosan films by metal treatment.

The passivated metal is labeled (a). The piranha treated metal is labeled (b).

Tables 4.74 – 4.79 show the high resolution scans of five of six elements present. The scan of phosphorous could not be analyzed as the peak area was too small to analyze accurately. Tables 4.74 – 4.75 show the peaks from the high resolution scans of carbon; there were seven peaks present, with all but one peak present on both metal treatments. The first peak, located at 284.8 ± 0.2 eV and identified as C, was not significantly different between the two metal treatments. The C – C peak, located at 285.6 ± 0.2 eV, showed a significant decrease from the passivated metal to the piranha treated metal, with values of 3370 ± 950 per unit area and 1530 ± 1280 per unit area, respectively. The third peak, located at 286.6 ± 0.3 eV and identified as C – O, showed a significant increase from the passivated metal to the piranha treated metal, with values of 2330 ± 590 per unit area and 3170 ± 700 per unit area, respectively. The peak located at 287.6 ± 0.3 eV and identified as C – N – H was not statistically different between the two metal treatments. The fifth peak, identified as C = O and located at 288.7 ± 0.2 eV, showed a significant increase from the passivated metal to the piranha treated metal, with values of 1070 ± 110 per unit area and 1390 ± 410 per unit area, respectively. The last peak present on both surfaces was identified as $CaCO_3$ and was located at 289.9 ± 0.2 eV. A significant increase between the passivated metal and the piranha treated metal was seen, with values of 370 ± 150 per unit area and 760 ± 150 per unit area, respectively. The final peak, identified as N – C and located at 290.8 ± 0.3 eV, was present only on the piranha treated surface. Figure 4.51 illustrates the differences between the film on passivated metal and the film on piranha treated metal.

Table 4.74. Carbon functional group peak areas based on XPS high resolution scans of the chitosan films based on metal treatment.

	C [4.1]	C-C [4.2]	C-O [4.3]	C-N-H [4.9]
Metal Treatment	284.8 ± 0.2 eV	285.6 ± 0.2 eV	286.6 ± 0.3 eV	287.6 ± 0.3 eV
Passivated	820 ± 80[a]	3370 ± 950	2330 ± 590	2450 ± 600[b]
Piranha	750 ± 160[a]	1530 ± 1280	3170 ± 700	2540 ± 540[b]

Values with the same superscript are not statistically different at the 5% significance level.

Table 4.75. Carbon functional group peak areas based on XPS high resolution scans of the chitosan films based on metal treatment.

	C=O [4.10]	$CaCO_3$ [4.37]	N-C [4.11]
Metal Treatment	288.7 ± 0.2 eV	289.9 ± 0.2 eV	290.8 ± 0.3 eV
Passivated	1070 ± 110	370 ± 150	---
Piranha	1390 ± 410	760 ± 310	260 ± 50

Values with the same superscript are not statistically different at the 5% significance level.

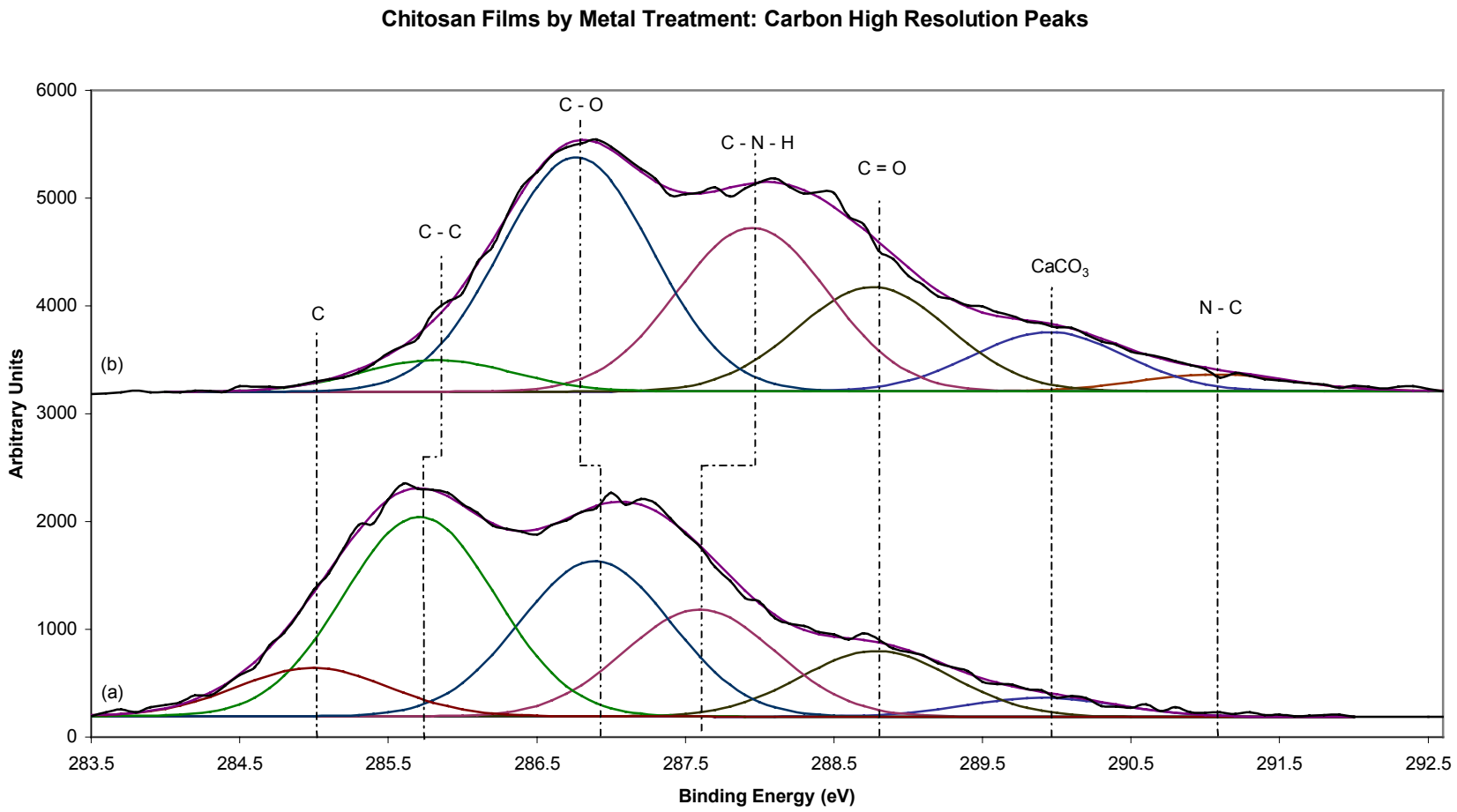

Figure 4.51. Representative carbon high resolution scans of the chitosan films by metal treatment.

The passivated metal is labeled (a). The piranha treated metal is labeled (b).

Table 4.76 shows the peaks from the high resolution scan of oxygen; there were five peaks present, with all peaks present on the film surface. The first peak, located at 531.6 ± 0.2 eV and identified as $CaCO_3$, was not significantly different between the two metal treatments. The CaO peak, located at 532.5 ± 0.4 eV, showed a significant decrease from the passivated metal to the piranha treated metal, with values of 2180 ± 660 per unit area and 1300 ± 490 per unit area, respectively. The third peak, located at 533.5 ± 0.3 eV and identified as SiO_2, was not significantly different between the two metal treatments. The peak located at 534.4 ± 0.3 eV and identified as NO, showed a significant increase from the passivated metal to the piranha treated metal, with values of 2140 ± 880 per unit area and 3830 ± 750 per unit area, respectively. The fifth peak, identified as C = O and located at 535.5 ± 0.3 eV, was not significantly different between the two metal treatments. Figure 4.52 illustrates the differences between the film on passivated metal and the film on piranha treated metal.

Table 4.76. Oxygen functional group peak areas based on XPS high resolution scans of the chitosan films based on metal treatment.

	$CaCO_3$ [4.38]	CaO [4.39]	SiO_2 [4.19]	NO [4.22]	C=O [4.21]
Metal Treatment	531.6 ± 0.2 eV	532.5 ± 0.4 eV	533.5 ± 0.3 eV	534.4 ± 0.3 eV	535.5 ± 0.3 eV
Passivated	690 ± 280[a]	2180 ± 660	4110 ± 730[b]	2140 ± 880	410 ± 290[c]
Piranha	200 ± 20[a]	1300 ± 480	3320 ± 930[b]	3830 ± 750	840 ± 380[c]

Values with the same superscript are not statistically different at the 5% significance level.

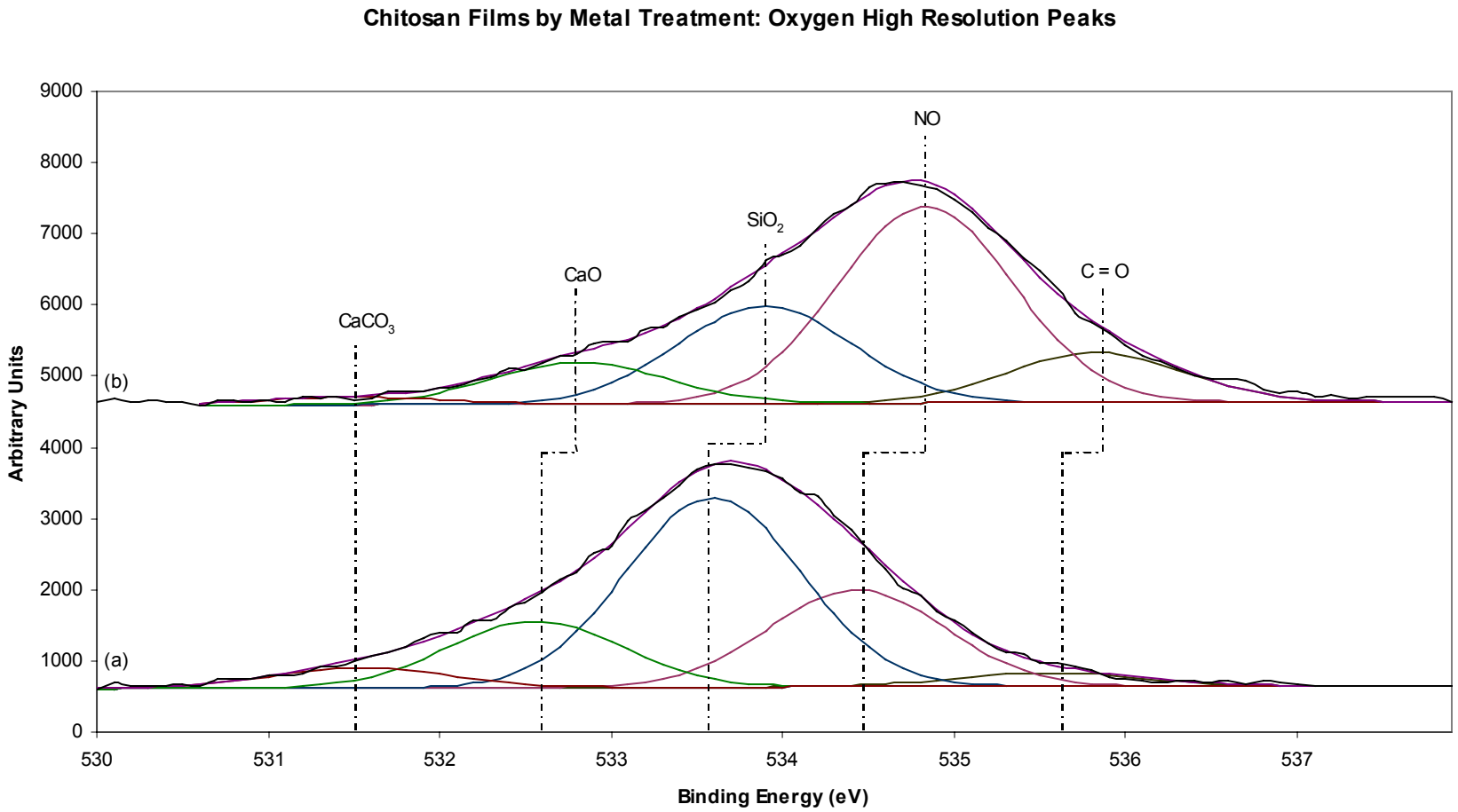

Figure 4.52. Representative oxygen high resolution scans of the chitosan films by metal treatment.

The passivated metal is labeled (a). The piranha treated metal is labeled (b).

Table 4.77 shows the peaks from the high resolution scans of calcium; there were three peaks present, all of which were present on both metal surfaces. The first peak, located at 347.8 ± 0.2 eV and identified as CaO, was not significantly different between the two metal treatments. The $CaHPO_4$ peak, identified as 348.7 ± 0.3 eV, was also not significantly different between the two metal treatments. The final peak, identified as $CaCO_3$ and located at 349.4 ± 0.3 eV, was not significantly different between the two metal treatments. Figure 4.53 illustrates the lack of differences between calcium peaks on the two films deposited on the metal treatments.

Table 4.78 shows the peaks from the high resolution scans of nitrogen; there were four peaks present, all of which were present on both metal surfaces. The N – C peak, located at 399.8 ± 0.2 eV, was not significantly different between the two metal treatments. The second peak, located at 400.9 ± 0.2 eV and identified as C – N – H, showed a significant increase between the passivated metal and the piranha treated metals, with values of 550 ± 140 per unit area and 680 ± 120 per unit area, respectively. The NH_4^+ peak, located at 401.9 ± 0.2 eV, was not significantly different between the two metal treatments. The final peak, located at 402.4 ± 0.2 eV and identified as NO, was also not significantly different between the two metal treatments. Figure 4.54 shows the differences between the nitrogen peaks present on the two films deposited on the metal treatments.

Table 4.77. Calcium functional group peak areas based on XPS high resolution scans of the chitosan films based on metal treatment.

	CaO [4.40]	**$CaHPO_4$ [4.41]**	**$CaCO_3$ [4.42]**
Metal Treatment	347.8 ± 0.2 eV	348.7 ± 0.3 eV	349. 4 ± 0.3 eV
Passivated	250 ± 130[a]	180 ± 140[b]	140 ± 240[c]
Piranha	240 ± 80[a]	280 ± 70[b]	270 ± 40[c]

Values with the same superscript are not statistically different at the 5% significance level.

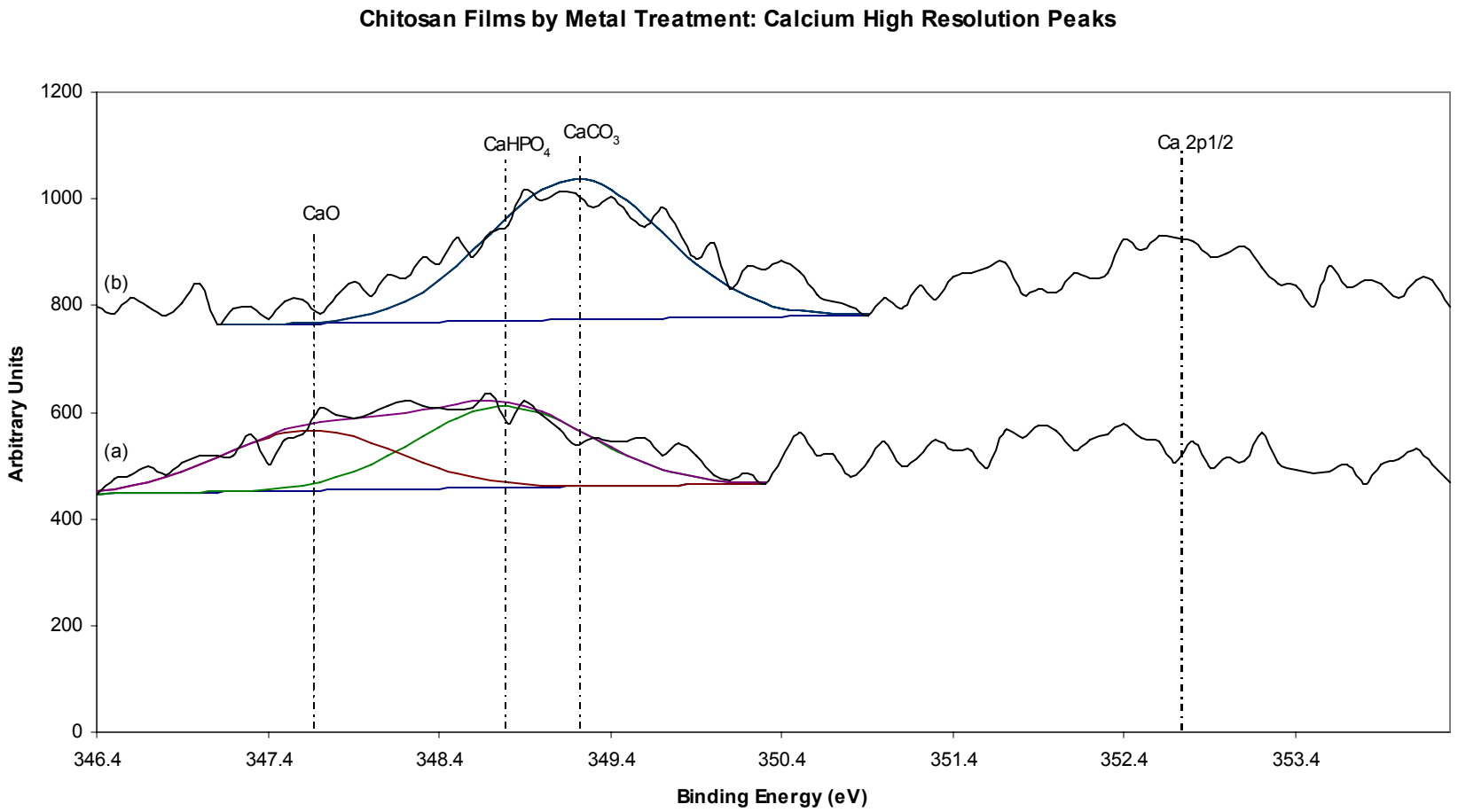

Figure 4.53. Representative calcium high resolution scans of the chitosan films by metal treatment.

The passivated metal is labeled (a). The piranha treated metal is labeled (b).

Table 4.78. Nitrogen functional group peak areas based on XPS high resolution scans of the chitosan films based on metal treatment.

	N-C [4.32]	C-N-H [4.33]	NH_4^+ [4.34]	NO [4.36]
Metal Treatment	399.8 ± 0.2 eV	400.9 ± 0.2 eV	401.9 ± 0.2 eV	402.4 ± 0.2 eV
Passivated	490 ± 170[a]	550 ± 140	210 ± 40[b]	270 ± 40[c]
Piranha	330 ± 150[a]	680 ± 120	280 ± 110[b]	340 ± 70[c]

Values with the same superscript are not statistically different at the 5% significance level.

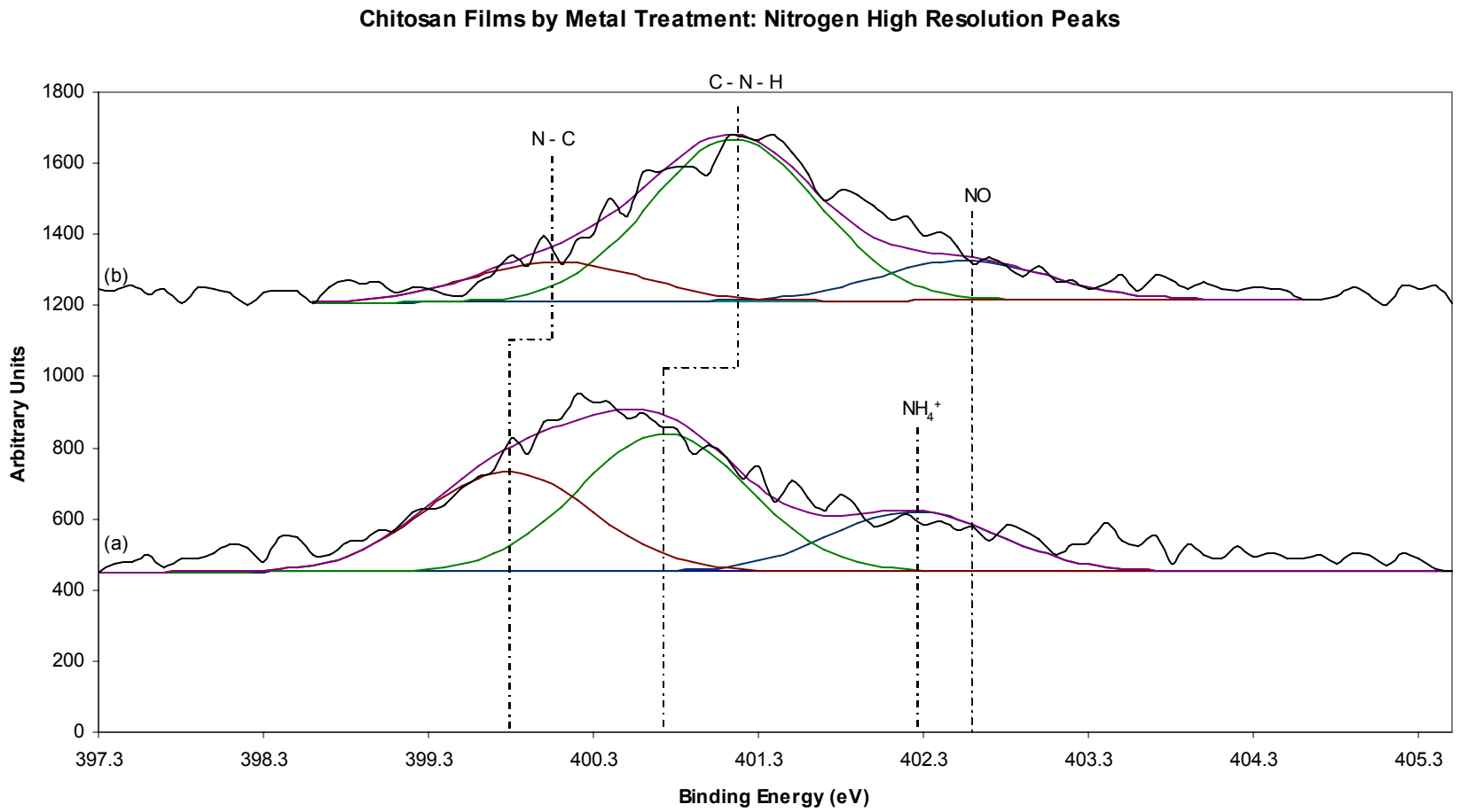

Figure 4.54. Representative nitrogen high resolution scans of the chitosan films by metal treatment.

The passivated metal is labeled (a). The piranha treated metal is labeled (b).

Table 4.79 shows the peaks from the high resolution scans of silicon; there were three peaks present, all of which were present on both metal surfaces. The SiO_x peak, located at 102.0 ± 0.2 eV, was not significantly different between the two metal treatments; however, there was only one scan out of nine that indicated the peak was present on the passivated metal. The second peak, located at 102.8 ± 0.2 eV and identified as SiO, also was not significantly different between the two metal treatments. The final peak, located at 103.7 ± 0.2 eV and identified as SiO_3, showed a significant decrease from the passivated metal to the piranha treated metal, with values of 210 ± 90 per unit area and 90 ± 90 per unit area, respectively. Figure 4.55 shows the differences between the silicon peaks present on the two films deposited on the metal treatments.

By comparing the films produced by using the two metal treatments, some minor changes were noticed. Most of these changes, including changes to the C – C, C – O, C = O, and C – N – H peaks, were likely caused by the arrangement of the chitosan chains, caused by the polar nature of the amine group positioning itself to be with the polar water molecules. The other changes, including the changes to the peak areas of CaO, $CaCO_3$ and SiO_3, were likely the result of incomplete demineralization, possibly caused by the different amounts of the compounds taken in by the different shellfish used to create the chitosan powder. All of the changes were minimal, showing the two metal treatments did not affect the chemical structure of the chitosan.

Table 4.79. Silicon functional group peak areas based on XPS high resolution scans of the chitosan films based on metal treatment.

	SiO_x [4.27]	**SiO [4.28]**	**SiO_3 [4.29]**
Metal Treatment	102.0 ± 0.2 eV	102.8 ± 0.2 eV	103.7 ± 0.2 eV
Passivated	170[a]*	270 ± 270[b]	210 ± 90
Piranha	130 ± 100[a]	260 ± 120[b]	90 ± 90

Values with the same superscript are not statistically different at the 5% significance level.
*Only one observation at given binding energy.

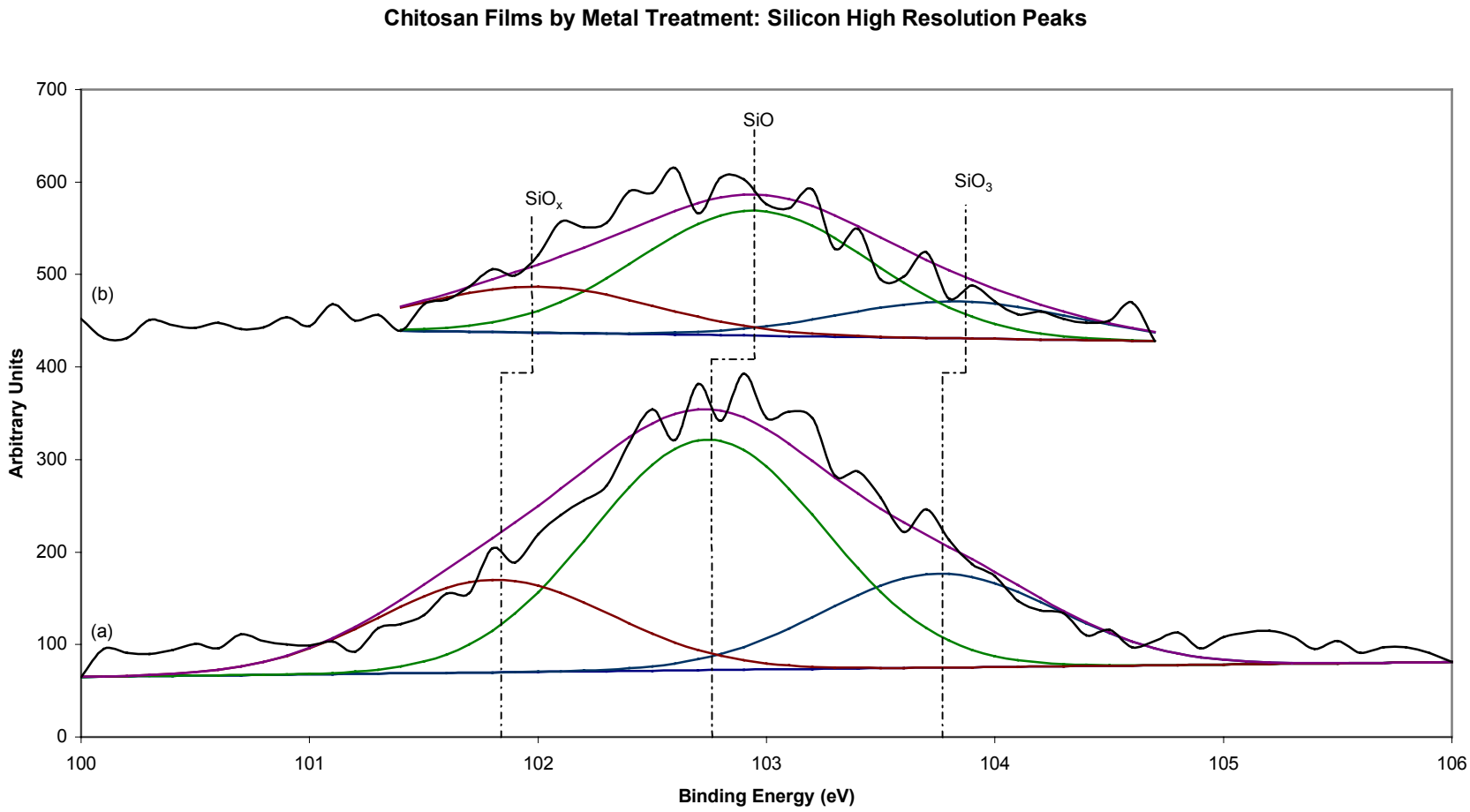

Figure 4.55. Representative silicon high resolution scans of the chitosan films by metal treatment.

The passivated metal is labeled (a). The piranha treated metal is labeled (b).

4.3.4.3 Chitosan Film Analysis based on Silane Treatment

The means and standard deviations from the survey scans of the chitosan films based on the two silane treatments are shown in Table 4.80 and are based on percentage. The peak areas of the chitosan films based on the silane treatment are shown in Tables 4.81 and 4.82. Based on percentage, the carbon peak using the aldehyde silane was significantly lower than the carbon peak using the amino silane, with values of 64 ± 2 % and 67 ± 2 %. The peak area of the carbon indicated an opposite trend, with a significantly higher amount present using the aldehyde silane as compared to the amino silane, with values of 24350 ± 1030 per unit area and 22920 ± 600 per unit area, respectively.

The oxygen peak using the aldehyde silane was not statistically different from the amino silane, based on percentage. However, the peak area of oxygen using the aldehyde silane was significantly higher than the amino silane, with values of 24010 ± 1640 per unit area and 21980 ± 1960 per unit area, respectively.

Based on percentage and peak area, there were no significant changes of the nitrogen peak between the two silane treatments. The calcium peak also did not show any significant changes between the two silane treatments, based on percentage and peak area.

Based on percentage, a significant decrease in the silicon peak was seen when comparing the aldehyde silane to the amino silane, with values of 4 ± 2 % and 0 ± 1 %, respectively. The peak area supported this trend, with values of 1400 ± 840 per unit area and 130 ± 200 per unit area, respectively. Based on percentage, there were no significant

changes between the two silane treatments for phosphorous; however, the peak area of phosphorous shows a significant decrease between the aldehyde silane and the amino silane, with values of 380 ± 190 per unit area and 140 ± 190 per unit area, respectively. Figure 4.56 shows the surface scans of the chitosan films based on metal treatments.

Table 4.80. Elemental percentage based on XPS survey scans of the chitosan films based on silane treatment.

Metal Treatment	Carbon	Oxygen	Nitrogen	Calcium	Silicon	Phosphorous
Aldehyde	64 ± 2 %	26 ± 1[a] %	5 ± 1[b] %	1 ± 1[c] %	1 ± 2 %	1 ± 1[e] %
Amino	67 ± 2 %	26 ± 2[a] %	5 ± 1[b] %	1 ± 1[c] %	0 ± 1 %	0 ± 1[e] %

Values with the same superscript are not statistically different at the 5% significance level.

Table 4.81. Elemental peak areas based on XPS survey scans of the chitosan films based on silane treatment.

Metal Treatment	Carbon	Oxygen	Nitrogen
Aldehyde	24350 ± 1030	24010 ± 1640	3080 ± 660[a]
Amino	22920 ± 600	21980 ± 1960	3050 ± 490[a]

Values with the same superscript are not statistically different at the 5% significance level.

Table 4.82. Elemental peak areas based on XPS survey scans of the chitosan films based on silane treatment.

Metal Treatment	Calcium	Silicon	Phosphorous
Aldehyde	1970 ± 700[b]	1400 ± 840	380 ± 190
Amino	1400 ± 830[b]	130 ± 210	140 ± 200

Values with the same superscript are not statistically different at the 5% significance level.

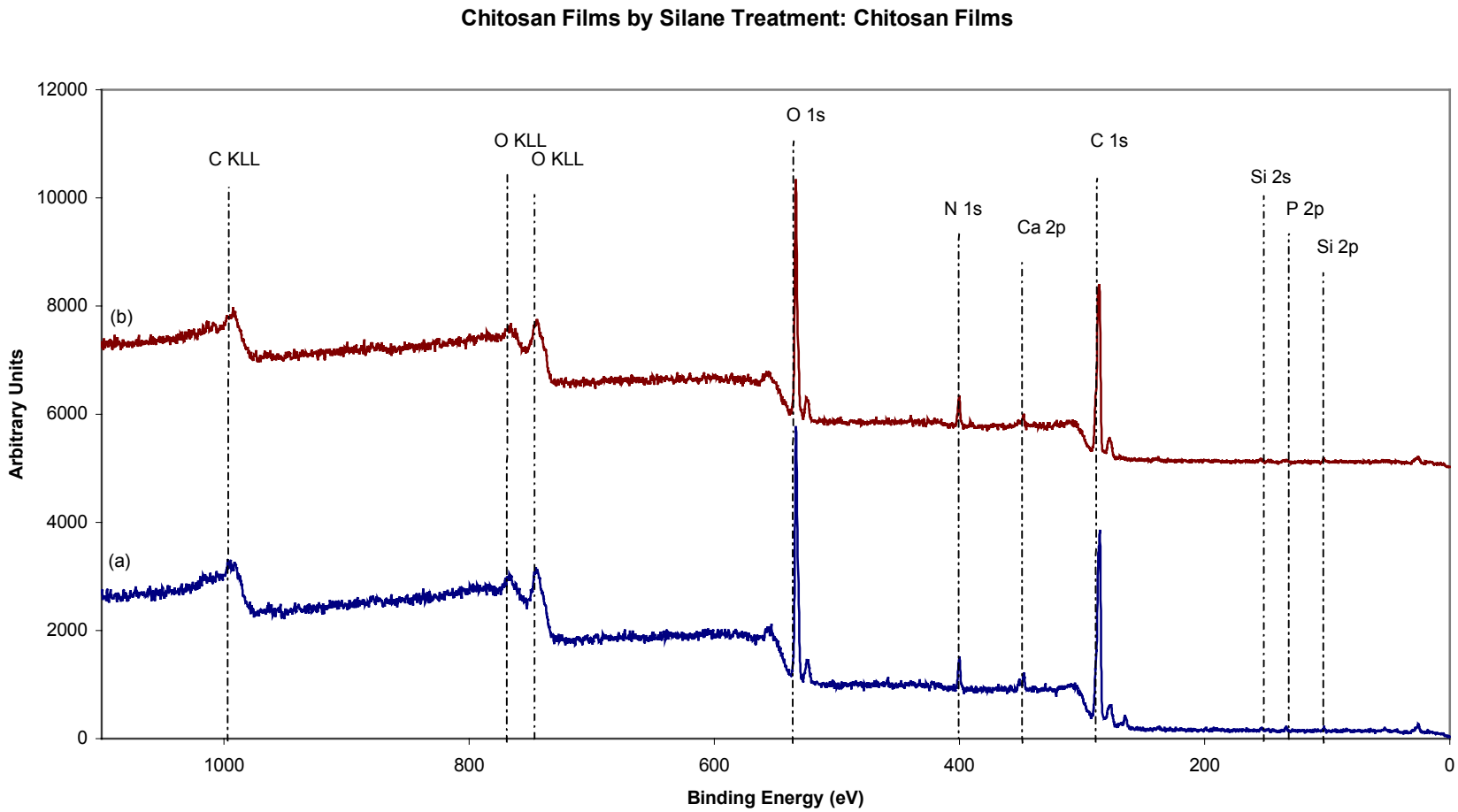

Figure 4.56. Representative survey scans of the chitosan films by silane treatment.

The aldehyde silane is labeled (a). The amino silane is labeled (b).

Tables 4.83 – 4.88 show the high resolution scans of five of six elements present. The scan of phosphorous could not be analyzed as the peak area was too small to analyze accurately. Tables 4.83 – 4.84 show the peaks from the high resolution scans of carbon; there were seven peaks present on all of the films. The first peak, located at 284.8 ± 0.2 eV and identified as C, was not significantly different between the two silane treatments. The C – C peak, located at 285.6 ± 0.2 eV, showed a significant decrease using the aldehyde silane as compared to using the amino silane, with values of 3130 ± 990 per unit area and 1780 ± 1550 per unit area, respectively. The third peak, located at 286.6 ± 0.3 eV and identified as C – O, showed a significant increase using the aldehyde silane as compared to using the amino silane, with values of 2340 ± 650 per unit area and 3160 ± 650 per unit area, respectively. The peak located at 287.6 ± 0.3 eV and identified as C – N – H was not statistically different between the two silane treatments. The fifth peak, identified as C = O and located at 288.7 ± 0.2 eV, showed a significant increase using the aldehyde silane as compared to using the amino silane, with values of 110 ± 110 per unit area and 1390 ± 410 per unit area, respectively. The sixth peak, identified as $CaCO_3$ and located at 289.9 ± 0.2 eV, showed no significant changes between the two silane treatments. The final peak, identified as N – C and located at 290.8 ± 0.3 eV, also showed no significant changes between the two silane treatments. Figure 4.57 illustrates the differences between the film using the aldehyde silane and the film using the amino silane.

Table 4.83. Carbon functional group peak areas based on XPS high resolution scans of the chitosan films based on silane treatment.

	C [4.1]	C-C [4.2]	C-O [4.3]	C-N-H [4.9]
Metal Treatment	284.8 ± 0.2 eV	285.6 ± 0.2 eV	286.6 ± 0.3 eV	287.6 ± 0.3 eV
Aldehyde	750 ± 160[a]	3130 ± 990	2340 ± 650	2470 ± 520[b]
Amino	820 ± 80[a]	1780 ± 1550	3170 ± 650	2510 ± 620[b]

Values with the same superscript are not statistically different at the 5% significance level.

Table 4.84. Carbon functional group peak areas based on XPS high resolution scans of the chitosan films based on silane treatment.

	C=O [4.10]	$CaCO_3$ [4.37]	N-C [4.11]
Metal Treatment	288.7 ± 0.2 eV	289.9 ± 0.2 eV	290.8 ± 0.3 eV
Aldehyde	1070 ± 110	430 ± 250[c]	230 ± 40[d]
Amino	1390 ± 410	670 ± 320[c]	290 ± 20[d]

Values with the same superscript are not statistically different at the 5% significance level.

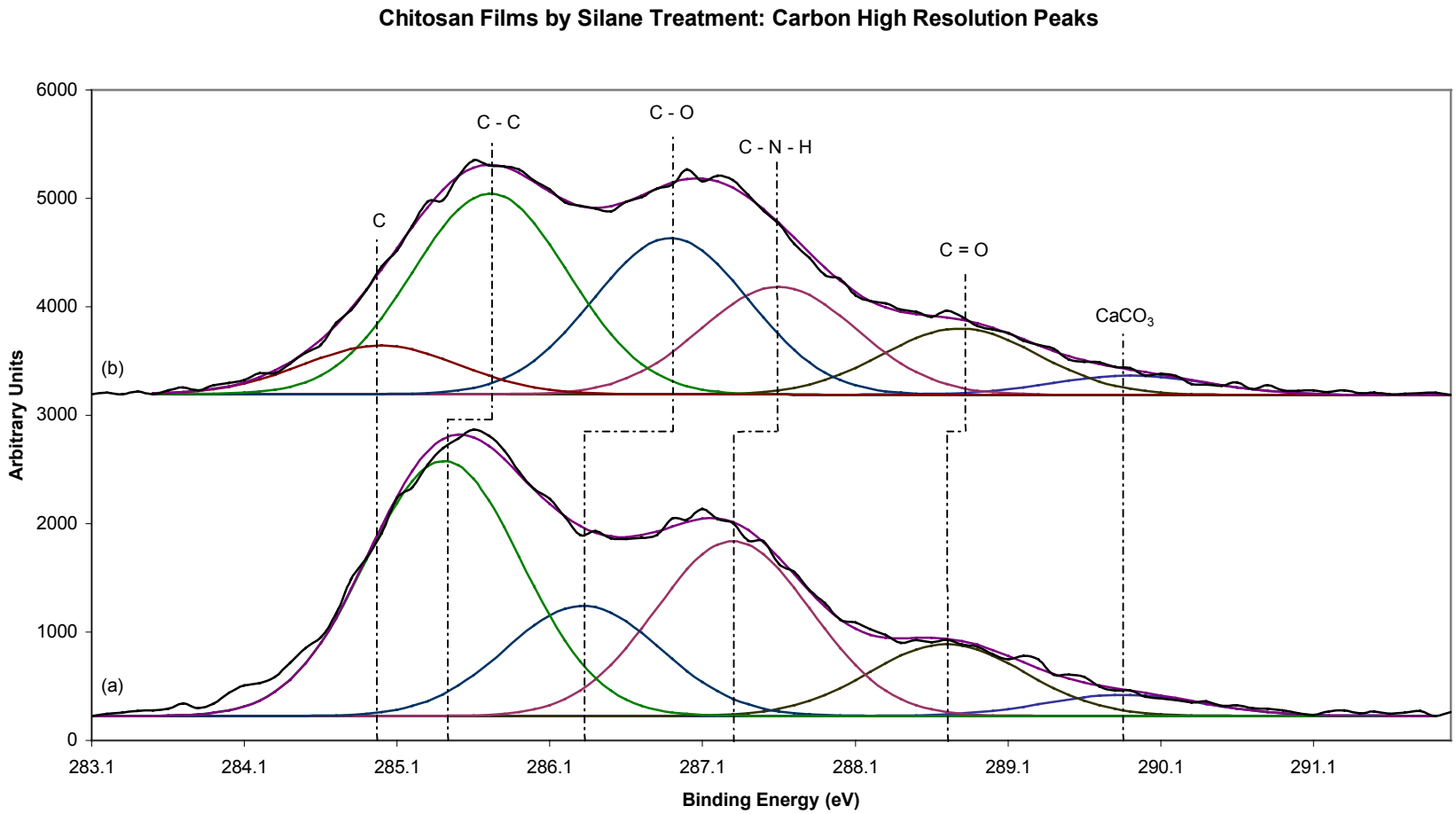

Figure 4.57. Representative carbon high resolution scans of the chitosan films by silane treatment.

The aldehyde silane is labeled (a). The amino silane is labeled (b).

Table 4.85 shows the peaks from the high resolution scan of oxygen; there were five peaks present, with all peaks present on the film surface. The first peak, located at 531.6 ± 0.2 eV and identified as $CaCO_3$, was not significantly different between the two silane treatments. The CaO peak, located at 532.5 ± 0.4 eV, showed a significant decrease using the aldehyde silane as compared to using the amino silane, with values of 2050 ± 690 per unit area and 1430 ± 630 per unit area, respectively. The third peak, located at 533.5 ± 0.3 eV and identified as SiO_2, was not significantly different between the two silane treatments. The peak located at 534.4 ± 0.3 eV and identified as NO, also was not significantly different between the two silane treatments. The fifth peak, identified as C = O and located at 535.5 ± 0.3 eV, was not significantly different between the two silane treatments. Figure 4.58 illustrates the differences between the film using the aldehyde silane and the film using the amino silane.

Table 4.86 shows the peaks from the high resolution scans of calcium; there were three peaks present, all of which were present on both silane surfaces. The first peak, located at 347.8 ± 0.2 eV and identified as CaO, was not significantly different between the two silane treatments. The $CaHPO_4$ peak, identified as 348.7 ± 0.3 eV, was also not significantly different between the two silane treatments. The final peak, identified as $CaCO_3$ and located at 349.4 ± 0.3 eV, was again, not significantly different between the two silane treatments. Figure 4.59 illustrates the lack of differences between calcium peaks based on the use of the aldehyde silane or the amino silane in the deposition of the chitosan films.

Table 4.85. Oxygen functional group peak areas based on XPS high resolution scans of the chitosan films based on silane treatment.

	$CaCO_3$ [4.38]	**CaO [4.39]**	**SiO_2 [4.19]**	**NO [4.22]**	**C=O [4.21]**
Metal Treatment	531.6 ± 0.2 eV	532.5 ± 0.4 eV	533.5 ± 0.3 eV	534.4 ± 0.3 eV	535.5 ± 0.275 eV
Aldehyde	720 ± 220[a]	2050 ± 690	3970 ± 670[b]	2800 ± 1230[c]	540 ± 420[d]
Amino	540 ± 350[a]	1430 ± 630	3460 ± 1070[b]	3160 ± 1130[c]	730 ± 350[d]

Values with the same superscript are not statistically different at the 5% significance level.

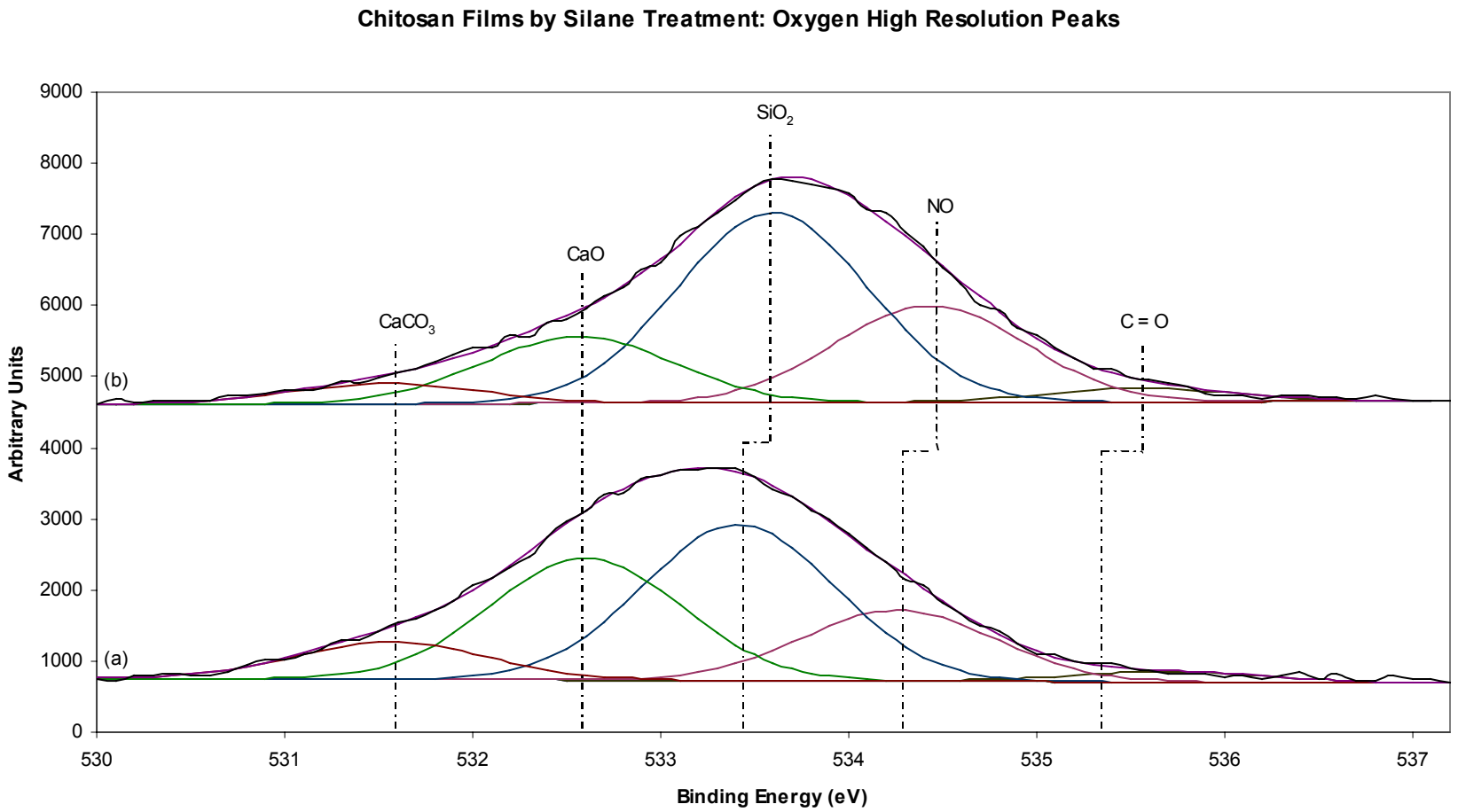

Figure 4.58. Representative oxygen high resolution scans of the chitosan films by silane treatment.

The aldehyde silane is labeled (a). The amino silane is labeled (b).

Table 4.86. Calcium functional group peak areas based on XPS high resolution scans of the chitosan films based on silane treatment.

	CaO [4.40]	**$CaHPO_4$ [4.41]**	**$CaCO_3$ [4.42]**
Metal Treatment	347.8 ± 0.2 eV	348.7 ± 0.3 eV	349. 4 ± 0.3 eV
Aldehyde	270 ± 70[a]	220 ± 100[b]	250 ± 40[c]
Amino	210 ± 190[a]	260 ± 130[b]	200 ± 190[c]

Values with the same superscript are not statistically different at the 5% significance level.

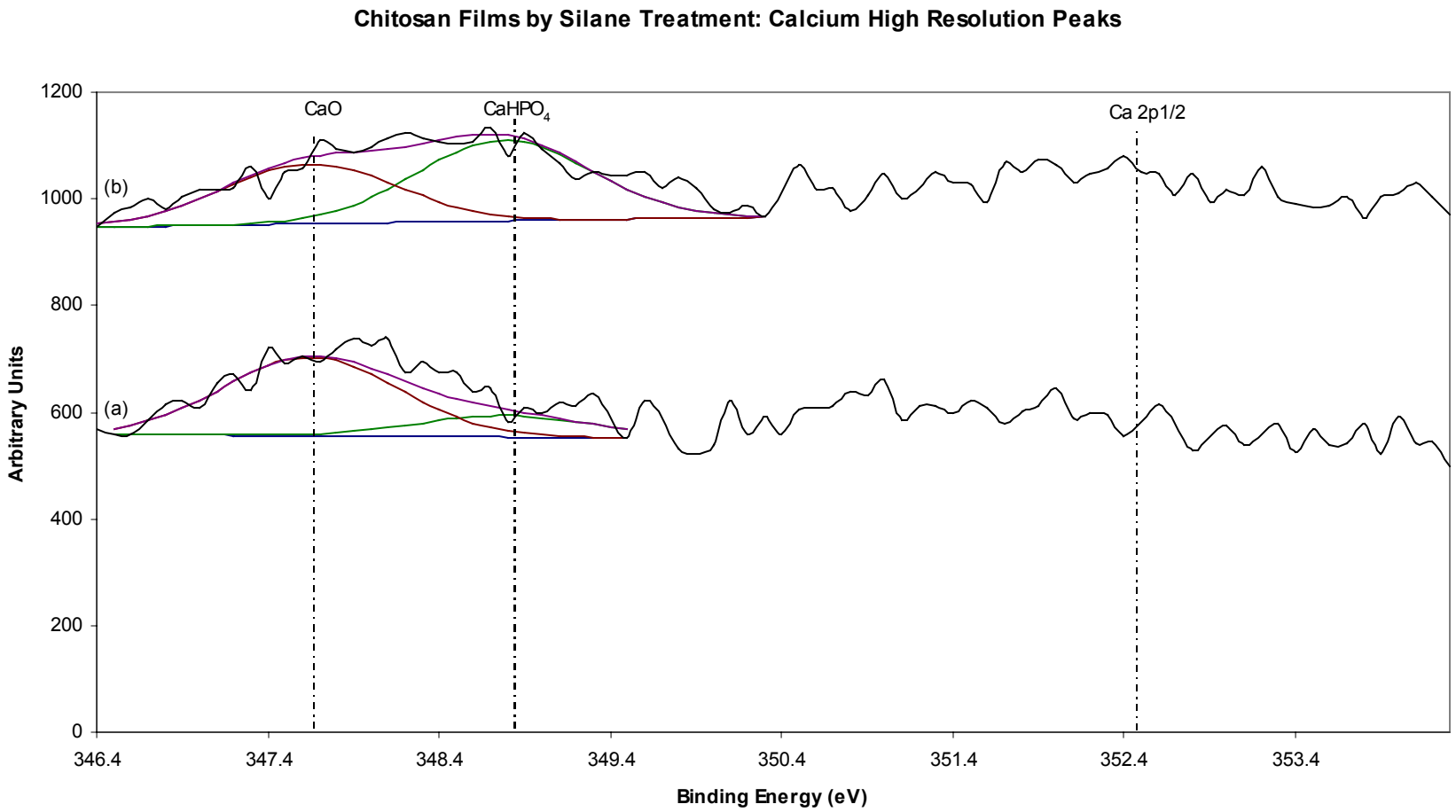

Figure 4.59. Representative calcium high resolution scans of the chitosan films by silane treatment.

The aldehyde silane is labeled (a). The amino silane is labeled (b).

Table 4.87 shows the peaks from the high resolution scans of nitrogen; there were four peaks present, two of which were present on both silane surfaces. The N – C peak, located at 399.8 ± 0.2 eV, was found on both silane surface; it was not significantly different between the two silane treatments. The second peak, located at 400.9 ± 0.2 eV and identified as C – N – H, showed a significant increase using the amino silane as compared to the aldehyde silane, with values of 690 ± 110 per unit area and 530 ± 130 per unit area, respectively. The NH_4^+ peak, located at 401.9 ± 0.2 eV, was not present using the amino silane, while the peak located at 402.4 ± 0.2 eV and identified as NO, was not present using the aldehyde silane. Figure 4.60 shows the differences between the nitrogen peaks present based on the silane treatment.

Table 4.88 shows the peaks from the high resolution scans of silicon; there were three peaks present, with two peaks present on both silane surfaces. The SiO_x peak, located at 102.0 ± 0.2 eV, was present only after using the aldehyde silane. The second peak, located at 102.8 ± 0.2 eV and identified as SiO, showed a significant decrease using the amino silane as compared to the aldehyde silane, with values of 20 ± 60 per unit area as compared to 400 ± 180 per unit area, respectively. The final peak, located at 103.7 ± 0.2 eV and identified as SiO_3, also showed a significant decrease using the amino silane as compared to the aldehyde silane, with values of 60 ± 90 per unit area as compared to 190 ± 80 per unit area, respectively. Figure 4.61 shows the differences between the silicon peaks present on the two films deposited using one of the two silane treatments.

By comparing the films produced by using the two silane treatments, some minor changes were noticed. Most of these changes, including changes to the C – C, C – O,

C = O, and C – N – H peaks, were likely caused by the arrangement of the chitosan chains, caused by the polar nature of the amine group positioning itself to be with the polar water molecules. The other changes, including the changes to the peak areas of CaO and SiO_3, were likely the result of incomplete demineralization, possibly caused by the different amounts of the compounds taken in by the different shellfish used to create the chitosan powder. All of the changes were minimal, showing the two silane treatments did not affect the chemical structure of the chitosan.

Table 4.87. Nitrogen functional group peak areas based on XPS high resolution scans of the chitosan films based on silane treatment.

	N-C [4.32]	C-N-H [4.33]	NH_4^+ [4.34]	NO [4.36]
Metal Treatment	399.8 ± 0.2 eV	400.9 ± 0.2 eV	401.9 ± 0.2 eV	402.4 ± 0.2 eV
Aldehyde	420 ± 110[a]	530 ± 130	250± 90	---
Amino	430 ± 260[a]	690 ± 110	---	300 ± 60

Values with the same superscript are not statistically different at the 5% significance level.

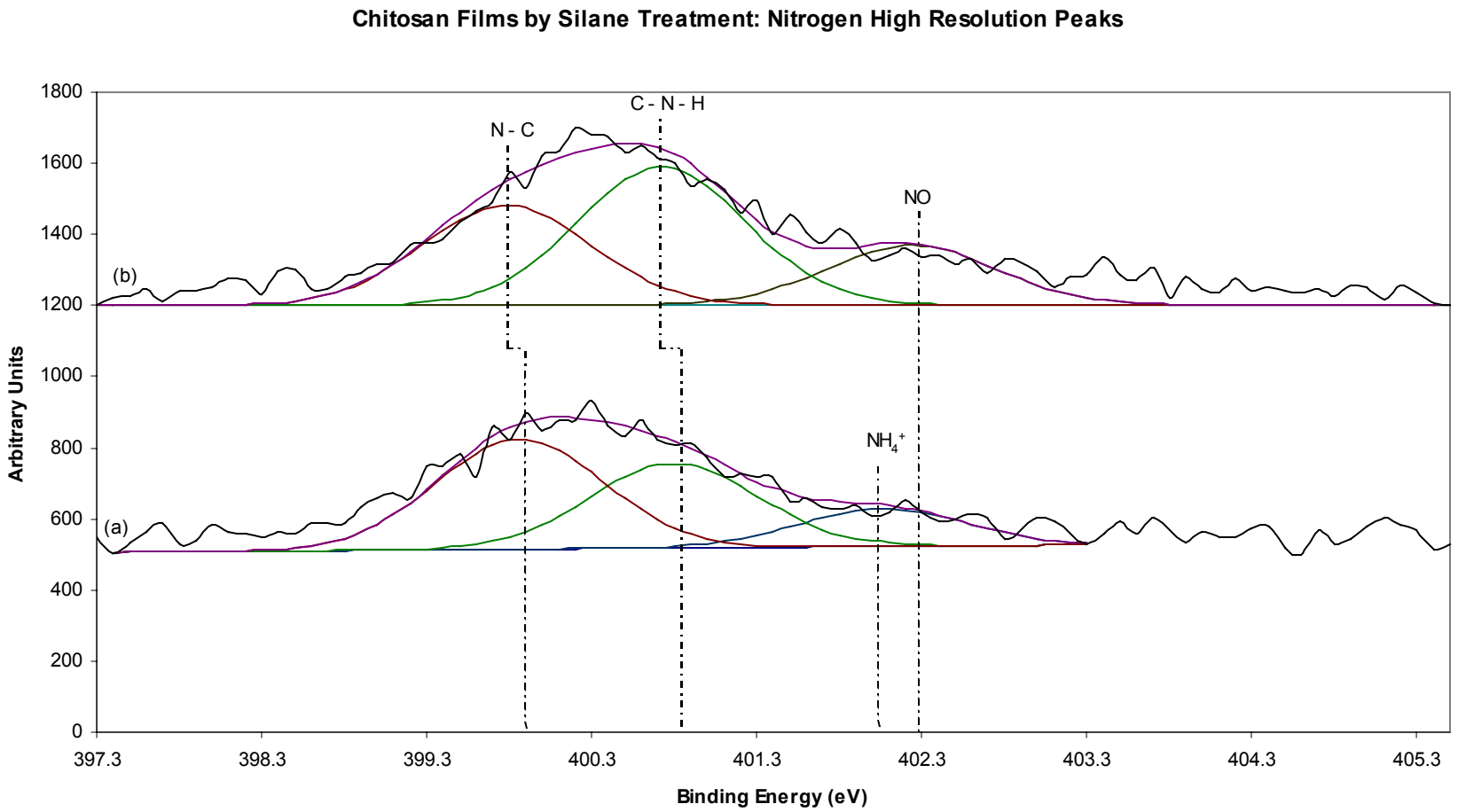

Figure 4.60. Representative nitrogen high resolution scans of the chitosan films by silane treatment.

The aldehyde silane is labeled (a). The amino silane is labeled (b).

Table 4.88. Silicon functional group peak areas based on XPS high resolution scans of the chitosan films based on silane treatment.

	SiO_x [4.27]	**SiO [4.28]**	**SiO_3 [4.29]**
Metal Treatment	102.0 ± 0.2 eV	102.8 ± 0.2 eV	103.7 ± 0.2 eV
Aldehyde	140 ± 90	400 ± 180	190 ± 80
Amino	---	20 ± 60	60 ± 90

Values with the same superscript are not statistically different at the 5% significance level.

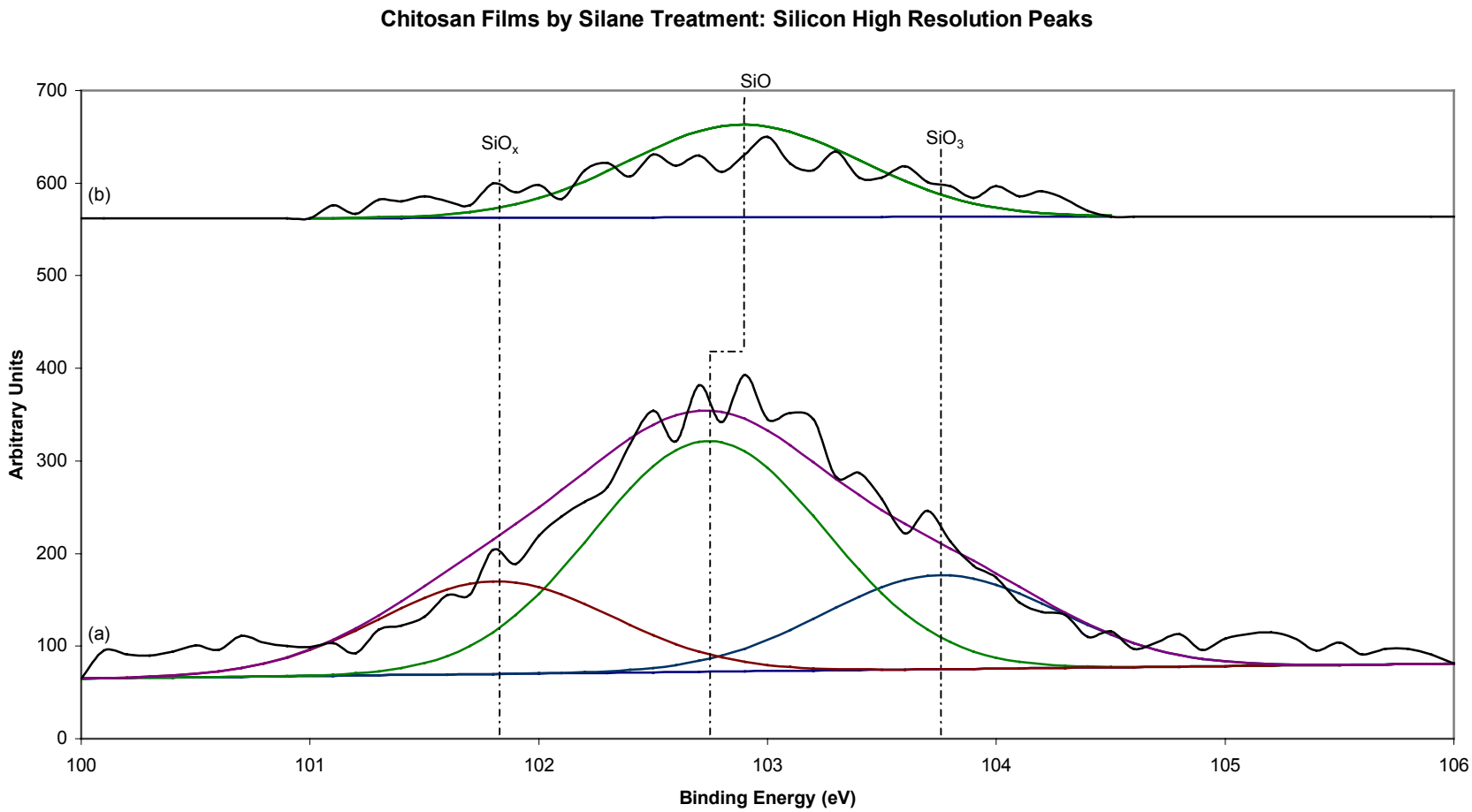

Figure 4.61. Representative silicon high resolution scans of the chitosan films by silane treatment.

The aldehyde silane is labeled (a). The amino silane is labeled (b).

4.4 Discussion

The results indicated different statistical trends for each of the treatments, from the metal treatments before the deposition of silane through the chitosan films deposited on each of the metal and silane treatment combinations. Therefore, the discussion will cover each of the sections present in the results portion of this chapter.

4.4.1 Metal Treatments

A significant difference was seen between each of the elements present on the metal surfaces, using either the passivated treatment or the piranha treatment. When comparing the carbon percentage, the piranha treated metal had a much lower amount of carbon present as compared to the passivated metal. The difference in carbon on the two metals resides solely in the treatment method; two of the three chemicals used in the cleaning of the titanium surface are acetone and ethanol, both organic solvents. The dilute nitric acid used to passivate the surface is not designed to remove the carbon, but instead form an oxide film, which completely covers the surface. However, the piranha treatment is designed to remove carbon, as the sulfuric acid – hydrogen peroxide combination reacts with carboneous materials, removing them from the surface. This reaction causes a significant drop in the carbon percentage. With the significant drop of carbon on the piranha treated surface, all of the high resolution peaks, except for the elemental carbon peak, were significantly lower than the passivated surface, indicating that the piranha treatment did remove a large quantity of carbon. The remaining amount of carbon could be the result of a reaction with carbon in the atmosphere, as the piranha

treated surface is highly reactive. The carbon present on the passivated surface is likely the result of the solvent used in cleaning the metal.

The oxygen percentage also shows a significant change between the two metal treatments; the oxygen percentage on the passivated surface is much less than the oxygen percentage on the piranha treated surface, as shown graphically in Figure 4.3. This difference is again related to the treatment protocol; the purpose of passivation is to create an oxide layer completely covering the surface to prevent the reaction of titanium with its environment [4.45]. The purpose of the piranha treatment, however, was to create a specific reacting group, TiO, that would be available to the silane molecules. The piranha reaction removed carbon and the passive oxide layer, due to its ability to etch and react with titanium, allowing the titanium to react with the ultra pure water to form the TiO groups [4.43]. Two of the other groups present, – OH and $– (OH)_3^{-3}$, are also highly reactive, creating a reactive oxygen surface to treat with the different silane molecules. The C – O group present on both surfaces is not significantly different between the two reactions; it is likely due to a reaction of the surface with the carbon in the atmosphere, but would have no effect on the binding of the silane molecules.

The biggest difference between the passivated metal and the piranha treated metal with respect to percentage is the amount of titanium present on the surface of the metals, as shown graphically in Figure 4.4. There is a significant increase between the passivated metal and the piranha treated metal, with the increase caused by the treatment method. The purpose of passivation is to create an oxide layer completely covering the surface of the titanium metal [4.45], while the purpose of the piranha treatment is to create a reactive oxide layer [4.46], in order to bind silane. The significant increase of titanium is

also seen in the high resolution peaks, with the amount of the desired TiO peak much higher on the piranha treated metal than on the passivated metal. This increase of TiO will allow for more silane molecules to bind to the surface of the metal, thereby possibly increasing the adhesion strength of the chitosan film. The TiO_2 peak does not show a significant difference between the two metals and does not play a role in the reaction of the silane molecules, as the TiO_2 species is non-reactive and part of the oxide film created in passivation. The last peak, TiC, is likely the result of a reaction with the atmosphere; the peak area is very small as compared to the TiO_2 and TiO peaks, indicating that its formation will not likely disrupt the reaction between the silane molecules and the titanium surface.

4.4.2 Aminopropyltriethoxysilane

The amino silane results were determined through each of the reaction steps, which include the deposition of the silane (1a) and the reaction with gluteraldehyde (2a). The reaction steps were also examined based on the metal treatment, which covered the chitosan reaction (3a). The chitosan reaction step was not covered in this section, but in Section 4.4.4, due to the thickness of the film; the thickness of the film prevented the examination of the interaction between the film and the gluteraldehyde, as discussed further in this section.

4.4.2.1 Silane Reaction Step 1a: Comparing Metal Treatments

A significant increase of carbon, nitrogen, and silicon between the passivated metal and the piranha treated metal were seen following the deposition of the amino silane molecule onto the titanium surface, while a significant decrease of titanium

between the passivated metal and the piranha treated metal was seen. The increase between the three elements possibly indicates a higher amount of the silane molecule was deposited on the surface of the piranha treated metal. In examining high resolution peaks for each of the elements, the reasons for the increase become clear. The carbon high resolution peak has two peaks, which are significantly higher on the piranha treated surface as compared to the passivated surface. The first peak, C – O, is present at the silane end of the molecule and connects to silicon to form Si – O – C. The significant increase of the C – O peak seen when examining the piranha treated metal compared to the passivated metal plausibly indicates a higher amount of the amino silane molecule on the piranha surface as compared to the passivated surface. The second peak, C – N – H, is present at the terminal end of the molecule, where the gluteraldehyde will bond in reaction step 2a. A significant difference in the peak areas also indicated a higher amount of the amino silane molecule on the piranha surface as compared to the passivated surface; the significant increase of the C – N – H group on the piranha treated surface also indicates that more places exist for the gluteraldehyde to bond, thereby likely strengthening the bond of the chitosan film to the surface.

The passivated metal and the piranha treated metal also show significant changes to two peaks of nitrogen. The first peak, N – C, is present at the terminal end of the amino silane group, to form the C – NH_2 group. The significant increase seen between the passivated metal and the piranha treated metal indicated that more of the amino silane is bonded to the piranha treated metal than to the passivated metal. The second peak, C – N – H, is also present at the terminal end of the amino silane group; the significant increase seen between the passivated metal and the piranha treated metal again indicated

that more of the amino silane was bonded to the piranha treated metal as compared to the passivated metal. The results of the nitrogen high resolution scan confirm the likely results of the carbon high resolution scan, in that more amino silane is bonded to the surface of the piranha treated metal than to the surface of the passivated metal.

The significant differences in the amount of silicon present following the amino silane deposition on the two metal surfaces provides additional evidence that more amino silane is bound to the piranha treated surface, as compared to the passivated surface. The significant increase of the SiO_3 peak on the surface of the piranha treated metal, as compared to the passivated metal, indicated the formation of a polysiloxane chain close to the surface of the metal; this formation is important because it can only develop if the silane molecules are close to each other, allowing the remaining ethoxy – groups ($CH_3 – CH_2 – O –$) to bond to nearby silane groups, forming a $[– O – Si – O]_n$ group and likely stabilizing the silicon – oxygen – titanium bond; the remaining oxygen bind the silicon to the titanium surface. The other peak, SiO, showed a significant decrease from the passivated metal to the piranha treated metal. The presence of SiO on the passivated surface indicated that there was some binding of the amino silane to the passivated metal. However, this peak also indicated that more "lone" amino silane molecules existed, as compared to the group presence on the piranha treated metal.

The titanium high resolution scan further supports the increased adhesion of the amino silane onto the piranha treated metal as compared to the passivated metal. The TiO_2 peak does not exist on the piranha treated metal following the amino silane reaction, as it initially did following the piranha treatment; however, it does appear on the passivated the surface. The lack of the TiO_2 peak on the piranha treated surface indicates

that the amino silane is more tightly packed and covering the TiO_2 peaks. Since XPS can only penetrate approximately 40 angstroms, and the amino silane molecules are approximately 18 angstroms long, without consideration for the angles within the molecule, it stands to reason that the photoelectrons excited by x-ray source cannot escape as frequently as the photoelectrons could when no silane molecules were covering the surface. The TiO peak is substantially less on the piranha treated metal as compared to the passivated metal; this difference indicated that more of the TiO peak is masked by the amino silane, which is the result of a higher amount of amino silane bound to the piranha treated surface.

There was no significant change seen in the percentage or peak areas of oxygen between the two metal surfaces following the amino reaction step (1a). However, the high resolution scans show some significant changes do occur. The TiO peak drops significantly from the passivated surface to the piranha treated surface, indicating that more silane is bonding to the surface and "hiding" the TiO peak. The SiO_2 peak increases significantly from the passivated surface to the piranha treated surface, also indicating that more silane is bonding to the surface and forming a polysiloxane group to stabilize the silane molecules across the surface of the metal. These two peaks with significant differences further confirm the results seen based on the carbon, nitrogen, silicon, and titanium high resolution scans.

4.4.2.2 Gluteraldehyde Reaction Step 2a: Comparing Metal Treatments

No significant changes were present between the two metal surfaces following the gluteraldehyde reaction (2a), based on percentage. However, based on peak area, carbon

and nitrogen were both significantly more on the piranha treated surface than on the passivated surface. The increase of the two elements further supports the likelihood that the piranha treated surface bound more amino silane molecules than the passivated surface.

Of the six carbon peaks present on the surfaces, only one peak shows any significant difference between the two metal treatments. The C – O peak is significantly higher on the piranha treated surface as compared to the passivated surface. Since there are more amino silane molecules on the surface of the piranha treated metal, as previously discussed, it would seem that there would be a higher amount of the C = O peak on the piranha treated surface, since that is the terminal group of gluteraldehyde. However, gluteraldehyde is present in water, which could prompt a reaction between the terminal group of gluteraldehyde and water to form a C – O group from the C = O group. With the significantly higher amount of amino silane on the piranha treated surface, there would then be a significantly higher amount of C – O on the piranha treated surface, as shown in the results.

Three of five nitrogen peaks present do not show any statistical variation between the two metal surfaces. However, two peaks, N – C and C – N – H, were significantly higher on the piranha treated surface than on the passivated surface. The higher amounts of the peaks N – C and C – N – H on the piranha treated surface are due to the fact that there are more amino silane molecules bound to the that surface, as compared to the passivated surface. Because gluteraldehyde reacts with the C – N – H group to form C = N = C, and the N – C peaks were already higher following the amino silane reaction (1a), no significant change is expected between the reaction series.

While oxygen was not significantly different based on percentage or peak area, one peak shows a significant difference between the two metal treatments. The SiO_2 peak is significantly higher on the piranha treated surface compared to the passivated surface. This difference is due to the fact that more amino silane molecules were bonded to the piranha treated surface prior to the gluteraldehyde reaction (2a). The gluteraldehyde molecule is not large enough to fully "mask" the silicon element from the x-ray beam; the difference between the SiO_2 peak on the passivated metal and the piranha treated metal just further support the increased binding of the amino silane molecule to the titanium surface.

Silicon is also not significantly different based on percentage or peak area. However, the SiO_3 peak is significantly higher on the piranha treated surface compared to the passivated surface. This difference is accounted for because of the size of the gluteraldehyde molecule, which cannot fully cover the silicon element. Therefore, the same polysiloxane chain that was present following the deposition of the amino silane is still present following the gluteraldehyde reaction.

There were no significant differences between the titanium peaks on the two metal treatments following the gluteraldehyde reaction. A large portion of the titanium peak is likely masked by the addition of the gluteraldehyde molecule; the photoelectrons released by the excitation of the electron beam cannot escape from the amino silane – gluteraldehyde complex for analysis. Since XPS can only penetrate approximately 40 angstroms, and the amino silane – gluteraldehyde molecules are approximately 34 angstroms long, without consideration for the angles within the molecule, it stands to

reason that the photoelectrons excited by x-ray source cannot escape as frequently as the photoelectrons could when gluteraldehyde was not bound to the amino silane molecules.

4.4.2.3 Passivated Metal Treatment: Comparing Reaction Steps

Significant changes were observed following each of the reaction steps performed on the passivated metal surface. Following the amino reaction step (1a), a significant decrease of carbon was seen from the passivated surface to the amino silane surface, while a significant increase was seen from the amino silane surface to the gluteraldehyde surface; however, only the C – C peak can be examined since all of the other peaks present on the passivated metal surface were not identified as the same peaks following the amino reaction step, as there was no silicon or nitrogen present on the passivated surface. The drop in the C – C peak likely indicates that not all of the hydrocarbons found on the passivated surface were not chemically bound to the surface, but instead were physically bound to the surface, through weak hydrogen bonds. When a more desirable compound was present, as was the case with the amino silane, the weak hydrogen bonds break, releasing the hydrocarbon and allowing the amino silane to bond to the surface. No significant changes were seen in the C – C peak following the gluteraldehyde reaction step (2a) or the chitosan reaction step (3a). A significant increase was seen in the C – O peak between the amino reaction step and the gluteraldehyde reaction step, while a significant decrease was seen in the same C – O peak following the chitosan reaction step. The increase in the C – O peak between the amino reaction step and the gluteraldehyde reaction step is likely due to the presence of water in the aqueous gluteraldehyde solution, creating a C – O molecule in place of the terminal C = O on

gluteraldehyde. A significant increase in the C – N – H group was seen between the amino silane surface and the gluteraldehyde surface and between the gluteraldehyde surface and the chitosan surface. The increase in this group is likely due to the possible physical bonding of toluene to the amino silane terminal group. With the addition of gluteraldehyde, the toluene is fully removed, allowing all of the C – N – H groups to be seen. The C – N – H group would still be present following the gluteraldehyde reaction, as the gluteraldehyde would not bind with every terminal amine group. The peak identified as C = O also showed a significant increase between the amino silane surface and the gluteraldehyde surface; this is to be expected, as the terminal group of gluteraldehyde is C = O. With the gluteraldehyde reacting with the one of the two terminal ends of the amino silane to form C = N = C, the other end, composed of C = O, would be present at the surface of the growing film. The last peak, N – C, also showed a significant increase between the amino silane surface and the gluteraldehyde surface, along with a significant increase following the chitosan reaction. This increase is likely due to the binding of gluteraldehyde to the C – N – H group, which would remove the – H portion, creating N – C. The changes of the C – O peak, the C – N – H peak, the C = O peak, and the N – C peak following the chitosan reaction are a part of the chitosan molecule and will be discussed in Section 4.4.4.

Significant changes were also seen in the oxygen peak. No significant changes were seen in the peak area of oxygen between the passivated surface and the amino silane; however, changes were seen in the high resolution peaks. Only one peak can be compared through all four reaction steps, as the peaks present on the passivated surface were not identified as the same peaks following the amino silane reaction step, since

there was no silicon or nitrogen present on the passivated surface. A significant decrease in the TiO peak was seen between the passivated metal surface and the amino silane surface, along with a significant decrease following the gluteraldehyde surface. There was no titanium present following the chitosan film deposition. This significant decrease between the passivated metal surface and the amino silane surface is the result of the coverage of the amino silane; as the amino silane reacted with the TiO species, the peak became "covered" by the amino silane molecule, which prevented the release of the photoelectrons excited by the x-ray beam. The amount of TiO dropped even further following the reaction with gluteraldehyde since the amino silane – gluteraldehyde prevented even more photoelectrons from escaping. Since XPS can only penetrate approximately 40 angstroms, and the amino silane – gluteraldehyde molecules are approximately 34 angstroms long, without consideration for the angles within the molecule, it stands to reason that the photoelectrons excited by x-ray source cannot escape as frequently as the photoelectrons could when gluteraldehyde was not bound to the amino silane molecules. There were no statistical differences between the amino reaction surface and the gluteraldehyde reaction surface in the peaks identified as SiO, SiO_2, or NO, nor were there statistical differences between the gluteraldehyde reaction and the chitosan surface with respect to SiO, NO, or C = O. There were significant changes between the gluteraldehyde reaction surface and the chitosan film of the SiO_2 peak. The lack of change is due to the inability of the amino silane – gluteraldehyde complex to fully mask the silicon element from the x-ray beam, since the molecule extending from the silicon was only 24 angstroms thick. There was a significant decrease between the amino reaction surface and the gluteraldehyde reaction surface with respect

to SiO_x, while there was no significant change between the gluteraldehyde reaction and the chitosan reaction. The decrease of SiO_x is likely due to the coverage that the gluteraldehyde molecule provides to the SiO_x groups at the base of the amino silane – gluteraldehyde complex; the photoelectrons excited by the x-ray beam may not be able to escape the pull of the complex and would therefore show a decrease in the SiO_x peak. The significant change of the SiO_2 peak and the lack of change in the SiO_x peak following the chitosan reaction are a part of the chitosan molecule and will be discussed in Section 4.4.4.

There was a significant change in the amount of nitrogen present between the amino reaction surface and the gluteraldehyde reaction surface, while there was no nitrogen present on the passivated surface. Two of the five peaks present varied significantly between the amino silane surface and the gluteraldehyde surface, while one peak was present only on the amino silane surface. The N – C peak showed no significant change between the amino silane surface and the gluteraldehyde surface, but a significant increase was seen with respect to the chitosan surface. This is due to the fact that N – C is part of the amino silane molecule; once gluteraldehyde reacts with the amino silane molecule, N – C is still present as part of the bond between the gluteraldehyde molecule and the amino silane molecule. A significant decrease was seen between the amino silane surface and the gluteraldehyde surface with respect to C – N – H; this decrease is expected since C – N – H reacts with gluteraldehyde to form C = N = C. A significant increase was seen in the C – N – H peak following the chitosan reaction. A significant decrease was seen in the NH_4^+ peak following the gluteraldehyde reaction, while the NH_4^+ peak was not present on the chitosan surface. This decrease is

the result of the reaction between gluteraldehyde and NH_4^+, forming N = C. The NO_2^- peak, present only on the amino silane surface, is probably the result of physical bonding between the amine terminal group of the amino silane and the atmosphere during transport between the laboratory and the XPS machine. The significant changes of the C – N – H and NH_4^+ peaks and the lack of change in the N – C and NO peaks following the chitosan reaction are a part of the chitosan molecule and will be discussed in Section 4.4.4.

A significant change in the amount of silicon is seen between each of the three reaction steps, with no silicon present on the surface of the passivated metal. A significant decrease in the SiO peak is seen between the amino silane surface and the gluteraldehyde surface, along with a significant drop following the chitosan reaction. This drop is due to the coverage provided by the addition of the gluteraldehyde molecule; all of the photoelectrons excited by the x-ray beam cannot escape from the amino silane – gluteraldehyde complex, thereby reducing the amount of SiO seen. No significant change occurs with respect to the SiO_3 peak between the amino silane reaction step and the gluteraldehyde reaction step. The SiO peak is reduced because the photoelectrons cannot escape the chain formed by the amino silane – gluteraldehyde complex; however, the SiO_3 peak is not reduced, because, instead of "sticking up" as the amino silane – gluteraldehyde complex does, the polysiloxane group runs along the metal surface. The SiO_3 peak is not as fully covered as the SiO peak, which results in no significant changes between the amino silane reaction surface and the gluteraldehyde reaction surface. The SiO_3 group is not present on the chitosan surface. The significant changes of the SiO and

SiO_3 peaks following the chitosan reaction are related to the chitosan molecule and will be discussed in Section 4.4.4.

A significant change in the titanium peak, based on both percentage and peak area, is observed between the passivated metal and the amino silane reaction step, along with the amino silane reaction step and the gluteraldehyde reaction step. No titanium is present following the chitosan reaction step. No significant decrease in the TiO_2 peak is seen between the passivated metal surface and the amino silane surface, indicating no reaction took place with respect to the TiO_2 peak. There was also no significant decrease in the TiO_2 peak between the amino silane surface and the gluteraldehyde surface, indicating that the TiO_2 peak is passive and non-reactive. A significant decrease was seen in the TiO peak between the passivated metal surface and the amino silane surface, as illustrated in Figure 4.22. This decrease of the TiO peak is the result of binding the amino silane to TiO, which prevents some of the photoelectrons from being detected, as the TiO peak was covered by the large amino silane molecule. There was no significant decrease of the TiO peak between the amino silane reaction and the gluteraldehyde reaction, since the gluteraldehyde molecule is a smaller molecule and would not greatly reduce the amount of photoelectrons escaping from the surface.

Because of the lack of titanium following the chitosan reaction step, and the closeness of the silicon element to the titanium surface, the adhered film, which is believed to be around 100 μm, is too thick to examine the reaction between the gluteraldehyde molecule and the chitosan film. It is this reason, the thickness of the film, that makes any statistical similarities or differences between the gluteraldehyde reaction step and the chitosan reaction solely the result of the chitosan molecule, not the result of

the chemistry between the amino silane – gluteraldehyde complex and the chitosan film; the chitosan films on all four treatment combinations will be discussed in Section 4.4.4.

4.4.2.4 Piranha Treated Metal: Comparing Reaction Steps

Significant changes in the percentage and the peak area of carbon were seen between the piranha treated metal surface, the amino silane surface, the gluteraldehyde surface, and the chitosan film surface. A significant increase was seen between the piranha treated surface and the amino silane surface; however, the only peak that can be compared, the C – C peak was statistically similar. The C – C peak was significantly higher on the chitosan surface than on the gluteraldehyde surface, however. The other peaks could not be compared between the piranha treated surface and the amino silane surface, as the peak identification was different since neither silicon nor nitrogen were present on the piranha treated surface. The C – O peak was not significantly different between the amino silane surface and the gluteraldehyde surface; this occurs because the C – O peak is present at the base of the silane molecule, connecting silicon to the propyl group, as an Si – O – C link. The C – O peak was significantly lower on the chitosan surface than on the gluteraldehyde surface, however. The C – N – H group was significantly higher on the gluteraldehyde surface than on the amino silane surface; this increase is likely due to the removal of physically bonded toluene to the terminal amine group. With the addition of the aqueous gluteraldehyde solution, the remaining toluene was removed, allowing an increase in the C – N – H peak to be seen. A significant increase between the gluteraldehyde reaction step and the chitosan reaction was also seen with respect to the C – N – H peak. The C = O group significantly increased when

comparing the amino silane surface with the gluteraldehyde surface. This increase is due to the bonding of one end of the gluteraldehyde molecule with the amino silane molecule to form C = N = C, leaving the other end of the gluteraldehyde molecule, composed of a C = O group, exposed. A significant increase between the gluteraldehyde reaction step and the chitosan reaction was also seen with respect to the C = O peak. No significant change occurred with respect to the N – C peak between the amino silane surface and the gluteraldehyde surface. The lack of change is likely due to the small size of the gluteraldehyde molecule, which did not cover the N – C bond between the amino silane molecule and the gluteraldehyde molecule. The last peak, CO_3^{-2}, is present on the gluteraldehyde reaction surface and the chitosan surface, only. The formation of the CO_3^{-2} peak is likely due to some contamination, as there is no explanation based on the reaction scheme that could account for the formation of the CO_3^{-2} peak. As previously stated, because of the thickness of the chitosan film, the significant changes of the peaks C – C, C – O, C – N – H, C = O, N – C, and CO_3^{-2} will be covered in Section 4.4.4.

Significant changes were also seen in the oxygen peak, between the piranha treated surface and the amino silane surface; however, no significant changes were seen in the peak area of oxygen between the amino surface and the gluteraldehyde silane. Of the four peaks present on the piranha treated surface, only one peak could be compared through all four reaction steps, as the peaks present on the piranha treated surface were not identified as the same peaks following the amino silane reaction step, since there was no silicon or nitrogen present on the piranha treated surface. The TiO peak showed a significant decrease between the piranha treated surface and the amino silane surface, while no significant change was seen between the amino silane surface and the

gluteraldehyde surface. The significant decrease of the TiO peak between the piranha surface and the amino surface is the result of the bonding of the amino silane molecule to the TiO molecule; this bonding reduced the ability of the photoelectrons to escape from the surface. Since XPS can only penetrate approximately 40 angstroms, and the amino silane molecules are approximately 18 angstroms long, without consideration for the angles within the molecule, it stands to reason that the photoelectrons excited by x-ray source cannot escape as frequently as the photoelectrons could when the amino silane molecules were not bound to metal surface. There was no significant change in the TiO peak between the amino silane surface and the gluteraldehyde surface; the lack of change can be contributed to the small size of the gluteraldehyde molecule, which did not prevent the escape of photoelectrons from the surface. The TiO peak was not present on the chitosan film surface. The SiO peak showed no significant change between the amino silane reaction step and the gluteraldehyde reaction step. The lack of change is likely due to the small size of the gluteraldehyde molecule, which did not prevent the release of photoelectrons, as the "top" of the silicon portion of the amino silane molecule to the top of the gluteraldehyde molecule is only 24 angstroms. However, this lack of change in the peak is a good thing, as it shows that the SiO peak is strongly bonded to the piranha treated surface and will not be removed by an aqueous gluteraldehyde solution. A significant decrease in the SiO was seen between the gluteraldehyde surface and the chitosan surface. The SiO_x peak between the amino silane surface and the gluteraldehyde surface also showed a significant decrease; the gluteraldehyde surface and the chitosan film surface again demonstrated a significant decrease in the SiO_x peak. This decrease likely the result of the amino silane – gluteraldehyde complex covering the SiO_x groups

at the base of the complex; the photoelectrons excited by the x-ray beam would be unable to escape the complex and be detected. A significant decrease in the SiO_2 peak was also seen; this decrease was seen between the amino silane surface and the gluteraldehyde surface along with a decrease between the gluteraldehyde surface and the chitosan surface. The decrease of the SiO_2 peak is due to the growth of the film as each reaction is performed; as the amino silane – gluteraldehyde chain is created, the SiO_2 peak at the based of the chain is masked from detection since the photoelectrons cannot escape. The peak identified as NO shows a significant increase between the amino silane surface and the gluteraldehyde surface, along with a significant increase between the gluteraldehyde surface and the chitosan surface. The NO peak is only present in a small amount on the amino silane surface, likely a reaction of the terminal group with the atmosphere; however, since a significant increase is seen between the amino silane surface and the gluteraldehyde surface, a reaction between the amine group and the water present in the aqueous gluteraldehyde solution is the likely cause for the formation of the NO peak. A C = O peak exists on the surface of the gluteraldehyde surface, but not on the amino silane surface; this occurs because the terminal group of gluteraldehyde, which is C = O, is present following the reaction between the terminal amine group of the amino silane and the gluteraldehyde molecule. The C = O peak shows a significant increase between the gluteraldehyde reaction and the chitosan reaction. The changes of the chitosan film with respect to the SiO, SiO_x, SiO_2, NO, and C = O peaks will be covered in Section 4.4.4, since the thickness of the film results in an inability to examine the reaction between the chitosan surface and the amino silane – gluteraldehyde complex.

A significant decrease between the amino silane surface and the gluteraldehyde surface occurs with respect to nitrogen, based on both percentage and peak area. A significant decrease also occurs between the gluteraldehyde surface and the chitosan surface, based on peak area. No nitrogen was present on the piranha treated metal. The first peak, N – C, shows a significant decrease between the amino silane reaction and the gluteraldehyde reaction. This occurs because the amino silane molecules are grouped so closely together as indicated by the polysiloxane groups present on the surface, as discussed in Section 4.4.2.1. When the gluteraldehyde reacts with the terminal amine groups, the resulting C = N = C bond is masked from detection because the photoelectrons cannot escape the tightly packed amino silane – gluteraldehyde complexes. The N – C peak is not present on the chitosan film surface, however. The second peak C – N – H also shows a significant decrease between the amino silane reaction and the gluteraldehyde reaction, while a significant increase is seen between the gluteraldehyde reaction and the chitosan reaction. This decrease occurs because the gluteraldehyde reacts with the C – N – H group to form C = N = C, thereby reducing the amount of the C – N – H peak present. The NH_4^+ peak is present only on the amino silane surface and the gluteraldehyde surface; a significant decrease is shown between the two surfaces. The formation of the NH_4^+ group occurred as the terminal amine group became protonated and highly reactive. The reaction of gluteraldehyde with the amino silane produced a reaction between the gluteraldehyde and the NH_4^+ group, to form C = N = C, and reducing the amount of NH_4^+. The NO peak was present only on the gluteraldehyde and chitosan surfaces; no significant change was seen between the two surfaces. The presence of NO on the gluteraldehyde surface indicated the reaction of the

terminal amine group with the aqueous gluteraldehyde solution, forming NO instead of reacting with the gluteraldehyde molecule. NO_2^- was present only on the amino silane surface, likely a reaction with the atmosphere during transport to the XPS machine. The significant changes of N – C, C – N – H, NH_4^+, and NO on the chitosan surface will be discussed in Section 4.4.4, as part of the chitosan molecule, since the chitosan film is too thick to examine the interaction between gluteraldehyde and the chitosan film.

Significant changes in the percentage and peak area of silicon were seen between the amino silane reaction step and the gluteraldehyde reaction step, along with significant changes between the gluteraldehyde reaction step and the chitosan reaction step. There was no silicon present on the piranha treated surface. No significant change occurred to the SiO peak between the amino silane surface and the gluteraldehyde surface. The lack of change is due to the small size of the gluteraldehyde molecule, which does not prevent the photoelectrons from escaping. The presence of this peak also demonstrated that the link between the silicon element and the propyl group was not disturbed by placing the metal samples in the aqueous gluteraldehyde solution. A significant decrease of the SiO_3 peak does occur between the amino silane surface and the gluteraldehyde surface, along with a significant decrease between the gluteraldehyde surface and the chitosan surface. This decrease occurs because, as previously stated, there were more amino silane molecules on the surface of the piranha treated metal, with more polysiloxanes formed. As the molecules reacted with gluteraldehyde, a thicker coverage of the metal surface occurred, thereby reducing the amount of photoelectrons released by the polysiloxanes that could escape and be detected, indicating that the amino silane molecules were more tightly packed on the piranha treated surface. The final peak, SiO_2, is present on the

amino silane surface and the gluteraldehyde surface, with a significant decrease occurring between the two reactions. The decrease of the SiO_2 peak indicated that the base of the amino silane – gluteraldehyde complex was masked from detection because of how tightly packed the complexes were, which did not allow the escape of the photoelectrons. The changes of the SiO, SiO_3, and SiO_2 peaks with respect to the chitosan film will be covered in Section 4.4.4.

Significant changes in the percentage and peak area of titanium were seen between the piranha treated metal and the amino reaction step; however, no significant changes were seen between the amino silane surface and the gluteraldehyde surface, based on percentage and peak area. Titanium was not present on the surface of the chitosan film. The TiO_2 peak was present on the piranha treated metal, but was not present on the amino silane surface or the gluteraldehyde surface. The lack of this peak further indicated how closely packed the amino silane – gluteraldehyde complexes were; since the TiO_2 peak is non-reactive, following the adhesion of the amino silane molecule to the TiO peaks, the formation of polysiloxanes took place, completely covering the non-reactive TiO_2 species. The TiO peak showed a significant decrease from the piranha treated surface to the amino silane surface, but no significant change was seen from the amino silane surface to the gluteraldehyde surface. The significant decrease is seen because of the reaction of the amino silane molecule with the TiO species, to the point of almost completely removing the peak, as seen in Figure 4.28. While there was no significant difference between the amino silane surface and the gluteraldehyde surface with respect to the TiO peak, there was very little that could be seen on the amino silane surface following the amino silane reaction. The amino silane reacted with the TiO

species to almost completely cover the piranha treated surface. The last remaining peak, TiC, saw a significant decrease from the piranha treated surface to the amino silane surface; the decrease is likely the result of the amino silane molecule binding to the TiO peaks and creating polysiloxane groups between the amino silane molecules, thereby covering the TiC peaks. There was no significant change between the amino silane surface and the gluteraldehyde surface, as the polysiloxanes had already formed.

4.4.3 Triethoxsilylbutyraldehyde

The aldehyde silane results were determined through each of the reaction steps, which include the deposition of the silane (1b). The reaction steps were also examined based on the metal treatment, which covered the chitosan reaction (2b). The chitosan reaction step was not covered in this section, but in Section 4.4.4, due to the thickness of the film, which prevented examination of the interaction between the film and the aldehyde silane, as further discussed in this section.

4.4.3.1 Silane Reaction Step 1b: Comparing Metal Treatments

No significant changes were seen between the two metal surfaces with respect to carbon, oxygen, silicon, or titanium, based on percentage. In fact, no significant change was seen in any of the high resolution carbon peaks. This can possibly be attributed to the high reactivity of the aldehyde silane molecule. The hydrocarbon peak would be identical because of the close packing of the aldehyde silane, likely caused by the silane molecule's strong reaction with itself and with the TiO species. This possible close packing would prevent the release of some of the excited photoelectrons, thereby reducing the C – C peak. The C – O and C = O peaks, located at the terminal end of the

aldehyde silane molecule, would not show a difference either. The lack of difference is because nothing would prevent the excitation of the electrons, producing a large quantity of photoelectrons released from the surface at the same binding energy. Since the aldehyde silane molecules were possibly very closely packed, the difference in detection of the C – O and C = O peak would be minimal. The COOH, CO_3^{+2}, and CO_3^{-2} peaks are not significantly different between the two surfaces either. These peaks are likely the reaction of the terminal end of the aldehyde silane group with the atmosphere during transport to the XPS machine, as the reaction does not support the formation of the three peaks.

Unlike the carbon high resolution peaks, there were significant changes in the oxygen high resolutions peaks. Of the six peaks, two peaks were statistically different, while one peak, the SiO peak, was not present on the passivated surface. The TiO peak showed no significant difference between the two metal surfaces; this indicated that the aldehyde silane would strongly bond to any TiO present on the surface of the metal. However, since the TiO peak was much less on the passivated surface than on the piranha treated surface, more aldehyde silane was bound to the piranha treated surface, since the TiO peak was the same following the reaction. The SiO peak was not present on the passivated surface, but the presence of the peak on the piranha treated surface indicated that the bond between the silicon portion of the silane molecule and the butyl portion of the silane molecule had not been disrupted. No significant change was seen in the SiO_x peak between the two metal surfaces, indicating that the polysiloxane chain formed regardless of the amount of aldehyde silane present, since there was more aldehyde silane on the piranha treated surface than on the passivated surface. There was a significant

decrease in the SiO_2 peak when comparing the passivated surface to the piranha treated surface. The decrease is indicative of the increased amount of aldehyde silane present on the piranha treated surface; not as many photoelectrons excited by the x-ray beam were able to escape the closely pack aldehyde silane molecules on the piranha treated surface, indicated by a lower peak area of SiO_2. No significant change occurred when comparing the C – O peak on the two metal surfaces. While there was more aldehyde silane on the piranha treated surface, the C – O species is located at the terminal end of the molecule and would allow more photoelectrons to be released; without the closely packed aldehyde silane molecules preventing the escape of the photoelectrons, the detection of the C – O species would be nearly identical since the photoelectrons on the aldehyde silane surface were excited at the same binding energy. While the C = O peak was much higher on the piranha treated surface than on the passivated surface, no real comparisons between the two surface can be made, as the C = O peak was present on only one of nine piranha treated surfaces.

When examining the silicon peak area, no significant changes were seen, with respect to both the overall peak area and the high resolution peak areas. The aldehyde silane is highly reactive, with both the surface and with itself. The lack of change in the silicon high resolution peaks just likely confirms the molecule's high reactivity. The SiO peak, or the peak at the silicon end of the aldehyde silane molecule, connected the silicon and the butyl group. This peak was not disturbed or broken during the aldehyde silane deposition, which is indicated by the lack of change between the two metal surfaces. SiO_3 is indicative of a polysiloxane chain, or the connection the aldehyde silane makes to itself; this peak is not significantly different between the two metals, an indication that it

didn't matter which surface the aldehyde silane was on, it would also react with itself to form the chains. The final peak, SiO_2, is located at the base of the aldehyde silane molecule, and connected the aldehyde silane molecule to the titanium surface; no significant change was seen here, indicating that the SiO_2 species formed with every possible TiO species, possibly leading to an increase in the adhesion strength of the chitosan film.

No significant changes were seen when examining titanium, in either the overall peak area or the high resolution peak areas. While there is no difference between the peaks, there was originally a difference between the TiO peak on the passivated metal and on the piranha treated metal. The lack of difference in the TiO peak following the aldehyde reaction indicated that the aldehyde silane reacted strongly with almost every TiO species available; there were less TiO species available on the passivated surface to react with, but the aldehyde silane reacted with every species it could find, covering the TiO species and reducing the amount of TiO detected. This indicated that there were likely more aldehyde silane molecules bound to the piranha treated surface than to the passivated surface, since more TiO species were present on the piranha treated surface. The TiO_2 peak is also not significantly different between the two metal treatments, although it was higher on the passivated metal surface than on the piranha treated surface. The lack of difference shows that the aldehyde silane not only reacted with the TiO species, but reacted with itself to form polysiloxane chains across the surface, hiding the non-reactive TiO_2 species from detection.

4.4.3.2 Passivated Metal Treatment: Comparing Reaction Steps

Significant changes were observed following each of the reaction steps performed on the passivated metal surface. Following the aldehyde reaction step (1b), a significant decrease of carbon was seen from the passivated surface to the aldehyde silane surface, while a significant increase was seen from the aldehyde silane surface to the chitosan surface, based on percentage. The peak area of carbon, however, showed a different trend, with no significant difference between the passivated surface and the aldehyde surface. Looking at the high resolution peaks, a significant change occurred on three peaks, while three peaks were not originally present on the passivated surface. No significant change occurred between the passivated surface and the peak identified as elemental carbon, while the peak was not present on the chitosan surface. The lack of change indicated that the presence of the elemental carbon did not affect bonding, but also was not removed by sonication following the deposition of the aldehyde silane; the elemental carbon is chemically bound to the passivated metal surface. The second peak, C – C, showed a significant decrease between the passivated metal surface and the aldehyde silane surface, while no significant change occurred between the aldehyde silane surface and the chitosan surface. The decrease of the C – C peak indicated that not all of the hydrocarbons present on the passivated surface were chemically bound to the surface; the hydrocarbons were instead physically bound to the surface, through weak hydrogen bonds. When the aldehyde silane was present, the weak hydrogen bonds were broken, allowing the aldehyde silane to bond to the passivated metal surface. The peak identified as C – O was not present on the passivated surface; however, the peak was present following the deposition of the aldehyde silane and a significant increase was

seen on the chitosan film. This peak can be attributed to aldehyde silane molecule, where the C – O group links the silicon element to the butyl group, to form Si – O – C. The fourth peak, identified as C = O, shows a significant decrease between the passivated metal surface and the aldehyde silane surface. This decrease is likely the result of the removal of the physically bonded C = O on the surface of the passivated metal; the aldehyde silane surface should have C = O present, as that group is the terminal group on the aldehyde silane molecule. COOH is not present on the passivated metal surface, but is present following the aldehyde silane reaction and following the chitosan reaction. The COOH peak present on the aldehyde silane surface is likely due to a reaction between the terminal group and the ethanol used to rinse the toluene from the surface, producing an O – C – OH group, instead of keeping the C = O terminal group. The CO_3^{+2} peak is present on the passivated surface and following the two reaction steps; it decreases significantly from the passivated surface to the aldehyde silane surface and it is not significantly different between the aldehyde silane surface and the chitosan surface. The CO_3^{+2} is likely the result of contamination in the solvent, as the reaction does not support the formation of the CO_3^{+2} group; it could also be the result of a reaction between the surface and the atmosphere during transport to the XPS machine. The final peak, CO_3^{-2}, is present only on the aldehyde silane surface and is likely the result of a reaction with the atmosphere during transport to the XPS machine. The changes of the C – C peak, the C – O peak, the C = O peak, the COOH peak, and the CO_3^{+2} peak following the chitosan reaction are a part of the chitosan molecule and will be discussed in Section 4.4.4.

No statistical changes were seen between the oxygen peak on the passivated metal and the aldehyde treated surface, based on percentage. However, a significant increase

was seen in the oxygen peak based on peak area. A significant decrease in the TiO peak was seen between the passivated metal and the aldehyde silane, while the peak was not present on the chitosan surface; this decrease is the result of the bonding of the aldehyde silane to the passivated metal, changing the peak to a Ti – O – Si peak, and also decreasing the amount of photoelectrons that could escape, as the aldehyde silane is slightly larger than the amino silane, with an addition carbon bond. In fact, the aldehyde silane is approximately 20 angstroms long, without consideration for the angles within the molecule, it stands to reason that the photoelectrons excited by x-ray source cannot escape as frequently as the photoelectrons could when the aldehyde silane was not bound to the metal surface. The –OH peak present on the passivated surface was not present following the aldehyde silane deposition; following the chitosan reaction, however, the peak was identified as SiO. The peak was not present following the aldehyde reaction because of the formation of the Ti – O – Si peak, which completely removed the – OH group from the surface due to the reaction between the aldehyde silane and the passivated metal. The third peak, identified as C – O on the passivated surface, was identified as SiO_x on the aldehyde silane surface. Therefore, no comparison between the two surfaces can be made. However, the presence of SiO_x on the aldehyde silane surface indicated that a reaction with the passivated surface did occur, resulting in the formation of SiO_x groups between the passivated surface and the aldehyde silane surface. The fourth peak was identified as $-(OH)_3^{-3}$ on the passivated surface and as SiO_2 on the aldehyde silane surface and the chitosan surface; once again, the peak cannot be compared between the passivated surface and the aldehyde silane surface. The presence of the SiO_2 peak following the deposition of the aldehyde silane indicated that the aldehyde silane

molecule was bound to the titanium surface at the silicon end of the molecule, forming the complex Ti – O – Si – O. A significant increase in the C – O peak was seen between the passivated metal and the aldehyde silane surface, while no significant change was seen between the aldehyde silane surface and the chitosan surface. The increase between the passivated surface and the aldehyde silane surface is due to the increased amount of C – O present at the silicon end of the aldehyde silane surface; the butyl portion of the aldehyde molecule is bound to the silane by an oxygen, forming the Si – O – C bond, which increased greatly from the passivated metal surface to the aldehyde silane surface. The C = O peak was not present on the passivated metal surface; it was present on the aldehyde silane surface, which was not significantly different from the chitosan surface. The presence of the C = O group is due to the terminal group of the aldehyde silane, which is C = O. The significant changes of the SiO, SiO_x, and SiO_2 peaks, along with the peaks which did not change, identified as C – O and C = O, following the chitosan reaction are a part of the chitosan molecule and will be discussed in Section 4.4.4.

The passivated metal surface did not have any silicon present, so all of the silicon peaks were attributed to the deposition of the aldehyde silane. The SiO_x peak was not present on the aldehyde silane surface, but was present on the chitosan film. A significant amount of SiO was present following the deposition of the aldehyde silane, with no statistical change between the aldehyde silane and the chitosan film. The presence of the SiO was due to the bond between silicon and the butyl group. The SiO_3 peak on the aldehyde silane surface was more numerous than the other three peaks, and was significantly higher than the SiO_3 peak present on the chitosan surface; this peak indicated the formation of the polysiloxane group, which helps stabilize the aldehyde

silane on the surface. The SiO_3 peak also indicated that the aldehyde silane was closely packed on the passivated metal surface. The SiO_2 peak was present on the aldehyde silane surface, but was not present on the chitosan surface. This peak further indicated a bond between the titanium surface and the aldehyde silane molecule, in support of the SiO_3 peak. The significant changes of the SiO_x, SiO_3, and SiO_2 peaks, along with the SiO peak which was not significantly different, present on the chitosan film will be covered in Section 4.4.4, as the differences are the result of the chitosan molecule and not indicative of the interaction between the aldehyde silane and the chitosan film.

A significant decrease in both the percentage and peak area of the titanium is seen between the passivated surface and the aldehyde silane surface; there was no titanium present following the chitosan reaction. A significant decrease was seen in the TiO peak from the passivated surface to the aldehyde silane surface. This decrease is the result of the aldehyde silane molecule reaction with the TiO peak to form Ti – O – Si. The decrease is also the result of the aldehyde silane, which is larger than the amino silane by a carbon bond; the increased size of the aldehyde silane molecule prevents the escape of some photoelectrons, thereby reducing the amount of TiO. Since XPS can penetrate to, at most a depth of 40 angstroms, and the aldehyde silane is approximately 20 angstroms long, without consideration for the angles within the molecule, it stands to reason that the photoelectrons excited by x-ray source cannot escape as frequently as the photoelectrons could when the aldehyde silane was not bound to the metal surface. The second peak, TiO_2, also shows a significant decrease between the passivated metal surface and the aldehyde silane surface. Because TiO_2 is non-reactive, the reduction in the peak size is the result of the polysiloxane group covering the surface and preventing the

photoelectrons from escaping and being detected. A second TiO_2 peak was present on the aldehyde silane surface, which was not present on the passivated metal surface. This second peak only confirms that there is the non-reactive TiO_2 species, supporting the presence of the first TiO_2 peak. The final peak, TiC, was present only on the passivated surface; the lack of this peak is the result of the polysiloxane chains covering the surface, preventing the escape and detection of photoelectrons.

Because of the lack of titanium following the chitosan reaction step, and the closeness of the silicon element to the titanium surface, the adhered film is too thick to examine the reaction between the aldehyde molecule and the chitosan film. The film is believed to be around 100 μm thick, based on the lower limit of thickness which can be detected by the human eye. Since XPS can only penetrate 40 angstroms, or 4 nm, the film is 10,000 times thicker than the penetration depth of XPS. It is this reason, the thickness of the film, that makes any statistical similarities or differences between the aldehyde reaction step and the chitosan reaction solely the result of the chitosan molecule, not the result of the chemistry between the aldehyde silane and the chitosan film; the chitosan films on all four treatment combinations will be discussed in Section 4.4.4.

4.4.3.3 Piranha Treated Metal: Comparing Reaction Steps

Significant changes were observed following each of the reaction steps performed on the piranha treated metal surface. Following the aldehyde reaction step, a significant increase of carbon was seen from the piranha treated surface to the aldehyde silane surface, along with a significant increase from the aldehyde silane surface to the chitosan

film surface, based on both percentage and peak area. Looking at the high resolution peaks, three peaks were not present on the piranha treated surface; the four peaks that were present on the piranha treated surface were not significantly different as compared to the aldehyde silane surface. The first peak, which showed no significant difference between the piranha treated surface and the aldehyde silane surface nor the aldehyde silane surface and the chitosan film surface, was the elemental carbon peak; the lack of difference indicated that the presence of elemental carbon did not affect bonding, but was not removed by sonication following the deposition of the aldehyde silane. The C – C peak was also present on all three surfaces, and showed no significant difference between any of the reaction steps. The lack of change indicated that the hydrocarbons present on the piranha treated surface were either not bound strongly and replaced by the aldehyde silane molecules or was strongly bound and the aldehyde silane molecules deposited around the bound hydrocarbons. The C – O peak was not present on the piranha treated surface; following the deposition of the aldehyde silane, a significant amount was present, while no significant increase was seen following the chitosan reaction. The C – O peak can be attributed to the aldehyde silane molecule, where the C – O group links the silicon element to the butyl group, to form Si – O – C. The fourth peak, C = O, does not change significantly between the piranha treated metal and the aldehyde silane surface, while a significant increase is seen following the chitosan reaction. The lack of change is probably due to a two-fold occurrence; first, the C = O species may be physically bonded to the piranha treated surface, which is removed when the aldehyde silane molecules are introduced to the surface. After the physically bonded C = O is removed, an increase is then seen since C = O is the terminal end of the aldehyde silane

molecule and should be present following the aldehyde silane reaction step. COOH is not present on the piranha treated surface, but is present following the aldehyde silane reaction and shows a significant increase following the chitosan reaction. The COOH peak present on the aldehyde silane surface is likely due to a reaction between the terminal group and the ethanol used to rinse the toluene off the surface, producing an O – C – OH group, instead of keeping the C = O terminal group. The CO_3^{+2} peak is present on the piranha treated surface and following the two reactions steps; there are no statistical differences between any of the reaction steps. The CO_3^{+2} peak is likely the result of a reaction between the surface and the atmosphere during transport to the XPS machine; it could also be contamination in the solvent, as the reaction does not support the formation of the CO_3^{+2} group. The CO_3^{-2} peak is not present on the piranha treated surface and shows no significant difference between the aldehyde silane surface and the chitosan film surface; it is likely the result of a reaction with the atmosphere during transport to the XPS machine. The significant changes of the C = O and COOH peaks, along with the peaks which showed no significant differences, following the chitosan reaction are a part of the chitosan molecule and will be discussed in Section 4.4.4.

The percentage and peak area of oxygen significantly decreased from the piranha treated surface to the aldehyde silane surface and from the aldehyde silane surface to the chitosan surface. A very significant decrease in the peak area of TiO occurred between the piranha treated surface and the aldehyde silane surface; the peak was not present following the chitosan reaction step. The significant decrease is the result of the bonding of the aldehyde silane to the piranha treated surface, changing the peak to a Ti – O – Si peak. The – OH peak present on the piranha treated surface could not be compared to the

aldehyde silane surface, as it was identified as SiO following the aldehyde silane reaction. The presence of the SiO peak indicates that the bond between the silicon element and the butyl group of the aldehyde silane molecule was not disturbed in the deposition and sonication process. The third peak, identified as C – O on the piranha treated surface, was identified as SiO_x following the reaction with the aldehyde silane. A significant decrease was seen from the aldehyde silane reaction to the chitosan reaction; the presence of the SiO_x on the aldehyde silane surface indicated that a reaction with the piranha metal surface, resulting in the formation of SiO_x groups between the piranha treated surface and the aldehyde silane molecules. The SiO_2 peak present on the aldehyde silane surface and the chitosan surface was also present on the piranha treated surface, although it was identified as $– (OH)_3^{-3}$, since silicon was not present on the piranha treated surface. The aldehyde silane surface and the chitosan surface showed no significant difference; however, the piranha treated surface and the aldehyde silane surface could not be compared as the identifications were different. The presence of the SiO_2 peak following the deposition of the aldehyde silane indicated that the aldehyde silane molecule was bound to the titanium surface at the silicon end of the molecule, forming the complex Ti – O – Si – O. The C – O peak was not present on the piranha treated surface, but was present following the aldehyde reaction series; no significant changes occurred between the aldehyde surface and the chitosan surface. The presence of the C – O peak is due to the increased amount of C – O present at the silicon end of the aldehyde silane molecule; the silicon is bound to the butyl portion of the aldehyde silane molecule by an oxygen, forming the Si – O – C bond. The C = O peak was also not present on the piranha treated surface; it was only present on the aldehyde silane surface

and was not significantly different from the chitosan film. However, the C = O peak was only present in one scan of nine, so no real comparisons could be made between the three surfaces. The significant changes related to the SiO and SiO_x peaks, along with the lack of change related to the SiO_2, C – O, and C = O peaks, following the chitosan reaction are a part of the chitosan molecule and will be discussed in Section 4.4.4.

The piranha treated surface did not have any silicon present, so all of the silicon peaks were attributed to the deposition of the aldehyde silane. The SiO_x peak showed no significant changes between the aldehyde silane surface and the chitosan film; however, the SiO_x peak was present on the aldehyde silane surface in only one scan out of nine, so no real comparisons between the aldehyde surface and the chitosan surface can be made. A significant amount of SiO was present following the deposition of the aldehyde silane; there was also a significant decrease of the SiO peak following the chitosan reaction. The presence of the SiO species was due to the bond between the silicon and the butyl group, forming the complex Si – O – C. The SiO_3 peak on the aldehyde silane surface showed a significant decrease following the chitosan reaction. The presence of the SiO_3 species indicated the formation of the polysiloxane group, which helps stabilize the aldehyde silane on the surface; it also indicated that the aldehyde silane was closely packed on the piranha treated metal surface. The SiO_2 peak was present on the aldehyde silane surface, but was not present on the chitosan film surface; this peak further indicated that a bond between the titanium surface and the aldehyde silane molecule formed, supporting the bond formation of the SiO_3 species. The significant changes of the SiO and SiO_3 peaks, along with the peaks which were not significantly different, following the chitosan film reaction will be covered in Section 4.4.4, as these changes are related to the chitosan

molecule and not to the reaction between the aldehyde silane molecules and the chitosan film.

A significant decrease in both percentage and peak area of the titanium element was seen between the piranha treated surface and the aldehyde silane surface; there was no titanium present following the chitosan reaction. A significant decrease was seen in the TiO peak from the piranha treated surface to the aldehyde silane surface; this decrease is the result of the aldehyde silane molecule reacting with the TiO peak to form Ti – O – Si. It is also the result of the increased size aldehyde silane, which is larger than the amino silane by a carbon bond, preventing the escape of photoelectrons excited by the x-ray beam, preventing the detection of the TiO peak. The TiO_2 peak also shows a significant decrease between the piranha treated metal and the aldehyde silane reaction step. Because TiO_2 is non-reactive, the reduction of the peak is likely the result of the polysiloxane group covering the surface, which prevented the photoelectrons from escaping, limiting the detection of TiO_2. Since XPS can penetrate to, at most a depth of 40 angstroms, and the aldehyde silane is approximately 20 angstroms long, without consideration for the angles within the molecule, it stands to reason that the photoelectrons excited by x-ray source cannot escape as frequently as the photoelectrons could when the aldehyde silane was not bound to the metal surface. The final peak, TiC, was present only on the piranha treated surface; the lack of this peak is likely the result of the coverage provided by the polysiloxane chains, preventing the escape and detection of the photoelectrons.

Because of the lack of titanium following the chitosan reaction step, and the closeness of the silicon element to the titanium surface, the adhered film is too thick to

examine the reaction between the aldehyde molecule and the chitosan film. It is this reason, the thickness of the film, that makes any statistical similarities or differences between the aldehyde reaction step and the chitosan reaction solely the result of the chitosan molecule, not the result of the chemistry between the aldehyde silane and the chitosan film; the chitosan films on all four treatment combinations will be discussed in Section 4.4.4.

4.4.4 Chitosan Films

The chitosan films were not analyzed within the different reaction series because the films were so thick. The films are believe to be around 100 μm thick, while XPS can only penetrate a depth of at most 100 angstroms, or around 10 nm; a nanometer is about 1000 times smaller (10^{-3}) smaller than a micron (μm). Therefore, the chitosan film is too thick for the x-ray beam to penetrate, which negates the ability to examine the interaction between the silane and the chitosan film. However, the chitosan film itself can be examined.

4.4.4.1 Chitosan Film Analysis based on Metal Treatment and Silane Treatment

The carbon peak area and percentage shows significant differences between each of the films produced on the four treatment combinations. However, the peak area does not support the trend set forth by the percentage. Based on percentage, the film produced on the PiAm (piranha treated metal with amino silane) is significantly higher; however, based on peak area, the film on PiAm is statistically the same as on the PaAm surface (passivated metal with amino silane). The other two films, PaAl (passivated metal with aldehyde silane) and PiAl (piranha treated metal with aldehyde silane), are significantly

higher based on peak area, but are significantly lower than PiAm based on percentage. The differences outlined are not the result of the treatment combination, but instead, the likely result of the arrangement of the chitosan chains. The high resolution peaks of carbon support the differences due to the arrangement of the chitosan chains. The significant differences based on the C – C peak and the C – O peak indicate a different arrangement of the chain, since the C – C bond is located on the opposite side of the C – O bond, as shown in Figure 4.62. The significant difference based on the C = O peak is also likely indicative of the different arrangement of the chitosan chain; the C = O bond is located on the same side as the C – C bond, which it would cover and prevent the release of photoelectrons. There is no significant change in the C – N – H peak between the four treatment combinations, indicating that the amine group is present on all of the chitosan films; this peak is necessary to bond to the aldehyde groups present on either the amino silane – gluteraldehyde complex or the aldehyde silane molecule. The difference in the amount of $CaCO_3$ relates solely to the preparation of chitosan; before chitosan is used in research, it is deacetylated and demineralized. The $CaCO_3$ compound is incorporated by shellfish in order to strength and stabilize the chitin exoskeleton; the presence of the compound likely indicated that not all of the $CaCO_3$ was pulled out in the demineralization process. The lack of N – C on the PaAl and PaAm surfaces only further indicates that the chain is arranged differently; the excited photoelectrons cannot escape the large chitosan molecule to be detected.

Based on percentage, oxygen is not statistically different between the PaAl and PiAm surface, while the peak area indicated that the PaAl and PaAm surfaces were not statistically different. The significant changes of the oxygen peaks can be attributed to

the minerals left behind following the demineralization process. $CaCO_3$, present on all but the PiAl surface, was not significantly different, while the CaO peak was significantly different. These differences just further support the incomplete removal of the calcium mineral. SiO_2 is also significantly different; the incomplete removal of silicon is also a likely the result of the demineralization process. The NO peak and the C = O peak are not significantly different, indicating that no significant changes exist with the chitosan chain, just with the minerals present due to incomplete demineralization.

The calcium peak is not statistically different based on either percentage or peak area. Shellfish take in calcium as a way to strengthen and stabilize the chitin exoskeletons. Most of the calcium is removed in the demineralization process, but not all of the calcium is removed. The three peaks present, CaO, $CaHPO_4$, and $CaCO_3$, are not statistically different based on the treatment combinations, indicating that while the demineralization process did not go to completion, a large amount of calcium was removed.

Based on percentage, there is no significant change in the amount of nitrogen, while the peak areas of the films supports this observation. There were some significant changes in the high resolution peaks of nitrogen, which indicated that the arrangement of the chitosan chain played a role in the detection of nitrogen. The N – C and C – N - H peaks are significantly different, but all of the surfaces are connected, indicating that some of the chains were turned with some of the amine group facing "up" and some of the amine group facing "down". This arrangement is likely due to twisting of the chitosan chain, which occurred to get the polar groups aligned with the water in the solvent, since similar molecules prefer to be together. The NH_4^+ peak on the surface of two of the films

further supports the amine group facing "up", since chitosan forms amine groups in water.

Two of the four treatment combinations of silicon indicate that the PaAm and PiAm surfaces are not significantly different; the peak area of silicon supports this. The difference in the amount of silicon is the result of the living conditions of the shellfish used to produce chitosan. Shellfish live on the bottom of the ocean, where sand, also known as silicon dioxide, is located. Since the shellfish are on the bottom of the ocean, it is likely that small crystals of silicon dioxide were present on the surface of the shellfish when they were harvested. While silicon dioxide would be removed during the demineralization process, residue may still remain as part of the ash content. The SiO, SiO_x, and SiO_3 peaks all indicate that the demineralization process did not go to completion.

The phosphorous peak is not statistically different based on either percentage or peak area. The high resolution scans could not be studied as the peaks were too small for accurate analysis. Phosphorous is taken in by shellfish to combine with calcium, as shown in the calcium high resolution scan which showed as $CaHPO_4$, to further support and strengthen the chitin exoskeleton.

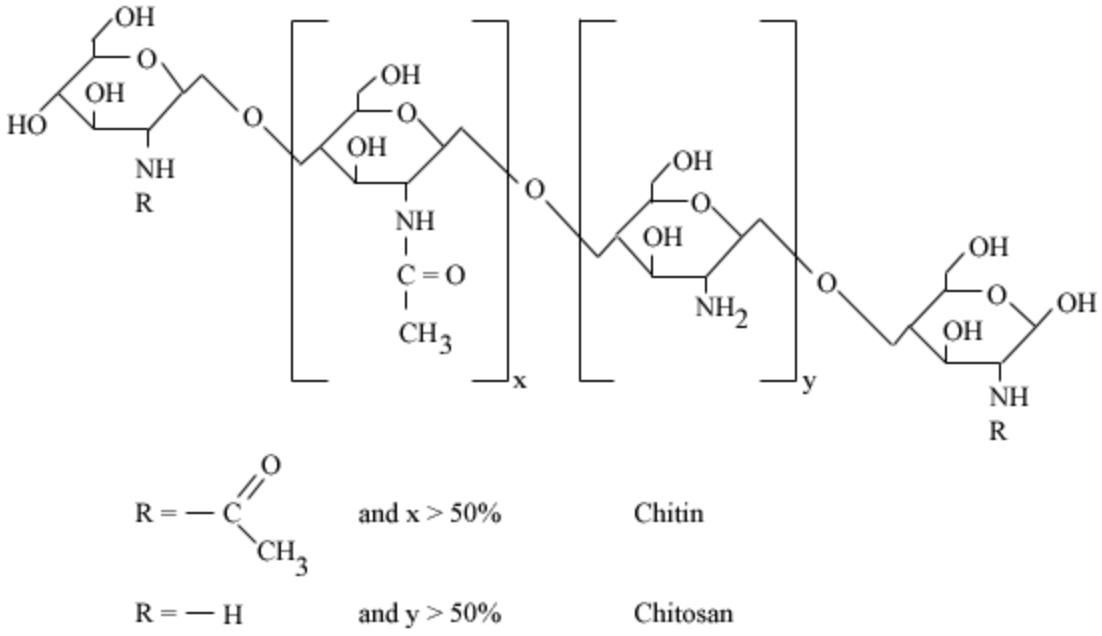

Figure 4.62. Schematic representation of chitin and chitosan [4.44].

4.4.4.2 Chitosan Film Analysis based on Metal Treatment

Because several of the elements were not statistically different based on the treatment combinations, the films were split apart by metal treatment and silane treatment to determine if any significant differences existed between the two treatments. The carbon peak area and percentage indicated that there were significant differences between the two metal treatments. The differences, however, are the result of the arrangement of the chitosan chains, as the C – C, C – O, and C = O peaks were significantly different, which indicate which way the chains were facing. The C – C and C – O peaks are on opposite sides of the chitosan chain, while the C = O peak would "mask" both the C – C and C – O peaks if it is facing "up". The $CaCO_3$ peak is also significantly different, indicating that the demineralization process was not fully completed.

The oxygen peak is significantly higher on the passivated metal based on percentage, but does not statistically change based on the peak area, with respect to the metal treatments. The two peaks that are statistically different indicate a change in the arrangement of the film and a chitosan film that is non-homogeneous. The change of the NO peak indicates that the arrangement of the film is different, as there is a possibility that the amine group reacted with the water when the chitosan was in solution to produce a NO group. That group would then be turned into the film, as is the case with the passivated metal, or on the surface of the film, as is the case with the piranha treatment. The presence of CaO in a statistically different amounts between the metal treatments just indicates that different amount of calcium were taken in by the shellfish used to produce the chitosan. The chitosan film can be called non-homogeneous because the films were all made from the same lot of chitosan.

The calcium peak is not statistically different for the metal treatments, based on either percentage or peak area. The demineralization process removed a large amount of the calcium, as indicated by the lack of statistical differences in the three calcium peaks present. However, the presence of the peaks does indicate that the shellfish did take in calcium, as no calcium was present in the chemicals used to deposit the chitosan film.

The nitrogen peak was not significantly different based on percentage or peak area for the metal treatments. The only significant difference is seen in the C – N – H peak, which would indicate the arrangement of the chitosan chain. The higher amount of the C – N – H peak on the piranha treated surface is the result of the amine group facing "up", as compared to facing "down" on the passivated surface.

The silicon percentage and peak area indicated that the two different metal treatments resulted in significantly different amounts of silicon present on the surface of the chitosan film. The differences are related to the demineralization process. Silicon would be present due small crystals of sand that were likely present on the surface of the shellfish when they were harvested. While the silicon would be removed during the demineralization process, residue may still remain.

As with the treatment combinations, the phosphorous peak is not statistically different based on either percentage or peak area. The high resolution scans could not be studied as the peaks were too small for accurate analysis. Phosphorous is taken in by shellfish to combine with calcium, as shown in the calcium high resolution scan which showed as $CaHPO_4$, to further support and strengthen the chitin exoskeleton.

4.4.4.3 Chitosan Film Analysis based on Silane Treatment

The carbon peak area and percentage indicated that there were significant differences between the two silane treatments. The differences, however, are, once again, the result of the arrangement of the chitosan chains, as the C – C, C – O, and C = O peaks were significantly different, which indicate which way the chains were facing. The C – C and C – O peaks are on opposite sides of the chitosan chain, while the C = O peak would "mask" both the C – C and C – O peaks if it is facing "up".

The oxygen peak does not statistically change based on percentage, but is varies significantly based on peak area. The high resolution peaks indicate a significant change in the CaO peak only; this change further indicates that the chitosan films are not homogeneous, but vary due to the number of shellfish used to create the chitosan powder.

The calcium peak is not statistically different based on either percentage or peak area, for the silane treatments. As previously stated, shellfish take in calcium as a way to strengthen and stabilize the chitin exoskeletons; the calcium is removed through a demineralization process, but not all of the calcium is removed in the process. The three peaks present, CaO, $CaHPO_4$, and $CaCO_3$, are not statistically different based on the treatment combinations, indicating that while the demineralization process did not go to completion, a large amount of calcium was removed.

The nitrogen peak was not significantly different based on percentage or peak area for the silane treatments. The C – N – H peak was present on both the aldehyde silane surface and the amino silane surface and was significantly higher on the amino silane surface. As with the metal treatment, the arrangement of the chain accounts for the difference in the C – N – H peak; the chitosan on the amino silane surface has the amine

group on the top of the film, while the chitosan on the aldehyde silane surface likely has the amine facing into the film.

The silicon percentage and peak area indicated that the two different silane treatments resulted in a significantly different amount of silicon present on the surface of the chitosan film. The differences are related to the demineralization process. All of the silicon peaks seen in the high resolution scans were significantly different; these differences are the result of the demineralization process and the heterogeneous nature of the individual shellfish, which would likely each have different amounts of the small sand crystals on their exoskeletons. While the sand would be removed during the demineralization process, residue may still remain.

As with the treatment combinations, the phosphorous peak is not statistically different based on the percentage; the peak area, however, is statistically different for the silane treatments. The high resolution scans could not be studied as the peaks were too small for accurate analysis. Phosphorous is taken in by shellfish to combine with calcium, as shown in the calcium high resolution scan which showed as $CaHPO_4$, to further support and strengthen the chitin exoskeleton. The statistical difference is solely related to the individual intake and use by the shellfish used to produce the chitosan, which results in a non-homogenous mixture.

4.5 Summary

In order to determine the major differences between the standard treatment method, which created a passivated titanium surface, and the new treatment method, which utilized piranha to create – OH groups on the titanium surface, XPS analysis was

performed on the metals surfaces following one of the two metal treatments. Significant changes were seen between the three elements present, with the most significant difference with respect to the silane reactions occurring to the titanium element. The highly reactive peak, TiO, was much more prevalent on the piranha treated surface than on the passivated surface, indicating that the piranha surface should bind more silane molecules than the passivated surface.

The first set of comparisons was made using the individual reactions steps of the amino silane reaction series on the two metal treatments. Significant changes in several elements occurred between the two different metal treatments following the first reaction step, the deposition of the amino silane with the metal surface. The changes that were seen, specifically a significant difference in the amount of nitrogen, silicon, and titanium, indicated that the piranha treated surface did likely bind more amino silane than the passivated surface. The higher amount of silane bound by the piranha treated surface was best illustrated by the significant differences in the C – N – H peak, which is the reactive amine group on the terminal end of the amino silane, and in the TiO peak, which was much less on the piranha treated surface than on the passivated surface, likely indicating more silane molecules were bound following the amino silane reaction, since the peak was originally higher on the piranha treated surface. The gluteraldehyde reaction step on the two metal treatments further indicated that more silane molecules were bound to the surface of the piranha treated metal, as the nitrogen peak, which would not be fully "covered" by the gluteraldehyde was still much higher on the piranha treated metal than on the passivated metal.

The second sets of comparisons were made by comparing the reaction steps of the amino silane reaction series on each of the two metal treatments. A significant drop between the passivated metal surface and the amino silane surface of the titanium peak, and specifically of the TiO peak, indicated that the anticipated surface reaction was likely occurring as desired. Since there was no nitrogen or silicon present on the passivated surface, the deposition of the amino silane is the only way nitrogen and silicon could become present on the metal surface; a decrease of the reactive C – N – H nitrogen peak further indicated that the anticipated surface reaction was likely occurring as desired. An even greater drop in the titanium peak between the piranha treated metal surface and the amino silane surface was seen when examining the second metal treatment. The highly reactive TiO peak also dropped significantly, again indicating that the anticipated surface reaction had likely occurred. As with the passivated metal, neither nitrogen nor silicon were present on the piranha treated surface; the only way for nitrogen and silicon to exist on the surface was through the deposition of the amino silane. The significant decrease of the amine group on the terminal end of the amino silane, identified as C – N – H, further serves as indication that the anticipated surface reaction is occurring as desired.

The third set of comparisons, and the first set of aldehyde silane comparisons, was made using the individual reaction step of the aldehyde silane reaction series on the two metal treatments. There were no significant differences between any of the elements present on the survey, while only a few significant differences between the high resolution peaks. The lack of difference between the two surfaces is an indication of how highly reactive the aldehyde silane molecule is, with both the titanium surface and with itself. There was significant polysiloxane formation, identified as SiO_3, on both surfaces,

indicative of the aldehyde silane molecule's reaction with itself, while there were very small TiO peaks, indicative of the aldehyde silane molecule's reaction with the metal surface.

The fourth sets of comparisons were made using the reaction steps of the aldehyde silane reaction series on each of the two metal treatments. A significant drop between the passivated surface and the aldehyde silane surface of the titanium peak and the TiO peak indicate that the anticipated surface reaction is occurring as drawn. Since there was no silicon present on the passivated surface, the deposition of the aldehyde silane is the only way silicon could become present on the metal surface; the increased presence of the C – O peak, or the base group on the aldehyde silane, also indicated that the reaction was likely proceeding as anticipated, since this peak should increase if the anticipated reaction was correct. The anticipated surface reaction between the piranha treated surface and the aldehyde silane molecule was seen also, because of the significant drop in the titanium peak and the TiO peak. As with the passivated metal, no silicon was present on the piranha treated surface. The increase in silicon can only be caused by the deposition of the aldehyde silane. The presence of the C – O peak, which is the species that connects the silicon to the butyl group, along with presence of COOH peak, or the terminal group of the aldehyde silane with a reaction with ethanol, demonstrated that the anticipated aldehyde reaction did occur as expected.

The chitosan films based on treatment combination showed several statistical variations, most of which were likely the result of an incomplete demineralization process. Also, the chitosan films showed variations based on the arrangement of the chains, with the majority of the significant differences caused by the photoelectrons that

were able to escape from the film in the most numerous quantities. The metal treatments and silane treatments further support the arrangement of the chitosan chains. The metal treatments and silane treatments also show that the films were not homogeneous, as the calcium oxide amounts varied. This variation is related to the uptake and use of calcium by the shellfish, as some shellfish would likely use more calcium than others would.

The research performed on the surfaces following the different reaction steps indicated that significant differences existed in the peak of importance. The significant decrease of the TiO peak, the significant increases of the SiO and SiO_3 peaks following both silane reactions, the significant increase of the C – N – H peak following the amino silane reaction, and the significant increases of the C = O and COOH peaks following the aldehyde silane reaction all indicated that the reactions were proceeding as anticipated. The anticipated amino silane reaction was further supported with the increase in the amount of the C = O and COOH peaks, along with the decrease of the C – N – H peak following the gluteraldehyde reaction. The treatment combinations did not affect the chemical structure of the chitosan films, however, as these films were not statistically different.

CHAPTER V

MECHANICAL ANALYSIS OF THE FOUR TREATMENT COMBINATIONS

5.1 Introduction

Chemical characterization of the chitosan films produced from the metal – silane treatment combinations does not adequately test all aspects of the films. Chemical characterization only allows the researcher to determine the reactions occurring. Therefore, a combination of both chemical and mechanical testing is necessary to fully characterize these films. Mechanical testing must be performed, to determine the adhesion strength of the film and to determine the effects of the treatment combinations on the bulk properties of the chitosan films.

5.2 XPS Examination of Films Used in Mechanical Testing

5.2.1 XPS Results

In order to ensure that the films produced for mechanical testing where similar to the films produced for chemical analysis, two samples were removed from each batch of films produced for mechanical testing. These two samples were run using XPS to ensure that the films were statistically similar. Table 5.1 shows the elemental percentage of the different elements present for all of the chitosan films produced as compared to the films

produced for the mechanical testing. The percentage of nitrogen, calcium, and phosphorous present in the films used in mechanical testing were not statistically different from the films used in chemical analysis. There was some variation between the elemental percentage and the peak area of the carbon, oxygen, and silicon peaks. Table 5.2 shows the peak areas of the chitosan films for the elements that varied significantly. However, even though variation occurred, the films produced for mechanical testing were not statistically different from at least one of the films used in chemical analysis. Figure 5.1 compares the survey scan graphs of the different chitosan films with the survey scan graphs of the films used in mechanical testing.

Table 5.1. Elemental percentage based on XPS survey scans of chitosan films.

Metal Treatment	Carbon	Oxygen	Nitrogen	Calcium	Silicon	Phosphorous
Passivated, Aldehyde	62.944 ± 2.606^{a} %	24.967 ± 1.766^{d} %	4.600 ± 1.109^{f} %	0.956 ± 0.364^{g} %	6.011 ± 1.522 %	0.656 ± 0.347^{k} %
Passivated, Amino	65.478 ± 1.209^{b} %	27.711 ± 1.152 %	5.533 ± 0.943^{f} %	0.722 ± 0.595^{g} %	0.167 ± 0.500^{h} %	0.344 ± 0.495^{k} %
Piranha, Aldehyde	$64.478 \pm 1.435^{a,b}$ %	26.233 ± 0.850 %	5.033 ± 0.707^{f} %	1.167 ± 0.409^{g} %	2.244 ± 1.549^{j} %	0.856 ± 0.425^{k} %
Piranha, Amino	68.322 ± 1.251^{c} %	$24.644 \pm 1.026^{d,e}$ %	5.100 ± 0.458^{f} %	0.978 ± 0.367^{g} %	$0.678 \pm 0.746^{h,j}$ %	0.289 ± 0.425^{k} %
Films for Oak Ridge	68.300 ± 1.010^{c} %	$23.817 \pm 1.430^{d,e}$ %	5.233 ± 1.145^{f} %	0.867 ± 0.350^{g} %	$1.317 \pm 1.093^{h,j}$ %	0.467 ± 0.585^{k} %
Films for Memphis	69.017 ± 1.003^{c} %	23.600 ± 0.540^{e} %	5.650 ± 0.712^{f} %	1.083 ± 0.417^{g} %	0.333 ± 0.816^{h} %	0.300 ± 0.35^{k} %

Values with the same superscript are not statistically different at the 5% significance level.

Table 5.2. Peak area of elements present based on XPS survey scans of chitosan films.

Metal Treatment	Carbon	Oxygen	Silicon
Passivated, Aldehyde	23908.11 ± 1135.918[a]	23266.83 ± 1837.595[c]	2030.278 ± 560.724
Passivated, Amino	22729.00 ± 683.113[b,c]	23494.94 ± 1202.418[c]	52.167 ± 156.500[e]
Piranha, Aldehyde	24787.11 ± 725.403	24753.33 ± 1047.742[c]	773.667 ± 532.505[f]
Piranha, Amino	23105.67 ± 457.128[c]	20468.56 ± 1237.012[d]	205.000 ± 228.642[e]
Films for Oak Ridge	23811.67 ± 385.904[a]	20388.92 ± 1628.339[d]	388.833 ± 317.235[e,f]
Films for Memphis	23467.25 ± 282.100[a,b]	19514.00 ± 606.265[d]	98.500 ± 241.275[e]

Values with the same superscript are not statistically different at the 5% significance level.

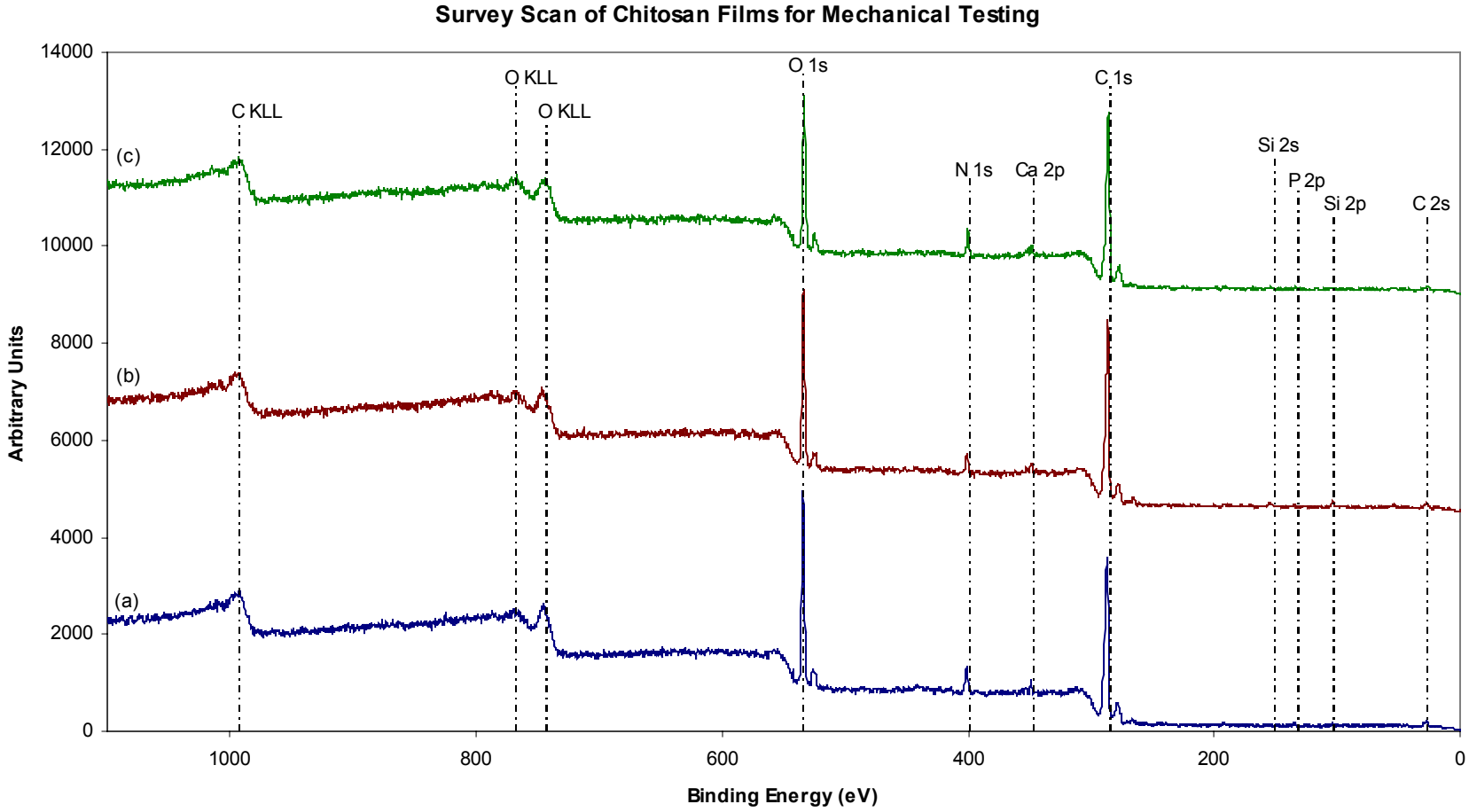

Figure 5.1. Survey scans of representative chitosan films used for mechanical testing.

(a) Representative scan from chemical analysis. (b) Representative scan for Mechanical Testing performed at Oak Ridge National Lab. (c) Representative scan for Mechanical Testing performed at the University of Memphis.

5.2.2 XPS Discussion

While statistically significant variation occurred among the films produced using different techniques, the variation did not affect the films produced for mechanical testing. For each of the elements present, the films were not significantly different from at least one of the films produced for the chemical analysis. The lack of statistical variation indicates that the films produced for mechanical testing match the films produced for chemical testing. Since the films for mechanical testing are statistically equivalent to the films for chemical analysis, any mechanical results that demonstrate an improvement in film quality can be attributed to the treatment combinations and not to a change in the chemistry of the film.

5.3 Results

Mechanical testing is an important part of determining the quality of the films. As part of this research, hardness, elastic modulus, bulk adhesion, and contact angle measurements were taken.

5.3.1 Hardness and Elastic Modulus

In order to determine the hardness and the elastic modulus of the films produced from the different metal – silane treatments, constant stiffness measurements, or CSM, nano-indentation tests were performed. CSM allows the computer to calculate the stiffness of the material, which is directly related to the hardness and the elastic modulus. There are several equations used in the calculation of stiffness, hardness, and elastic modulus. To begin with, the load applied to the test material is first calculated, using equation 5.1.

$$P = B\left(h - h_f\right)^m \tag{5.1}$$

where B and m are empirically fitted parameters, h is the resulting penetration, and h_f is the final displacement after complete unloading [5.1]. Following the determination of B and m, the stiffness of the material can be calculated, using equation 5.2.

$$S = \frac{B * m * \left(h - h_f\right)^{m-1}}{h = h_{\max}} \tag{5.2}$$

where h_{max} is the maximum depth of penetration [5.1]. The calculation of the stiffness of the material allows the researcher to calculate the contact depth, h_c, using equation 5.3.

$$h_c = \frac{h - \varepsilon P}{S} \tag{5.3}$$

where ε is a constant that depends on the indenter geometry [5.1]. The contact depth then allows the researcher to calculate the projected contact area, which is a function of contact depth as shown in equation 5.4.

$$A = f\left(h_c\right) \tag{5.4}$$

The determination of the projected contact area, A, and the load applied to the surface, P, allows the researcher to calculate the hardness of the material by using equation 5.5 [5.1].

$$H = \frac{P}{A} \tag{5.5}$$

Since the researcher has also determined the stiffness, the reduced elastic modulus can be calculated from equation 5.6.

$$E_r = \frac{\sqrt{\pi} * S}{2\beta\sqrt{A}} \tag{5.6}$$

where β is a constant that depends only on the geometry of the indenter [5.1]. The elastic modulus is then calculated from equation 5.7.

$$\frac{1}{E_r} = \frac{\left(1-\nu^2\right)}{E} + \frac{\left(1-\nu_i{}^2\right)}{E_i} \tag{5.7}$$

where ν is Poisson's ratio and E_i and ν_i are the elastic modulus and Poisson's ratio of the indenter, respectively [5.1]. The only major difference that is apparent when using the continuous stiffness measurements (CSM) as compared to the above equations is the equation needed for stiffness. When using CSM, equation 5.8 is used instead of equation 5.2.

$$S = \left[\frac{1}{\frac{F_o}{z_o}\cos\phi - \left(K_s - m\omega^2\right)} - \frac{1}{K_f}\right]^{-1} \tag{5.8}$$

where F_o is the excitation amplitude, z_o is the displacement amplitude, ϕ is the phase angle, K_s is the stiffness of the support springs, m is the indenter column, ω is the excitation frequency, and K_f is the load-frame stiffness [5.2].

The mean and standard deviation for each of the four different treatment combinations are shown in Table 5.3. Since all of the means were not significantly different, analysis was also performed to determine if differences existed between the individual metal treatments and the individual silane treatments. The means and standard deviations of the individual metal treatments are shown in Table 5.4, while the means and standard deviations of the individual silane treatments are shown in Table 5.5. No significant statistical variation occurs based on the combinations, with means ranging from 0.14 ± 0.08 GPa to 0.19 ± 0.08 GPa, or the individual treatments, with means

between the range of the combinations. Thus, no significant difference in the hardness of the films was observed as a function of film preparation.

Table 5.3. Hardness and elastic modulus of the chitosan films.

Treatment Combination	Hardness (GPa)	Elastic Modulus (GPa)
Passivated, Aldehyde	0.14 ± 0.08^{a}	4.82 ± 2.33^{b}
Passivated, Amino	0.19 ± 0.08^{a}	4.90 ± 1.82^{b}
Piranha, Aldehyde	0.15 ± 0.06^{a}	4.53 ± 1.20^{b}
Piranha, Amino	0.18 ± 0.04^{a}	4.78 ± 0.64^{b}

Values with the same superscript are not statistically different at the 5% significance level.

Table 5.4. Hardness and elastic modulus of the chitosan films based on metal treatment.

Metal Treatment	**Hardness (GPa)**	**Elastic Modulus (GPa)**
Passivated	0.16 ± 0.08^{a}	4.86 ± 2.08^{b}
Piranha	0.17 ± 0.05^{a}	4.67 ± 0.94^{b}

Values with the same superscript are not statistically different at the 5% significance level.

Table 5.5. Hardness and elastic modulus of the chitosan films based on silane treatment.

Silane Treatment	**Hardness (GPa)**	**Elastic Modulus (GPa)**
Aldehyde	0.15 ± 0.07^{a}	4.69 ± 1.89^{b}
Amino	0.18 ± 0.06^{a}	4.84 ± 1.34^{b}

Values with the same superscript are not statistically different at the 5% significance level.

5.3.2 AFM and SEM Pictures of Indentation Marks

Significant effects of the hardness and the elastic modulus values were not evident based on the calculations performed. In order to determine if the films were similar in their topography before testing and in their reaction to the applied stress after testing, AFM and SEM were performed. Both the untouched films and the indentation locations were examined for all of the treatment combinations. The passivated metal with aldehyde silane AFM pictures are shown in Figure 5.2, while the SEM pictures are shown in Figure 5.3. The passivated metal with amino silane AFM pictures are shown in Figure 5.4, while the SEM pictures are shown in Figure 5.5. The piranha treated metal with aldehyde silane AFM pictures are shown in Figure 5.6, while the SEM pictures are shown in Figure 5.7. Finally, the piranha treated metal with amino silane AFM pictures are shown in Figure 5.8, while the SEM pictures are shown in Figure 5.9. No apparent differences were seen between topography or the films' reaction to stress based on both the AFM and SEM pictures.

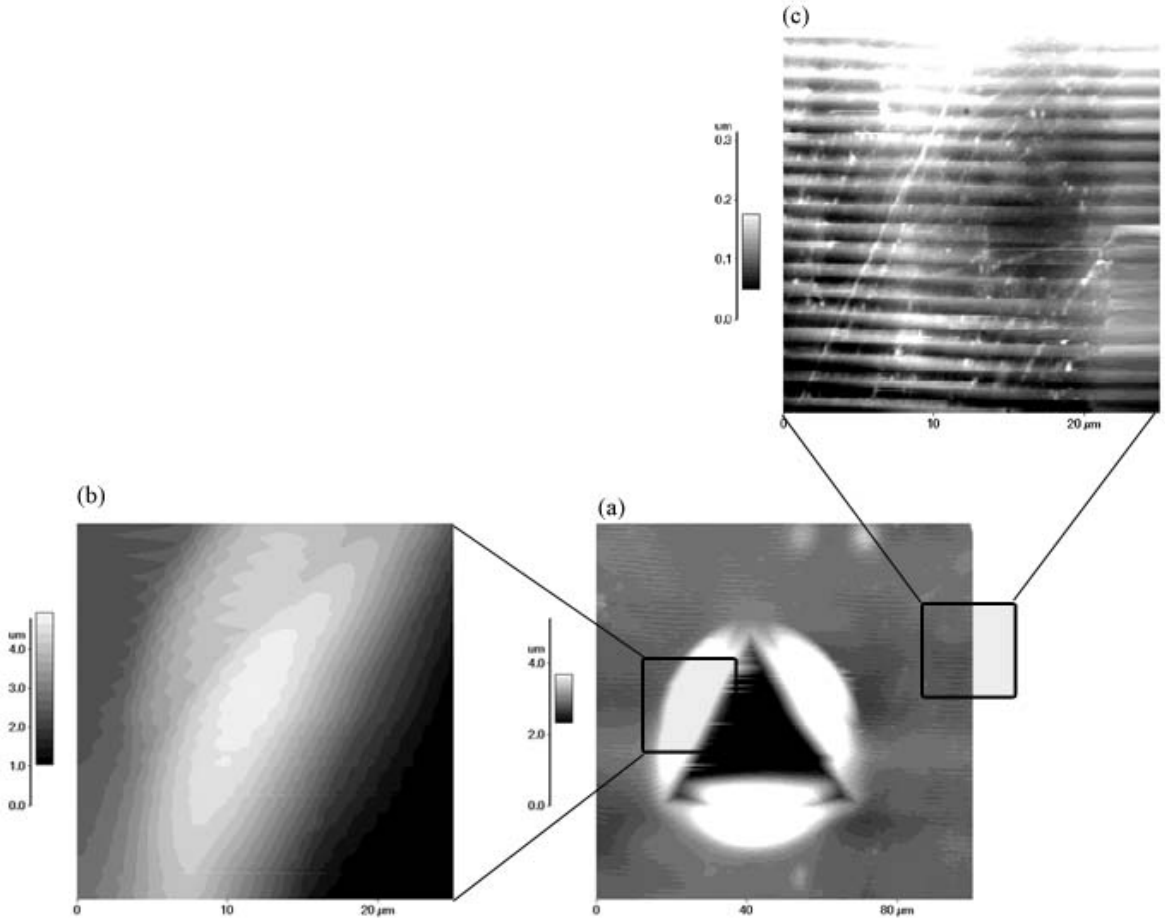

Figure 5.2. AFM pictures of passivated metal with aldehyde silane.

(a) Shows the full indentation mark. (b) Shows the pile-up produced by the indentation tip. (c) Shows the nearby film.

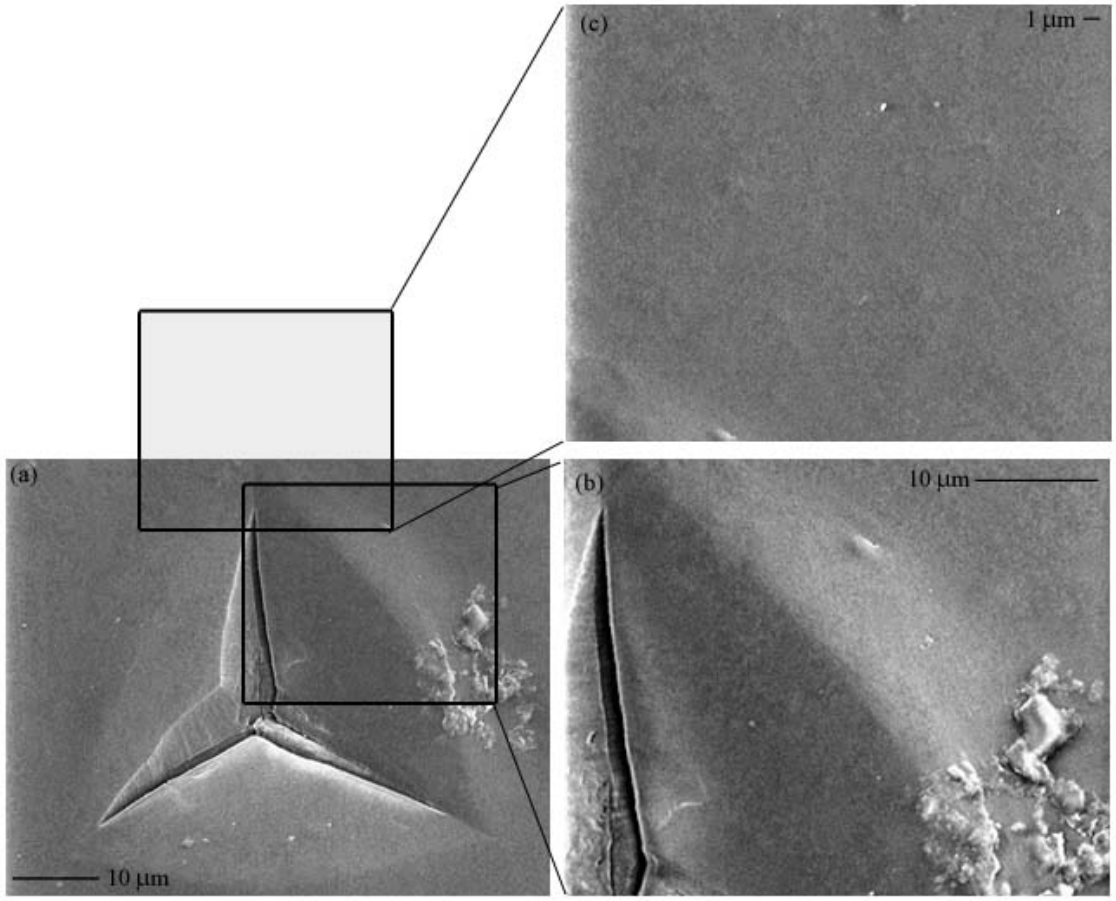

Figure 5.3. SEM pictures of passivated metal with aldehyde silane.

(a) Shows the full indentation mark. (b) Shows the pile-up produced by the indentation tip. (c) Shows the nearby film.

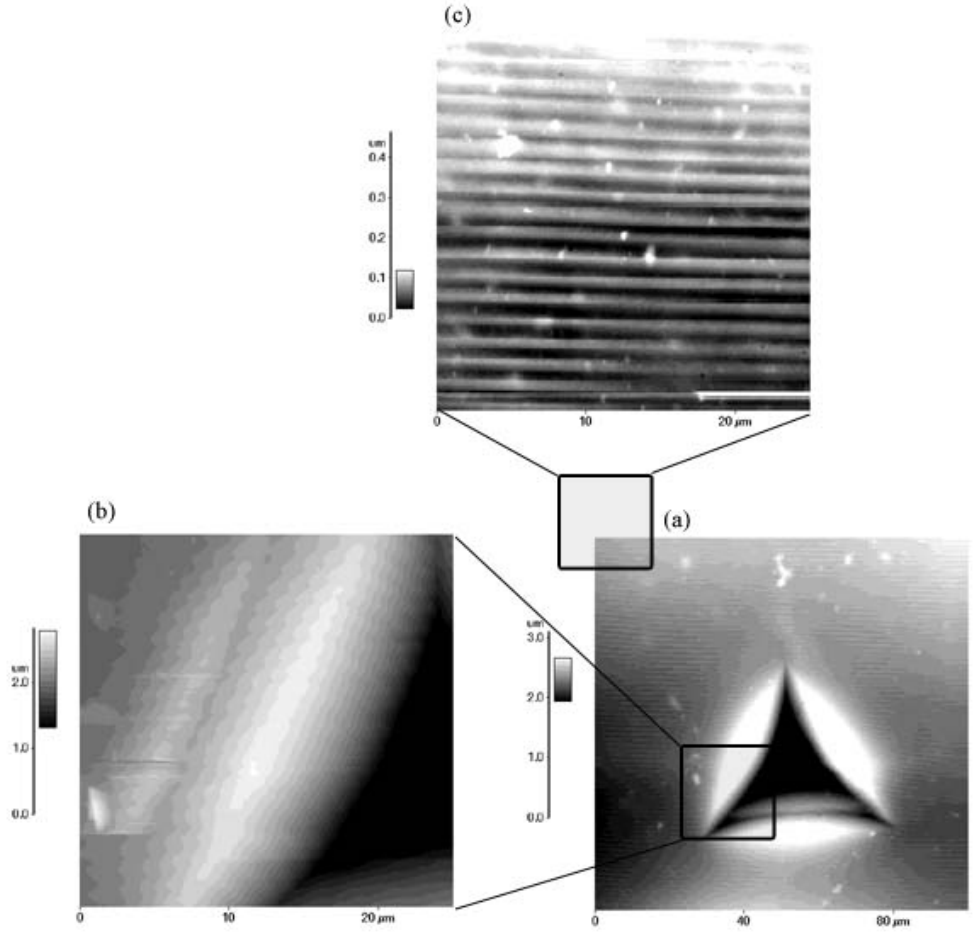

Figure 5.4. AFM pictures of passivated metal with amino silane.

(a) Shows the full indentation mark. (b) Shows the pile-up produced by the indentation tip. (c) Shows the nearby film.

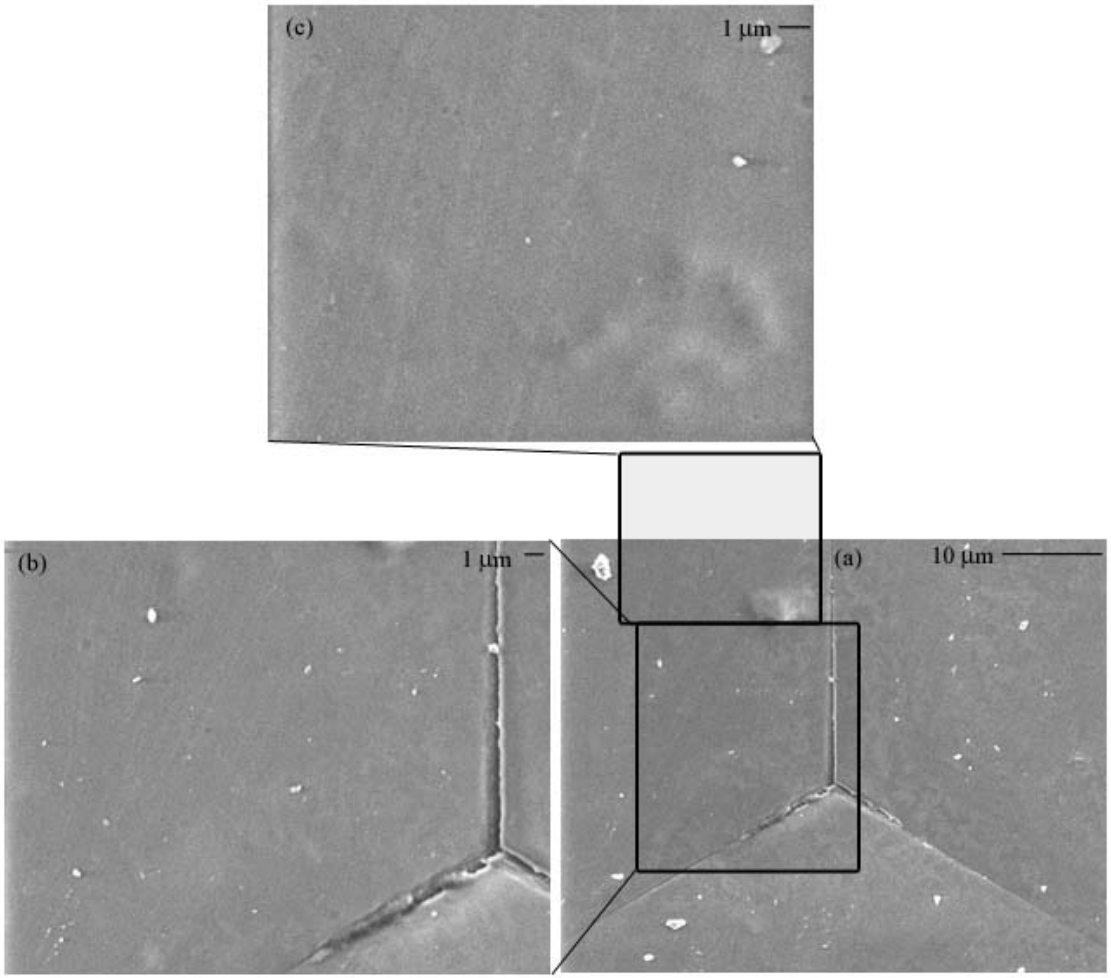

Figure 5.5. SEM pictures of passivated metal with amino silane.

(a) Shows the full indentation mark. (b) Shows the pile-up produced by the indentation tip. (c) Shows the nearby film.

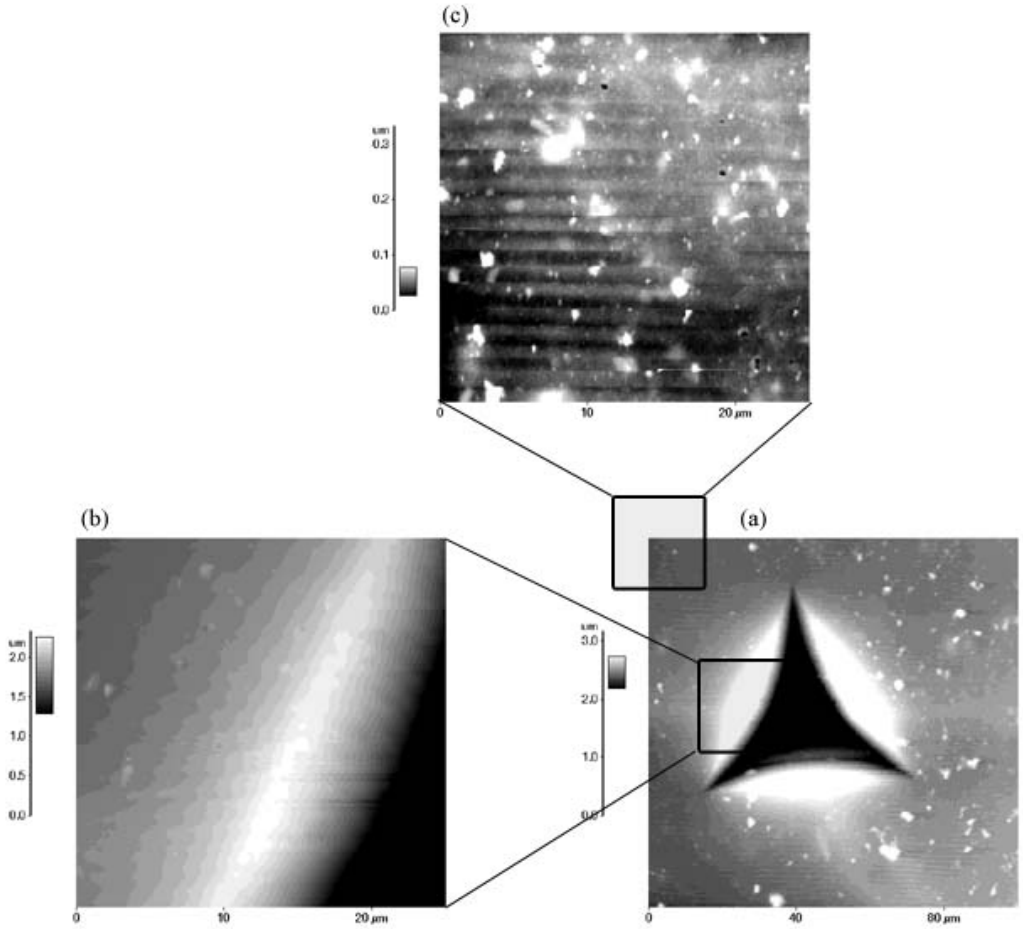

Figure 5.6. AFM pictures of piranha treated metal with aldehyde silane.

(a) Shows the full indentation mark. (b) Shows the pile-up produced by the indentation tip. (c) Shows the nearby film.

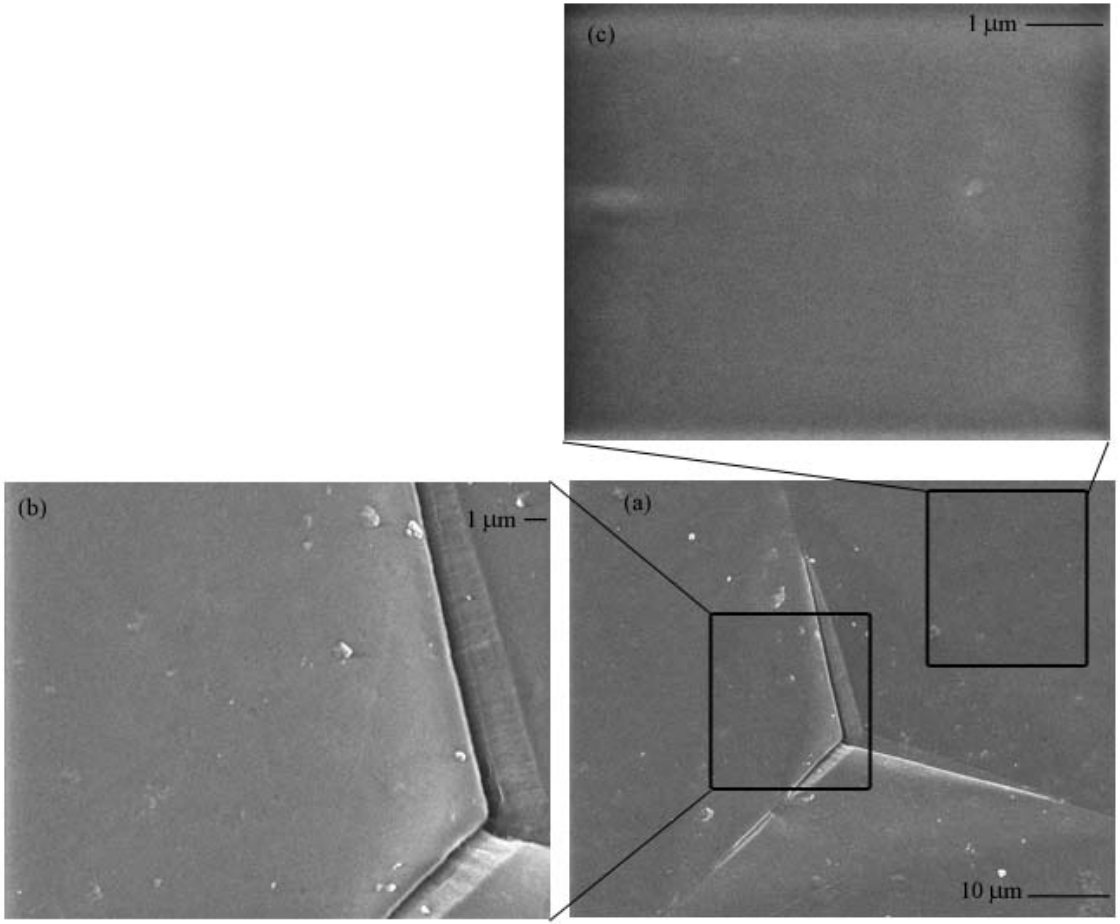

Figure 5.7. SEM pictures of piranha treated metal with aldehyde silane.

(a) Shows the full indentation mark. (b) Shows the pile-up produced by the indentation tip. (c) Shows the nearby film.

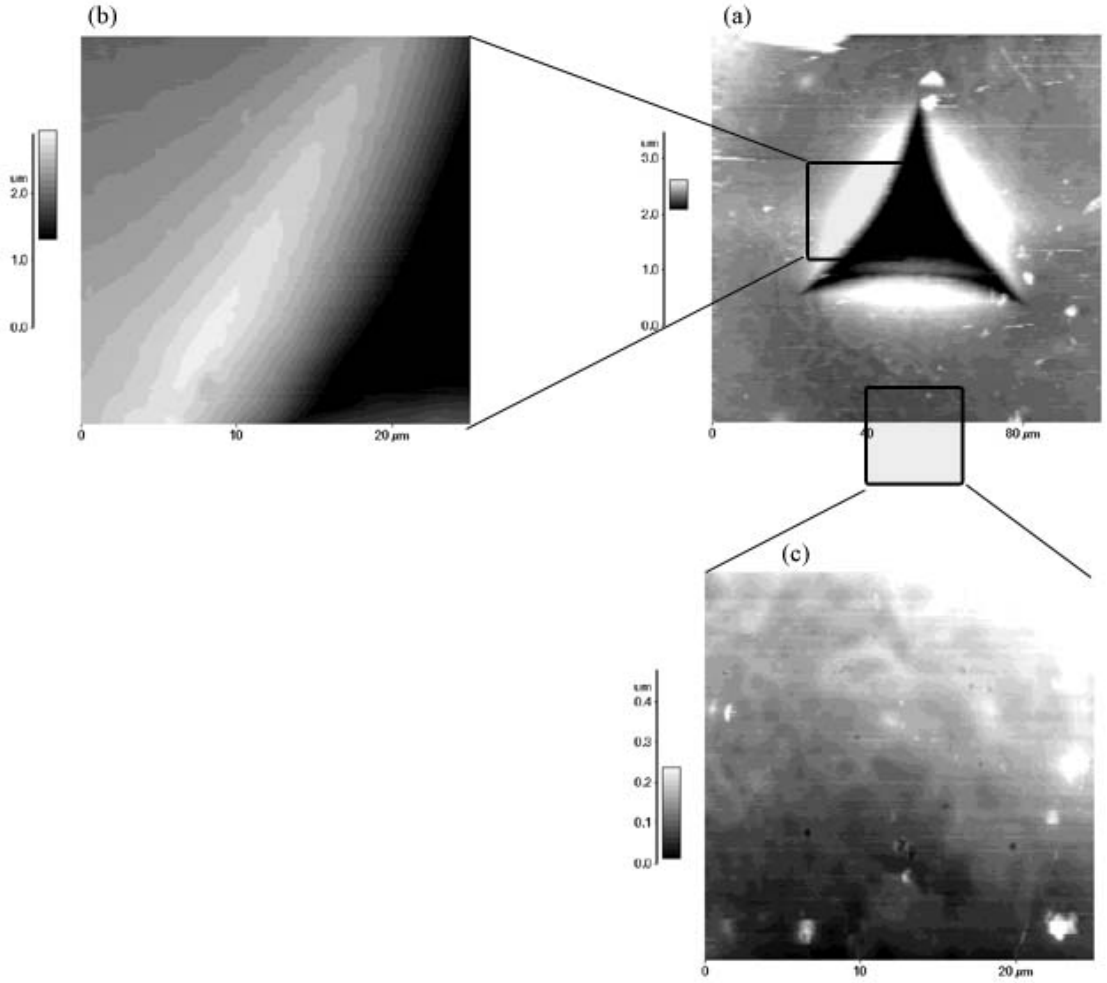

Figure 5.8. AFM pictures of piranha treated metal with amino silane.

(a) Shows the full indentation mark. (b) Shows the pile-up produced by the indentation tip. (c) Shows the nearby film.

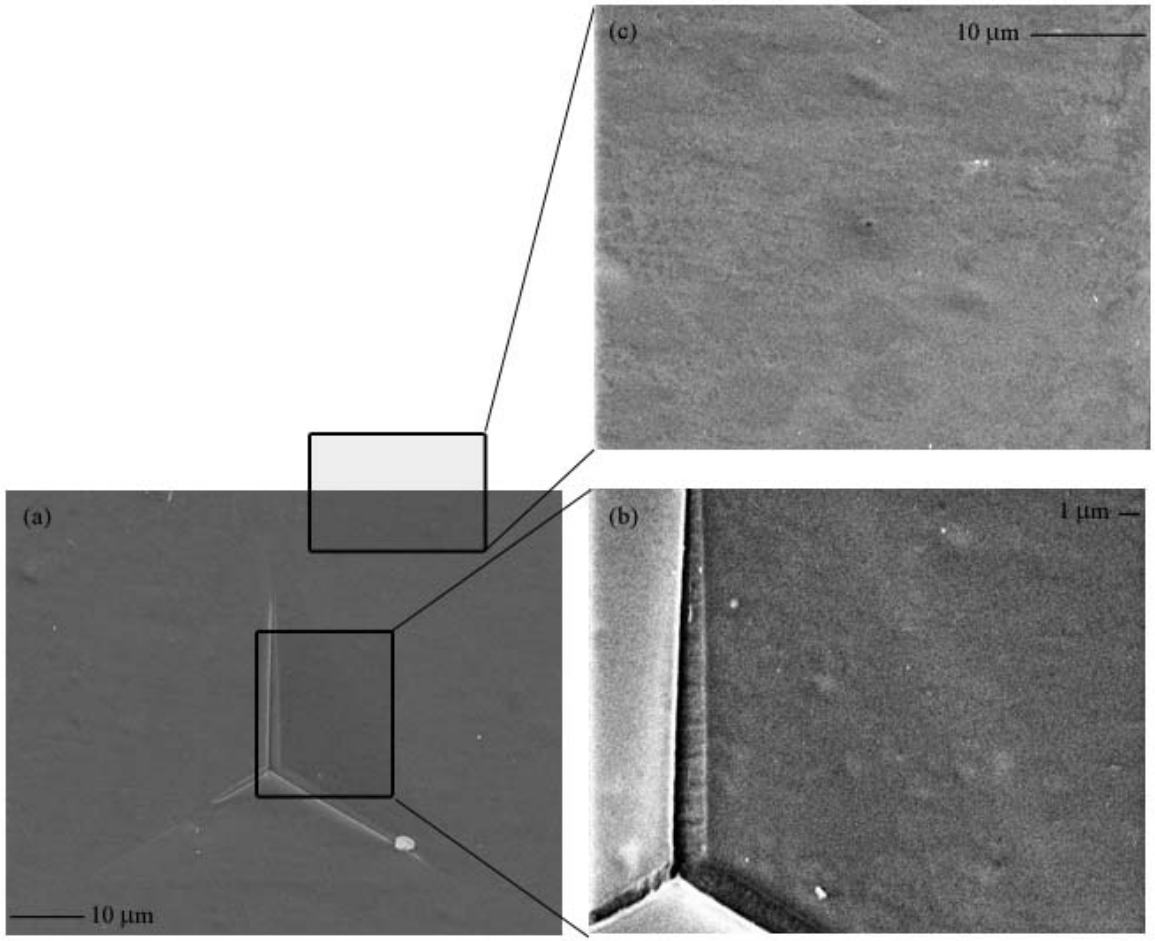

Figure 5.9. SEM pictures of piranha treated metal with amino silane.

(a) Shows the full indentation mark. (b) Shows the pile-up produced by the indentation tip. (c) Shows the nearby film.

5.3.3 Roughness

The hardness and elastic modulus results were determined using CSM nano-indentation. In order to determine the roughness of the different films, AFM was used to analyze the chitosan films. Table 5.6 shows the means and standard deviations of the roughness of the chitosan films based on metal – silane treatment; measurements were taken on both the x-axis and the y-axis, as demonstrated in Figure 5.10. Since no statistically significant differences were present, analysis was also performed on the individual metal treatments, as shown in Table 5.7, and the individual silane treatments, as shown in Table 5.8. No significant statistical variation occurs based on the combinations, with the roughness means ranging from 244.10 ± 100.62 nm to 352.52 ± 122.15 nm for the x-axis and means ranging from 270.51 ± 111.77 nm to 346.72 ± 127.95 nm, or the individual treatments, with means between the range of the combinations. The locations for the roughness measurements were chosen to minimize the dust deposited during the evaporation of the films. Figure 5.11 graphically shows the roughness of the four different films as determined using the x-axis measurements, while Figure 5.12 graphically shows the roughness of the four different films as determined using the y-axis measurements. All of the figures show no apparent differences in topography as a result of the sample treatment, further confirming the statistical analysis that no significant differences in film roughness occurred.

Table 5.6. Roughness of the chitosan films.

Treatment Combination	X Axis Roughness (nm)	Y Axis Roughness (nm)
Passivated, Aldehyde	352.52 ± 122.15[a]	346.72 ± 127.95[b]
Passivated, Amino	279.16 ± 126.92[a]	280.42 ± 124.26[b]
Piranha, Aldehyde	244.10 ± 100.62[a]	270.51 ± 111.77[b]
Piranha, Amino	328.85 ± 98.60[a]	290.99 ± 155.43[b]

Values with the same superscript are not statistically different at the 5% significance level.

Table 5.7. Roughness of the chitosan films based on metal treatment.

Metal Treatment	X Axis Roughness (nm)	Y Axis Roughness (nm)
Passivated	315.84 ± 126.60^{a}	313.57 ± 127.11^{b}
Piranha	283.98 ± 105.91^{a}	280.15 ± 130.11^{b}

Values with the same superscript are not statistically different at the 5% significance level.

Table 5.8. Roughness of the chitosan films based on silane treatment.

Silane Treatment	X Axis Roughness (nm)	Y Axis Roughness (nm)
Aldehyde	298.31 ± 122.05^{a}	308.62 ± 122.97^{b}
Amino	302.54 ± 113.85^{a}	285.39 ± 135.35^{b}

Values with the same superscript are not statistically different at the 5% significance level.

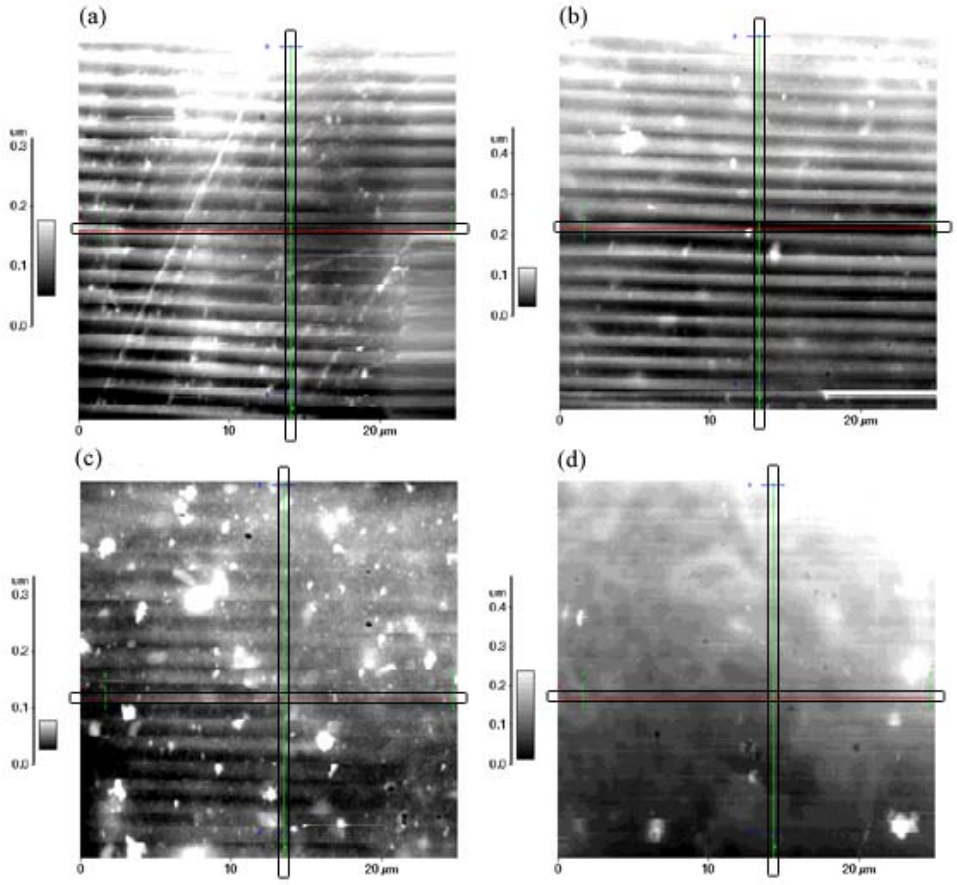

Figure 5.10. AFM pictures of the films.

The X-Axis is determined from calculations horizontal black lines, while the Y-Axis is determined from calculations using the vertical black lines. (a) Passivated Metal with Aldehyde Silane. (b) Passivated Metal with Amino Silane. (c) Piranha Treated Metal with Aldehyde Silane. (d) Piranha Treated Metal with Amino Silane.

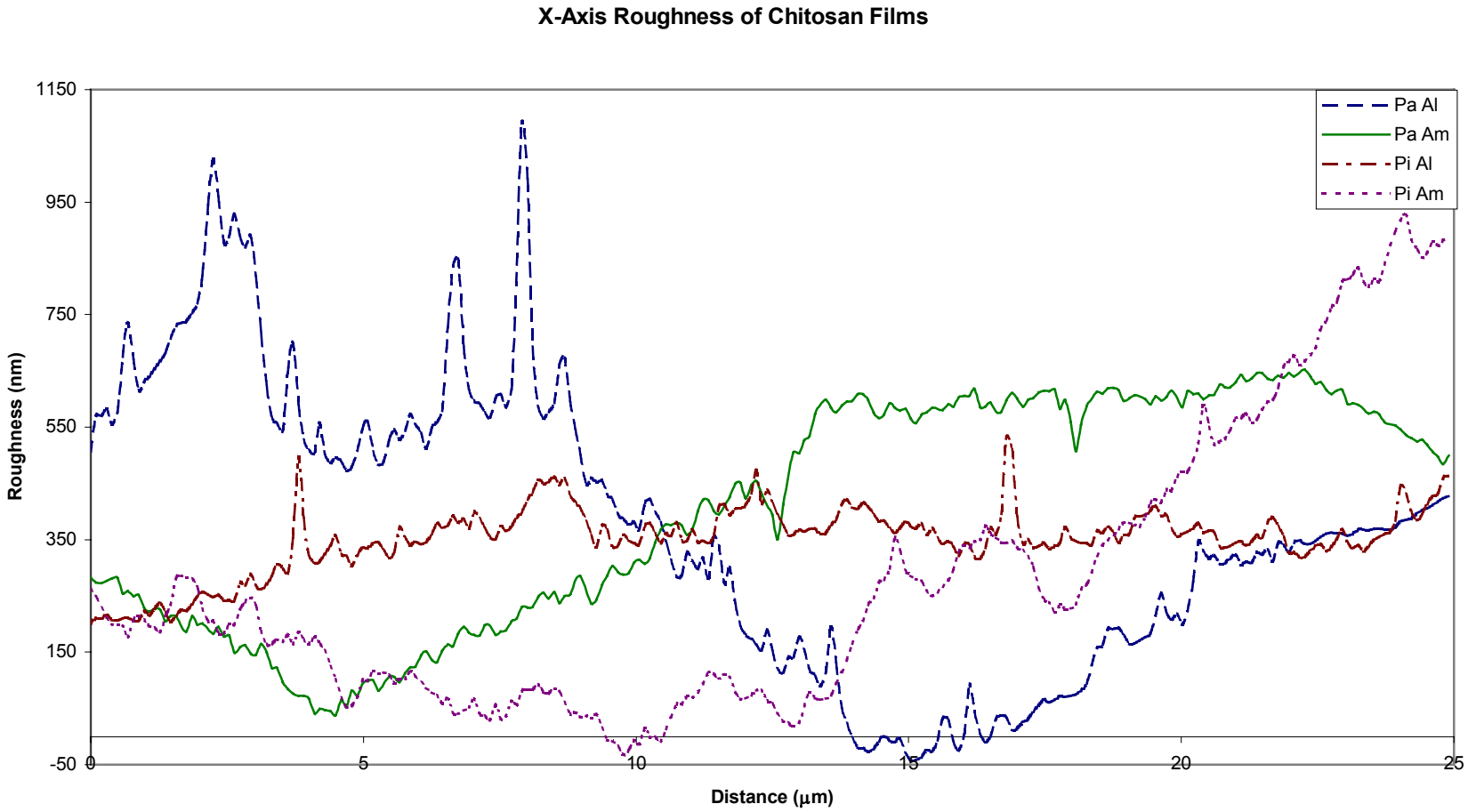

Figure 5.11. X-Axis roughness diagrams for the chitosan films produced by the four treatment combinations.

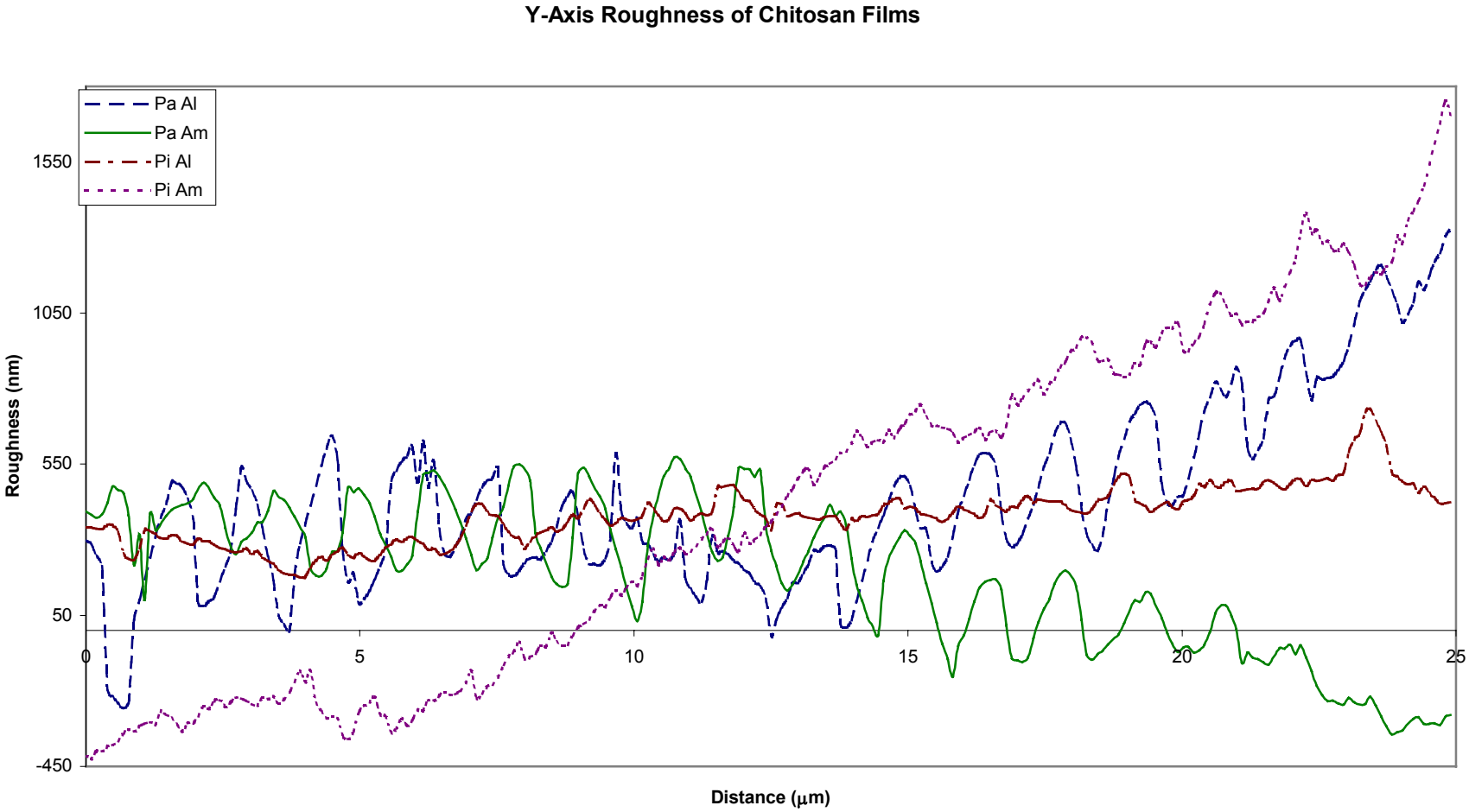

Figure 5.12. Y-Axis roughness diagrams for the chitosan films produced by the four treatment combinations.

5.3.4 Scratch Testing

Scratch testing was used to establish the adhesive strength of the films and to determine if any of the metal-silane combinations increased that adhesive strength. The means and standard deviations of the critical load applied to the films, along with depth of the scratch and the scratch width are shown in Table 5.9. Since there were values that were not statistically different, analysis was also performed on the critical load, scratch depth, and scratch width of the individual metal treatments and silane treatments, as shown in Table 5.10 and Table 5.11, respectively. The piranha treated films did experience higher critical loads, deeper scratch depths, and wider scratch widths, but the different silanes only experienced a difference in the scratch width, with the amino treated films having a more narrow scratch than the aldehyde treated films.

The means and standard deviations of the scratch height, residual depth, and pile – up height for each of the four treatment combinations are shown in Table 5.12. Since some of the values were not statistically different, analysis was also performed on the individual metal treatments and individual silane treatments, as shown in Table 5.13 and Table 5.14, respectively. The silane treated films shows a difference in scratch height and residual depth, but no difference in pile – up height; the aldehyde treated films had much deeper scratches and the residual depth was also much deeper. The films produced on the different metal treatments showed only a statistical difference in pile – up height, with the passivated films having much higher piling than the piranha treated films.

SEM was used to analyze the scratches produced. Figure 5.13 shows the scratches produced on the passivated metal with aldehyde silane, while Figure 5.14

shows the scratches produced on the passivated metal with amino silane. Figure 5.15 shows the scratches produced on the piranha treated metal with aldehyde silane, while Figure 5.16 shows the scratches produced on the piranha treated metal with amino silane. Some differences in the films were noticed, but no delamination events occurred; the lack of delamination events negated the ability to use any work of adhesion or shearing force equations.

Table 5.9. Critical load, depth, and scratch width of the chitosan films.

Treatment Combination	Critical Load (mN)	Depth (nm)	Scratch Width (μm)
Passivated, Aldehyde	234.91 ± 238.30[a]	3764.07 ± 2029.53[c]	69.33 ± 4.43[d]
Passivated, Amino	322.32 ± 76.52[a]	6507.44 ± 2045.33[c]	69.66 ± 1.29[d]
Piranha, Aldehyde	539.93 ± 18.90[b]	10534.75 ± 397.85	84.54 ± 5.04
Piranha, Amino	583.18 ± 0.27[b]	5454.87 ± 3958.11[c]	73.20 ± 1.64[d]

Values with the same superscript are not statistically different at the 5% significance level.

Table 5.10. Critical load, depth, and scratch width of the chitosan films based on metal treatment.

Metal Treatment	Critical Load (mN)	Depth (nm)	Scratch Width (μm)
Passivated	283.47 ± 195.08	5288.16 ± 2393.09	69.51 ± 2.87
Piranha	559.15 ± 37.58	8277.02 ± 3622.46	79.50 ± 7.03

Values with the same superscript are not statistically different at the 5% significance level.

Table 5.11. Critical load, depth, and scratch width of the chitosan films based on silane treatment.

Silane Treatment	Critical Load (mN)	Depth (nm)	Scratch Width (μm)
Aldehyde	404.37 ± 219.16^{a}	7525.56 ± 3789.15^{b}	77.78 ± 9.19
Amino	438.26 ± 183.14^{a}	6039.63 ± 2876.53^{b}	71.23 ± 2.31

Values with the same superscript are not statistically different at the 5% significance level.

Table 5.12. Scratch height, residual depth, and pile-up height of the chitosan films.

Treatment Combination	Scratch Height (nm)	Residual Depth (nm)	Pile-Up Height (nm)
Passivated, Aldehyde	5884.02 ± 1142.58[a]	3889.56 ± 833.61[a]	1994.45 ± 696.29[c]
Passivated, Amino	3890.07 ± 92.72[c]	2382.14 ± 65.21[b]	1597.93 ± 86.78[c]
Piranha, Aldehyde	5163.55 ± 524.72[a,b]	4144.36 ± 475.53[a]	1019.19 ± 331.96
Piranha, Amino	4462.58 ± 262.54[b,c]	2754.67 ± 174.06[b]	1707.91 ± 100.54[c]

Values with the same superscript are not statistically different at the 5% significance level.

Table 5.13. Scratch height, residual depth, and pile-up height of the chitosan films based on metal treatment.

Metal Treatment	Scratch Height (nm)	Residual Depth (nm)	Pile-Up Height (nm)
Passivated	4826.27 ± 1225.07[a]	3052.11 ± 945.47[b]	1774.16 ± 478.80
Piranha	4852.00 ± 547.72[a]	3526.72 ± 812.95[b]	1325.29 ± 436.63

Values with the same superscript are not statistically different at the 5% significance level.

Table 5.14. Scratch height, residual depth, and pile-up height of the chitosan films based on silane treatment.

Silane Treatment	Scratch Height (nm)	Residual Depth (nm)	Pile-Up Height (nm)
Aldehyde	5483.75 ± 878.30	4031.12 ± 625.85	1452.64 ± 707.89[a]
Amino	4194.52 ± 307.92	2547.71 ± 228.11	1646.81 ± 104.48[a]

Values with the same superscript are not statistically different at the 5% significance level.

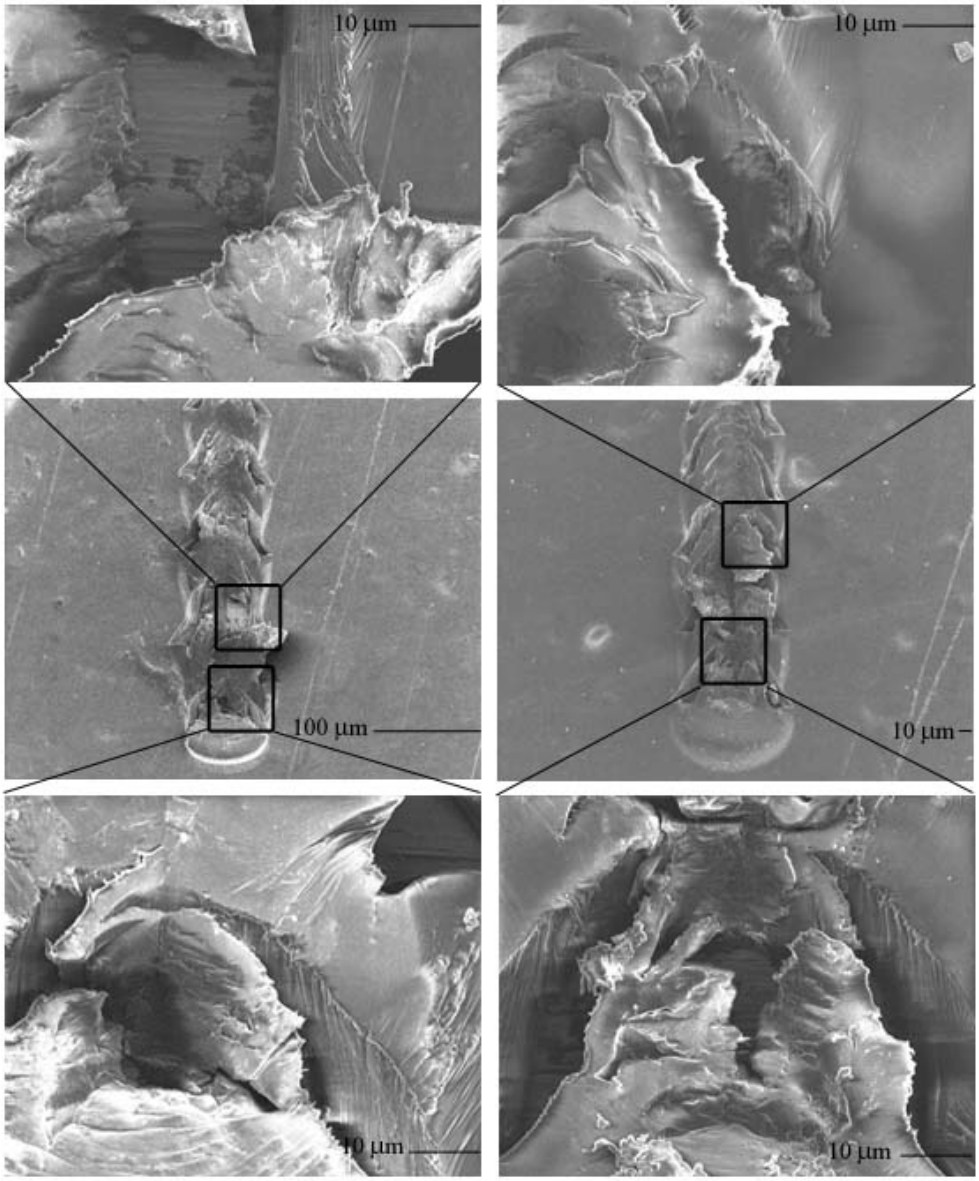

Figure 5.13. SEM pictures of the scratches produced on passivated metal with aldehyde silane.

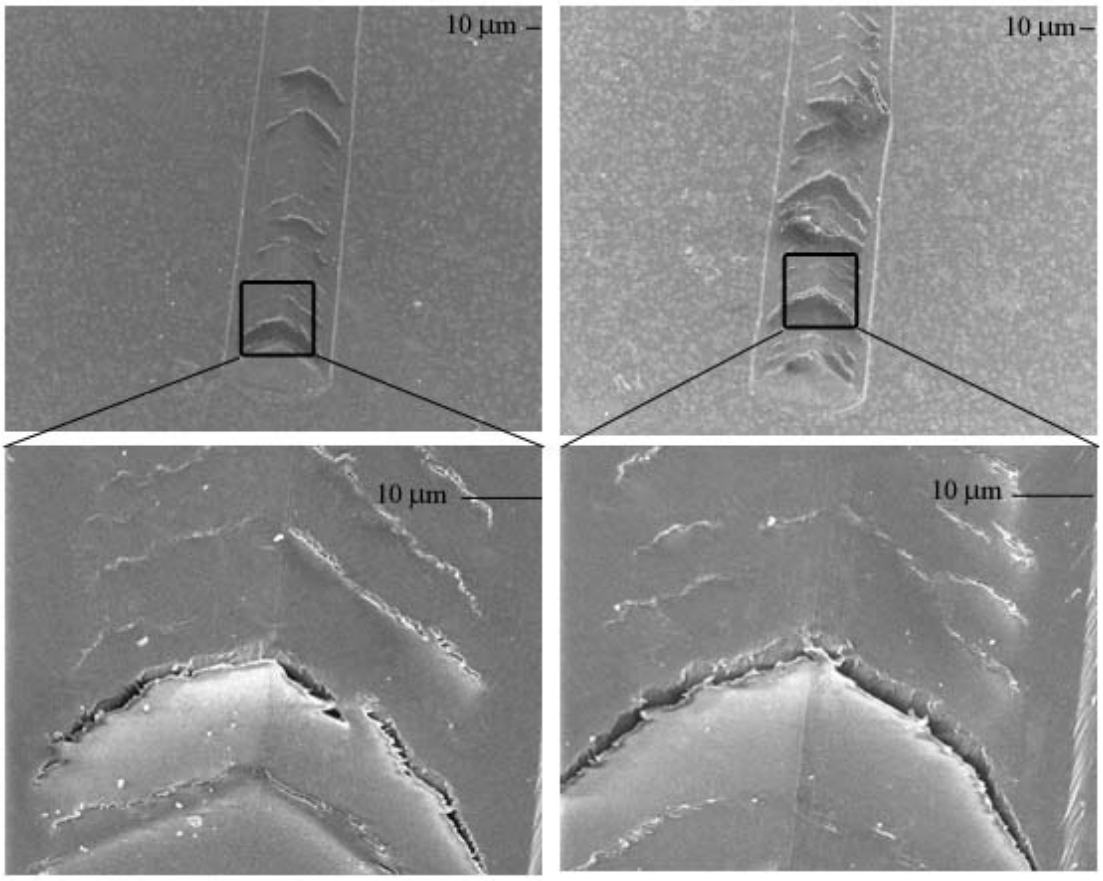

Figure 5.14. SEM pictures of the scratches produced on passivated metal with amino silane.

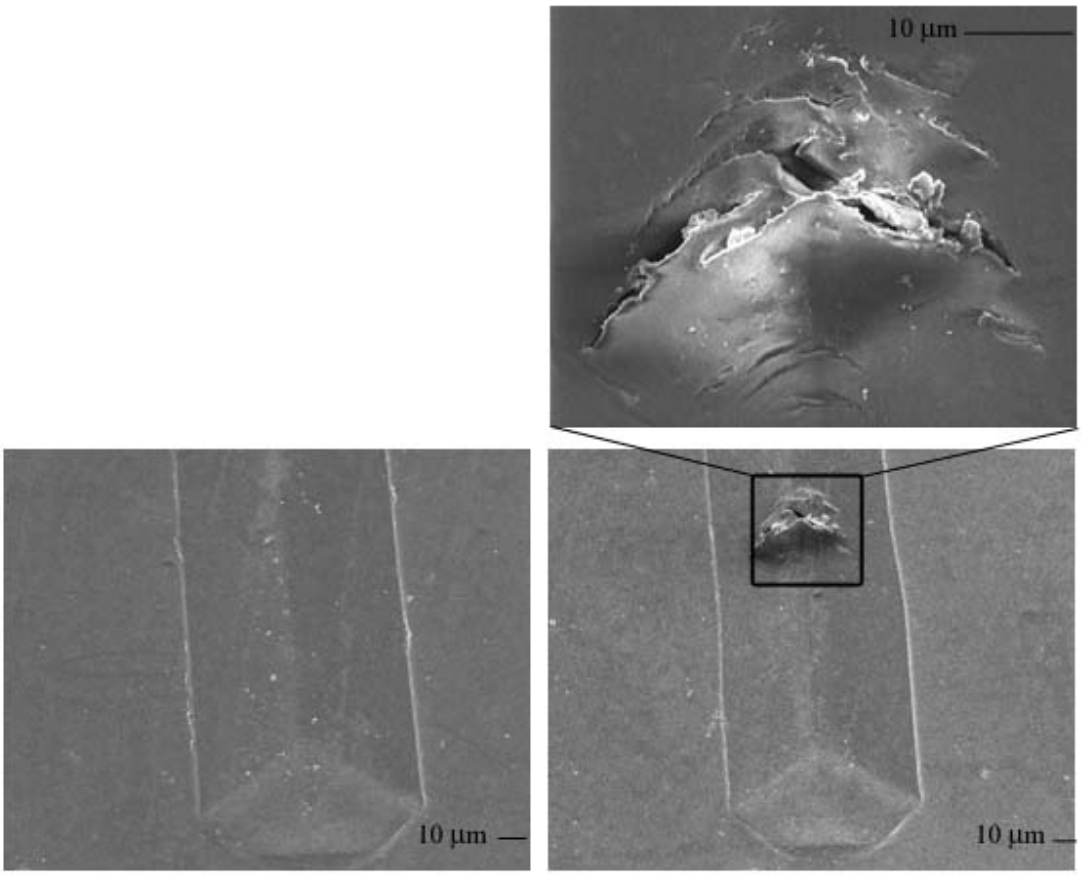

Figure 5.15. SEM pictures of the scratches produced on piranha treated metal with aldehyde silane.

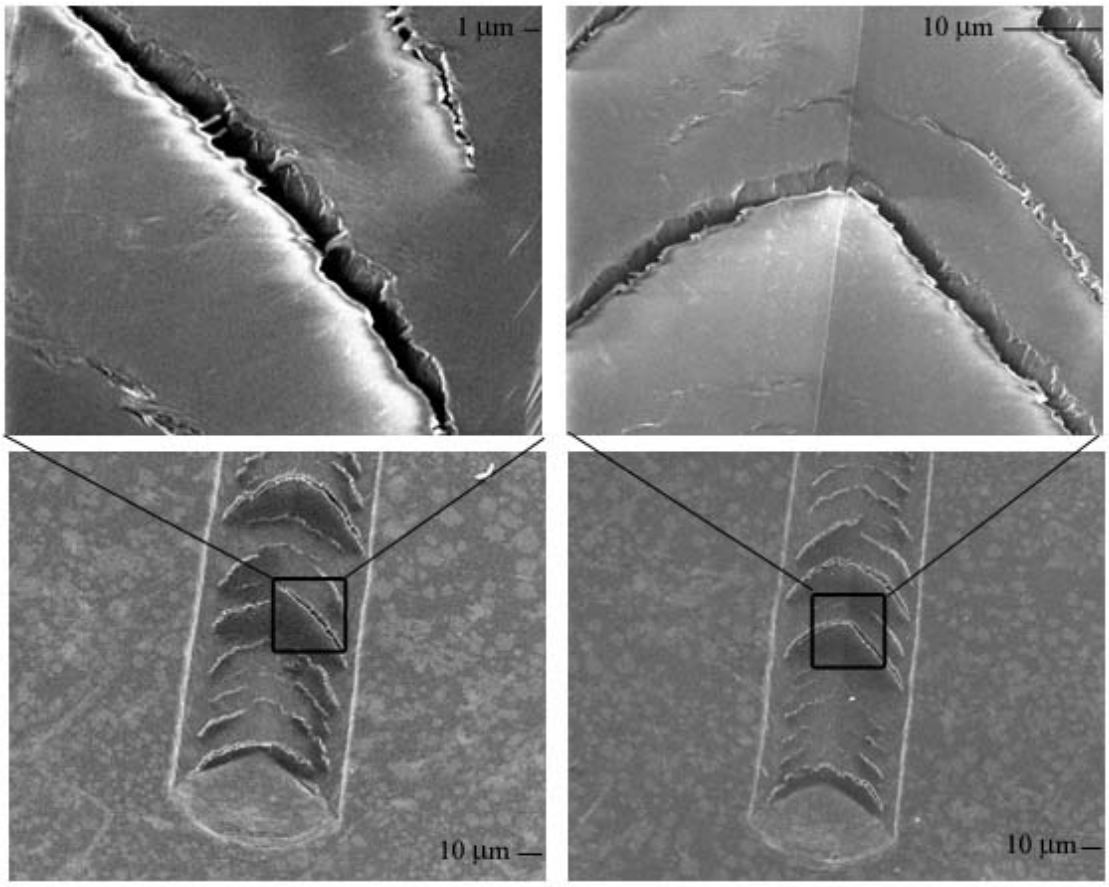

Figure 5.16. SEM pictures of the scratches produced on piranha treated metal with amino silane.

5.3.5 Bulk Adhesion

Because no delamination events occurred using scratch tests, bulk adhesion tests were performed. A standard protocol, as developed at the University of Memphis, was used to ensure that comparisons with the literature were accurate. A glue baseline was first produced, in order to determine if the failure occurred in the glue, within the film, or at the metal – film interface. Following the glue baseline, the four different treatment combinations were tested. Bulk adhesion tests the tensile strength of the glue, the film, and the film-metal interface. A load is applied over a specified contact area; tensile strength is then calculated from those specifications using the following formula:

$$Stress(MPa) = \frac{Load(N)}{Area(mm^2)} \tag{5.8}$$

The load was applied by the machine, while the area was set at 123 mm^2, as determined by the diameter of the pin. Table 5.15 shows the means and standard deviations of maximum load at break and the tensile stress applied to the films; only one film, a passivated metal with amino silane, was pulled from the surface of the metal, but its adhesion strength was not significantly different from the other tests. Since the values were not statistically different, analysis was performed on the individual metal treatments and individual silane treatments, with the means and standard deviations shown in Table 5.16 and Table 5.17, respectively. No significant statistical variation occurs based on the combinations, with the means for the maximum load at break ranging from 2055.67 ± 440.18 N to 2403.33 ± 200.85 N and the means for tensile strength ranging from 16.69 ± 3.57 MPa to 19.50 ± 1.63 MPa; also, no significant statistical variation occurs based on the individual treatments, with both the maximum load at break and tensile strength

means located in between the range of the combinations. The maximum load at break for the glue and the tensile strength of the glue were much less, with means of 635.76 ± 222.36 N and 5.22 ± 1.77 MPa, respectively. SEM images of the films and pins were taken following the bulk adhesion tests. Figure 5.17 shows the fracture of the glue on the chitosan and the fracture of the glue on the aluminum pin, which was representative of eleven of the twelve samples. Figure 5.18 shows the fracture of the chitosan film on the metal surface and the fracture of the chitosan film on the aluminum pin, which occurred on only one sample.

Table 5.15. Maximum load at break and tensile stress of the chitosan films.

Treatment Combination	Maximum Load (N)	Tensile Stress (MPa)
Glue	635.76 ± 222.36	5.22 ± 1.77
Passivated, Aldehyde	2190.33 ± 831.22[a]	17.77 ± 6.72[b]
Passivated, Amino	2055.67 ± 440.18[a]	16.69 ± 3.57[b]
Piranha, Aldehyde	2403.33 ± 200.85[a]	19.50 ± 1.63[b]
Piranha, Amino	2081.33 ± 1113.99[a]	16.88 ± 9.05[b]

Values with the same superscript are not statistically different at the 5% significance level.

Table 5.16. Maximum load at break and tensile stress of the chitosan films based on metal treatments.

Metal Treatment	Maximum Load (N)	Tensile Stress (MPa)
Glue	635.76 ± 222.36	5.22 ± 1.77
Passivated	2123.00 ± 599.43[a]	17.23 ± 4.85[b]
Piranha	2242.33 ± 737.31[a]	18.19 ± 5.99[b]

Values with the same superscript are not statistically different at the 5% significance level.

Table 5.17. Maximum load at break and tensile stress of the chitosan films based on silane treatments.

Silane Treatment	Maximum Load (N)	Tensile Stress (MPa)
Glue	635.76 ± 222.36	5.22 ± 1.77
Aldehyde	2296.39 ± 533.28[a]	18.64 ± 4.48[b]
Amino	2068.50 ± 757.69[a]	16.79 ± 6.16[b]

Values with the same superscript are not statistically different at the 5% significance level.

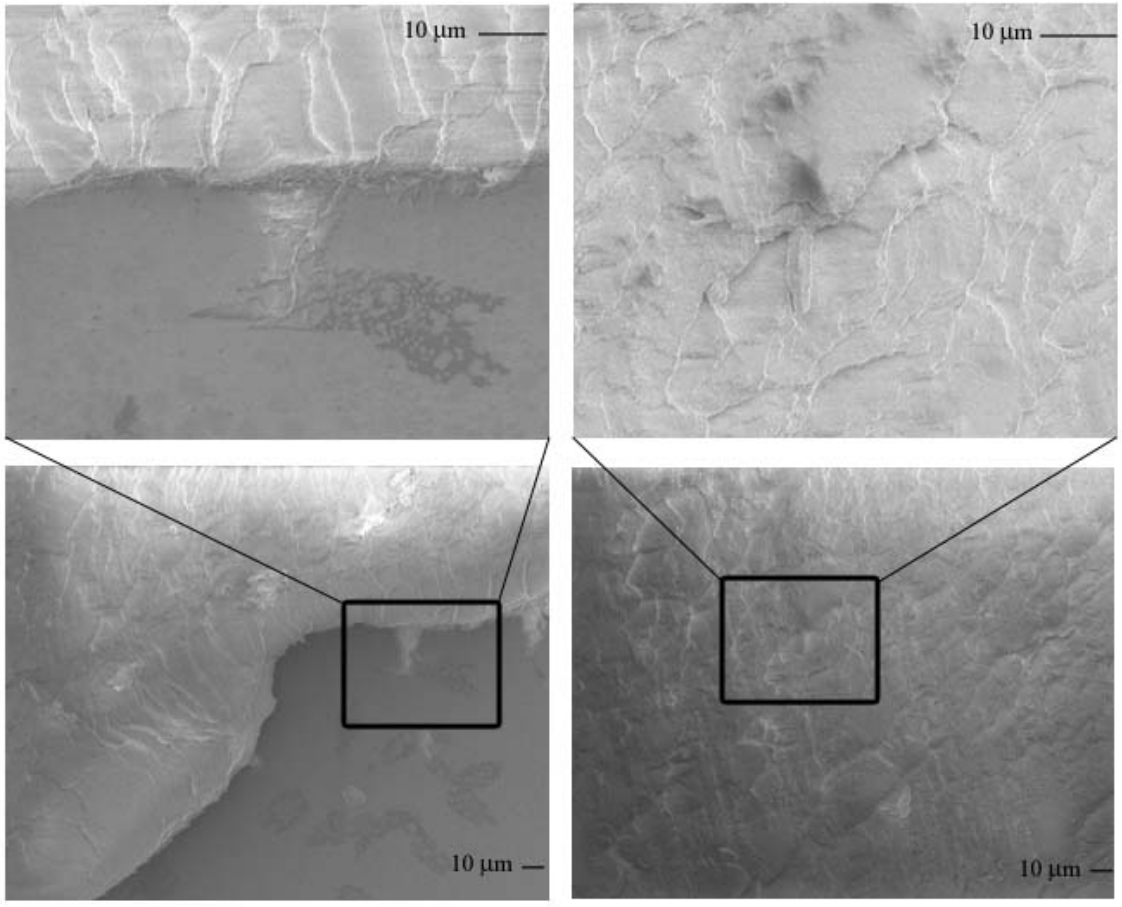

Figure 5.17. SEM pictures of the fracture of the glue after bulk adhesion tests.

The fracture of the glue on the chitosan film surface is shown in (a), while the fracture of the glue on the pin surface is shown in (b).

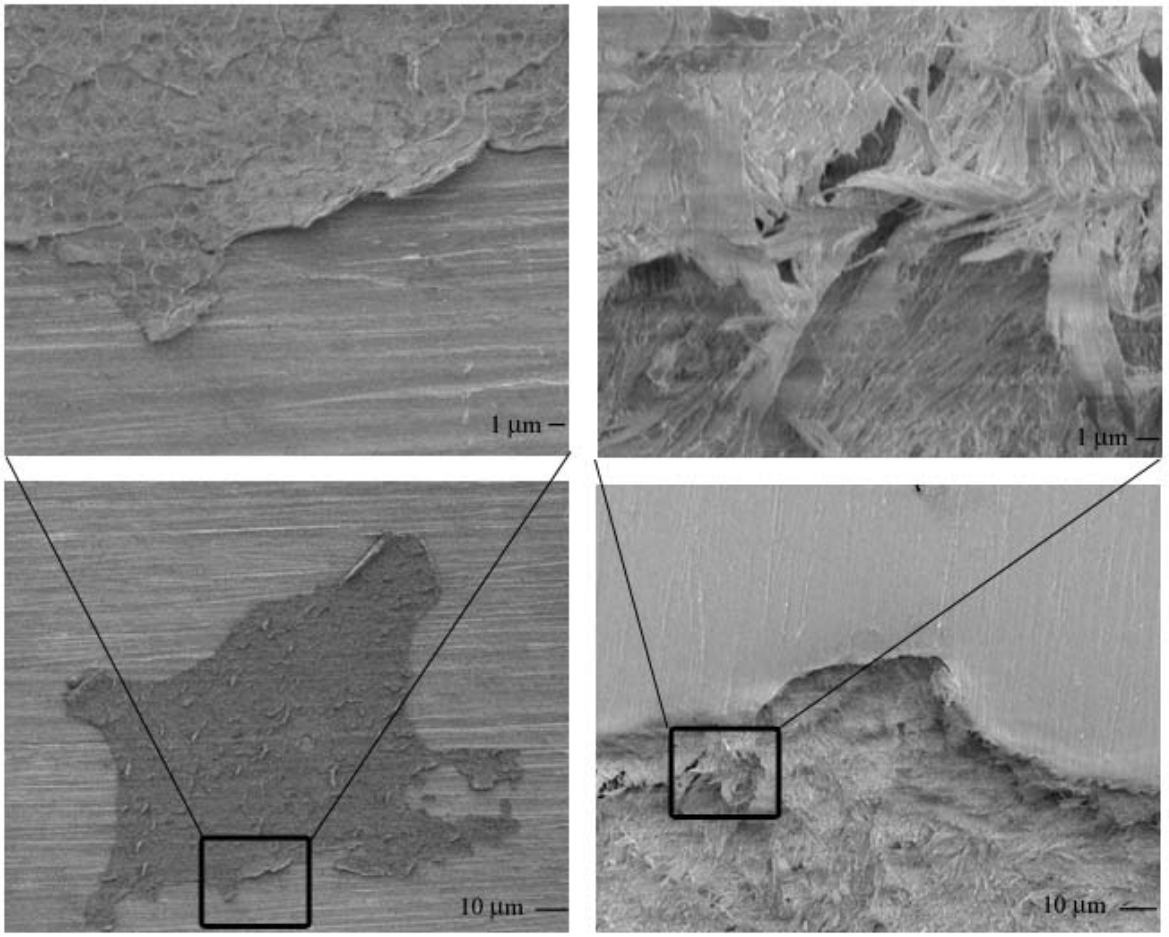

Figure 5.18. SEM pictures of the fracture of the chitosan film after bulk adhesion tests.

The fracture of the chitosan film on the metal surface is shown in (a), while the fracture of the chitosan film on the pin surface is shown in (b).

5.3.6 Contact Angle

Contact angle tests were performed to determine if the chitosan films were hydrophilic or hydrophobic. The films produced from the four treatment combinations were tested to determine if the treatment caused a change in the hydrophilicity of the films. Table 5.18 shows the means and standard deviations of the contact angles produced on the right side and the left side of the water droplet. Since there were no statistical differences in the treatment combinations, analysis was performed on the individual metal treatments and individual silane treatments, with the means and standard deviations shown in Table 5.19 and Table 5.20, respectively. No significant statistical variation occurs based on the combinations, with means for the left contact angles ranging from 93.6 ± 7.0^{o} to 97.7 ± 3.3^{o} and means for the right contact angles ranging from 93.6 ± 7.0^{o} to 98.0 ± 3.611^{o}; the means of the left and right contact angles were not statistically different either, which were in the range of the contact angles for the combinations. All of the contact angles indicated that the four treatment combinations resulted in slightly hydrophobic films. Figure 5.19 shows the contact angles on each of the four treatment combinations.

Table 5.18. Contact angles of the chitosan films.

Treatment Combination	Left Contact Angle	Right Contact Angle
Passivated, Aldehyde	$97.7 \pm 3.3^{o\ a}$	$98.0 \pm 3.6^{o\ b}$
Passivated, Amino	$94.3 \pm 5.3^{o\ a}$	$94.1 \pm 4.9^{o\ b}$
Piranha, Aldehyde	$93.6 \pm 7.0^{o\ a}$	$93.6 \pm 7.0^{o\ b}$
Piranha, Amino	$94.9 \pm 3.3^{o\ a}$	$95.1 \pm 3.3^{o\ b}$

Values with the same superscript are not statistically different at the 5% significance level.

Table 5.19. Contact angles of the chitosan films based on metal treatments..

Metal Treatment	Left Contact Angle	Right Contact Angle
Passivated	$96.0 \pm 4.7^{o\ a}$	$96.1 \pm 4.7^{o\ b}$
Piranha	$94.3 \pm 5.4^{o\ a}$	$94.4 \pm 5.4^{o\ b}$

Values with the same superscript are not statistically different at the 5% significance level.

Table 5.20. Contact angles of the chitosan films based on silane treatments.

Silane Treatment	Left Contact Angle	Right Contact Angle
Aldehyde	95.7 ± 5.8^{a}	95.8 ± 5.9^{b}
Amino	$94.6 \pm 4.3^{o\,a}$	$94.6 \pm 4.1^{o\,b}$

Values with the same superscript are not statistically different at the 5% significance level.

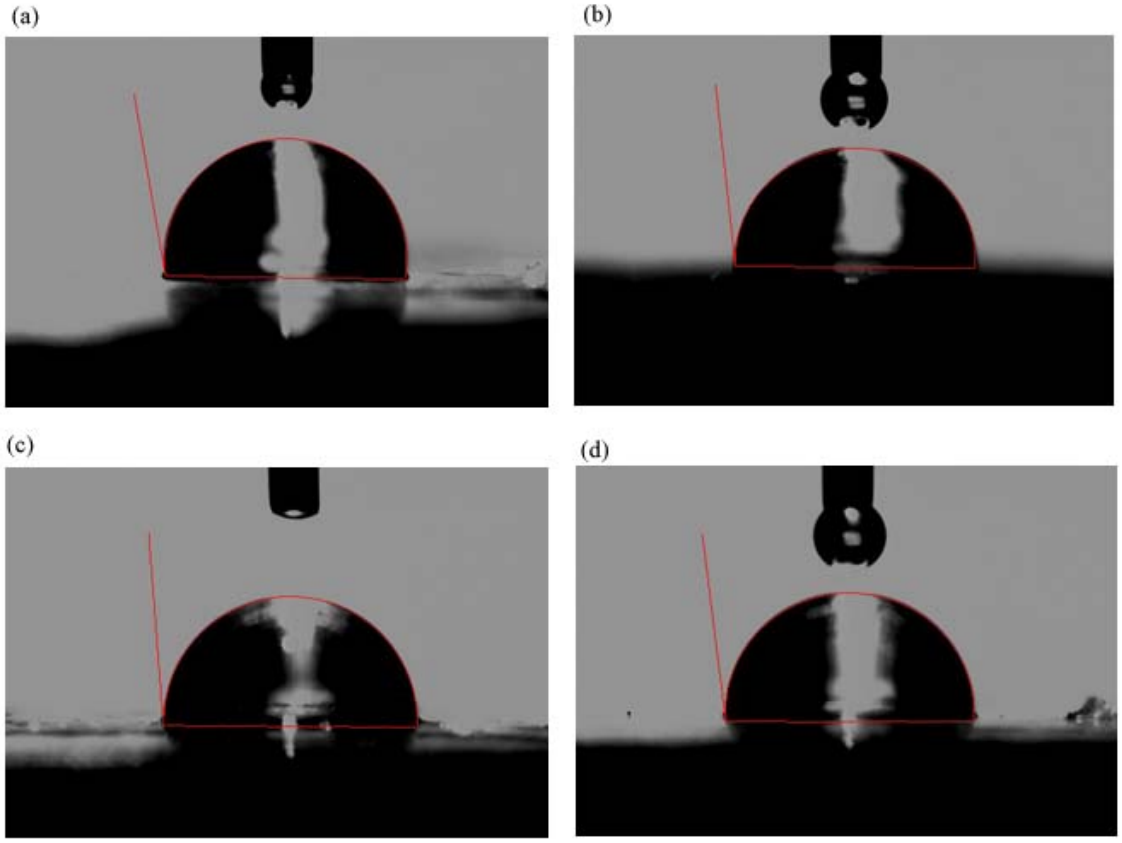

Figure 5.19. Contact angle pictures of the water drop on the four treatment combinations.

(a) Passivated Metal with Aldehyde Silane. (b) Passivated Metal with Amino Silane. (c) Piranha Treated Metal with Aldehyde Silane. (d) Piranha Treated Metal with Amino Silane.

5.4 Discussion

The results obtained from mechanical testing provide significant insight into the quality of the chitosan films. The hardness and elastic modulus of a film provide information about the ability of the material to withstand outside stresses, while scratch testing and bulk adhesion testing provide information about the strength of the metal – film interface. The roughness of the film provides information that will be useful in determining the ability of cells to adhere to the surface; contact angle measurements provide information about the hydrophilicity of the film, which relates to the ability of the film to adhere proteins and allow cell attachment.

5.4.1 Hardness and Elastic Modulus

The hardness values and the elastic modulus values for each of the four treatment combinations were not statistically different from the other values, or from literature values. A comparison of the hardness and elastic modulus of our films with literature values is shown in Table 5.21. The hardness values and the elastic modulus values did not change because of the nature of nano-indentation. The nano-indenter could only indent to a depth of 20 μm using a load of 500 mN; the chitosan film is close to 100 μm and the reaction occurs at the metal – film interface, where the nano-indenter did not reach. Therefore, the nano-indenter was only testing the chitosan film and not the effect of the treatment on the film. By using nano-indentation, it has been demonstrated that the chemical reaction does not affect the entire film; it has not been demonstrated how the chemical reaction affects the chitosan at the metal – film interface however. Chitosan films have demonstrated the ability to promote cell attachment and growth [5.7]; the lack

of difference between our films and literature values with respect to the hardness and elastic modulus should not affect the attachment and growth of bone cells.

Table 5.21. Literature values for hardness and elastic modulus of chitosan films.

Researcher	Chitosan Used	Hardness (GPa)	Elastic Modulus (GPa)
Wang et. al. [5.3]	Chitosan	0.12*	1.08 ± 0.04
	0.2% MWNT	0.13*	1.33 ± 0.06
	0.4% MWNT	0.17*	1.92 ± 0.07
	0.6% MNWT	0.15*	2.08 ± 0.05
	0.8% MNWT	0.15*	2.15 ± 0.09
Wang et. al. [5.4]	HAc-Cs	0.119 ± 0.006	3.76 ± 0.15
	2.5% MMT	0.136 ± 0.002	4.13 ± 0.09
	5.0% MMT	0.147 ± 0.008	4.39 ± 0.20
	10.0% MMT	0.164 ± 0.009	4.74 ± 0.34
	Cs	0.176 ± 0.004	4.39 ± 0.06
	2.5% MMT	0.195 ± 0.008	4.69 ± 0.15
	5.0% MMT	0.195 ± 0.022	4.71 ± 0.47
	10.0% MMT	0.199 ± 0.023	4.92 ± 0.41
Majd et. al. [5.5]	76% DDA- RT	0.13 ± 0.05	3.66 ± 0.68
	92.3% DDA- RT	0.12 ± 0.01	3.56 ± 0.25
	95.6% DDA- RT	0.12 ± 0.04	4.02 ± 0.85
	76% - 40°C	0.14 ± 0.29	3.76 ± 0.55
	92.3% - 40°C	0.12 ± 0.01	3.65 ± 0.19
	95.6% - 40°C	0.13 ± 0.04	4.02 ± 0.85
	76% - 70°C	0.14 ± 0.29	3.77 ± 0.57
	92.3% - 70°C	0.13 ± 0.01	3.70 ± 0.22
	95.6% - 70°C	0.11 ± 0.04	4.09 ± 0.84
	76% - 90°C	0.12 ± 0.26	3.56 ± 0.45
	92.3% - 90°C	0.12 ± 0.01	3.60 ± 0.21
	95.6% - 90°C	0.11 ± 0.04	4.00 ± 0.87
This Research	Passivated, Aldehyde	0.14 ± 0.08	4.82 ± 2.33
	Passivated, Amino	0.19 ± 0.08	4.90 ± 1.82
	Piranha, Aldehyde	0.15 ± 0.06	4.53 ± 1.20
	Piranha, Amino	0.18 ± 0.04	4.78 ± 0.64

*Values were read from a graph and no standard deviations were given.
MWNT: Multi-Walled Nanotubes
HAc: Acetic Acid
MMT: Montmorillonite
DDA: Degree of Deacetylation
RT: Room Temperature

5.4.2 AFM and SEM Picture of Indentation Marks

Significant pile – up of the chitosan film could be seen in all of the AFM pictures taken of the indentation locations, regardless of the treatment combination. However, the actual height of the pile-up could not be determined, as AFM could only measure 7.5 μm on the z-axis. The pile-up present was at least 4.0 μm, as shown in Figures 5.2, 5.4, 5.6, and 5.8, but that number is not accurate due to the thickness of the film. Even with the significant pile – up, there were no delamination events visible, a very desirable feature of coatings used for biomedical implants. The lack of delamination is likely the result of the film thickness; since the films were thicker than the nano-indenter could press, the nano-indenter never approached the metal – film interface and therefore did not place enough energy at the metal – film interface to cause any delamination events. The film surrounding the pile – up was smooth, with no outward pressing of the film demonstrated, as shown in Figures 5.2 – 5.9. The chitosan did crack under the pressure of the indenter, but the depth of the crack was not through to the metal underneath, as shown in Figures 5.3, 5.5, 5.7, and 5.9. Neither the metal treatment nor the silane treatment showed any major differences in the appearance of the nano-indentation mark. The lack of influence on the film surrounding the indentation mark is an indication of the film's ability to absorb applied stress, thereby reducing the chance that damage to the film will adversely affect the coating. Since the film stays attached to the metal surface when stress was applied, no flaking of the coating occurred, which is a major problem of hydroxyapatite coatings [5.9]. Unlike hydroxyapatite coatings, which flake and allow macrophage cells to cause crevice corrosion [5.9], the chitosan coatings absorb the applied stress, stay attached to the metal surface, and can prevent the crevice corrosion

that results from the coating flaking off the surface. The stronger attachment of the chitosan coating also allows for better growth of bone cells into the film, improving the osseointegration of the implant into the surrounding bone.

5.4.3 Roughness

The roughness of the films is determined by analyzing graphs produced from the pictures taken using AFM. The analysis was performed in an effort to avoid the dust particles left from the evaporation method used to deposit the chitosan films. The roughness of the film was not statistically different for any of the treatment combinations, nor for the individual metal treatments or individual silane treatments. The films were considered smooth, with values ranging between 0.24 ± 0.10 μm and 0.35 ± 0.12 μm. The smoothness of the film in all of the locations analyzed indicates that the chitosan film is comparatively homogeneous throughout the surface layer of the film.

No published literature on the roughness of untreated chitosan exists. The values measured here are once again for the surface of the films and do not measure the roughness of the film due to the treatment. The statistically indifferent roughness values indicate that the treatment does not affect the bulk properties of the film. However, this research was not able to measure the roughness of the films near the metal surface to determine if the treatment method changed film properties at the surface of the metal. The slight roughness values are desired for implant coatings, as it increases the surface area for proteins to adhere to [5.8].

5.4.4 Scratch Testing

Scratch testing can be very useful in analyzing how effectively a film is adhered to a surface. This includes measuring the amount of shear stress it takes to disrupt the film, in the form of shearing force, and how strongly the film is adhered, in the form of work of adhesion. Like roughness values, no published literature exists with respect to the chitosan film adhesion using scratch testing. In order to determine this, however, delamination events, or places where the film pulls off the surface, are required. The results from the scratch testing proved to be inconclusive; there were no delamination events so no determinations on the strength of the metal – film interface could be made. The lack of delamination is probably due to the thickness of the film, where the energy from the applied load could not reach the metal – film interface and therefore could not disrupt it.

The critical load applied to the films did vary significantly with respect to the metal treatment. The passivated surfaces had a much smaller critical load applied; for the amount of load that was applied, much larger breaks within the film were seen for the passivated films, as shown in Figures 5.13 – 5.14, as compared to the piranha treated films, as shown in Figures 5.15 – 5.16. This difference in critical load may well be affected by the breaks; the films with more breakage could not have the same critical load applied as the films without the severe breakage. However, the cause of the film surface cracks is probably the result of the method of deposition instead of any changes brought on by the metal treatment. Because evaporation of chitosan is used, the chitosan polymer chains align themselves in a random fashion. Several layers of chitosan chains exist within the film; chains in the top layer could get intertwined with chains in the lower

levels, increasing the resistance to cracking. However, chains in the top layer may not intertwine with chains in the lower levels, thereby possibly reducing the ability of the chitosan to resist cracking.

It is interesting to note that, while the passivated films cracked more than the piranha treated films, the cracks did not propagate outside of the line created by the nano-indenter. This seems to indicate an ability of chitosan to absorb applied stress and not allow it to move throughout the film surface. This lack of crack propagation would reduce the ability of the film to flake off the metal when shear stresses are applied in implantation, thereby preventing or reducing the chance of pitting and crevice corrosion.

5.4.5 Bulk Adhesion

In order to determine if the fracture of the surface takes place within the glue, within the film, or at the film-metal interface, the strength of the glue first had to be determined. The strength of the glue in this research was determined to be 5.22 ± 1.77 MPa. Therefore, if the film could withstand more the 5.22 ± 1.77 MPa, the fracture should occur within the glue.

The results show a significant increase in the strength of the glue, from 5.22 ± 1.77 MPa to 19.50 ± 1.63 MPa. The increase in strength of the glue indicates that a reaction between the chitosan and the glue took place, thereby increasing the strength of the glue. This reaction could be the result of a slightly porous chain organization in the chitosan and/or the solvent of the glue reacting with the chitosan. Whatever the reason, the strength of the glue was significantly increased. One way to determine if the strength of the film is stronger than literature values would be to use a different glue, with a higher

bond strength. The increased bond strength of the glue would allow for a better determination of the strength of the bond between the metal surface and the chitosan film.

However, even with an increase in glue strength, 19.50 ± 1.63 MPa was not enough to disrupt the chitosan film – metal interface. Of nine samples tested, only one sample of passivated, amino treated metal showed any film fracture, as shown in Figure 5.17. All of the other samples, and even the sample with the small film fracture, broke at the glue – aluminum pin interface, with the glue remaining on the film, indicating that the tensile strength of the glue – film exceeded the glue strength between the glue and the aluminum pin. The strength of the film – metal bond has far exceeded the previously published film strengths of 1.5 – 1.8 MPa [5.6]; the film – metal bond also possesses the same general tensile strength as hydroxyapatite coatings, which range between 6.7 MPa to 26.0 MPa [5.6]. While no significant changes could be seen between the four treatment combinations, the increase in time that the substrates spent in the silane solution from ten minutes to twenty-four hours and the use of toluene as the solvent in place of 95% ethanol – 5% water did greatly affect the bond strength between the silane and the metal surface.

5.4.6 Contact Angle

The contact angle measurements are used to determine the hydrophilic nature of a surface. Contact angle values greater than 90^{o} are considered hydrophobic, while contact angle values less than 90^{o} are considered hydrophilic. There were no significant differences between the four treatment combinations; all of the films are considered hydrophobic, although the amount of hydrophobicity is low, with the largest contact

angle being 98.0 ± 3.6°. This number is higher than published values of 76.4 ± 5.1° [5.7]. The increase in hydrophobicity is likely due to the method of film preparation. Acetic acid was used to dissolve the chitosan in water. Following the evaporation of excess water and acetic acid, the films were not rinsed with either ethanol or sodium hydroxide to remove the acetic acid. The presence of the acid likely affected the contact angle readings.

A slightly hydrophobic film may actually be desired, as hydrophobic films bind more proteins. This occurs because the proteins are able to align more tightly together with their hydrophobic ends attached to the film [5.8]. An increase in protein attachment is actually desired, as cells adhere to proteins on the surface of a material, not to the actual material [5.8].

5.4.7 Final Mechanical Properties Comparison

The previous discussion has provided insight into the differences between the films produced in this research and published films. Table 5.22 shows the best published values, if available, and the values produced in this research. The roughness values and the values for scratch testing were not listed in the table, since there were no published values to compare to this research.

Table 5.22. Mechanical property comparisons between this research and published values.

Mechanical Property	**Published Literature Values**	**Values from This Research**
Hardness (GPa)	0.14 ± 0.29 [5.5]	0.19 ± 0.06
Elastic Modulus (GPa)	4.09 ± 0.84 [5.5]	4.90 ± 1.82
Bulk Adhesion (MPa)	1.8 [5.6*]	19.50 ± 1.63
Contact Angles (^{o})	76.4 ± 5.1 [5.7]	98.0 ± 3.6

* No significant values were listed for these values.

As the Table 5.22 shows, the bulk adhesion value for this research was much higher than previously published bulk adhesion values. This significant increase to the adhesion strength demonstrates that the films produced are considerably higher quality than previous films. The bulk properties of the film, such as hardness and elastic modulus, did not change as a result of the surface treatments; therefore, the surface treatments did not change the structure of the chitosan film.

5.5 Summary

In order to ensure that the results obtained from the mechanical tests were comparable to the films produced for chemical analysis, XPS was run on a sample of the films produced for mechanical testing. There were no statistical differences between the films produced for chemical analysis or the films produced for mechanical analysis. Therefore, all of the results from mechanical testing were considered relevant to the films created using the four different treatment combinations.

The hardness and elastic modulus values for each of the four treatment combinations were not statistically different. Also, the hardness and elastic modulus values for the individual metal treatments and individual silane treatments were not statistically different. Finally, the hardness and elastic modulus values were not statistically different from published literature values for chitosan. This indicates that the treatment used in creating the films did not affect the bulk properties of the film, as the treatment was located at the metal – film interface; the hardness and elastic modulus values were determined at the film surface and did not penetrate the thickness of the film to reach the metal – film interface.

The roughness values obtained from analysis of the AFM pictures indicate relatively smooth films, with no statistical differences between the different treatment combinations. The slightly rough surface is desirable for implant coatings, as this increases the surface area for proteins to adhere to.

Scratch testing indicated a difference in critical load for films created using a passivated metal as compared to films using a piranha treated metal. However, no delamination events were seen and therefore, no shearing force or work of adhesion values can be determined. The difference in critical load, and the cracks produced, were probably the result of the chitosan chain interaction rather than a statement on the metal treatment method.

Bulk adhesion indicated a significant increase in the metal – film interface bonding as compared to published results. There were no significant differences associated with the treatment combinations, but the glue strength was significantly increased after being placed on the chitosan surface. Even with the increase in glue strength, however, the films did not pull off the surface and were able to withstand 19.50 ± 1.63 MPa of tensile stress; the point of break occurred at the glue – aluminum pin interface. The time increase of the titanium substrates in the silane solution and the effect of toluene as the solvent, instead of 95% ethanol – 5% water, are likely the sources of an increase in bulk adhesion strength.

The chitosan films were considered hydrophobic following contact angle measurements. This research also had much larger contact angles than published research, with values as large as 98.0 ± 3.6^{o} compared to 76.4 ± 5.1^{o}. The increase in hydrophobicity is likely due to acetic acid residue instead of the result of film treatment,

as the contact angles from the different treatment combinations were not statistically different. A hydrophobic surface is desirable, however, as it has been proven to increase protein adsorption which is directly related to cell adhesion, since cells bind to proteins adhered to the surface, not the surface itself.

Overall, mechanical testing indicated that the treatment combination did not affect the bulk properties of the film, as indicated by the hardness, elastic modulus, and roughness values of the films. Also, the method followed to deposit the different silanes significantly increased the quality of the films as demonstrated by the increased bulk adhesion values. Scratch testing and contact angle tests indicate several differences can occur, which is likely due to the organization of the chitosan chains and the interaction of the surface chains with the chains located beneath those surface chains.

CHAPTER VI

SUMMARY AND CONCLUSIONS

6.1 Introduction

Several different methods were used to determine if the films produced in this research were higher quality than films previously produced. Four treatment combinations were used for the majority of this research, following the determination that the first reaction resulted in poor film adhesion. Chemical analysis was performed on each step of the reactions in order to confirm, or reject, the anticipated surface reaction. Mechanical testing was then performed on the final films to determine the films' hardness, elastic modulus, roughness, adhesion, and contact angle. The results from the chemical analysis and the mechanical analysis allowed us to determine if our films were of higher quality than previously published films.

6.2 Chemical Analysis

Using X-Ray Photoelectron Spectroscopy (XPS), the anticipated surface reactions could be confirmed, or rejected. The surface analysis of the original silane reaction, using isocyanatopropyltriethoxysilane, provided evidence that the anticipated surface reaction was not occurring. The low presence of the TiO, the removal of the reactive terminal groups, and an inability to form a silane monolayer were all contributing factors

in the development of a new method to treat the titanium surface and in a new solvent to deposit the silane molecules.

Following the realization that the anticipated surface reaction was not occurring, the titanium metal was treated with a piranha solution, to encourage the formation of TiO groups. A significant increase in the presence of the TiO groups as compared to the passivated metal was seen using XPS. These groups are ultimately responsible for binding the silane molecules to the surface.

The silane molecules were also placed in toluene, instead of a water – ethanol mixture, to reduce the chances of unwanted polysiloxane formation and removal of the reactive terminal groups. Two silanes were chosen to provide more information about the binding of the chitosan film to the titanium surface. One silane, aminopropyltriethoxysilane, needed a linker molecule, gluteraldehyde, in order to bind chitosan; the second silane, triethoxsilylbutyraldehyde, did not need a linker molecule.

Four treatment combinations were created, using either passivated titanium or piranha treated titanium, and using either the amino silane or the aldehyde silane. The anticipated surface reactions were then examined using XPS. The use of a different solvent likely resulted in closely packed silane molecules, using both the aldehyde silane and the amino silane. The piranha treated metal also appeared to bond more silane than the passivated metal, as there were more TiO groups present originally.

The chitosan films were too thick to examine the reaction between the silane molecules and the chitosan films using XPS. However, XPS was able to show that the chitosan films still contained some residual minerals from the original starting materials, even following the demineralization process. Also, XPS showed that the chitosan films

are not completely homogeneous, a fact explained by the multiple shellfish exoskeletons used to create the chitosan powder, even though all of the powder used came from one batch. Since each shellfish is different in its uptake of minerals and production of chitin, the precursor of chitosan, the deacetylation and demineralization processes would not make the chitosan from each shellfish exactly the same. However, the chitosan films did not have major differences, indicating that the treatment combination did not affect the chemical structure of the chitosan film.

XPS was also used to analyze the films used in mechanical testing. It showed that all of the films used fell within the range of films produced using one of the four treatment combinations. This allowed all of the results from the mechanical tests to be considered relevant to the films used in chemical analysis.

6.3 Mechanical Analysis

The films produced were tested to determine if any major changes were made to the chitosan using the four treatment combinations. The hardness and elastic modulus of the films were examined using nano-indentation. These values were unchanged, in part due to the thickness of the film. However, the lack of change indicated that the silane reactions did not change the structure or bulk properties of the chitosan. The roughness of the films were determined and showed no significant differences between the four treatment combinations. The lack of significant difference again showed that the treatment combinations did not affect the bulk chitosan properties.

The films were too thick to gather much information from scratch testing. No delamination events occurred, indicating that at least the film could withstand more than

the energy exerted by a force of 600 mN. Bulk adhesion testing was also performed on the films, to determine the tensile strength of the films attached to the surface. Our results were much higher than any previously published results with regard to the adhesion strength of the chitosan film. In fact, the adhesion strength of the chitosan film was in between values published for the adhesion strength of hydroxyapatite, a ceramic. The chitosan films were also slightly hydrophobic, a possible advantage to binding proteins.

6.4 Relation to the Research Objectives

The primary goal of this research was to produce higher quality films than had been previously published. This goal was obtained: the films produced were more tightly bound to the titanium surface than any previously published results.

A complete understanding of the surface chemical reactions helped lead to these higher quality films. Without the surface analysis performed on the published silane reaction, the reasons for the film failure would never have been known. The first "sub-objective", analyzing the surface of a published silane reaction, allowed us to develop a different treatment protocol to increase the TiO group, reduce the loss of the reactive terminal groups, and prevent the unwanted formation of polysiloxanes. The poor quality of the films was best illustrated by the inability of the films to stay bound once the films were subjected to the high vacuum necessary for SEM; the films were unable to enter the XPS ultra – high vacuum chamber for the fear that the film would pull off the surface and become lodged in the ion pump, causing a significant downtime for the XPS machine.

The second "sub-objective", analyzing the surface of four treatment combinations, allowed us to determine that the anticipated surface reactions were indeed occurring as desired. The indications of these anticipated surface reactions included the reduction in TiO groups between the metal surface and the silane treated surface, the increasing amount of silicon on the surface following the silane reaction step, and the ability of the chitosan films to stay attached in the ultra – high vacuum system required for XPS.

The third "sub-objective", analyzing the final films to determine the mechanical properties, showed us that the metal treatments and silane reactions did not chemically alter the structure of the chitosan, as the surface properties of the film were statistically similar to published results. The mechanical analysis also showed that the films were tightly bound to the titanium surface, as neither scratch testing nor bulk adhesion testing caused the films to delaminate, or pull off, the surface. The lack of delamination will prevent the film from flaking off the titanium surface. The ability to prevent flaking of the film will also prevent crevice corrosion and pitting caused by the macrophages attacking a foreign body; without places for the macrophages to get into to begin degrading the implant, the less of chance for failure of the implant.

The chemical analysis performed on the surfaces allowed us to determine that the anticipated surface reactions were occurring. The mechanical analysis performed on the final films allowed us to determine that the bulk properties of the chitosan film were not changed, but that the chitosan films were tightly bound to the titanium surface. These two sets of analyses provided significant evidence that the films produced in this research are high quality films and are better than any of the results previously published.

CHAPTER VII

FUTURE WORK

7.1 Introduction

The research area that deals with improving implants and implant coatings is very broad, with several different avenues of investigation ongoing at the same time. While this research presented begins to cover the film – implant interface, it by no means exhausts all possibilities available for exploration. The research presented in this dissertation covers only the surface science of the chemical reactions and the mechanical effects of the chemical reactions. Specifically, this research presented two different silane reactions on two different metal treatments, but did not address other methods of deposition; this research also did not focus on the biological effects that may occur in the chitosan coating because of the different treatment schemes. Future research into the biological effects of the treatments and into other methods of deposition can further characterize and improve upon the bonding of a coating to a metal implant surface. Several methods to further characterize the films presented in this research and to improve upon the chitosan binding should be considered for future work.

7.2 Sterilization Effects

Chitosan has been sterilized using different techniques, such as autoclaving, ethylene oxide, and gamma irradiation. Each of the techniques sterilizes the bulk, and the

surface, of the chitosan. While bulk tests on the sterilized chitosan films have been performed, and changes in the tensile strength, contact angle, and hemolysis properties have been detected, no tests to determine if changes occur at the nano-scale have been conducted. The previously presented research did determine properties on the nano-scale, but these tests were conducted on "as-cast" chitosan. However, no material can be implanted into any animal without sterilization. Therefore, mechanical properties at the nano-scale need to be gathered and compared to present research, in order to determine if any major structural changes have occurred due to sterilization. Nano-indentation and scratch testing on the sterilized surfaces will provide the sterilized elastic modulus and sterilized hardness; it may also provide information about the bond strength, and if that bond was degraded during sterilization. These two tests can provide valuable information relating to how these sterilized films would stand up during implantation.

Nano-indentation properties are very useful to determine how a film will react during implantation. However, if the thickness of the film is not greatly affected, scratch testing may not provide any valuable information about the bond strength. Therefore, other mechanical properties will need to be investigated. Nano-indentation properties should be investigated with equipment that allows greater depth penetration as compared to the equipment used in this research. Also, bulk adhesion tests, where the film is pulled off the metal substrate, will provide information about the bond strength. By comparing this bond strength to the bond strength of the unsterilized films, one will be able to determine if the underlying silane layers were affected by the sterilization. Also, contact angle treatments will allow the researcher to determine if the films hydrophilic nature

changes; a major change in the nature of the film may present a problem to cell attachment and growth.

7.3 Biological Effects of Chitosan Treatments

The films developed in this research were produced using two different silanes and two metal treatments. While the chitosan film is thick, there is still a chance that the metal treatments and/or silane treatments may affect the make up of the chitosan film; while XPS could not determine this change, osteoblasts may notice the change and be unable to attach and/or grow. Therefore, cell studies will need to be performed on the films produced in this research to determine if cell attachment and cell growth is affected. As previously stated, only sterilized material may be used in implants; therefore, the chitosan films should be sterilized before testing the cell attachment and growth, in order to determine if major changes are present from previous literature.

7.4 Applications to Different Implant Metals

In this research, all of the data was collected using only commercially pure titanium – grade 4. However, multiple different implant metals exist. Titanium – 6 Aluminum – 4 Vanadium and Cobalt – Chrome implant quality metals should also be used to determine the effects of the two different silanes. This research would include X-Ray Photoelectron Spectroscopy to determine the reactions occurring at the surface of the implant metals, nano-indentation to determine if any mechanical properties change as a result of the metal substrate, bulk adhesion to determine if the binding strength is the same, and contact angles to determine if the hydrophilicity of the chitosan film is affected by the metal substrate. Also, sterilization effects and biological effects should be

examined for each of the metals to determine if any changes occur because of the metal substrate or reaction series.

7.5 Effects of Solvents

In the presented research, toluene was used as the solvent with which to carry the silanes. This solvent was chosen because it contains no water, which reacts with the silanes to remove the reactive terminal end groups and cause a polysiloxane to form. However, toluene is dangerous and mutagenic effects have been demonstrated in the laboratory [7.1]. It is not considered a carcinogen, because insufficient research has been performed on the chemical; however, damaging effects have been seen in a multitude of different human systems, including cardiac, lungs, and brain [7.1]. While it produced results superior to previous films, the use of toluene needs to be eliminated. Therefore, another solvents without the known toxicity effects of toluene need to be investigated.

These solvents all must have two major properties similar to toluene. First, the solvents should not absorb water from the air. If the solvent does absorb water, even in small amounts, as toluene can, then the procedure given in chapter two, where the solvent is placed in sealed containers covered with parafilm, should be followed to minimize the intake of water. However, if the solvent absorbs water just because the top of the bottle was removed, then these solvents should not be used. The solvents also need to be organic, since silanes dissolve in the organic solvent and do not separate. However, substituting a toxic, carcinogenic solvent with a toxic, non-carcinogenic solvent only solves one half of the problem. Therefore, the solvents need to be relatively non-toxic

and non-carcinogenic. Some solvents to investigate include 200 proof ethanol, ethyl ether, and acetone. Other suitable solvents may exist and should be investigated.

Once several suitable solvents have been identified, a comparison between the results of the varying solvents should be compared to toluene. This includes a chemical reaction analysis to determine the percentage of carbon, oxygen, titanium, silicon, and possibly nitrogen, and the different species of compounds present. A major decrease would not be desired, as this would affect the bonding of the film to the surface. However, values that only decrease slightly, stay the same, or even increase, would be highly desirable as the solvent then removes the toxicity and carcinogenicity of toluene. The mechanical properties of the produced films using the desirable solvents would also need to be compared with films produced using toluene. Nano-indentation, scratch testing, bulk adhesion, and contact angle measurements would all be necessary in order to determine if the new solvent had any effect on the bond strength and hydrophilicity of the films. The newly produced films would also need to be sterilized and the same mechanical tests would need to be performed in order to determine if the sterilization affected the silane molecules in any way. Finally, biological tests, including cell attachment and growth, would need to be performed to determine if there were any major changes detectable by the osteoblasts but undetectable by chemical means.

7.6 Effects of Deposition

An offshoot of determining the best solvent to deposit the silane from would also be to investigate methods to deposit the silane without the presence of a solvent, or a very minimal amount of solvent. A commonly used method of depositing silane is chemical

vapor deposition (CVD) [7.2 – 7.3]. In CVD, the silane is vaporized at a relatively mild temperature (90°C – 130°C) [7.3]; following a set time to allow the silane to react with the substrate, the reactor is then purged with nitrogen gas to remove physisorbed molecules, instead of the sonication performed when using toluene [7.2].

Activation of the metal substrate can also be accomplished without the use of silanes. This activation would be performed using other deposition methods, including plasma deposition and laser deposition. Plasma polymerization takes place at low temperature and low pressure, using plasma that has been produced by a glow discharge through an organic vapor or gas [7.4]. The organic compound used determines the minimum wattage needed, as this differs dramatically between organic monomers [7.4]. Commonly used organic compounds are allyl amine and hexamethyldisiloxane in oxygen [7.4 – 7.5]. This method produces large peaks of either nitrogen or oxygen, respectively [7.5 – 7.6]. There are two main types of laser deposition: pulsed laser deposition (PLD) and matrix – assisted pulsed laser evaporation (MAPLE). In PLD, a laser is aimed at a target containing the reactive material. The laser causes the "significant material removal . . . in the form of an ejected forward-directed plume" [7.7]. A laser is used because it is able to readily vaporize almost any material, making thin film deposition of any material possible [7.7]. MAPLE is also pulsed laser, but is used when the ultraviolet laser light interacts with the organic target [7.7]. With MAPLE, the target is a frozen matrix of solvent and polymer; when the laser light hits the matrix, it heats the solvent until it vaporizes [7.7]. This heating causes enough kinetic energy to releases the polymer into the gas phase; MAPLE allows the use of the polymer without any significant decomposition [7.7]. In fact MAPLE has been used to deposit pullulan, a polysaccharide

of glucose [7.8]. The major difference between plasma deposition and laser deposition, especially matrix-assisted pulsed laser evaporation, is the ability to actually use the polymer to coat the metal, which is not possible using plasma deposition.

Chemical vapor deposition of silane, plasma deposition of allyl amine or hexamethyldisiloxane, and laser deposition of chitosan or a silane are just three methods that can be used in an effort to improve the metal – substrate interface. Since the three techniques use different beginning materials, a study in the chemical reactions should be done. Several chemical tests should be performed on the final films; these tests will compare the different techniques to ensure that the chitosan film was not affected by the chemical treatment. In order to determine if these methods improved the interface, several mechanical tests will also need to be conducted. These mechanical tests include nano-indentation, scratch testing, and bulk adhesion. Nano-indentation tests would be used to determine if the chemical treatments affected the film in any way, including changing the elastic modulus or changing the hardness of the chitosan film. Based on the deposition method, there may also be linker molecule thickness differences that could affect the binding of the chitosan films. This binding difference may result in delamination of the film when a scratch is induced. If no differences are seen, however, bulk adhesion tests would be used to determine the strength of the bond created by the different deposition techniques. Finally, biological tests, such as contact angle, cell attachment studies, and cell growth studies would need to be performed to determine if major changes to the film occurred because of the treatment; these changes may not be seen chemically, but would be "seen" biologically if the cells failed to attach and/or grow.

7.7 Coating Methods to Control Thickness

Currently, the chitosan films are around 100 μm, which is the lower end of thickness that can be seen by the human eye; these films are considered thick. This thickness could very easily affect the binding properties of the films produced. Only a small portion of the chitosan film binds to the metal surface by way of a silane and a linker molecule, as in the case of aminopropyltriethoxysilane, or just a silane, as in the case of triethoxsilylbutyraldehyde; the rest of the film intertwines with itself. Therefore, it would be beneficial to determine ways to control the thickness of the film, which includes investigations into how to lower the thickness, which could possibly produce higher quality films that are bonded more to the metal than to itself.

As part of controlling the thickness, however, care must be taken to ensure that the film produced is not too thin; a film that is too thin would easily be degraded, exposing the silane/gluteraldehyde combination or the metal surface. The effects of the silanes on bone cells would need to be investigated to determine what toxicity values are present and how these silanes affect bone cell growth, metabolism, and proliferation. Once a minimum thickness has been determined, then mechanical tests would need to be performed to determine if an improvement has been made in the binding of the film to the metal surface. Scratch testing could be very useful in these tests, as the film may be considered thin, in the upper nanometer or lower micron range, and delamination could occur. Contact angle tests would also need to be performed to determine if the thickness affected the hydrophilicity of the chitosan films. Biological tests would have already performed to determine the minimum thickness of the chitosan films to be used for further testing.

7.8 Coating Additives

One of the many properties that make chitosan so useful is its ability to bind to proteins and other materials, such as calcium. The addition of proteins and/or other materials can help to improve the differentiation and proliferation of bone cells.

The addition of proteins, such as bone morphogenetic protein, can help promote differentiation. However, proteins are more sensitive to chemicals than polysaccharides are. Therefore, care must be given to prevent the protein from becoming denatured. Tests of the activity of the protein will need to be performed at every step of the reaction scheme. This includes testing of the protein after evaporation of the chitosan film and testing of the protein after sterilization. Should the protein not become denatured, then mechanical testing to determine if bond strength, hardness, and elastic modulus of the film are affected would be performed. Also, biological testing of both cell attachment and cell proliferation would need to be performed and compared to the chitosan film that does not contain the protein.

Chitosan readily absorbs calcium, which in turn causes the uptake of phosphate ions [7.9]. Also, chitosan has been shown to be a good transportation tool for hydroxyapatite [7.10]. Studies have been performed on the different uptake of chemicals and ceramics, which include testing the hardness and elastic modulus of the film. However, bonding these composites to a substrate has not been examined. The bond strength of these modified chitosan films is of significance to coating quality and the prevention of flaking and cracking.

7.9 Coating Materials

Chitosan, as previously stated, is a copolymer of glucosamine and N-acetyl glucosamine. There are several other compounds present in the human body that resemble chitosan, differing only by the acetamide group or the amine group. Hyarulonate and glucosamine are two such compounds. These compounds could be used in conjunction with, or in place of, chitosan to improve the bioactivity of the coating. Figure 7.1 shows chitosan compared to hyarulonate, with the molecular differences shown in bold italics; glucosamine was not shown as it is a part of chitosan.

In order to determine if the addition of hyarulonate or glucosamine improves the chitosan coating, or should replace the coating, several tests will need to be performed. To begin with, the chemistry of the reactions will need to be determined using X-Ray Photoelectron Spectroscopy. This will allow the researcher to ensure that the reaction scheme is similar to the reaction scheme presented in this research. The mechanical properties will also need to be tested. Because hyarulonate and glucosamine are both polymers, the possibility exists that no major changes to the hardness and elastic modulus of the coating will occur. However, this would need to be proven. Since the chemistry of the compounds differ from chitosan, as demonstrated in Figure 7.1, the bond strength of the modified chitosan coating and the coatings without chitosan will need to be examined using bulk adhesion tests. Contact angle tests will also need to be performed to determine if the addition of hyarulonate or glucosamine affects the hydrophilicity of the chitosan films; contact angle tests will also need to be performed on the coating without chitosan to determine if any changes to the hydrophilicity of the polymers occur because of the chitosan.

Following sterilization, the mechanical properties will need to be reexamined to determine if sterilization affects either the modified chitosan films or the individual polymer films. This includes the determination of hardness and elastic modulus, along with bulk adhesion tests. Contact angle tests will also need to be performed to determine if the sterilization method affected the hydrophilicity of the modified chitosan films or the individual polymer films. Finally, biological tests will need to be performed to determine if the attachment, differentiation, and proliferation of bone cells is affected by the modified chitosan films or the individual polymer films.

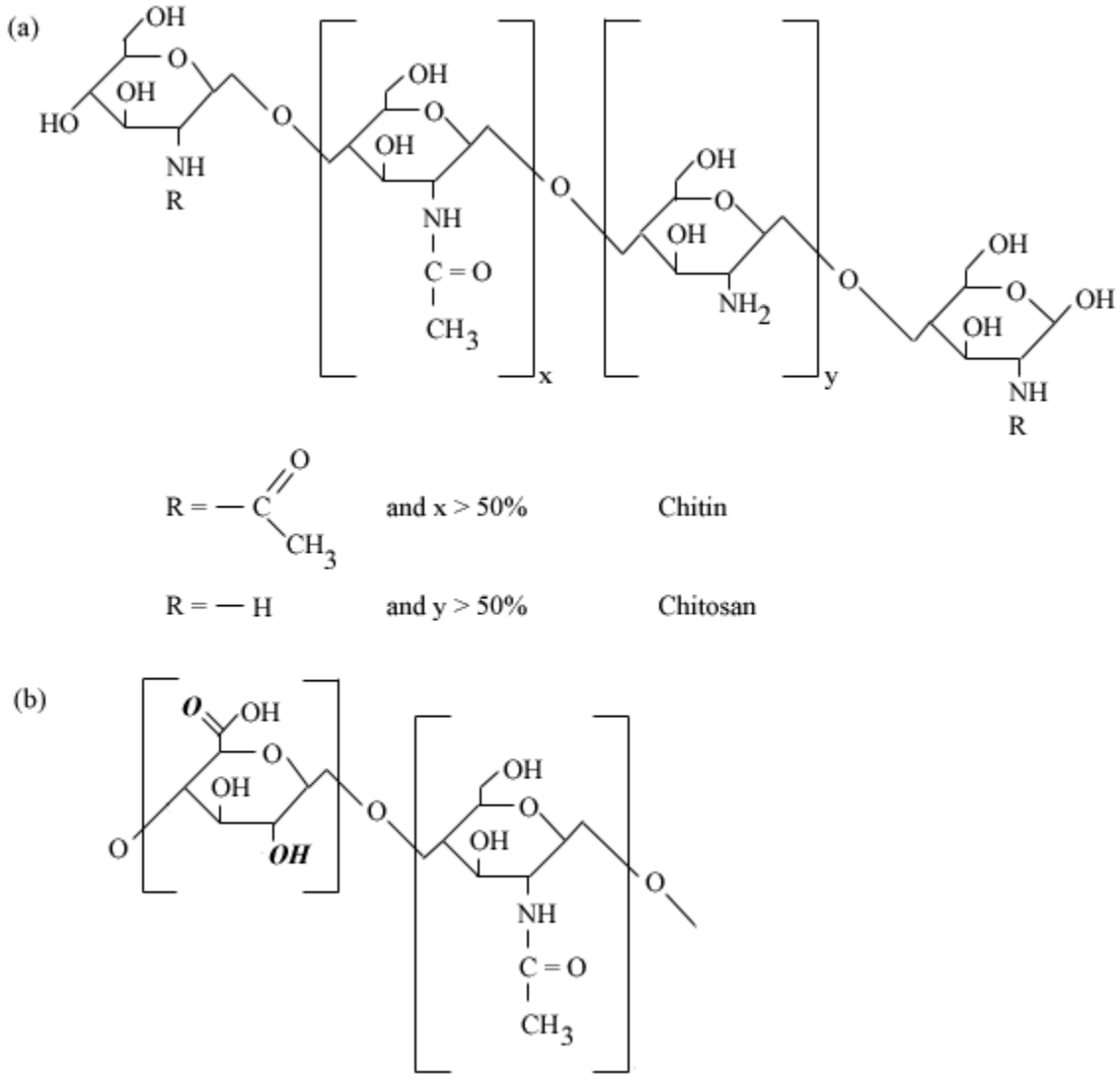

Figure 7.1. The differences in biological molecules.

(a) chitosan and (b) hyarulonate [8.11], shown in bold italics.

7.10 Conclusions

As demonstrated in this chapter, plenty of areas exist which can improve the metal – coating interface to improve implant life and the quality of tissue growth. Many different areas exist to explore, including changes in implant metals, modification of the solvent, alteration of the deposition method, and additions to the chitosan film. These adjustments would need to be individually tested in order to determine the best method to improve the metal – coating interface, while improving the coating – tissue interface or affecting the interface minimally.

WORKS CITED

Abstract References

[A.1] Ratner, B. D. and A. S. Hoffman. *Biomaterials Science: An Introduction to Materials in Medicine*. California: Academic Press, Inc., 1996, Foreword, 1-8.

[A.2] S.D. Cook, K.A. Thomas, J.F. Kay. "Experimental Coating Defect in Hydroxylapatite-Coated Implants." *Clinical Orthopaedics and Related Research*, 1992, 265, 280-290.

[A.3] A.K. Singla, M. Chawla. "Chitosan: some pharmaceutical and biological aspects-an update." *Journal of Pharmacy and Pharmacology*, 2001, 53, 1047-1067.

[A.4] Q. Li, E.T. Dunn, E.W. Grandmaison, M.F.A. Goosen. "Application and Properties of Chitosan." *Journal of Bioactive and Compatible Polymers*, 1992, 7, 370-397.

[A.5] M. Prasitsilp, R. Jenwithisuk, K. Kongsuwan, N. Damrongchai, P. Watts. "Cellular responses to chitosan *in vitro*: The importance of deacetylation." *Journal of Materials Science: Materials in Medicine*, 2000, 11, 773-778.

[A.6] R.A.A. Muzzarelli, M. Mattioli-Belmonte, A. Pugnaloni, G. Biagini. "Biochemistry, histology, and clinical uses of chitins and chitosans in wound healing." *Chitin and Chitinases*, ed. P. Jolles, R.A.A. Muzzarelli, Switzerland: Birkhauser Verlag Basel, 1990.

[A.7] P. Klokkevold, L. Vandemark, E.B. Kenney, G.W. Bernard. "Osteogenesis Enhanced by Chitosan (Poly-N-Acetyl Glucosaminoglycan) *In Vitro*." *Journal of Periodontology,* 1996, 67, 1170-1775.

[A.8] J.D. Bumgardner, R. Wiser, P.D. Gerard, P. Bergin, B. Chestnutt, M. Marini, V. Ramsey, S.H. Elder, J.A. Gilbert. "Chitosan: potential use as a bioactive coating for orthopaedic and craniofacial/dental implants." *Journal of Biomaterials Science, Polymer Edition*, 2003, 14 (5), 423-438.

Chapter 1 References

[1.1] Ratner, B. D. and A. S. Hoffman. *Biomaterials Science: An Introduction to Materials in Medicine*. California: Academic Press, Inc., 1996, Chapter 2, 37-131.

[1.2] Ratner, B. D. and A. S. Hoffman. *Biomaterials Science: An Introduction to Materials in Medicine*. California: Academic Press, Inc., 1996, Foreword, 1-8.

[1.3] Ratner, B. D. and A. S. Hoffman. *Biomaterials Science: An Introduction to Materials in Medicine*. California: Academic Press, Inc., 1996, Chapter 5, 215-242.

[1.4] "What Does LD50 mean?" *OSH Answers*. June 16th, 2005. Canadian Centre for Occupational Health and Safety (CCOHS). June 14th, 2006. <http://www.ccohs.ca/oshanswers/chemicals/ld50.html>

[1.5] Black, J. *Biological Performance of Materials: Fundamentals of Biocompatibility*. Third Edition. New York: Marcel Dekker, Inc., 1999. Chapter 1, pg. 6. August 9th, 2006. <http://library.msstate.edu:2116/Reader/>

[1.6] Ratner, B. D. and A. S. Hoffman. *Biomaterials Science: An Introduction to Materials in Medicine*. California: Academic Press, Inc., 1996, Chapter 7, 283-388.

[1.7] Callister, Jr., W. D. *Materials Science and Engineering: An Introduction*. New York: John Wiley & Sons, Inc., 2000, Chapter 11, 328-350.

[1.8] Callister, Jr., W. D. *Materials Science and Engineering: An Introduction*. New York: John Wiley & Sons, Inc., 2000, Chapter 7, 153-183.

[1.9] Callister, Jr., W. D. *Materials Science and Engineering: An Introduction*. New York: John Wiley & Sons, Inc., 2000, Chapter 12, 351-380.

[1.10] Callister, Jr., W. D. *Materials Science and Engineering: An Introduction*. New York: John Wiley & Sons, Inc., 2000, Appendix B, 789-816.

[1.11] Callister, Jr., W. D. *Materials Science and Engineering: An Introduction*. New York: John Wiley & Sons, Inc., 2000, Chapter 4, 66-91.

[1.12] Black, J. *Biological Performance of Materials: Fundamentals of Biocompatibility*. Third Edition. New York: Marcel Dekker, Inc., 1999. Glossary, pg. 450. August 9th, 2006. <http://library.msstate.edu:2116/Reader/>

[1.13] Fontana, M.G. *Corrosion Engineering*. Third Edition. Massachusetts: McGraw-Hill, 1986, Chapter 3, 39-152.

[1.14] J. Walczak, F. Shahgaldi, F. Heatley. "In vivo corrosion of 316L stainless-steel hip implants: morphology and elemental compositions of corrosion products." *Biomaterials*, 1998, 19, 229-237.

[1.15] M.-F. Harmand. "*In vitro* study of biodegradation of a Co-Cr alloy using a human cell culture model." *Journal of Biomaterial Science, Polymer Edition*, 1994, 6 (9), 809-814.

[1.16] S. A. Brown, K. Zhang, K. Merritt, J. H. Payer. "*In vivo* transport and excretion of corrosion products from accelerated anodic corrosion of porous coated F75 alloy." *Journal of Biomedical Materials Research*, 1993, 27, 1007-1017.

[1.17] Fontana, M.G. *Corrosion Engineering*. Third Edition. Massachusetts: McGraw-Hill, 1986, Chapter 2, 12-38.

[1.18] O. E. M. Pohler. "Failures of Metallic Orthopedic Implants." *Metals Handbook*. Ninth Edition. American Society for Metals. Metals Parks :ASM International, 1986, 11, 668-694.

[1.19] Pinchuk, G. *Schaum's Outline of Theory and Problems of Immunology*. New York: McGraw- Hill, 2002.

[1.20] "Iron: What is it?" *Dietary Supplement Fact Sheet: Iron*. July 26th, 2005. Office of Dietary Supplements, NIH Clinical Center, National Institutes of Health. June 14th, 2006. <http://dietary-supplements.info.nih.gov/factsheets/iron.asp.>

[1.21] J. Black. "Systemic effects of biomaterials." *Biomaterials*, 1984, 5, 11-18.

[1.22] N. Hallab, K. Merritt, J. J. Jacobs. "Current Concepts Review: Metal Sensitivity in Patients with Orthopaedic Implants." *The Journal of Bone & Joint Surgery*, 2001, 83-A (3), 428-436.

[1.23] J. D. Bumgardner, L. C. Lucas. "Cellular Response to Metallic Ions Released from Nickel-Chromium Dental Alloys." *Journal of Dental Research*, 1995, 74 (8), 1521-1527.

[1.24] *Plasma Spray Process*. Gordon England. June 14th, 2006. <http://www.gordonengland.co.uk/ps.htm>

[1.25] F.J. Kummer, W.L. Jaffe. "Stability of Cyclically Loaded Hydroxyapatite Coating: Effect of Substrate Materials, Surface Preparation, and Testing Environment." *Journal of Applied Biomaterials*, 1992, 3, 211-215.

[1.26] S.D. Cook, K.A. Thomas, J.F. Kay. "Experimental Coating Defect in Hydroxylapatite-Coated Implants." *Clinical Orthopaedics and Related Research*, 1992, 265, 280-290.

[1.27] R.J. Friedman, T.W. Bauer, K. Garg, M. Jiang, Y.H. An, R.A. Draughn. "Histological and Mechanical Comparison of Hydroxyapatite-Coated Cobalt-Chrome and Titanium Implants in the Rabbit Femur." *Journal of Applied Biomaterials*, 1995, 6, 231-235.

[1.28] J. Schrooten, J.A. Helsen. "Adhesion of bioactive glass coating to Ti6Al4V oral implant." *Biomaterials*, 2000, 21 (14), 1461-1469.

[1.29] W.R. Lacefield. "Hydroxyapatite Coatings." *Annals New York Academy of Sciences*. Year, Vol, 72-80.

[1.30] Callister, Jr., W. D. *Materials Science and Engineering: An Introduction*. New York: John Wiley & Sons, Inc., 2000, Chapter 14, 421-445.

[1.31] *Sputtering*. July 26th, 2006. Wikipedia, the free encyclopedia. June 14th, 2006. <http://en.wikipedia.org/wiki/Sputtering>

[1.32] Y. Yang, C.M. Agrawal, K.H. Kim, H. Martin, K. Schulz, J.D. Bumgardner, J.L. Ong. "Characterization and Dissolution Behavior of Sputter Calcium Phosphate Coatings After Different Postdeposition Heat Treatment Temperatures." *Journal of Oral Implantology*. 2003, 29 (6), 270-277

[1.33] A. Nanci, J.D. Wuest, L. Peru, P. Brunet, V. Sharma, S. Zalzal, M.D. McKee. "Chemical modification of titanium surfaces for covalent attachment of biological molecules." *Journal of Biomedical Materials Research*, 1998, 40, 324-335.

[1.34] D.A. Puleo. "Retention of enzymatic activity immobilized on silanized Co-Cr-Mo and Ti-6Al-4V." *Journal of Biomedical Materials Research*, 1997, 37, 222-228.

[1.35] D.A. Puleo. "Activity of enzyme immobilized on silanized Co-Cr-Mo." *Journal of Biomedical Materials Research*, 1995, 29, 951-957.

[1.36] S.H. Maxian, J.P. Zawadsky, M.G. Dunn. "Effect of Ca/P coating resorption and surgical fit on the bone/implant interface." *Journal of Biomedical Materials Research*, 1994, 28 (11), 1311-1319.

[1.37] Callister, Jr., W. D. *Materials Science and Engineering: An Introduction*. New York: John Wiley & Sons, Inc., 2000, Chapter 6, 112-152.

[1.38] Callister, Jr., W. D. *Materials Science and Engineering: An Introduction*. New York: John Wiley & Sons, Inc., 2000, Chapter 13, 381-420.

[1.39] F. Chen, Z.C. Wang, C.J. Lin. "Preparation and characterization of nano-sized hydroxyapatite particles and hydroxyapatite/chitosan nano-composite for use in biomedical materials." *Materials Letters*, 2002, 57, 848-861.

[1.40] T. Furukawa, Y. Matsusue, T. Yasunaga, Y. Shikinami, M. Okuno, T. Nakamura. "Biodegradation behavior of ultra-high-strength hydroxyapatite/poly (L-lactide) composite rods for internal fixation of bone fractures." *Biomaterials*, 2000, 21 (9), 889-898.

[1.41] T. Kasuga, Y. Ota, M. Nogami, Y. Abe. "Preparation and mechanical properties of polylactic acid composites containing hydroxyapatite fibers." *Biomaterials*, 2001, 22 (1), 19-23.

[1.42] M.C. Change, T. Ikoma, M. Kikuchi, J. Tanaka. "Preparation of a porous hydroxyapatite/collagen nanocomposite using gluteraldehyde as a crosslinkage agent." *Journal of Materials Science Letters,* 2001, 20 (13), 1199-1201.

[1.43] S. Viala, M. Freche, J.L. Lacout. "Preparation of a new organic-mineral composite: chitosan-hydroxyapatite." *Annales de Chimie: Science des Materiaux*, 1998, 23 (1-2), 69-72.

[1.44] M. Wang, W. Bonfield. "Chemically coupled hydroxyapatite-polyethylene composites: Structure and properties." *Biomaterials*, 2002, 22 (11), 1311-1320.

[1.45] M. Wang, S. Deb, W. Bonfield. "Chemical coupled hydroxyapatite-polyethylene composites: Processing and characterization." *Material Letters*, 2000, 44 (2), 119-124.

[1.46] D.A. Puleo, R.A. Kissling, M.S. Sheu. "A technique to immobilize bioactive proteins, including bone morphogenetic protein-4 (BMP-4), on titanium alloy." *Biomaterials*, 2002, 23, 2079-2087.

[1.47] Q. Li, E.T. Dunn, E.W. Grandmaison, M.F.A. Goosen. "Application and Properties of Chitosan." *Journal of Bioactive and Compatible Polymers*, 1992, 7, 370-397.

[1.48] A.K. Singla, M. Chawla. "Chitosan: some pharmaceutical and biological aspects-an update." *Journal of Pharmacy and Pharmacology*, 2001, 53, 1047-1067.

[1.49] E. Khor, L.Y. Lim. "Implantable applications of chitin and chitosan." *Biomaterials*, 2003, 24, 2339-2349.

[1.50] J.D. Bumgardner, R. Wiser, P.D. Gerard, P. Bergin, B. Chestnutt, M. Marini, V. Ramsey, S.H. Elder, J.A. Gilbert. "Chitosan: potential use as a bioactive coating for orthopaedic and craniofacial/dental implants." *Journal of Biomaterials Science, Polymer Edition*, 2003, 14 (5), 423-438.

[1.51] O.C. Agboh, Y. Qin. "Chitin and Chitosan Fibers." *Polymers for Advanced Technologies,* 1997, 8, 355-365.

[1.52] R.A.A. Muzzarelli, C. Muzzarelli, R. Tarsi, M. Miliani, F. Gabbanelli, M. Cartolari. "Fungistatic Activity of Modified Chitosans against *Saprolegnia parasitica*." *Biomacromolecules*, 2001, 2, 165-169.

[1.53] N.R. Sudarshan, D.G. Hoover, D. Knorr. "Antibacterial Action of Chitosan." *Food Biotechnology*, 1992, 6 (3), 257-272.

[1.54] R.A.A. Muzzarelli, R. Tarsi, O. Filippini, E. Giovanetti, G. Biagini, P.E. Varaldo. "Antimicrobial Properties of *N*-Carboxybutyl Chitosan." *Antimicrobial Agents and Chemotherapy*, 1990, 34 (10), 2019-2023.

[1.55] J.F. Prudden, P. Migel, P. Hanson, L. Friedrich, L. Balassa. "The Discovery of a Potent Pure Chemical Wound-Healing Accelerator." *The American Journal of Surgery*, 1970, 119, 560-564.

[1.56] K. Tomihata, Y. Ikada. "*In vitro* and *in vivo* degradation of films of chitin and its deacetylated derivatives." *Biomaterials*, 1997, 18, 567-575.

[1.57] M. Prasitsilp, R. Jenwithisuk, K. Kongsuwan, N. Damrongchai, P. Watts. "Cellular responses to chitosan *in vitro*: The importance of deacetylation." *Journal of Materials Science: Materials in Medicine*, 2000, 11, 773-778.

[1.58] P. Kohn, R.J. Winzler, R.C. Hoffman. "Metabolism of D- Glucosamine and *N*-Acetyl-D-glucosamine in the Intact Rat." *The Journal of Biological Chemistry*, 1962, 237 (2), 304-308.

[1.59] R.A.A. Muzzarelli, M. Mattioli-Belmonte, A. Pugnaloni, G. Biagini. "Biochemistry, histology, and clinical uses of chitins and chitosans in wound healing." *Chitin and Chitinases*, ed. P. Jolles, R.A.A. Muzzarelli, Switzerland: Birkhauser Verlag Basel, 1990.

[1.60] P. Klokkevold, L. Vandemark, E.B. Kenney, G.W. Bernard. "Osteogenesis Enhanced by Chitosan (Poly-N-Acetyl Glucosaminoglycan) *In Vitro*." *Journal of Periodontology,* 1996, 67, 1170-1775.

[1.61] A. Lahiji, A. Sohrabi, D. S. Hungerford, C. G. Frondoza. "Chitosan supports the expression of extracellular matrix proteins in human osteoblasts and chondrocytes." *Journal of Biomedical Materials Research*, 2000, 51, 586-595.

[1.62] H. Ueno, F. Nakamura, M. Murakami, M. Okumura, T. Kadosawn, T. Fujinaga. "Evaluation effects of chitosan for the extracellular matrix production by fibroblasts and the growth factors production by macrophages." *Biomaterials*, 2000, 22, 2125-2130.

[1.63] M. Haque, A. C. Beekley, A. Gutowska, R. A. Reardon, P. Groo, S. P. Murray, C. Anderson, K. Azarow. "Bioabsorption Qualities of Chitosan-Absorbable Vascular Templates." *Current Surgery*, 2001, 58 (1), 77-80.

[1.64] K. Vårum, M. M. Myhr, R. J. N. Hjerde, O. Smidsrød. "*In vitro* degradation rates of partially *N*-acetylated chitosans in human serum." *Carbohydrate Research*, 1997, 299, 99-101.

[1.65] S. H. Pangburn, P. V. Trescony, J. Heller."Lysozyme degradation of partially deacetylated chitin, its film and hydrogels." *Biomaterials*, 1982, 3, 105-108.

[1.66] E. Belamie, A. Domard, H. Chanzy, M.-M. Giraud-Guille. "Spherulitic Crystallization of Chitosan Oligomers." *Langmuir*, 1999, 15, 1549-1555.

[1.67] S. B. Rao, C. P. Sharma. "Use of chitosan as a biomaterial: Studies on its safety and hemostatic potential." *Journal of Biomedical Materials Research*, 1997, 34, 21-28.

[1.68] S. B. Rao, C. P. Sharma. "Sterilization of Chitosan: Implications." *Journal of Biomaterials Applications*, 1995, 10, 136-143.

[1.69] L.-Y. Lim, E. Khor, C.-E. Ling. "Effects of Dry Heat and Saturated Steam on the Physical Properties of Chitosan." *Journal of Biomedical Materials Research*, 1999, 48, 111-116.

[1.70] L.-Y. Lim, E. Khor, O. Koo. "γ Irradiation of Chitosan." *Journal of Biomedical Materials Research*, 1998, 43, 282-290.

[1.71] C. Jarry, C. Chaput, A. Chenite, M.-A. Renaud, M. Buschmann, J.-C. Leroux. "Effects of Steam Sterilization on Thermogelling Chitosan-Based Gels." *Journal of Biomedical Research (applied Biomaterials)*, 2001, 58, 127-135.

[1.72] P.R. Marreco, P.d.L. Moreira, S.C. Genari, A.M. Moraes. "Effects of Different Sterilizaton Methods on the Morphology, Mechanical Properties, and Cytotoxicity of Chitosan Membranes Used as Wound Dressings." *Journal of Biomedical Materials Research Part B: Applied Biomaterials*, 2004, 71B, 268-277.

[1.73] K.T. Hwang, J.T. Kim, S.T. Jung, G.S. Cho, H.J. Park. "Properties of Chitosan-Based Biopolymer Films with Various Degrees of Deacetylation and Molecular Weights." *Journal of Applied Polymer Science*, 2003, 89, 3476-3484.

[1.74] M.F. Cervera, J. Heinamaki, K. Krogars, A.C. Jorgensen, M. Karjalainen, A.I. Colarte, J. Yliruusi. "Solid-State and Mechanical Properties of Aqueous Chitosan-Amylose Starch Films Plasticized with Polyols." *AAPS PharmSciTech*, 2004, 5 (1), Article 15, http://www.aapspharmscitech.org.

[1.75] S.F. Wang, L. Shen, W.D. Zhang, Y.J. Tong. "Preparation and Mechanical Properties of Chitosan/Carbon Nanotubes Composites." *Biomacromolecules*, 2005, 6, 3067-3072.

[1.76] S.F. Wang, L. Shen, Y.J. Tong, L. Chen, I.Y. Phang, P.Q. Lim, T.X. Liu. "Biopolymer chitosan/montmorillonite nanocomposites: Preparation and characterization." *Polymer Degradation and Stability,* 2005, 90, 123-131.

[1.77] R. A. A. Muzzarelli, M. Mattioli-Belmonte, C. Tietz, R. Biagini, G. Ferioli, M. A. Brunelli, M. Fini, R. Giardino, P. Ilari, G. Biagini. "Stimulatory effect on bone formation exerted by a modified chitosan." *Biomaterials*, 1994, 15 (13) 1075-1081.

[1.78] R. A. A. Muzzarelli, G. Biagini, M. Bellardini, L. Simonelli, C. Castaldini, G. Fratto. "Osteoconduction exerted by methylpyrrolidinone chitosan used in dental surgery." *Biomaterials*, 1993, 14 (1), 39-43.

[1.79] R. Muzzarelli, V. Baldassarre, F. Conti, P. Ferrara, G. Biagini, G. Gazzanelli, V. Vasi. "Biological activity of chitosan: ultrastructural study." *Biomaterials*, 1988, 9, 247-252.

[1.80] J.L. Lopez-Lacomba, J.M. Garcia-Cantalejo, J.V. Sanz Casado, A. Abarrategi, V. Correas Magana, V. Ramos. "Use of rhBMP-2 Activated Chitosan Films to Improve Osseointegration." *Biomacromolecules*, 2006, 7, 792-798.

[1.81] J. Redepenning, G. Venkataraman, J. Chen, N. Stafford. "Electrochemical preparation of chitosan/hydroxapatite composite coatings on titanium substrates." *Journal of Biomedical Materials Research*, 2003, 66A, 411-416.

[1.82] J. Wang, J. de Boer, K. de Groot. "Preparation and Characterization of Electrodeposited Calcium Phosphate/Chitosan Coating on Ti6Al4V Plates." *Journal of Dental Research*, 2004, 83 (4), 296-301.

[1.83] B. Thierry, F.M. Winnik, Y. Merhi, J. Silver, M. Tabrizian. "Bioactive Coatings of Endovascular Stents Based on Polyelectrolyte Multilayers." *Biomacromolecules*, 2003, 4, 1564-1571.

[1.84] K. Cai, A. Rechtenbach, J. Hao, J. Bossert, K.D. Jandt. "Polysaccharide-protein surface modification of titanium via a layer-by-layer technique: Characterization and cell behaviour aspects." *Biomaterials*, 2005, 26, 5960-5971.

[1.85] R.A.A. Muzzarelli, G. Biagini, A. DeBenedittis, P. Mengucci, G. Majni, G. Tosi. "Chitosan-oxychitin coatings for prosthetic materials." *Carbohydrate Polymers*, 2001, 45, 35-41.

[1.86] J.D. Bumgardner, R. Wiser, S.H. Elder, R. Jouett, Y. Yang, J.L. Ong. "Contact angle, protein adsorption, and osteoblast precursor cell attachment to chitosan coatings bonded to titanium." *Journal of Biomaterials Science, Polymer Edition*, 2003, 14 (12), 1401-1409.

[1.87] *Cobalt Chromium (CoCr) Material for EOSINT M-Series Machines*. Morris Technologies. July 28th, 2006. <http://www.morristech.com/graphics/cobaltchromium.pdf>

[1.88] Ohring, M. *The Materials Science of Thin Films*. California: Academic Press, Inc., 1992.

Chapter 2 References

[2.1] K.R. Williams, R.S. Muller. "Etch Rates for Micromachining Processing." *Journal of Microelectromechanical Systems*, 1996, 5 (4), 256-269.

[2.2] J.D. Bumgardner, R. Wiser, P.D. Gerard, P. Bergin, B. Chestnutt, M. Marini, V. Ramsey, S.H. Elder, J.A. Gilbert. "Chitosan: potential use as a bioactive coating for orthopaedic and craniofacial/dental implants." *Journal of Biomaterials Science, Polymer Edition*, 2003, 14 (5), 423-438.

[2.3] Moulder, J. F., W. F. Stickle, P. E. Sobol, and K. D. Bomben. *Handbook of X-ray Photoelectron Spectroscopy*. Minnesota: Perkin-Elmer Corporation, 1992.

[2.4] *Electron Shell*. July 23rd, 2006. Wikipedia, the free encyclopedia. June 28th, 2006. <http://en.wikipedia.org/wiki/Electron_shell>

[2.5] Garbassi, F., M. Morra, E. Occhiello. *Polymer Surfaces: From Physics to Technology*. New York: John Wiley and Sons, Inc., 1994.

[2.6] Postek, M. T., K. S. Howard, A. H. Johnson, and K. L. McMichael. *Scanning Electron Microscopy: A Student's Handbook*. Vermont: Ladd Research Industries, 1980.

[2.7] *Manual for TestWorks 4 Software*. Tennessee: MTS Systems Corporation, Version 16, 2001, Chapter 4, 27-38.

[2.8] *Manual for TestWorks 4 Software*. Tennessee: MTS Systems Corporation, Version 16, 2001, CSM Option, 200-208.

[2.9] *Manual for TestWorks 4 Software*. Tennessee: MTS Systems Corporation, Version 16, 2001, Instrumented Scratch Testing, 299-314.

[2.10] J. Ahn, K.L. Mittal, R.H. MacQueen. "Hardness and Adhesion of Filmed Structures as Determined by the Scratch Technique." *Adhesion Measurement of Thin Films, Thick Films, and Bulk Coatings.* K.L. Mittal, ed. Pennsylvania: American Society for Testing and Materials, 1978.

[2.11] J.A. Schneider, S.E. Guthrie, W.M. Clift, N.R. Moody. "Quantifying the effect of carbon on the practical adhesion of aluminum films to sapphire substrates." *Adhesion Aspects of Thin Films,* 2000, 1, 1-12.

[2.12] *User's Guide to Autoprobe M5*. California: Park Scientific Instruments, 1998.

[2.13] Ohring, M. *The Materials Science of Thin Films*. California: Academic Press, Inc., 1992.

[2.14] Tredgold, R.H. *Order in Thin Organic Films*. New York: Cambridge University Press, 1994.

[2.15] Dee, K.C., D.A. Puleo, R. Bizios. *An Introduction to Tissue-Biomaterial Interactions*. New Jersey: John Wiley and Sons, Inc., 2002.

Chapter 3 References

[3.1] A. Nanci, J.D. Wuest, L. Peru, P. Brunet, V. Sharma, S. Zalzal, M.D. McKee. "Chemical modification of titanium surfaces for covalent attachment of biological molecules." *Journal of Biomedical Materials Research*, 1998, 40, 324-335.

[3.2] D.A. Puleo. "Retention of enzymatic activity immobilized on silanized Co-Cr-Mo and Ti-6Al-4V." *Journal of Biomedical Materials Research*, 1997, 37, 222-228.

[3.3] D.A. Puleo. "Activity of enzyme immobilized on silanized Co-Cr-Mo." *Journal of Biomedical Materials Research*, 1995, 29, 951-957.

[3.4] H. M. Liao, R. N. S. Sodhi, T. W. Coyle. "Surface composition of AlN powders studied by x-ray photoelectron spectroscopy and bremsstrahlung-excited Auger electron spectroscopy." *Journal of Vacuum Science and Technology*, 1993, 11 (5), 2681-2686.

[3.5] G. Hollinger, G. Marest, H. Jaffrezic, J. Tousset, N. Moncoffre. "Temperature influence during nitrogen implantation into stell." *Nuclear Instruments and Methods in Physics Research*, 1985, B7/8, 177-183.

[3.6] D. Rats, J. Sevely, L. Vandenbulcke, R. Benoit, R. Erre, R. Herbin, V. Serin. "Characterization of diamond films deposited on titanium and its alloys." *Thin Solid Films*, 1995, 270, 177-183.

[3.7] A. D. Romaschin, L. N. Bui, M. Thompson, N. B. McKeown, P. G. Kalman. "Surface Modification of the Biomedical Polymer Poly(ethylene terephthalate)." *Analyst*, 1993, 118, 463-474.

[3.8] C. Jones, E. Sammann. "The effect of low power plasmas on carbon fibre surfaces." *Carbon*, 1990, 28 (4), 509-514.

[3.9] B. J. Meenan, J. A. Hewitt, N. M. D. Brown. "X-ray induced Beam Damage Observed during X-ray Photoelectron Spectroscopy (XPS) Studies of Palladium Electrode Ink Materials." *Surface and Interface Analysis*, 1992, 18, 187-198.

[3.10] A. D. Romaschin, L. N. Bui, M. Thompson, N. B. McKeown, P. G. Kalman, "Surface Modification of the Biomedical Polymer Poly(ethylene terephthalate)." *Analyst*, 1993, 118, 463-474.

[3.11] A. S. Vanini, J. P. Audouard, P. Marcus. "The Role of Nitrogen in the Passivity of Austenitic Stainless Steels." *Corrosion Science*, 1994, 36 (11), 1825-1834.

[3.12] P. Bertrand, V. B. Wiertz, "Identification of the n-containing functionalities introduced at the surface of ammonia plasma treated carbon fibres by combined TOF SIMS and XPS." *Unité de Physico-Chimie et de Physique des Materiaux*, Univ. Louvain 1348 Editor, Louvain.

[3.13] B. F. Dzhurinskii, D. Gati, N. P. sergushin, V. I. Nefedov, Y. V. Salyn. "Simple and coordination compounds. An X-ray photoelectron spectroscopic study of certain oxides." *Russian Journal of Inorganic Chemistry*, 1975, 20, 2307-2314.

[3.14] C. Cardinaud, G. Lemperiere, M. C. Peignon, P. Y. Jouan. "Characterisation of TiN coatings and of TiN/Si interface by x-ray photoelectron spectroscopy and Auger electron spectroscopy." *Applied Surfae Science*, 1993, 68, 595-603.

[3.15] T. L. Barr. "The nature of the relative bonding chemistry in zeolites: an XPS study." *Journal of Physical Chemistry*, 1990, 10, 760-765.

[3.16] J. M. Martin, L. Vovelle, M. Bou, T. L. Mogne. "Chemistry of the interface between aluminium and polyethyleneterephtalate by X PS." *Applied Surface Science*, 1991, 47, 149-161.

[3.17] G. Hollinger. "Structures Chimique Et Electronique De L'Interface SiO_2-Si." *Applications of Surface Science*, 1981, 8, 318-336.

[3.18] M. J. Graham. "The application of surface techniques in understanding corrosion phenomena and mechanisms." *Corrosion Science*, 1995, 37 (9), 1377-1397.

[3.19] B. A. De Angelis, C. Rizzo, S. Contarini, S. P. Howlett. "XPS study on the dispersion of carbone additives in silicon carbide powders." *Applied Surface Science*, 1991, 51, 177-183.

[3.20] C. D. Wagner. "X-ray photoelectron spectroscopy with X-ray photons of higher energy." *Journal of Vacuum Science and Technology*, 1978, 15 (2), 518-523.

[3.21] A. Weninger, J. E. Davies, K. Sreenivas, R. N. S. Sodhi. "X-ray photoelectron spectroscopic comparison of sputtered Ti, Ti6Al4V, and passivated bulk metals for use in cell culture techniques." *Journal of Vacuum Science and Technology*, 1991, A9 (3), 1329-1333.

[3.22] A. Fahlman, C. Nordling, G. Johansson, K. Hamrin. "Charge transfer in transition metal carbides and related compounds studied by esca." *Journal of Physical and Chemical Solids*, 1969, 30, 1835-1847.

[3.23] B. F. Lowenberg, B. W. Callen, J. E. Davies, R. N. S. Sodhi, S. Lugowski. "Nitric acid passivation of Ti6Al4V reduces Thickness of surface oxide layer and increases trace element release." *Journal of Biomedical Materials Research*, 1995, 29, 279-290.

[3.24] "Isopropyltriethoxysilane." *Material Safety Data Sheet*. July 13th, 2005. Alfa Aesar. May 12th, 2006.
<http://www.alfa.com/CGI-BIN/LANSAWEB?WEBEVENT+L0B59798F96760100F356038+ALF+ENG>

[3.25] P.A. Heiney, K. Gruneberg, J. Fang. "Structure and Growth of Chromophore-Functionalized (3-Aminopropyl)triethoxysilane Self-Assembled on Silicon." *Langmuir*, 2000, 16, 2651-2657.

[3.26] E.T. Vandenberg, L. Bertilsson, B. Liedberg, J. Uvdal, R. Erlandsson, H. Elwing, I. Lundstrom. "Structure of 3-Aminopropyl Triethoxy Silane on Silicon Oxide." *Journal of Colloid and Interface Science*, 1991, 147, 1, 103-118.

[3.27] W. Qian, B. Xu, L. Wu, C. Wang, D. Yao, F. Yu, C. Yuan, Y. Wei. "Controlled Site-Directed Assembly of Antibodies by Their Oligosaccaride Moieties onto APTES Derivatized Surfaces." *Journal of Colloid and Interface Science*, 1999, 214, 16-19.

[3.28] J.D. Bumgardner, R. Wiser, P.D. Gerard, P. Bergin, B. Chestnutt, M. Marini, V. Ramsey, S.H. Elder, J.A. Gilbert. "Chitosan: potential use as a bioactive coating for orthopaedic and craniofacial/dental implants." *Journal of Biomaterials Science, Polymer Edition*, 2003, 14 (5), 423-438.

Chapter 4 References

[4.1] H. M. Liao, R. N. S. Sodhi, T. W. Coyle. "Surface composition of AlN powders studied by x-ray photoelectron spectroscopy and bremsstrahlung-excited Auger electron spectroscopy." *Journal of Vacuum Science and Technology*, 1993, 11 (5), 2681-2686.

[4.2] G. Hollinger, G. Marest, H. Jaffrezic, J. Tousset, N. Moncoffre. "Temperature influence during nitrogen implantation into steel." *Nuclear Instruments and Methods in Physics Research*, 1985, B7/8, 177-183.

[4.3] D. Rats, J. Sevely, L. Vandenbulcke, R. Benoit, R. Erre, R. Herbin, V. Serin. "Characterization of diamond films deposited on titanium and its alloys." *Thin Solid Films*, 1995, 270, 177-183.

[4.4] Moulder, J. F., W. F. Stickle, P. E. Sobol, and K. D. Bomben. *Handbook of X-ray Photoelectron Spectroscopy*. Minnesota: Perkin-Elmer Corporation, 1992.

[4.5] A. D. Romaschin, L. N. Bui, M. Thompson, N. B. McKeown, P. G. Kalman. "Surface Modification of the Biomedical Polymer Poly(ethylene terephthalate)." *Analyst*, 1993, 118, 463-474.

[4.6] C. Jones, E. Sammann. "The effect of low power plasmas on carbon fibre surfaces." *Carbon*, 1990, 28 (4), 509-514.

[4.7] C. D. Wagner, J. F. Moulder, L. E. Davis, W. M. Riggs. *Handbook of X-ray Photoelectron Spectroscopy*. Minnesota: Perkin-Elmer Corporation, 1992.

[4.8] C. H. Shan, W. Kowebel. "The mechanism of fiber - matrix interactions in carbon - carbon composites." *Carbon*, 1990, 28 (2/3), 287-299.

[4.9] A. D. Romaschin, L. N. Bui, M. Thompson, N. B. McKeown, P. G. Kalman. "Surface Modification of the Biomedical Polymer Poly(ethylene terephthalate)." *Analyst*, 1993, 118, 463-474.

[4.10] D. T. Clark, H. R. Thomas. "Applications of ESCA to Polymer Chemistry Em Dash 10. Core and Valence Energy Levels of a Series of Polyacrylates." *Journal of Polymer Science, Polymer Chemistry Edition*, 1976, 14 (7), 1671-1700.

[4.11] A. D. Romaschin, L. N. Bui, M. Thompson, N. B. McKeown, P. G. Kalman. "Surface Modification of the Biomedical Polymer Poly(ethylene terephthalate)." *Analyst*, 1993, 118, 463-474.

[4.12] A. Casagrande, A. Glisenti, E. Lanzoni, E. Tondello, L.Mirenghi, M. Casarin, R. Bertoncello. "TiN, TiC and Ti(C,N) film characterization and its relationship to tribological behaviour." *Surface and Interface Analysis*, 1992, 18, 525-531.

[4.13] A. Atrens, A. S. Lim. "ESCA studies of Nitrogen-Containing Stainless Steels." *Applied Physics A*, 1990, 51, 411-418.

[4.14] F. Beguin, I. Rashkov, N. Manolova, R. Benoit, R. Erre, S. Delpeux. "Fullerene core star-like polymers-1. Preparation from fullerenes and monoazidopolyehers." *European Polymer Journal*, 1998, 34 (7), 905-915.

[4.15] A. Nylund, I. Olefjord. "Surface Analysis of Oxidized Aluminium - 1. Hydration of Al2O3 and Decomposition of Al(OH)3 in a Vacuum as Studied by ESCA." *Surface and Interface Analysis*, 1994, 21, 283-289.

[4.16] Garbassi, F., M. Morra, E. Occhiello. *Polymer Surfaces: From Physics to Technology.* New York: John Wiley and Sons, Inc., 1994.

[4.17] B. A. De Angelis, C. Rizzo, S. Contarini, S. P. Howlett. "XPS study on the dispersion of carbone additives in silicon carbide powders." *Applied Surface Science*, 1991, 51, 177-183.

[4.18] A. Cros, R. Saudi, C. A. Hewett, S. S. Lau, G. Hollinger. "An x-ray photoemission spectroscopy investigation of oxides grown on Au_xSi_{1-x} layers." *Journal of Applied Physics*, 1990, 67, 1826-1830.

[4.19] T. A. Clarke, E. N. Rizkalla. "X-ray photoelectron spectroscopy of some silicates." *Chemical Physics Letters*, 1976, 37, 523-526.

[4.20] D. T. Clark, H. R. Thomas. "Applications of ESCA to Polymer Chemistry Em Dash 10. Core and Valence Energy Levels of a Series of Polyacrylates." *Journal of Polymer Science, Polymer Chemistry Edition*, 1976, 14 (7), 1671-1700.

[4.21] Garbassi, F., M. Morra, E. Occhiello. *Polymer Surfaces: From Physics to Technology.* New York: John Wiley and Sons, Inc., 1994.

[4.22] M. W. Roberts, M. H. Matloob. "Electron spectroscopic study of nitrogen species adsorbed on copper." *School of Chemistry: University of Bradford*, 1977, BD7 (1DP), 1393-1405.

[4.23] J. F. Huravlev, M. V. Kuznetsov, V. A. Gubanov. "XPS analysis of adsorption of oxygen molecules on the surface of Ti and TiNx films in vacuum." *Journal of Electron Spectroscopy and Related Phenomena*, 1992, 38, 169-176.

[4.24] A. Fahlman, C. Nordling, G. Johansson, K. Hamrin. "Charge transfer in transition metal carbides and related compounds studied by esca." *Journal of Physical and Chemical Solids*, 1969, 30, 1835-1847.

[4.25] A. Luches, A. Perrone, B. Dubreuil, B. Rousseau, C. Boulmer-Leborgne, G. Blondiaux, H. Estrade, J. Hermann, J. L. Debrun, M. L. Degiorgi, M. Martino, P. Brault. "Direct carbidation of titanium as a result of multipulse UV-laser irradiation of titanium samples in an ambient methane gas." *Applied Surface Science*, 1992, 54, 349-352.

[4.26] B. F. Lowenberg, B. W. Callen, J. E. Davies, R. N. S. Sodhi, S. Lugowski. "Nitric acid passivation of Ti6Al4V reduces Thickness of surface oxide layer and increases trace element release." *Journal of Biomedical Materials Research*, 1995, 29, 279-290.

[4.27] B. Carriere, D. Brion, J. Escard, J. P. Deville. "X-Ray Photoelectron study of some silicon-oxygen compounds." *Journal of Electron Spectroscopy and Related Phenomena*, 1977, 10, 85-91.

[4.28] T. L. Barr. "An ESCA Study of Termination of the Passivation of Elemental Metals." *The Journal of Physical Chemistry*, 1978, 82 (16), 1801-1810.

[4.29] G. Mink, G. Varsanyi, I. Bertoti, J. Grabis, J. Vaivads, T. Millers, T. Szekely. "XPS Characterization of Ultrafine Si3N4 Powders." *Surface and Interface Analysis*, 1998, 12, 527-530.

[4.30] M. J. Graham. "The application of surface techniques in understanding corrosion phenomena and mechanisms." *Corrosion Science*, 1995, 37 (9), 1377-1397.

[4.31] B. E. Chenhall, J. Ellis, P. T. Crisp, R. Payling, R. K. Tandon, R. S. Baker. "Application of X-ray photoelectron spectroscopy to the analysis of stainless-steel welding aerosols." *Applications of Surface Science*, 1985, 20, 527-537.

[4.32] F. Beguin, I. Rashkov, N. Manolova, R. Benoit, R. Erre, S. Delpeux "Fullerene core star-like polymers-1. Preparation from fullerenes and monoazidopolyehers." *European Polymer Journal*, 1998, 34 (7), 905-915.

[4.33] L. Qingliang, Y. Huaming, Z. Xiong, Z. Zude. "Structural study of compartmental complexes of europium and copper." *Journal of Molecular Structure*, 1999, 478, 23-27.

[4.34] A. S. Vanini, J. P. Audouard, P. Marcus. "The Role of Nitrogen in the Passivity of Austenitic Stainless Steels." *Corrosion Science*, 1994, 36 (11) 1825-1834.

[4.35] Moulder, J. F., W. F. Stickle, P. E. Sobol, and K. D. Bomben. *Handbook of X-ray Photoelectron Spectroscopy*. Minnesota: Perkin-Elmer Corporation, 1992.

[4.36] A. Pashutski, M. Folman. "Low temperature XPS studies of NO and N_2O adsorption on Al(100)." *Surface Science*, 1989, 216, 395-408.

[4.37] A. B. Christie, J. Lee, I. Sutherland, J. M. Walls. "An XPS study of ion-induced compositional changes with group II and group IV compounds." *Applications of Surface Science*, 1983, 15, 224-237.

[4.38] Briggs, D. and M. P. Seah. *Practical Surface Analysis.* New York: John Wiley & Sons, Inc., 1993, Vol 1, 2nd Ed.

[4.39] Y. Kanedo, Y. Suginohara. "Observation of Si2p binding energy by ESCA and determination of O, O- and O2- ions in silicates." *Graduate School.* 1977, Tohoku University, Sendai, 285-289.

[4.40] Briggs, D. and M. P. Seah. *Practical Surface Analysis.* New York: John Wiley & Sons, Inc., 1993, Vol 1, 2nd Ed.

[4.41] W. J. Landis, J. R. Martin. "X-ray photoelectron spectroscopy applied to gold-decorated mineral standards of biological interest." *Journal of Vacuum Science and Technology*, 1984, A 2, 1108-1111.

[4.42] B. E. Chenhall, J. Ellis, P. T. Crisp, R. Payling, R. K. Tandon, R. S. Baker. "Application of X-ray photoelectron spectroscopy to the analysis of stainless-steel welding aerosols." *Applications of Surface Science*, 1985, 20, 527-537.

[4.43] K.R. Williams, R.S. Muller. "Etch Rates for Micromachining Processing." *Journal of Microelectromechanical Systems*, 1996, 5 (4), 256-269.

[4.44] E. Khor, L.Y. Lim. "Implantable applications of chitin and chitosan." *Biomaterials*, 2003, 24, 2339-2349.

Chapter 5 References

[5.1] *Manual for TestWorks 4 Software*. Tennessee: MTS Systems Corporation, Version 16, 2001, Chapter 4, 27-38.

[5.2] *Manual for TestWorks 4 Software*. Tennessee: MTS Systems Corporation, Version 16, 2001, CSM Option, 200-208.

[5.3] S.F. Wang, L. Shen, W.D. Zhang, Y.J. Tong. "Preparation and Mechanical Properties of Chitosan/Carbon Nanotubes Composites." *Biomacromolecules*, 2005, 6, 3067-3072.

[5.4] S.F. Wang, L. Shen, Y.J. Tong, L. Chen, I.Y. Phang, P.Q. Lim, T.X. Liu. "Biopolymer chitosan/montmorillonite nanocomposites: Preparation and characterization." *Polymer Degradation and Stability,* 2005, 90, 123-131.

[5.5] S. Majd, Y. Yuan, W.O. Haggard, J.L. Ong, Y. Yang, S. Mishra, J.D. Bumgardner. "Quasi-Static Nanomechanical Characterization of Chitosan Films."

[5.6] J.D. Bumgardner, R. Wiser, P.D. Gerard, P. Bergin, B. Chestnutt, M. Marini, V. Ramsey, S.H. Elder, J.A. Gilbert. "Chitosan: potential use as a bioactive coating for orthopaedic and craniofacial/dental implants." *Journal of Biomaterials Science, Polymer Edition*, 2003, 14 (5), 423-438.

[5.7] J.D. Bumgardner, R. Wiser, S.H. Elder, R. Jouett, Y. Yang, J.L. Ong. "Contact angle, protein adsorption, and osteoblast precursor cell attachment to chitosan coatings bonded to titanium." *Journal of Biomaterials Science, Polymer Edition*, 2003, 14 (12), 1401-1409.

[5.8] Dee, K.C., D.A. Puleo, R. Bizios. *An Introduction to Tissue-Biomaterial Interactions*. New Jersey: John Wiley and Sons, Inc., 2002.

Chapter 7 References

[7.1] "Toluene." *Material Safety Data Sheet*. March 7th, 2006. Alfa Aesar. July 5th, 2006. <http://www.alfa.com/CGI-BIN/LANSAWEEB?PROCFUN+WEBOEP+SRCHCHK+alf+ENG>

[7.2] S. Ek, E.I. Iiskola, L. Niinisto. "Gas-Phase Deposition of Aminopropylalkoxysilanes on Porous Silica." *Langmuir*, 2003, 19, 3461-3471.

[7.3] S. Ek, E.I. Iiskola, L. Niinisto, J. Vaittinen, T.T. Pakkanen, J. Keranen, A. Auroux. "Atomic Layer Deposition of a High-Density Aminopropylsiloxane Network on Silica through Sequential Reaction of γ-Aminopropyltrialkoxysilanes and Water." *Langmuir*, 2003, 19, 10601-10609.

[7.4] S. Gaur, G. Vergason. "Plasma Polymerization: Theory and Practice." *Society of Vacuum Coatings: 43rd Annual Technical Conference Proceedings*, 2000, 267-271.

[7.5] F.J. Boerio, V.H. Wagh, R.G. Dillingham. "Vapor-Phase Silanation of Plasma-Polymerized Silica-Like Films by γ-Aminopropyltriethoxysilane." *The Journal of Adhesion*, 2005, 81, 115-142.

[7.6] D.A. Puleo, R.A. Kissling, M.S. Sheu. "A technique to immobilize bioactive proteins, including bone morphogenetic protein-4 (BMP-4), on titanium alloy." *Biomaterials*, 2002, 23, 2079-2087.

[7.7] D.B. Chrisey, A. Pique, R.A. McGill, J.S> Horwitz, B.R. Ringeisen, D.M. Bubb, P.K. Wu. "Laser Deposition of Polymer and Biomaterial Films." *Chemical Review*, 2003, 103, 553-576.

[7.8] R. Cristescu, I. Stamatin, D.E. Mihaieseu, C. Ghica, M. Albulescu, I.N. Mihailescu, D.B. Chrisey. "Pulsed laser deposition of biocompatible polymers: a comparative study in case of pullulan." *Thin Solid Films*, 2004, 453-454, 262-268.

[7.9] E. Khor, L.Y. Lim. "Implantable applications of chitin and chitosan." *Biomaterials*, 2003, 24, 2339-2349.

[7.10] F. Chen, Z.C. Wang, C.J. Lin. "Preparation and characterization of nano-sized hydroxyapatite particles and hydroxyapatite/chitosan nano-composite for use in biomedical materials." *Materials Letters*, 2002, 57, 848-861.

[7.11] J.K. Francis Suh, H.W.T. Matthew. "Application of chitosan-based polysaccharide biomaterials in cartilage tissue engineering: a review." *Biomaterials*, 2000, 21, 2589-2598.